IL
NUOVO CIMENTO
ORGANO DELLA SOCIETÀ ITALIANA DI FISICA
SOTTO GLI AUSPICI DEL CONSIGLIO NAZIONALE DELLE RICERCHE
E DEL COMITATO NAZIONALE PER L'ENERGIA NUCLEARE

VOL. XXII, N. 4 *Serie decima* 16 Novembre 1961

Il calcolo dell'intensità di diffrazione dei raggi X da parte di strutture denotanti disordine monodimensionale.

II - Applicazioni della teoria ad alcuni modelli strutturali con disordine monodimensionale.

G. ALLEGRA
Istituto di Chimica Industriale del Politecnico - Milano

(ricevuto il 19 Luglio 1961)

Riassunto. — Daremo in questa seconda nota alcuni esempi di calcolo, secondo la teoria precedentemente sviluppata, dell'intensità media diffratta ai raggi X da parte di alcune strutture ipotetiche denotanti disordine monodimensionale, costituite sia da strati dello stesso tipo che da strati di tipo diverso. Supporemo inoltre la sfera di influenza di successione probabilistica (s) variabile tra 1 e 3.

1. – Il calcolo dell'intensità media diffratta da parte di una struttura costituita da strati dello stesso tipo che si possono succedere secondo due differenti vettori di traslazione t_1 e t_2, con $s = 2$.

Questo caso comprende, nella sua generalità, il problema già trattato da WILSON [1] nel caso delle imperfezioni in alcune strutture di cobalto metallico, e da HENDRICKS e TELLER [2] nel caso del disordine monodimensionale nella grafite; può inoltre trovare utile applicazione in diversi problemi di disordine monodimensionale connessi con i silicati naturali [3-6].

(1) A. J. C. WILSON: *Proc. Roy. Soc.*, A **180**, 277 (1942).
(2) S. B. HENDRICKS ed E. TELLER: *Journ. Chem. Phys.*, **10**, 147 (1942).
(3) J. MERING: *Acta Cryst.*, **2**, 371 (1949).
(4) J. MERING: *Trans. Int. Congress of Soil Science*, **3**, 21 (Amsterdam, 1950).
(5) M. CESARI, G. L. MORELLI e L. FAVRETTO: *Journ. Acta Universitatis Carolinae*, Serie Geologica, in corso di stampa (Praga, 1961).
(6) G. BROWN e R. GREENE-KELLY: *Acta Cryst.*, **7**, 101 (1954).

Siano: f la frequenza di comparizione delle traslazioni di tipo $\boldsymbol{t}_1$; $(1-f)$ la corrispondente frequenza delle traslazioni di tipo $\boldsymbol{t}_2$; q_1 e q_2 le probabilità che alle traslazioni $\boldsymbol{t}_1$ e $\boldsymbol{t}_2$ succedano ordinatamente le stesse traslazioni $\boldsymbol{t}_1$ e $\boldsymbol{t}_2$; $(1-q_1)$ e $(1-q_2)$ le probabilità che alle traslazioni $\boldsymbol{t}_1$ e $\boldsymbol{t}_2$ succedano ordinatamente le traslazioni alternative $\boldsymbol{t}_2$ e $\boldsymbol{t}_1$; φ_1 e φ_2 gli angoli di fase corrispondenti ai vettori $\boldsymbol{t}_1$ e $\boldsymbol{t}_2$:

$$(1) \qquad \varphi_1 = 2\pi \boldsymbol{t}_1 \times \boldsymbol{S}\,; \qquad \varphi_2 = 2\pi \boldsymbol{t}_2 \times \boldsymbol{S}\,; \qquad |\boldsymbol{S}| = \frac{2\sin\theta}{\lambda}\,;$$

V il fattore di struttura di ogni strato, riferito ad una terna d'assi solidale con lo strato stesso.

Il sistema lineare omogeneo dato dalla (A.10) della Nota I (*) diviene nel caso presente:

$$(2) \qquad \begin{cases} f = fq_1 + (1-f)(1-q_2) \\ 1-f = f(1-q_1) + (1-f)q_2\,. \end{cases}$$

Dal sistema (2) si ricavano le seguenti relazioni, non indipendenti tra f, q_1, e q_2:

$$(3) \qquad f_1 = f = \frac{1-q_2}{2-(q_1+q_2)}\,; \qquad f_2 = 1-f = \frac{1-q_1}{2-(q_1+q_2)}\,.$$

Esprimendo nel seguito tutti i parametri di probabilità in funzione di q_1 e q_2, avremo:

$$(4) \qquad \begin{cases} \mathscr{F}\ (\text{vedi la (A.12)}) = |f\exp[-i\varphi_1],(1-f)\exp[-i\varphi_2]| = \\ \quad = \left|\dfrac{1-q_2}{2-(q_1+q_2)}\exp[-i\varphi_1],\ \dfrac{1-q_1}{2-(q_1+q_2)}\exp[-i\varphi_2]\right|\,; \\ \boldsymbol{Q} = \begin{vmatrix} q_1\exp[-i\varphi_1] & (1-q_1)\exp[-i\varphi_2] \\ (1-q_2)\exp[-i\varphi_1] & q_2\exp[-i\varphi_2] \end{vmatrix}\,. \end{cases}$$

Il calcolo della matrice inversa $(\boldsymbol{E}-\boldsymbol{Q})^{-1}$ conduce al seguente risultato:

$$(5) \qquad (\boldsymbol{E}-\boldsymbol{Q})^{-1} = \frac{1}{1-[1-(q_1+q_2)]\exp[-i(\varphi_1+\varphi_2)]-q_1\exp[-i\varphi_1]-q_2\exp[-i\varphi_2]} \cdot \begin{vmatrix} 1-q_2\exp[-i\varphi_2] & (1-q_1)\exp[-i\varphi_2] \\ (1-q_2)\exp[-i\varphi_1] & 1-q_1\exp[-i\varphi_1] \end{vmatrix}\,;$$

(*) G. ALLEGRA: *Nuovo Cimento*, **21**, 783 (1961), nel seguito indicato con I.

dove il termine che precede la matrice a secondo membro si intende che moltiplichi tutti i termini della matrice stessa. L'espressione $\mathscr{F}(\boldsymbol{E}-\boldsymbol{Q})^{-1}\mathbf{1}$ diviene quindi:

$$(6)\qquad \mathscr{F}(\boldsymbol{E}-\boldsymbol{Q})^{-1}\mathbf{1} =$$

$$= \frac{\left\{(1-q_2)e^{-i\varphi_1}\left[1-q_2e^{-i\varphi_2}+(1-q_1)e^{-i\varphi_2}\right]+(1-q_1)e^{-i\varphi_2}\left[1-q_1e^{-i\varphi_1}+(1-q_2)e^{-i\varphi_1}\right]\right\}}{[2-(q_1+q_2)]\left\{1-[1-(q_1+q_2)]\,e^{-(i\varphi_1+\varphi_2)}-q_1\,e^{-i\varphi_1}-q_2\,e^{-i\varphi_2}\right]\right\}};$$

ed infine, dopo alcune semplificazioni, l'espressione (A.15) (Nota I) per I_{A_v} diviene:

$$(7)\qquad I_{A_v}=\frac{I}{N_1}=VV^*\,\frac{(q_1+q_2)(1-q_1)(1-q_2)(1-\cos(\varphi_1-\varphi_2))}{[2-(q_1+q_2)]\{[1-(q_1+q_2)]+(q_1^2+q_2^2+q_1q_2)\}+[q_2-q_1-q_2(q_1+q_2)]\cos\varphi_1+[q_1-q_2-q_1(q_1+q_2)]\cos\varphi_2-[1-(q_1+q_2)]\cos(\varphi_1+\varphi_2)+q_1q_2\cos(\varphi_1-\varphi_2)]}.$$

Passando quindi all'analisi, nel caso presente, delle condizioni per cui la (A.5) (Nota I) non converge, e quindi la (7) non è più valida, osserviamo che l'espressione (vedi (A.18) Nota I):

$$\mathrm{Det}\,(\boldsymbol{E}-\boldsymbol{Q}) = 1-[1-(q_1+q_2)]\cdot$$

$$\cdot\exp[-i(\varphi_1+\varphi_2)]-q_1\exp[-i\varphi_1]-q_2\exp[-i\varphi_2],$$

si annulla per una delle quattro seguenti combinazioni di valori dei parametri di probabilità e del vettore reciproco:

$$(8)\qquad \begin{cases} \alpha)\ \varphi_1=2\pi n; & \varphi_2=2\pi m\ (n \text{ ed } m \text{ interi};\ q_1 \text{ e } q_2 \text{ qualunque});\\ \beta)\ q_1=1; & \varphi_1=2\pi n\ (n \text{ intero})\ (q_2 \text{ e } \varphi_2 \text{ qualunque});\\ \gamma)\ q_2=1; & \varphi_2=2\pi n\ (n \text{ intero})\ (q_1 \text{ e } \varphi_1 \text{ qualunque});\\ \delta)\ q_1=q_2=0; & \varphi_1+\varphi_2=2\pi n\ (n \text{ intero}). \end{cases}$$

Le ultime tre combinazioni parametriche caratterizzano strutture tridimensionalmente regolari e valori di $\boldsymbol{S}$ in corrispondenza dei quali si hanno le riflessioni nette secondo Bragg. La seconda e la terza combinazione parametrica caratterizzano strutture in cui tutti gli strati si succedono sempre rispettivamente secondo la traslazione $\boldsymbol{t}_1$ o la traslazione $\boldsymbol{t}_2$; la quarta caratterizza una struttura in cui ad ogni traslazione $\boldsymbol{t}_1$ succede $\boldsymbol{t}_2$ e viceversa. La prima relazione definisce una struttura regolare solo nel caso banale in cui $\varphi_1 \equiv \varphi_2$ (per ogni valore di $\boldsymbol{S}$); in tal caso si avrebbe $\boldsymbol{t}_1=\boldsymbol{t}_2=\boldsymbol{t}$. Altrimenti,

anche nel caso più generale, la α) dell'espressione (8) ci dice che si otterranno sempre riflessioni nette (tipo Bragg) lungo tutte le rette dello spazio reciproco caratterizzate dalle relazioni indicate, che possono vettorialmente così rappresentarsi:

$$(8') \qquad \boldsymbol{t}_1 \times \boldsymbol{S} = n; \qquad \boldsymbol{t}_2 \times \boldsymbol{S} = m\,.$$

Facciamo rilevare a questo proposito una proprietà del tutto generale dell'espressione di I_{Av} ottenibile secondo la presente teoria per qualsivoglia tipo di struttura generalmente statistica: nei casi limite in cui i parametri di probabilità assumano i valori caratteristici di strutture tridimensionalmente regolari, il numeratore di I_{Av} si annulla; per i valori di $\boldsymbol{S}$ corrispondenti alle riflessioni di Bragg, I_{Av} assume tuttavia la forma indeterminata (0/0) e con un procedimento al limite si riconosce facilmente che questo rapporto tende all'infinito. Tale proprietà, perfettamente in accordo con la teoria generale della diffrazione da parte di un cristallo infinitamente grande, è ben rilevabile nel terzo membro della (7) dove i quattro termini che compongono il numeratore, eventualmente nulli, corrispondono alle quattro possibili strutture regolari esaminate.

In particolare, possiamo facilmente applicare la (7) al caso già studiato [1,2] di strutture a strati a simmetria trigonale o esagonale che possono succedersi con $s = 2$, secondo le due traslazioni equivalenti,

$$(9) \qquad \begin{cases} \boldsymbol{t}_1 = \frac{1}{3}\boldsymbol{a} + \frac{2}{3}\boldsymbol{b} + \boldsymbol{c} \\ \\ \boldsymbol{t}_2 = \frac{2}{3}\boldsymbol{a} + \frac{1}{3}\boldsymbol{b} + \boldsymbol{c} \end{cases} \qquad \begin{array}{l} (\boldsymbol{a} \text{ e } \boldsymbol{b} \text{ sono i vettori di ripetizione del} \\ \text{reticolo piano; } \boldsymbol{c} \text{ il vettore distanza sup-} \\ \text{posta costante, tra gli strati).} \end{array}$$

A causa della simmetria, potremo porre:

$$(10) \qquad q_1 = q_2 = (1 - \alpha); \qquad (1 - q_1) = (1 - q_2) = \alpha\,.$$

Potremo ora applicare la relazione (7) quando si abbia $\alpha \neq 0$ e $\neq 1$ (si avrebbero in caso contrario strutture ordinate), a meno che siano verificate le relazioni (8'). Queste nel caso presente divengono:

$$(8'') \qquad \begin{cases} h - k = 3r, \qquad l = s \ (r \text{ ed } s \text{ interi}), \\ \\ (h \text{ (intero)} = \boldsymbol{a} \times \boldsymbol{S};\ k \text{ (intero)} = \boldsymbol{b} \times \boldsymbol{S};\ l \text{ (continuo in generale)} = \boldsymbol{c} \times \boldsymbol{S}). \end{cases}$$

Queste relazioni caratterizzano i punti del reticolo reciproco in cui la radiazione diffratta presenta i picchi infinitamente concentrati secondo Bragg.

Per $h - k = 3r \pm 1$ la radiazione diffratta presenterà andamento continuo lungo l (la (A.5') di Nota I risulterà convergente), e sarà applicabile la (7),

dove $\varphi_1 = 2\pi(n + l \pm \frac{1}{3})$ e $\varphi_2 = 2\pi(m + l \mp \frac{1}{3})$:

$$(7') \quad I_{Av} = VV^* \frac{3\alpha(1-\alpha)}{(3 - 6\alpha + 5\alpha^2) + 4(1-\alpha)^2 \cos 2\pi l + 2(1-2\alpha)\cos 2\pi 2l}.$$

Questa formula equivale in modo esatto alle più involute formule ricavate da Wilson (formula (14), [1] pag. 281) e di Hendricks e Teller (formula (34), [2] pag. 166).

2. – Il calcolo dell'intensità media diffratta da parte di una struttura costituita da strati, a simmetria trigonale o esagonale, dello stesso tipo, che si possono succedere, con $s=2$, secondo le tre diverse traslazioni: $\boldsymbol{t}_0 = \boldsymbol{c}$; $\boldsymbol{t}_1 = \frac{1}{3}\boldsymbol{a} + \frac{2}{3}\boldsymbol{b} + \boldsymbol{c}$; $\boldsymbol{t}_2 = \frac{2}{3}\boldsymbol{a} + \frac{1}{3}\boldsymbol{b} + \boldsymbol{c}$ ($\boldsymbol{a}$ e $\boldsymbol{b}$ essendo i vettori di ripetizione della cella piana esagonale; $\boldsymbol{c}$ essendo il vettore che rappresenta la distanza, supposta costante, fra gli strati; $\boldsymbol{t}_1$ e $\boldsymbol{t}_2$ siano simmetricamente equivalenti).

Questo modello di successione statistica ha avuto per noi particolare interesse per essere stato applicato alla struttura della modificazione α del $TiCl_3$; è stato inoltre applicato da F. Halla, H. Jagodzinski e W. R. Ruston [7] al disordine monodimensionale presente in alcuni tipi cristallini di dodecaidrotrifenilene. La simmetria impone che siano egualmente probabili le successioni (01) e (02); (10) e (20); (12) e (21); (11) e (22). Se aggiungiamo a queste le condizioni di normalizzazione per le probabilità di successione p_{ij}: $\sum_{j=0}^{2} p_{ij} = 1$, possiamo descrivere l'intero complesso dei parametri, di probabilità con i tre soli parametri: $p_{00} = a$; $p_{11} = p_{22} = b$; $p_{12} = p_{21} = c$, e la matrice $\boldsymbol{Q}$ diviene:

$$\boldsymbol{Q} = \begin{vmatrix} a\exp[-2\pi i l] & \frac{1-a}{2}\exp[-2\pi i](\frac{1}{3}h + \frac{2}{3}k + l) & \frac{1-a}{2}\exp[-2\pi i(\frac{2}{3}h + \frac{1}{3}k + l)] \\ [1-(b+c)]\exp[-2\pi i l] & b\exp[-2\pi i](\frac{1}{3}h + \frac{2}{3}k + l) & c\exp[-2\pi i](\frac{2}{3}h + \frac{1}{3}k + l) \\ [1-(b+c)]\exp[-2\pi i l] & c\exp[-2\pi i(\frac{1}{3}h + \frac{2}{3}k + l)] & b\exp[-2\pi i](\frac{2}{3}h + \frac{1}{3}k + l) \end{vmatrix}$$

(h e k interi, l continuo in generale).

La soluzione del sistema (10) (I) conduce in questo caso ai seguenti valori

---

[7] F. Halla, H. Jagodzinski e W. R. Ruston: *Acta Cryst.*, 6, 478 (1953).

per le frequenze di comparizione f_i:

$$(12) \qquad f_0 = \frac{1-b-c}{2-(a+b+c)}; \qquad f_1 = f_2 = \frac{1-a}{2[2-(a+b+c)]}.$$

Usando per brevità i simboli: $\eta = \frac{1}{3}h + \frac{2}{3}k$; $\theta = \frac{2}{3}h + \frac{1}{3}k$, il determinante della matrice $(\boldsymbol{E} - \boldsymbol{Q})$ vale:

$$(13) \quad \mathrm{Det}\,(\boldsymbol{E}-\boldsymbol{Q}) = 1 + \exp[-2\pi i l]\Big[-a - b\big(\exp[-2\pi i\eta] + \exp[-2\pi i\theta)\big] +$$

$$+ \exp[-2\pi i 2l]\Big[(b^2-c^2) + \Big(ab + \tfrac{1}{2}(1-a)(b+c-1)\Big)(\exp[-2\pi i\eta] +$$

$$+ \exp[-2\pi i\theta])\Big] + \exp[-2\pi i 3l](b-c)[1-(a+b+c)]\,.$$

La (13) si annulla per le seguenti combinazioni di valori dei parametri e del vettore reciproco:

$$(14) \quad \begin{cases} \alpha)\ h-k = 3n \ (n \text{ intero}) \text{ ed } l \text{ intero } (a,\ b \text{ e } c \text{ qualunque}); \\ \beta)\ a = 1, \quad l = n \ (h,\ k,\ b \text{ e } c \text{ qualunque}); \\ \gamma)\ b = 0, \quad c = 1, \qquad l = \dfrac{n}{2} \quad (h,\ k \text{ e } a \text{ qualunque}), \\ \delta)\ b = 1, \quad c = 0, \qquad h-k+3l = 3n \ (a \text{ qualunque}). \end{cases}$$

Le condizioni α) caratterizzano, come nel caso precedente, una famiglia di rette del reticolo reciproco lungo le quali la radiazione diffratta presenta l'interferenza di Bragg, sia che la struttura si presenti statistica o no; le condizioni β), γ) e δ) caratterizzano strutture regolari, la prima a strati tutti sovrapposti lungo $\boldsymbol{c}$, la seconda a strati che si sovrappongono ogni due, (*ABABAB*... indicando con *A*, *B* e *C* strati occupanti posizioni non sovrapposte lungo $\boldsymbol{c}$); la terza a strati che si sovrappongono ogni tre (*ABCABCABC*...).

Nel caso che $h-k \neq 3n$, e per combinazioni di valori dei parametri di probabilità diverse dalla β), γ) e δ), la (A.15′) della I diviene nel caso presente, dopo alcune semplificazioni e ponendo per semplicità: $p = 1-(a+b+c)$ $q = 1-a$; $r = 1+(b-c)$:

$$(15) \qquad I_{ss} = VV^* \frac{\frac{2}{9}q(1+p)(1+p-q)(1+(r-1)\cos 2\pi l] + \frac{2}{9}qr(r-2)[(3q(p-1)+2(1-2p^2))-6p\cos 2\pi l]}{(1+p)\{1+\frac{1}{9}[(3q-p+r-3)e^{-2\pi i l}+\frac{1}{9}[r(-2p+3q-1)+3p-3q+1]e^{-4\pi i l}+p(r-1)e^{-6\pi i l}\}\{\text{compl. con.}\}}.$$

Com'è da attendersi, I_{Av} si annulla in generale per $a = 1$ $(q = 0)$; $b = 0$, $c = 1$ $(r = 0,\ q = 1 + p)$; $b = 1$, $c = 0$ $(r = 2,\ q = 1 + p)$.

Si può inoltre rilevare come, ponendo $c = \alpha$, $b = 1 - \alpha$ e $a = 0$ (cioè $p = 0$, $q = 1$, $r = 2\alpha$), il modello attuale comprenda quello studiato nell'ultima parte del paragrafo precedente; si ottiene infatti dalla (15) ancora la (7′).

3. – Il calcolo dell'intensità diffratta da parte di una struttura costituita da strati a simmetria trigonale o esagonale dello stesso tipo, che si possano succedere, con $s = 3$, secondo le due traslazioni equivalenti: $\boldsymbol{t}_1 = \frac{1}{3}\boldsymbol{a} + \frac{2}{3}\boldsymbol{b} + \boldsymbol{c}$; $\boldsymbol{t}_2 = \frac{2}{3}\boldsymbol{a} + \frac{1}{3}\boldsymbol{b} + \boldsymbol{c}$.

Il modello ora proposto può trovare applicazione, in particolare, nello studio di diverse strutture metalliche monodimensionalmente disordinate o difettose, e in altri casi di strutture statistiche a strati esagonali, quali, tipicamente, certe modificazioni di carburo di silicio [8] e suoi derivati [9].

Data la simmetria esagonale la matrice quadrata delle probabilità di successione $|p_{uu'}|$ (dove u e u' possono corrispondere alle quattro coppie di indici di traslazione: 11, 12, 21 e 22) è la seguente:

$$
(16) \qquad |p_{uu'}| = \begin{array}{c|cccc} & (11) & (12) & (21) & (22) \\ (11) & 1-\sigma & \sigma & 0 & 0 \\ (12) & 0 & 0 & 1-\tau & \tau \\ (21) & \tau & 1-\tau & 0 & 0 \\ (22) & 0 & 0 & \sigma & 1-\sigma \end{array} ,
$$

avendo indicato con σ la probabilità che ad una successione di tipo romboedrico di 2 traslazioni adiacenti $(\boldsymbol{t}_1\boldsymbol{t}_1)$ o $(\boldsymbol{t}_2\boldsymbol{t}_2)$ segua una successione che denomineremo di tipo esagonale (rispettivamente $\boldsymbol{t}_1\boldsymbol{t}_2$ o $\boldsymbol{t}_2\boldsymbol{t}_1$), e con τ la probabilità che, inversamente, ad una successione di tipo esagonale segua una successione di tipo romboedrico. $(1 - \sigma)$ e $(1 - \tau)$ sono evidentemente le probabilità di sequenza rispettivamente romboedrica-romboedrica ed esagonale-esagonale; tutti gli altri accoppiamenti di indici u e u' sono fisicamente non significativi, e le corrispondenti probabilità sono poste eguali a 0 (vedi I a pag. 796).

---

[8] H. JAGODZINSKI: *Acta Cryst.*, 7, 300 (1954).

[9] R. GEVERS: *Acta Cryst.*, 7, 337 (1954).

La risoluzione del sistema (A.22) (I) rispetto alle frequenze di comparizione delle possibili successioni di $(s-1)$ traslazioni conduce alla seguente soluzione:

$$f_{11} = f_{22} = \frac{\tau}{2(\sigma+\tau)}\,; \quad f_{12} = f_{21} = \frac{\sigma}{2(\sigma+\tau)}\,. \tag{17}$$

La matrice $\boldsymbol{Q}'$ assume in questo caso la forma:

$$\boldsymbol{Q}' = \begin{vmatrix} (1-\sigma)\,e^{-2\pi i(\eta+l)} & \sigma\,e^{-2\pi i(\theta+l)} & 0 & 0 \\ 0 & 0 & (1-\tau)\,e^{-2\pi i(\eta+l)} & \tau\,e^{-2\pi i(\theta+l)} \\ \tau\,e^{-2\pi i(\eta+l)} & (1-\tau)\,e^{-2\pi i(\theta+l)} & 0 & 0 \\ 0 & 0 & \sigma\,e^{-2\pi i(\eta+l)} & (1-\sigma)\,e^{-2\pi i(\theta+l)} \end{vmatrix} \tag{18}$$

$$(\eta = \tfrac{1}{3}h + \tfrac{2}{3}k\,, \quad \theta = \tfrac{2}{3}h + \tfrac{1}{3}k)\,.$$

e il determinante della matrice $(\boldsymbol{E}-\boldsymbol{Q}')$ risulta:

$$\begin{aligned} \text{Det}\,(\boldsymbol{E}-\boldsymbol{Q}') = {} & 1-(1-\sigma)(\exp[-2\pi i\eta] + \exp[-2\pi i\theta])\exp[-2\pi il] + \\ & + [(1-\sigma)^2 - (1-\tau)^2]\exp[-2\pi i 2l] + (1-\tau)(1-\sigma-\tau)\cdot \\ & \cdot(\exp[-2\pi i\eta] + \exp[-2\pi i\theta])\exp[-2\pi i 3l] - (1-\sigma-\tau)^2\exp[-2\pi i 4l]\,. \end{aligned} \tag{19}$$

Le condizioni di annullamento della (19) sono fornite dalle relazioni seguenti:

$$\begin{cases} \alpha)\ h-k = 3n,\ l \text{ intero } (\sigma \text{ e } \tau \text{ qualsiasi}); \\ \beta)\ \sigma = 0;\ \ h-k+3l = 3n; \\ \gamma)\ \tau = 0\,,\ l = \dfrac{n}{2}\ (h,\ k \text{ e } \sigma \text{ qualsiasi})\,; \\ \delta)\ \sigma = 1\,,\ \tau = 1\,,\ l = \dfrac{n}{4}\ (h \text{ e } k \text{ qualsiasi})\,. \end{cases} \tag{20}$$

Delle condizioni $\alpha)$, già riscontrate analogamente nelle Sezioni **1** e **2**, non diremo più oltre. Le condizioni $\beta)$, analoghe alle $\delta)$ della Sezione **2**, caratterizzano una struttura ordinata di tipo romboedrico, così come le condizioni $\gamma)$

corrispondono alle γ) della precedente sezione caratterizzando una struttura ordinata di tipo esagonale. Infine, le condizioni δ) corrispondono ad una struttura ordinata caratterizzata dalla successione di traslazioni ($\boldsymbol{t}_1\boldsymbol{t}_1\boldsymbol{t}_2\boldsymbol{t}_2\boldsymbol{t}_1\boldsymbol{t}_1\boldsymbol{t}_2\boldsymbol{t}_2$...), ovvero, con riferimento alle successioni di strati in posizioni definite, dalla successione ($ABCBABCBA$...). Quando le condizioni di convergenza siano soddisfatte, in particolare $h - k \neq 3n$, la (28′) della I diviene nel caso presente:

$$) \quad I_{Av} = VV^* \cdot$$

$$3\sigma\tau(2-\sigma-\tau)\{[1+(1-\sigma-\tau)^2]+(1-\sigma-\tau)\cos 2\pi l\}$$

$$\{1+(1-\sigma)^2+(2-\sigma-\tau)^2(\sigma-\tau)^2+(1-\tau)^2(1-\sigma-\tau)^2+(1-\sigma-\tau)^4\}+$$

$$2\{(1-\sigma)+(1-\sigma)(2-\sigma-\tau)(\tau-\sigma)+(2-\sigma-\tau)(\tau-\sigma)(1-\tau)(\sigma+\tau-1)-(1-\tau)(\sigma+\tau-1)^3\}\cos 2\pi l+$$

$$2\{(2-\sigma-\tau)^2(\tau^2-\sigma^2)+(1-\tau)(1-\sigma)(\sigma+\tau-1)\}\cos 2\pi 2l+$$

$$2(\sigma+\tau-1)[1-\tau-(1-\sigma)(\sigma+\tau-1)]\cos 2\pi 3l-$$

$$2(\sigma+\tau-1)^2\cos 2\pi 4l\,.$$

Il numeratore a secondo membro della (21) si annulla identicamente per: $\sigma = 0$; $\tau = 0$; $\sigma = \tau = 1$ (cfr. le osservazioni svolte a pag. 664. Anche il modello statistico presente comprende quello studiato al termine del primo paragrafo; quando infatti si ponga nella (21):

$$\sigma = 1 - \tau = \alpha$$

si ottiene immediatamente la formula (7′).

4. – Il calcolo dell'intensità diffratta da parte di una struttura costituita da strati eguali aventi simmetria trigonale che si succedono statisticamente con $s = 1$ secondo le tre possibili traslazioni: $\boldsymbol{t}_0 = \boldsymbol{c}$; $\boldsymbol{t}_1 = \frac{1}{3}\boldsymbol{a} + \frac{2}{3}\boldsymbol{b} + \boldsymbol{c}$; $\boldsymbol{t}_2 = \frac{2}{3}\boldsymbol{a} + \frac{1}{3}\boldsymbol{b} + \boldsymbol{c}$. Si ammette che ogni strato possa essere generato dal precedente, oltre che per traslazione semplice, anche per traslazione e rotazione di $(2n+1)(\pi/3)$ (n intero) attorno ad un asse passante per l'origine dello strato ed ortogonale ad esso.

Questo modello statistico è stato da noi introdotto nello studio di una modificazione disordinata (forma δ) del tricloruro di titanio. Pur essendo gli strati tutti eguali, dovremo considerare di tipo diverso, giusta la definizione data all'inizio della I, gli strati aventi i rispettivi vettori $\boldsymbol{a}$ e $\boldsymbol{b}$ paralleli

tra loro e quelli i cui vettori corrispondenti si possono ritenere ottenuti dai precedenti per rotazione di $\pm 60°$ (o multipli dispari di questi angoli). Indicheremo con $V(1)$ e $V(2)$ i fattori di struttura dei due tipi di strati, riferiti a terne intrinseche agli strati stessi e parallele tra loro, e applicheremo a questo caso la teoria sviluppata nella Sezione (B.1) della Nota I. Semplici considerazioni dedotte dalla simmetria ternaria di ogni strato portano alla conclusione che i parametri indipendenti di probabilità di successione tra i due tipi di strati secondo le diverse possibili traslazioni sono cinque; il quadro complessivo di tali parametri si presenta come segue:

(22)

tipo di strato di partenza	tipo di strato successivo	vettore di traslazione	probabilità che abbia luogo la successione
(1)	(1)	$\boldsymbol{t}_0$	p_0
	(1)	$\boldsymbol{t}_1$	p_1
	(1)	$\boldsymbol{t}_2$	p_2
	(2)	$\boldsymbol{t}_0$	p_0'
	(2)	$\boldsymbol{t}_1$	p_1'
	(2)	$\boldsymbol{t}_2$	p_2'
(2)	(2)	$\boldsymbol{t}_0$	p_0
	(2)	$\boldsymbol{t}_1$	p_2
	(2)	$\boldsymbol{t}_2$	p_1
	(1)	$\boldsymbol{t}_0$	p_0'
	(1)	$\boldsymbol{t}_1$	p_2'
	(1)	$\boldsymbol{t}_2$	p_1'

Inoltre si deve avere:

$$p_0 + p_1 + p_2 + p_0' + p_1' + p_2' = 1 \,. \tag{23}$$

La risoluzione del sistema (B.2) porta ai seguenti ovvii valori delle frequenze di comparizione dei due tipi di strati:

$$f(1) = f(2) = \tfrac{1}{2} \,.$$

La matrice quadrata del secondo ordine $\boldsymbol{Q}$ (vedi la (5) della Sezione (B.1)

della I) è costituita in questo caso dai seguenti elementi:

$$
(24)\quad \begin{cases}
Q_{11}=p_0\exp[-2\pi i l]+p_1\exp[-2\pi i(\frac{1}{3}h+\frac{2}{3}k+l)]+p_2\exp[-2\pi i(\frac{2}{3}h+\frac{1}{3}k+l)]= \\
\qquad = \exp[-2\pi i l](p_0+p_1\exp[-2\pi i\eta]+p_2\exp[-2\pi i\theta]), \\
Q_{12}=\exp[-2\pi i l](p_0'+p_1'\exp[-2\pi i\eta]+p_2'\exp[-2\pi i\theta]), \\
Q_{21}=\exp[-2\pi i l](p_0'+p_1'\exp[-2\pi i\theta]+p_2'\exp[-2\pi i\eta]); \\
Q_{22}=\exp[-2\pi i l](p_0+p_1\exp[-2\pi i\theta]+p_2\exp[-2\pi i\eta]);
\end{cases}
$$

avendo posto, come in casi precedenti, $\eta=\frac{1}{3}h+\frac{2}{3}k$, $\theta=\frac{2}{3}h+\frac{1}{3}k$.

Poichè risulta che $\exp[-2\pi i\eta]=\exp[+2\pi i\theta]$, le grandezze complesse Q_{11} e Q_{22} e rispettivamente Q_{12} e Q_{21} risultano tra loro coniugate. Potremo quindi porre:

$$
(25)\quad \begin{cases}
p_0+p_1\exp[-2\pi i\eta]+p_2\exp[-2\pi i\theta] = A\exp[-i\alpha]; & (A \text{ numero reale}) \\
p_0+p_1\exp[-2\pi i\theta]+p_2\exp[-2\pi i\eta] = A\exp[+i\alpha]; & \\
p_0'+p_1'\exp[-2\pi i\eta]+p_2'\exp[-2\pi i\theta] = B\exp[-i\beta]; & (B \text{ numero reale}) \\
p_0'+p_1'\exp[-2\pi i\theta]+p_2'\exp[-2\pi i\eta] = B\exp[+i\beta]. &
\end{cases}
$$

Il determinante della matrice $(\boldsymbol{E}-\boldsymbol{Q})$ assume il valore:

$$
(26)\quad \mathrm{Det}\,(\boldsymbol{E}-\boldsymbol{Q})=1-2A\cos\alpha\exp[-2\pi i l]+(A^2-B^2)\exp[-2\pi i 2l].
$$

Le condizioni di annullamento della (26) sono le seguenti:

$$
(27)\quad \begin{cases}
\alpha)\ h-k=3n \text{ (intero) } (\eta=m,\ \theta=p,\ m \text{ e } p \text{ interi) e } l=r \text{ (intero)}; & \\
\beta)\quad h-k\neq 3n; \quad p_0'=1; \quad l=\dfrac{n}{2} & (n \text{ intero}); \\
\gamma)\quad h-k\neq 3n; \quad p_1'=1; \quad l=\dfrac{n}{2} & (n \text{ intero}); \\
\delta)\quad h-k\neq 3n; \quad p_2'=1; \quad l=\dfrac{n}{2} & (n \text{ intero}); \\
\varepsilon)\quad h-k\neq 3n; \quad p_0=1; \quad l=n & (n \text{ intero}); \\
\theta)\quad h-k\neq 3n; \quad p_1=1; \quad l=n\pm\frac{1}{3} & (n \text{ intero}); \\
\eta)\quad h-k\neq 3n; \quad p_2=1; \quad l=n\pm\frac{1}{3} & (n \text{ intero}).
\end{cases}
$$

A parte le condizioni α), che abbiamo già ritrovato nei casi precedentemente trattati, tutte le successive caratterizzano strutture ordinate che è facile identificare. Per $h - k \neq 3n$ e tutti i coefficienti di probabilità diversi da 1, l'espressione (B.12) della I per $I_{\Lambda\nu}$ diviene:

$$(28)\quad I_{\Lambda\nu} = \frac{(V(1)V(1)^* + V(2)V(2)^*)[1-(A^2-B^2)^2] - 2A(1-A^2+B^2)[V(1)V(1)^*\cos(2\pi l-\alpha) + V(2)V(2)^*\cos(2\pi l+\alpha)] + 2(V(1)V(2)^* + V(2)V(1)^*)B\cos\beta[(1+A^2-B^2)\cos 2\pi l - 2A\cos\alpha]}{2\{[1+(A^2-B^2)^2+4A^2\cos^2\alpha] - 4A(1+A^2-B^2)\cos\alpha\cos 2\pi l + 2(A^2-B^2)\cos 2\pi 2l\}}$$

Qualora uno qualunque dei parametri di probabilità venga posto eguale ad uno, deve essere necessariamente:

$$A = 0 \quad \text{e} \quad B = 1; \quad \text{ovvero} \quad A = 1 \quad \text{e} \quad B = 0\,.$$

In queste condizioni, come è da attendersi (vedi pag. 664) il numeratore della (28) si annulla identicamente.

Facciamo infine rilevare come, secondo la trattazione di HENDRICKS e TELLER [2], il presente problema statistico avrebbe potuto trovare risoluzione solo mediante la diagonalizzazione di una matrice quadrata del 6° ordine. 6 sono infatti i tipi di strati diversi per posizione assoluta, che potremo indicare con A B e C (tipi di strati paralleli tra loro e aventi l'origine in $(0\ 0.\ c)$, $(\frac{1}{3}, \frac{2}{3}, c)$ e $(\frac{2}{3}, \frac{1}{3}, c)$) e con A', B' e C' (corrispondenti ai precedenti e ruotati di 60°).

SUMMARY

In this second note, according to the theory precedingly developed, we give some examples of calculation of the X-ray mean diffracted intensity by some hypothetical structures, either constituted by one-type layers or by different-type layers, showing monodimensional disorder. We will also suppose that the range of influence of probabilistic succession (s) is variable between 1 and 3.

IL NUOVO CIMENTO Vol. XXII, N. 4 16 Novembre 1961

Conformal Invariance of Massless Dirac-Like Wave Equations.

J. S. Lomont

Polytechnic Institute of Brooklyn - Brooklyn, N. Y.

(ricevuto il 19 Luglio 1961)

Summary. — It is shown that all Dirac-like wave equations with positive integral or half-integral spin, zero rest mass, and no interaction are conformally invariant. The transformation of Ψ under the conformal group, and the associated conservation laws are given in a very simple form.

1. – Introduction.

Conformal transformations were introduced into physics via electromagnetic theory by Bôcher [1], Bateman [2], and Cunningham [3], the latter two of whom showed that the Maxwell equations without sources are conformally invariant. The conformal invariance of the Maxwell equations was then used by Bessel-Hagen [4] in conjunction with Noether's theorem [5] to obtain some new conservation laws. It was subsequently shown by McLennan [6,7] that conformal invariance is a property shared by practically all massless, relativistic wave equations without interaction. Consequently, massless wave equations in general have conservation laws other than the usual relativistic conservation laws.

McLennan proved the conformal invariance of Gårding's [8] very general

---

[1] M. Bôcher: *Über die Reihenentwicklungen der Potentialtheorie* (Leipzig, 1894).
[2] H. Bateman: *Proc. London Math. Soc.*, **7**, 70 (1909); **8**, 223, 469 (1910).
[3] E. Cunningham: *Proc. London Math. Soc.*, **8**, 77 (1910).
[4] E. Bessel-Hagen: *Math. Ann.*, **84**, 258 (1921).
[5] E. Noether: *Nachr. Akad. Wiss. Göttingen, Math. Phys. Kl.*, 235 (1918).
[6] J. A. McLennan jr.: *On the invariance properties and conservation laws for relativistic wave equations, particularly for zero rest mass*, Diss. (Lehigh University, 1952).
[7] J. A. McLennan: *Nuovo Cimento*, **3**, 1360 (1956).
[8] L. Gårding: *Proc. Cambr. Phil. Soc.*, **41**, 49 (1945).

class of massless wave equations. Because of the generality of McLennan's analysis, however, the results were rather complicated.

The purpose of the present work is to consider a more restricted class of massless, relativistic wave equations, the so-called Diraclike wave equations [9], and obtain the transformation laws and conservation laws in a very simple form. For these equations the discussion becomes relatively transparent.

For convenience a number of other papers dealing with conformal transformations in physics are listed [10].

2. – Preliminaries.

It was shown in (L) that for every integral and half-integral spin $s > 0$ there is a unique $4s$-dimensional wave equations of the form [11]

$$\alpha^\mu \nabla_\mu \Psi = 0 \,, \tag{2.1}$$

where

$$\alpha^0 = I \,, \tag{2.2}$$

$$\alpha_1^2 = \alpha_2^2 = \alpha_3^2 = 1 \,, \tag{2.3}$$

$$\alpha_1 \alpha_2 = i\alpha_3 \qquad \text{(cycl. 1, 2, 3)} \,, \tag{2.4}$$

$$[\alpha_1, \alpha_2]_+ = 0 \qquad \text{(cycl. 1, 2, 3)} \,, \tag{2.5}$$

$$\alpha_\mu^\dagger = \alpha_\mu \,, \tag{2.6}$$

[9] J. S. Lomont: *Phys. Rev.*, **111**, 1710 (1958); hereafter referred to as (L).

[10] H. Weyl: *Sitzungsber. d. Preuss. Akad. d. Wiss.*, 265 (1918); H. Weyl: *Space, Time, and Matter*, pp. 285, 324; P. A. M. Dirac: *Ann. of Math.*, **37**, 429 (1936); H. J. Bhabha: *Proc. Cambr. Phil. Soc.*, **32**, 622 (1936); J. A. Schouten and J. Haantjes: *Proc. Kon. Akad. v. Wet.*, **39**, 1059 (1936); W. Pauli: *Helv. Phys. Acta*, **13**, 204 (1940); J. Haantjes: *Proc. Kon. Akad. v. Wet.*, **43**, 1288 (1940); J. A. Schouten: *Rev. Mod. Phys.*, **21**, 421 (1949); R. L. Ingraham: *Proc. Kon. Akad. v. Wet.*, **54**, 315 (1951); E. L. Hill: *Phys. Rev.*, **84**, 1165 (1951); I. E. Segal: *Duke Math. Journ.*, **18**, 221 (1951); W. Brittin: *Phys. Rev.*, **87**, 898 (1952); R. L. Ingraham: *Proc. Nat. Acad. Sci. U.S.A.*, **38**, 921 (1952); *Nuovo Cimento*, **9**, 886 (1952); **10**, 27 (1953); B. Hoffmann: *Phys. Rev.*, **89**, 49, 53 (1953); F. Bopp: *Proc. Int. Conf. Theor. Phys.* (Kyoto and Tokyo, 1953), pp. 289, 295; R. L. Ingraham: *Proc. Nat. Acad. Sci. U.S.A.*, **40**, 237 (1954); Y. Murai: *Progr. Theor. Phys.*, **11**, 441 (1954); R. L. Ingraham: *Nuovo Cimento*, **12**, 825 (1954); **1**, 82 (1955); A. Popovici: *Com. Acad. R. P. Romine*, **8**, 877 (1958); **9**, 671 (1959); *Rev. Math. Pures Appl.*, **4**, 577 (1959); V. I. Ogievetski and I. V. Polubarinov: *Sov. Phys. JETP*, **10**, 335 (1960); F. Calogero: *Nuovo Cimento*, **20**, 297 (1961).

[11] We take $c = \hbar = 1$, $-g_{00} = g_{11} = g_{22} = g_{33} = 1$, $x^0 = t$, $x^1 = x$, $x^2 = y$, $x^3 = z$, $\nabla_\mu = (\partial/\partial x)\mu$, I = unit matrix, † means adjoint. Greek indices run from 0 to 3, Latin indices from 1 to 3.

and when the α's have the correct form the last $2s-1$ components of Ψ are zero ([12]). Under the Lorentz transformation

$$\delta x^{\lambda} = \omega^{\lambda\mu} x_{\mu} , \tag{2.7}$$

where the parameters $\omega^{\lambda\mu}$ satisfy

$$\omega^{\lambda\mu} = -\omega^{\mu\lambda} , \tag{2.8}$$

Ψ transforms according to the equation

$$\delta\Psi = -\tfrac{1}{2}\omega^{\mu\nu} K_{\mu\nu}\Psi . \tag{2.9}$$

The $4s\times 4s$ matrices $K_{\mu\nu}$ satisfy the following relations

$$K_{\mu\nu} = -K_{\nu\mu} , \tag{2.10}$$

$$[K_{\varkappa\lambda}, K_{\mu\nu}] = -g_{\lambda\mu}K_{\varkappa\nu} + g_{\lambda\nu}K_{\varkappa\mu} + g_{\varkappa\mu}K_{\lambda\nu} - g_{\varkappa\nu}K_{\lambda\mu} , \tag{2.11}$$

$$[\alpha_{\lambda}, K_{\mu\nu}] = \alpha_{\mu}(g_{\nu\lambda} + g_{\nu 0}\alpha_{\lambda}) - \alpha_{\nu}(g_{\mu\lambda} + g_{\mu 0}\alpha_{\lambda}) . \tag{2.12}$$

If we let

$$\boldsymbol{K} \equiv (K_{23}, K_{31}, K_{12}) , \tag{2.13}$$

$$\boldsymbol{\varkappa} \equiv (K_{01}, K_{02}, K_{03}) , \tag{2.14}$$

then (see (L) eqs. (9.5), (9.6))

$$\boldsymbol{K} = i\boldsymbol{\varkappa} , \tag{2.15}$$

$$\boldsymbol{K}^{\dagger} = -\boldsymbol{K} . \tag{2.16}$$

Let us always suppose α_{λ} and $K_{\mu\nu}$ to be chosen so that the last $2s-1$ components of Ψ are zero, and let P be the matrix which projects onto the top $2s+1$ components

$$P = \begin{pmatrix} I & 0 \\ 0 & 0 \end{pmatrix}, \tag{2.17}$$

where P is $4s$-dimensional and I is $(2s+1)$-dimensional. A relation which

([12]) See eq. (9.14)-(9.22) in (L).

was not proved in (L) but will be needed here is

$$\alpha^{\nu} K_{\mu\nu} P = (s-1)\alpha_{\mu} P \,. \tag{2.18}$$

This identity can be proved in a straightforward but tedious way by using the explicit forms of the matrices α_{λ} and $K_{\mu\nu}$ given in (L) (9.13)-(9.22).

3. – Conformal invariance.

The conformal group consists of the proper, orthochronous, inhomogeneous Lorentz transformations together with the linear scale transformations

$$x'_{\lambda} = e^{b} x_{\lambda} \,, \quad (\lambda = 0, 1, 2, 3) \ (b = \text{real constant}) \,, \tag{3.1}$$

and the non-linear transformations

$$x'_{\lambda} = \frac{x_{\lambda} - a_{\lambda} x^{\mu} x_{\mu}}{1 - 2a^{\mu} x_{\mu} + a^{\mu} a_{\mu} x_{\nu} x_{\nu}} \qquad (\lambda = 0, 1, 2, 3) \,, \tag{3.2}$$

a_{λ} = any real 4-tuple.

Thus the conformal group is a 15-parameter group. The corresponding infinitesimal transformations are

$$\delta x_{\lambda} = b x_{\lambda} \,, \tag{3.3}$$

$$\delta x_{\lambda} = 2a^{\mu} x_{\mu} x_{\lambda} - a_{\lambda} x^{\mu} x_{\mu} \,. \tag{3.4}$$

We will now define the transformation of Ψ under the infinitesimal coordinate transformations (3.3) and (3.4) in such a way that the wave eq. (2.1) is form-invariant. Under (3.3) we let

$$\delta \Psi = b' b \Psi \,, \tag{3.5}$$

where b' is any constant. Then since $\delta \nabla_{\mu} = - b \nabla_{\mu}$

$$\delta(\alpha^{\mu} \nabla_{\mu} \Psi) = \alpha^{\mu} (\delta \nabla_{\mu}) \Psi + \alpha^{\mu} \nabla_{\mu} \delta \Psi = - b \alpha^{\mu} \nabla_{\mu} \Psi + b' b \alpha^{\mu} \nabla_{\mu} \Psi = 0 \,. \tag{3.6}$$

The transformation of Ψ under (3.4) is somewhat more complicated, but still quite simple relative to McLennan's transformation law for the Gårding wave functions.

Under (3.4) we let

$$\delta\Psi = 2\{-(s+1)(a^\mu x_\mu) + a^\mu x^\nu K_{\mu\nu}\}\Psi\,. \tag{3.7}$$

Since

$$\delta\nabla_\lambda = -2a^\mu x_\mu \nabla_\lambda + 2x_\lambda a^\mu \nabla_\mu - 2a_\lambda x^\mu \nabla_\mu\,, \tag{3.8}$$

we have

$$\delta(\alpha^\lambda \nabla_\lambda \Psi) = \alpha^\lambda(\delta\nabla_\lambda)\Psi + \alpha^\lambda \nabla_\lambda(\delta\Psi) = -2(ax)(\alpha\nabla)\Psi + 2(\alpha x)(a\nabla)\Psi - \tag{3.9}$$
$$-2(a\alpha)(x\nabla)\Psi - 2(s+1)(\alpha\nabla)(ax\Psi + 2(\alpha\nabla)a^\mu x^\nu K_{\mu\nu}\Psi\,,$$

where the parentheses indicate the invariant inner product of the vectors. Substituting

$$(\alpha\nabla)(ax)\Psi = (a\alpha)\Psi + (ax)(\alpha\nabla)\Psi\,, \tag{3.10}$$

and

$$(\alpha\nabla)a^\mu x^\nu K_{\mu\nu}\Psi = a^\mu \alpha^\nu K_{\mu\nu}\Psi + (a\alpha)(x\nabla)\Psi - \tag{3.11}$$
$$-(x\alpha)(a\nabla)\Psi + \{a^\mu x^\nu K_{\mu\nu} + x_0(a\alpha) - a_0(x\alpha)\}(\alpha\nabla)\Psi\,,$$

into (3.9) we obtain

$$\delta\{(\alpha\nabla)\Psi\} = 2a^\mu\{\alpha^\nu K_{\mu\nu} - (s+1)\alpha_\mu\}\Psi + \tag{3.12}$$
$$+2\{a^\mu x^\nu K_{\mu\nu} + x_0(a\alpha) - a_0(x\alpha) - (s+2)(ax)\}(\alpha\nabla)\Psi\,.$$

Using the wave equation $(\alpha\nabla)\Psi = 0$ we have

$$\delta\{(\alpha\nabla)\Psi\} = 2a^\mu\{\alpha^\nu K_{\mu\nu} - (s+1)\alpha^\mu\}\Psi\,, \tag{3.13}$$

and using the identity (2.18) we have the desired result

$$\delta\{(\alpha\nabla)\Psi\} = 0\,. \tag{3.14}$$

4. – Conservation laws.

GOOD ([13]) has shown how conservation laws can be derived very simply from Dirac-like wave equations without recourse to Lagrangians and Noether's

([13]) R. H. GOOD jr.: *Phys. Rev.*, **105**, 1914 (1957).

theorem. Let $\Psi(x)$ satisfy the wave eq. (2.1) (*i.e.*, $(\alpha\nabla)\Psi = 0$), and under the coordinate transformation $x' = x'(x)$ let $\Psi'(x) = O\Psi(x)$, where O is a linear operator and $(\alpha\nabla')\Psi'(x') = 0$. Then, if we let $j_\mu = \Psi^\dagger \alpha_\mu O\ \Psi$ we have $\nabla^\mu j_\mu = 0$.

For the infinitesimal scale transformation (3.3) we have

$$O_b = -b(x\nabla) + bb' , \tag{4.1}$$

and for the infinitesimal non-linear transformation (3.4)

$$O_a = -\{2(ax)x^\lambda - x^2 a^\lambda\}\nabla_\lambda - 2(s+1)(ax) + 2a^\mu x^\nu K_{\mu\nu} . \tag{4.2}$$

Thus the quantities

$$j_b^\lambda = \Psi^\dagger \alpha^\lambda \{-b(x\nabla) + b'\}\Psi , \tag{4.3}$$

and

$$j_a^\lambda = \Psi^\dagger \alpha^\lambda \{-2(ax)(x\nabla) + x^2(a\nabla) - 2(s+1)(ax) + 2a^\mu x^\nu K_{\mu\nu}\}\Psi , \tag{4.4}$$

are divergenceless. The coefficients of the arbitrary real parameters b and a^λ must also be divergenceless. Hence, if

$$B_\lambda = \Psi^\dagger \alpha_\lambda (x\nabla)\Psi , \tag{4.4}$$

and

$$A_{\lambda\mu} = \Psi^\dagger \alpha_\lambda \{-2x_\mu (x\nabla) + x^2\nabla_\mu - 2(s+1)x_\mu + 2x^\nu K_{\mu\nu}\}\Psi ,$$

we have the five conservation laws

$$\nabla^\lambda B_\lambda = 0 , \tag{4.5}$$

$$\nabla^\lambda A_{\lambda\mu} = 0 . \tag{4.6}$$

Good [13], and Hammer and Good [14] have observed that the conservation laws

$$\nabla^\mu \{\Psi^\dagger \alpha_\mu O\Psi\} = 0 , \tag{4.7}$$

[14] C. L. Hammer and R. H. Good jr.: *Phys. Rev.*, **108**, 882 (1957).

differ in form from the usual conservation laws essentially because Ψ is not the wave function. However, the quantity

$$\varphi \equiv |H|^{-(s-\frac{1}{2})}\Psi , \tag{4.8}$$

where

$$H = -i\boldsymbol{\alpha}\cdot\boldsymbol{\nabla} , \tag{4.9}$$

is the wave function, and if

$$O_\varphi \equiv |H|^{-(s-\frac{1}{2})} O\, |H|^{(s-\frac{1}{2})} ,$$

then

$$\nabla^\mu \left\{ \varphi^\dagger \alpha_\mu \frac{H}{|H|} O_\varphi \varphi \right\} = 0 , \tag{4.10}$$

is the usual form of the conservation equations.

RIASSUNTO (*)

Si dimostra che tutte le equazioni d'onda di tipo Dirac con spin positivo intero o semintero, massa a riposo nulla, e prive d'interazione, sono conformemente invarianti. Si danno in forma molto semplice la trasformazione di Ψ rispetto al gruppo conforme e le leggi di conservazione associate.

(*) *Traduzione a cura della Redazione.*

On the Analyticity of Partial Wave Amplitudes for Unstable Particles in Perturbation Theory.

A. W. Hendry

Department of Natural Philosophy, Glasgow University - Glasgow

(ricevuto il 29 Luglio 1961)

Summary. — Two-particle scattering processes with one outgoing particle unstable are investigated. The singularities of the physical scattering amplitude and the corresponding partial wave amplitudes are obtained.

1. – Introduction.

In this paper, we consider two-particle scattering processes of the type $a+b \to c+d$, in which one of the outgoing particles is unstable in the sense that an external stability condition ([1,2]) is violated. If one considers the analytic properties of scattering amplitudes in terms of Feynman diagrams, as for example in Fig. 1, then the external stability condition is said to be violated at the (14) vertex, say, if $p_{14}^2 > (m_1+m_4)^2$.

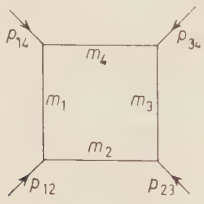

Fig. 1.

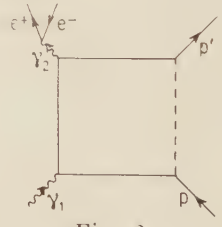

Fig. 2.

Such a situation might occur, for example, in the wide-angle pair production of electrons by photons on protons, as in Fig. 2. For sufficiently high energy

([1]) R. Karplus, C. M. Sommerfield and E. H. Wichmann: *Phys. Rev.*, **111**, 1187 (1958); **114**, 376 (1959).

([2]) J. Tarski: *Journ. Math. Phys.*, **1**, 149 (1960).

of the incident photon γ_1, an electron-positron pair may be produced by a virtual photon γ_2 whose 4-momentum squared is large enough to violate an external stability condition in the proton Compton scattering amplitude.

Another situation is in the consideration of the production of particles using an isobar model ([3]), as in

$$\pi + \mathcal{N} \to \pi + \mathcal{N}^* ,$$

$$\gamma + \mathcal{N} \to \pi + \mathcal{N}^* ,$$

where $\mathcal{N}^*$ is a nucleon isobaric state (that is, a resonance of the $\pi\mathcal{N}$ system) which subsequently decays into a nucleon and a pion. For these amplitudes, the external stability condition may be violated at the $\mathcal{N}^*$ corner of a graph.

In Section 2 (for completeness), we write down briefly some essential expressions and the equations of the surfaces of possible singularity for the scattering amplitude corresponding to the fourth order loop diagram in Fig. 1. There is also a discussion of the physical sheet and of the contours of integration. In Section 3, we investigate the behaviour of the scattering amplitude on these surfaces, and finally in Section 4 describe the singularities of the corresponding partial wave amplitudes.

2. – The scattering amplitude and the Landau surfaces.

The scattering amplitude for the fourth order loop diagram in Fig. 1 can be written (apart from a constant) in the form

$$\mathcal{F} = \lim_{\varepsilon \to 0+} \int_0^1 \dots \int_0^1 \mathrm{d}\alpha_1 \dots \mathrm{d}\alpha_4 \, \frac{\delta(1 - \sum \alpha_i)}{[D_1(\alpha_i; p_{jk}) - i\varepsilon]^2} , \tag{1}$$

where

$$D_1(\alpha_i; p_{jk}) = \sum_{i=1}^{4} \alpha_i m_i^2 - \sum_{i<j} \alpha_i \alpha_j p_{ij}^2 , \tag{2}$$

and we have taken $p_{13} = p_{12} + p_{23}$, $p_{24} = p_{23} + p_{34}$. It is more convenient ([1,2]) to introduce the quantities $y_{ij} (= y_{ji})$, defined by the equations

$$\begin{cases} p_{ij}^2 = m_i^2 + m_j^2 - 2 m_i m_j y_{ij} , & \text{for } i \neq j , \\ y_{ii} = 1 ; \end{cases} \tag{3}$$

([3]) S. J. Lindenbaum and R. M. Sternheimer: *Phys. Rev.*, **105**, 1874 (1957); R. F. Peierls: *Phys. Rev. Lett.*, **5**, 166 (1960).

and to change the integration variables to x_i, given by

$$x_i = \frac{\alpha_i m_i}{(\sum_{j=1}^{4} \alpha_j m_j)} . \tag{4}$$

The amplitude $\mathscr{F}$ then reduces to the simple form

$$\mathscr{F} = \lim_{\varepsilon \to 0+} \int_0^1 \ldots \int_0^1 \mathrm{d}x_1 \ldots \mathrm{d}x_4 \frac{N(x_i)\,\delta(1-\sum x_i)}{[D(x_i; y_{jk}) - i\varepsilon]^2} , \tag{5}$$

where

$$D(x_i; y_{jk}) = \sum_{i,j=1}^{4} x_i x_j y_{ij} . \tag{6}$$

Let us suppose that the quantities y_{12}, y_{23}, y_{34} all satisfy both internal and external stability conditions, while y_{14} violates an external stability condition: that is,

$$-1 < y_{12}, y_{23}, y_{34} < +1 ; \qquad y_{14} < -1 . \tag{7}$$

y_{13} and y_{24} are the variables in the theory; by (3), they are directly proportional to the more familiar energy-squared variables, s and t.

As can be seen directly from (2), the amplitude $\mathscr{F}$ defined in (1) and (5) (with y_{13}, y_{24} in their real physical scattering regions) is precisely the Feynman amplitude, which is obtained by associating a small negative imaginary part to each m_i^2 $(i = 1, \ldots, 4)$, the squares of the internal masses. So long as $\varepsilon \neq 0$, the contours of integration may be taken along the real x_i-axes, and the integral in (5) is well defined. However, $\mathscr{F}$ may become singular in the limit as ε tends to zero, due ([4]) to either an end-point singularity or a coincident singularity (pinching the contour) in each of the integrations.

As a consequence of $y_{14} < -1$, all of the contours of integration in (5) may no longer be taken as real when ε is put equal to zero. For if $x_2 = x_3 = 0$ we find immediately that D vanishes at the points

$$x_1 = \frac{1}{2} \pm \frac{1}{2}\left(1 - \frac{2}{1-y_{14}}\right)^{\frac{1}{2}}, \qquad x_4 = \frac{1}{2} \mp \frac{1}{2}\left(1 - \frac{2}{1-y_{14}}\right)^{\frac{1}{2}}; \tag{8}$$

and it is important to note that D vanishes at these points for all values of the variables y_{13}, y_{24}. These points obviously do not pinch their respective

([4]) R. J. Eden: *Proc. Roy. Soc.*, A **210**, 388 (1952); J. C. Polkinghorne and G. R. Screaton: *Nuovo Cimento*, **15**, 289 (1960).

contours, and so they may be avoided by deforming these contours off the real axes. This deformation must be carried out in such a way that $\mathscr{F}$ remains the physical scattering amplitude. By finding the zeros of the denominator in (5) with $x_2 = x_3 = 0$ and $\varepsilon \neq 0$, and observing their movement as $\varepsilon \to 0$, we may deduce that, when $\varepsilon = 0$, the x_1- and x_4-contours are of the form indicated in Fig. 3.

Fig. 3.

Also, the amplitude $\mathscr{F}$ may be extended outside the physical scattering regions by continuing analytically in the variables y_{13}, y_{24}; this constitutes the physical sheet ([5]). In our subsequent investigations, we shall therefore consider the multi-sheeted function $F(y_{13}, y_{24})$ defined by

$$F = \int_0^1 \ldots \int_0^1 \mathrm{d}x_1 \ldots \mathrm{d}x_4 \, \frac{N(x_i)\,\delta(1 - \sum x_i)}{[D(x_i; y_{jk})]^2}, \tag{9}$$

where the x_1-, x_4-contours are as indicated in Fig. 3, and the x_2-, x_3-contours are real: and determine in particular the singularities of F on its physical sheet.

It can easily be shown that F is certainly on its physical sheet when y_{13}, y_{24} both have small negative imaginary parts. Expanding D, we have

$$\begin{aligned} D(x_i; y_{13} - i\varepsilon', y_{24} - i\varepsilon') &= 2x_1x_3y_{13} + 2x_2x_4y_{24} + \\ &+ \Big[\sum_{i=1}^{4} x_i^2 + 2(x_1x_2y_{12} + x_2x_3y_{23} + x_3x_4y_{34} + x_1x_4y_{14})\Big] - 2i\varepsilon'(x_1x_3 + x_2x_4), \end{aligned} \tag{10}$$

and here the y_{13}, y_{24} on the right-hand side are assumed to be in their real physical regions.

With all the x_i real and so $(x_1x_3 + x_2x_4)$ positive, (10) obviously gives the Feynman denominator, as in (5). However the factor $(x_1x_3 + x_2x_4)$ can vanish in the four cases $x_1 = x_2 = 0$, $x_1 = x_4 = 0$, $x_3 = x_4 = 0$ and $x_2 = x_3 = 0$. For the first three of these cases, it is easy to show that (10) reduces to a positive quantity (again giving the correct Feynman limit as ε' tends to zero); for example, for $x_1 = x_2 = 0$, (10) becomes

$$x_3^2 + x_4^2 + 2x_3x_4y_{34} = 1 - 2(1 - y_{34})\,x_3(1 - x_3)$$

by eliminating x_4 (using $\sum x_i = 1$), and this has the positive minimum value of $\frac{1}{2}(1 + y_{34})$; similarly for the second and third cases. The fourth case, $x_2 = x_3 = 0$, corresponds precisely to the situation where we have the small contour deformations discussed above. Eliminating x_4, say, and putting $x_1 = \xi + i\eta$ (where η is small, and ξ is in a neighbourhood of the points in (8)),

([5]) R. J. Eden: *Phys. Rev.*, **119**, 1763 (1960); **121**, 1567 (1961).

we find that (10) contains the imaginary part

$$-2i(1-y_{14})(1-2\xi)\eta\,; \qquad (y_{14}<-1).$$

For the lower deformation, $\xi<\frac{1}{2}$ and $\eta>0$, while for the upper deformation $\xi>\frac{1}{2}$ and $\eta<0$. Thus at each of the deformations, (10) still possesses a small negative imaginary part, and so again is the correct Feynman denominator. (This is of course what we would have expected, since these contour deformations were in fact chosen to correspond to the Feynman limit). Hence when y_{13} and y_{14} approach their real axes from their lower half-planes, F becomes identical with the Feynman amplitude $\mathcal{F}$ and is therefore on its physical sheet.

The surfaces on which F may be singular, are given by the vanishing of the determinant and principal minors of the matrix $\mathcal{D}$:

$$\mathcal{D}=\begin{pmatrix} 1 & y_{12} & y_{13} & y_{14} \\ y_{12} & 1 & y_{23} & y_{24} \\ y_{13} & y_{23} & 1 & y_{34} \\ y_{14} & y_{24} & y_{34} & 1 \end{pmatrix}. \tag{11}$$

Explicity, the equations of these surfaces are

$$y_{13}=\pm 1\,, \quad \text{and} \quad y_{24}=\pm 1\,; \tag{12}$$

$$\begin{cases} L_4^{\pm}: & y_{13}=y_{12}y_{23}\pm\{(1-y_{12}^2)(1-y_{23}^2)\}^{\frac{1}{2}}\,, \\ L_2^{\pm}: & y_{13}=y_{14}y_{34}\pm\{(1-y_{14}^2)(1-y_{34}^2)\}^{\frac{1}{2}}\,, \\ L_3^{\pm}: & y_{24}=y_{12}y_{14}\pm\{(1-y_{12}^2)(1-y_{14}^2)\}^{\frac{1}{2}}\,, \\ L_1^{\pm}: & y_{24}=y_{23}y_{34}\pm\{(1-y_{23}^2)(1-y_{34}^2)\}^{\frac{1}{2}}\,. \end{cases} \tag{13}$$

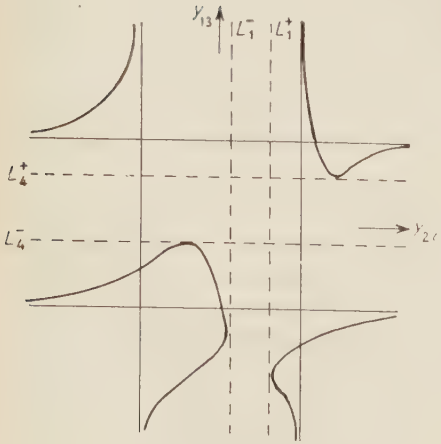

Fig. 4.

and

$$\Lambda(y_{ij})\equiv\det\mathcal{D}=0\,. \tag{14}$$

It will be noticed that, since $y_{14}<-1$, the surfaces $L_2^{\pm}$ and $L_3^{\pm}$ are complex. In Fig. 4, we have drawn a typical curve Γ corresponding to the real solutions (y_{13}, y_{14}) of the eq. (14). ($y_{13}=\pm 1$ and $y_{24}=\pm 1$ are asymptotes to Γ; $L_4^{\pm}$ and $L_1^{\pm}$ are the horizontal and vertical tangents respectively.)

A picture of the surface Σ which connects the various parts of Γ and which arises from the complex conjugate

roots of (14), may be obtained by using the usual search-line technique ([2]).

We must now investigate whether F is singular or regular on the surfaces (12), (13) and (14) on its physical sheet.

3. – The singularities of F.

One method ([6]) of determining the singularities of a scattering amplitude is to perform an analytic continuation in the (real) external masses from a region of known analyticity to a more extensive region containing the desired values of the external masses, and to observe the gradual development of the Landau surfaces. However, if one attempts to make a continuation in one of the external masses through the point where an external stability condition is violated, a singularity is found at that point. This may cause the sudden appearance and disappearance of singularities on the physical sheet of F, and so invalidates the above method.

The procedure adopted in the present paper is to consider the analytic continuation from a region $\mathscr{R}$ which has $\operatorname{Im} y_{13} < 0$, $\operatorname{Im} y_{24} < 0$ (regular for the physical sheet of F), up to and on to each of the various Landau surfaces (12), (13) and (14) separately.

For the surfaces $y_{13} = \pm 1$, we firstly note that we can continue analytically from $\mathscr{R}$ up to neighbourhoods of these surfaces without needing to deform the contours of integration (other than the small deformations indicated in Fig. 3, of course) since we can go by a route along which D does not vanish. Further, on these surfaces (which correspond to $x_2 = x_4 = 0$), D reduces to

$$D = 1 + 2x_1(1 - x_1)(y_{13} - 1) ,$$

where we have eliminated x_3 by the δ-function in (5). As x_1 varies along its contour from 0 to 1 (Fig. 3), we see that D is always positive if $y_{13} = +1$, but vanishes (two coincident roots) at the point $x_1 = \frac{1}{2}$ if $y_{13} = -1$ (D certainly does not vanish on the complex parts of the x_1-contour, since D acquires a non-zero imaginary part there). These roots pinch the contour (as may be shown by taking y_{14} slightly greater than -1). Thus F is regular on the surface $y_{13} = +1$, but singular on the surface $y_{13} = -1$.

Similarly F is regular on $y_{24} = +1$, but singular on $y_{24} = -1$.

It may likewise be seen that no further contour deformations are necessary to reach the real tangential surfaces $L_1^{\pm}$, $L_4^{\pm}$, and in fact F is regular on

---

([6]) P. V. Landshoff, J. C. Polkinghorne and J. C. Taylor: *Nuovo Cimento*, **19**, 939 (1961); R. J. Eden, P. V. Landshoff, J. C. Polkinghorne and J. C. Taylor: *Phys. Rev.*, **122**, 307 (1961).

these four surfaces provided that the conditions

$$y_{12}+y_{23}\geqslant 0\,,\qquad y_{23}+y_{34}\geqslant 0 \tag{15}$$

are satisfied. For example, on $L_4^{\pm}$ (which correspond to $x_4=0$), D reduces to

$$D=x_1^2+x_2^2+x_3^2+2x_1x_2y_{12}+2x_2x_3y_{23}+2x_1x_3y_{13}\,,$$

with $x_1+x_2+x_3=1$. For x_1 real, KARPLUS *et al.* [1] have shown that this D can be expressed as a positive definite quadratic form ($y_{13}>-1$ on $L_4^{\pm}$) if the first of the conditions (15) holds. For complex $x_1=\xi-i\eta$, where ξ is in the neighbourhood of the points in (8), D can be written (eliminating x_3, say) in the form

$$D=(ax_2^2+bx_2+c)+i\eta(dx_2+e)\,.$$

For D to vanish, both its real and imaginary parts must vanish simultaneously. However, the resulting quadratic and linear equations in x_2 are not consistent, and so D is non-zero also on the complex parts of the x_1-contour. Therefore, because of the non-vanishing of D, F is regular on $L_4^{\pm}$; and similar arguments apply for $L_1^{\pm}$. It may be noted that the conditions (15) are not really very restrictive, and are certainly satisfied for the examples mentioned in Section **1** (in fact, y_{12}, y_{23}, y_{24} are all positive there).

Similar results of regularity do not hold, however, on all of the complex tangential surfaces $L_2^{\pm}$, $L_3^{\pm}$ [7], as may be deduced from the investigations of LANDSHOFF and TREIMAN [8] who considered the reduced vertex diagram to which these surfaces correspond; they showed that, whereas L_2, L_3^- are regular, L_2^+, L_3^+ are singular. That F is regular on L_2^-, L_3^- follows from the fact that we may easilu continue analytically from $\mathscr{R}$ up to and on to these surfaces without D vanishing. However, in order to go from the region $\mathscr{R}$ (which has $\operatorname{Im} y_{13}<0$, $\operatorname{Im} y_{24}<0$) to a neighbourhood of L_2^+, say (which has $\operatorname{Im} y_{13}>0$), we must pass through the real point where $\operatorname{Im} y_{13}=0$ and D can vanish for a point on the previously chosen integration contours. This singularity may nevertheless be avoided by further deforming these contours; this can certainly be done, since we are not yet on any of the Landau surfaces and these are the only surfaces where we may have unavoidable singularities. Thus we must continually deform the contours as we enter the upper half y_{13}-plane and approach L_2^+ until, when we finally reach L_2^+, the contours can retreat no further

(7) J. C. POLKINGHORNE: private communication. The author would like to thank Dr. POLKINGHORNE for pointing this out, and also for enlightening correspondence.

(8) P. V. LANDSHOFF and S. B. TREIMAN: *Nuovo Cimento*, **19**, 1249 (1961).

and are pinched by coincident singularities. Hence we are unable to continue F analytically from $\mathscr{R}$ on to L_2^+, or similarly on to L_3^+. F is therefore singular on L_2^+, L_3^+ on its physical sheet.

Just as for the real tangents $L_1^{\pm}$, $L_4^{\pm}$ we may continue from $\mathscr{R}$ up to the real curve Γ without further contour deformation. For the behaviour of F on Γ, the method of Fowler *et al.* [9] was used: D vanishes on Γ at the points x_i $(i=1, ..., 4)$ given by

$$\frac{x_1}{\Delta_1^k} = \frac{x_2}{\Delta_2^k} = \frac{x_3}{\Delta_3^k} = \frac{x_4}{\Delta_4^k}, \qquad \text{for any } k \ (k=1, ..., 4), \tag{16}$$

where Δ_j^i is the co-factor of y_{ij} in the expansion of $\Delta \equiv \det \mathscr{D}$. Since all the co-factors in (16) are real, and $\sum x_i = 1$, it may be deduced that (16) is satisfied only when the x_i $(i=1, ..., 4)$ are real. Therefore, since the allowed real values of the x_i in (5) are only positive, we must determine the region R in the real y_{13}-, y_{24}-plane (Fig. 4) where the co-factors in (16), regarded as functions of y_{13} and y_{24}, have the same sign.

It is convenient here to take $k=2$ because, for $y_{14}<-1$, Δ_2^2 is negative for all real y_{13}, y_{24}. The regions where the other three co-factors are negative can easily be obtained, and it is found that no part of Γ lies in the intersection (R) of these regions. Therefore D does not vanish anywhere on Γ for the allowed positive values of the x_i-variables of integration; and thus F is regular both on Γ and also on that part of Σ sprouting out along Γ.

However, F is not regular on the whole of Σ; it is singular on that section which is separated off from the rest of Σ by the branch cut joining the points of contact of L_2^+ and L_3^+ with Σ (the 1-dimensional branch cut on this 2-dimensional surface Σ which lies in the 4-dimensional y_{13}-, y_{24}-space, divides Σ into two separate sections).

The singularities of the scattering amplitude F are therefore the real threshold singularities at $y_{13}=-1$, $y_{24}=-1$, and the complex singularities at values of y_{13}, y_{24} corresponding to L_2^+, L_3^+ and the above singular section of Σ. The presence of these complex singularities invalidates a Mandelstam representation for F.

4. – The singularities of the partial wave amplitudes.

The singularities of the partial wave amplitudes of F:

$$f_l(s) = \int_{-1}^{+1} \mathrm{d}(\cos\theta)\, F(s, \cos\theta)\, P_l(\cos\theta)\,,$$

[9] M. Fowler, P. V. Landshoff and R. W. Lardner: *Nuovo Cimento*, **17**, 956 (1960).

are slightly simpler than those of F itself, as a result of the theory of Taylor and Warburton ([10]). They showed that, in the case when all the stability conditions are satisfied, the partial wave amplitudes do not possess complex singularities due to the singular parts of Σ, since these singularities depend on the internal masses squared m_i^2 only as differences. By a slight extension of their argument, the same is true even when an external stability condition is violated; and $f_l(s)$ has no complex singularities arising from the singular section of Σ.

In Fig. 5, we have indicated a typical cut s-plane for $f_l(s)$. Besides the usual physical cut and the u-, t-cuts, there are branch cuts arising from L_2^+, L_3^+. The cut due to L_2^+ starts at the complex point A, and may be taken so that it joins up with the physical cut BC. The surface L_3^+ produces a similar cut in the t-plane, and this becomes the cut DEF (the locus of branch points) shown in the s-plane.

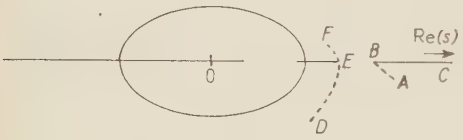

Fig. 5.

However, it may be remarked that these latter branch cuts from L_2^-, L_3^- are not directly related to any physical process, and so it is no longer easy to determine the discontinuities across them. It also seems very difficult at present to see what new singularities will be introduced into the above s-plane from higher order perturbation diagrams.

* * *

The author wishes to express his sincere thanks to Dr. R. G. Moorhouse for his guidance and assistance, and to Professor J. C. Gunn for his interest and encouragement. He also acknowledges the receipt of a D.S.I.R. Studentship.

([10]) J. G. Taylor and A. E. A. Warburton: *Phys. Rev.*, **120**, 1506 (1960).

RIASSUNTO (*)

Si esaminano i processi di scattering a due particelle, in cui una delle particelle è instabile. Si ottengono le singolarità dell'ampiezza di scattering fisica e le corrispondenti ampiezze dell'onda parziale.

(*) *Traduzione a cura della Redazione.*

IL NUOVO CIMENTO Vol. XXII, N. 4 16 Novembre 1961

The Determination of the Scattering Potential from the Spectral Measure Function.

V. – The Gelfand-Levitan Equation for the Three-Dimensional Scattering Problem.

I. Kay (*)

Institute for Mathematical Sciences, New York University - New York

H. E. Moses (**)

Department of Physics, Polytechnic Institute of Brooklyn - Brooklyn

(ricevuto il 29 Luglio 1961)

Summary. — A Gelfand-Levitan equation is introduced which enables one to calculate scattering potentials from part of the scattering amplitude in the three-dimensional scattering problem. The Gelfand-Levitan equation is a generalization of the one-dimensional Gelfand-Levitan equation of Kay and Moses. The part of the scattering amplitude which is required is an analogue of the reflection coefficient in one dimension. The potential which is obtained is more general than that usually assumed in the three-dimensional scattering problem in that it is diagonal in the radius variable but is a real integral operator in terms of the angular variables. The purely local potential (*i.e.* the potential which is diagonal in both the radial and angular variables) appears as a special case. In the present paper we assume that the perturbed Hamiltonian has a purely continuous spectrum which coincides with that of the unperturbed Hamiltonian. The case where there are also point eigenvalues is omitted in order to present the main ideas without unnecessary complications. We shall derive the Gelfand-Levitan equation from the very general Gelfand-Levitan method of Kay and Moses. This formalism already guarantees that the potential which is

(*) The work of I. Kay was supported by the National Science Foundation, NSF G-14000.

(**) The work of H. E. Moses was supported by the Office of Naval Research, contract Nonr-839(30), Project no. NR-013-106. Present address: Geophysics Corporation of America, Bedford, Mass.

obtained will reproduce the reflection coefficient and that the equation is correct. In a later paper, however, we shall prove that the Gelfand-Levitan equation which we derive is correct by an elementary formalism which makes no use of the general Gelfand-Levitan technique at all; the advantage of this procedure being that one is immediately convinced that the equation is the right one.

1 – Introduction and summary of results: the Gelfand-Levitan equation in three dimensions.

Various forms of the Gelfand-Levitan equation have been introduced for the purpose of reconstructing the scattering potential from scattering data, in particular scattering problems. A bibliography is given in references (1) and (2). It was noted by the present authors that these various Gelfand-Levitan equations could be considered as special cases of a general formalism, which they gave in reference (1). It was shown that the Gelfand-Levitan equation could be interpreted as an operator equation in Hilbert space for the operator which transforms the unperturbed Hamiltonian into the perturbed Hamiltonian. This operator could be obtained in terms of a positive-definite operator which was called the weight operator. In special cases, the weight operator could be obtained from suitable elements of the scattering operator.

In the present paper we shall use our generalized Gelfand-Levitan technique to obtain the Gelfand-Levitan equation for the three-dimensional scattering problem. Instead of assuming that the scattering potential is simply a real function of the co-ordinates, we shall consider a somewhat more general class of scattering potentials, namely those which, when expressed in terms of polar co-ordinates, are diagonal in terms of the radius variable but are real integral operators in terms of the angular variables. The general Gelfand-Levitan procedure of reference (1) shows that if the Gelfand-Levitan equation has a unique solution, then the potential which gives rise to the scattering will be reproduced by the Gelfand-Levitan procedure. Hence, if the scattering operator was given by a potential which is a multiplicative operator, it will be reproduced.

In the present paper we shall assume familiarity with reference (1). However, we shall change some of the notation in order to simplify various expressions. Also for simplicity, we shall assume there are no point eigenvalues.

(1) I. KAY and H. E. MOSES: *Nuovo Cimento*: part I, **2**, 917 (1955); part II, **3**, 66 (1956); part III, **3**, 276 (1956).

(2) L. D. FADDEEV: *Usp. Math. Nauk*, **14** (88), 57 (1959).

For those familiar with the general Gelfand-Levitan procedure it will be clear how they are to be introduced.

In a later paper, we shall use an elementary procedure to verify that it is the correct one, even though, this proof is not really needed, since the general Gelfand-Levitan procedure automatically gives the correct equation. The advantage of this proof is that one need not have much background in the subject to be persuaded of the validity of the proof.

After the introduction of some notation we shall give the Gelfand-Levitan equation which we shall derive in subsequent sections.

Generally speaking it will be convenient to use polar co-ordinates both for the $\boldsymbol{x}$-representation and the $\boldsymbol{p}$- (*i.e.* momentum) representation. The polar co-ordinates of $\boldsymbol{x}$ will be denoted by $r = |\boldsymbol{x}|$, the angle λ $(0 \leqslant \lambda \leqslant \pi)$ which is the angle made by $\boldsymbol{x}$ with the z-axis and the angle σ $(0 \leqslant \sigma \leqslant 2\pi)$ which is the angle made by the projection of $\boldsymbol{x}$ on the x-y plane with the x-axis. Similarly the vector $\boldsymbol{p}$ will have the polar co-ordinates $p = |\boldsymbol{p}|$, $\theta(0 \leqslant \theta \leqslant \pi)$, and $\varphi(0 \leqslant \varphi \leqslant 2\pi)$. When primes are put on the vectors it is to be understood that the corresponding polar co-ordinates also have primes and conversely.

The unperturbed Hamiltonian H_0 will be taken as

$$H_0 = -\nabla^2 , \tag{1.1}$$

while the perturbed Hamiltonian H is given by

$$H = H_0 + V , \tag{1.2}$$

where V is the scattering potential which in the $\boldsymbol{x}$ representation we assume has the form of an integral operator with the kernel

$$V(\boldsymbol{x}\,|\,\boldsymbol{x}') = \delta(r - r')V(r\,|\,\lambda, \sigma; \lambda', \sigma') , \tag{1.3}$$

where $V(r\,|\,\lambda, \sigma; \lambda', \sigma')$ is real and is the kernel of the integral operator in the angular variables, *i.e.*,

$$\int V(\boldsymbol{x}\,|\,\boldsymbol{x}')f(\boldsymbol{x}')\,\mathrm{d}\boldsymbol{x}' = r^2 \int_0^{\pi} \sin\lambda'\,\mathrm{d}\lambda' \int_0^{2\pi} \mathrm{d}\sigma'\, V(r\,|\,\lambda, \sigma; \lambda', \sigma')f(r, \lambda', \sigma') .$$

Here $f(\boldsymbol{x})$ is a state vector in the $\boldsymbol{x}$-representation and

$$f(\boldsymbol{x}) = f(r, \lambda, \sigma) .$$

A purely local potential is just a special case of the class of potentials which we are considering.

It will be convenient to express the eigenfunctions of H_0 in terms of three different representations. The first representation is the usual momentum representation. These eigenfunctions are denoted by $\Psi_0(\boldsymbol{x}\,|\,\boldsymbol{p})$ where

$$\Psi_0(\boldsymbol{x}\,|\,\boldsymbol{p}) = \left(\frac{1}{2\pi}\right)^{\frac{3}{2}} \exp\left[i\boldsymbol{p}\cdot\boldsymbol{x}\right]. \tag{1.4}$$

These eigenfunctions satisfy the orthogonality and completeness relations

$$\begin{cases} \int \Psi_0^*(\boldsymbol{x}\,|\,\boldsymbol{p})\Psi_0(\boldsymbol{x}\,|\,\boldsymbol{p}')\,\mathrm{d}\boldsymbol{x} = \delta(\boldsymbol{p}-\boldsymbol{p}')\,, \\ \int \Psi_0(\boldsymbol{x}\,|\,\boldsymbol{p})\Psi_0^*(\boldsymbol{x}'\,|\,\boldsymbol{p})\,\mathrm{d}\boldsymbol{p} = \delta(\boldsymbol{x}-\boldsymbol{x}')\,. \end{cases} \tag{1.5}$$

The second way of expressing the eigenfunctions is in terms of polar coordinates of the momentum vector $\boldsymbol{p}$. Let us denote this set by $\Psi_0(\boldsymbol{x}\,|\,p,\,\theta,\,\varphi)$ where

$$\Psi_0(\boldsymbol{x}\,|\,p,\,\theta,\,\varphi) = p\sqrt{\sin\theta}\,\Psi_0(\boldsymbol{x}\,|\,\boldsymbol{p})\,. \tag{1.6}$$

They satisfy the orthogonality and completeness relations

$$\begin{cases} \int \Psi_0^*(\boldsymbol{x}\,|\,p,\,\theta,\,\varphi)\Psi_0(\boldsymbol{x}\,|\,p',\,\theta',\,\varphi')\,\mathrm{d}\boldsymbol{x} = \delta(p-p')\delta(\theta-\theta')\,\delta(\varphi-\varphi')\,, \\ \int_0^\infty \mathrm{d}p \int_0^\pi \mathrm{d}\theta \int_0^{2\pi} \mathrm{d}\varphi\, \Psi_0(\boldsymbol{x}\,|\,p,\,\theta,\,\varphi)\Psi_0^*(\boldsymbol{x}'\,|\,p,\,\theta,\,\varphi) = \delta(\boldsymbol{x}-\boldsymbol{x}')\,. \end{cases} \tag{1.7}$$

The third way of expressing the eigenfunctions of H_0 is through the use of the energy and angle variables. We denote this set by $\Psi_0(\boldsymbol{x}\,|\,E,\,\theta,\,\varphi)$ where

$$\Psi_0(\boldsymbol{x}\,|\,E,\,\theta,\,\varphi) = \frac{(E)^{\frac{1}{4}}}{\sqrt{2}}\,\sqrt{\sin\theta}\,\Psi_0(\boldsymbol{x}\,|\,\boldsymbol{p})\,, \qquad (E = |\boldsymbol{p}|^2 = p^2), \tag{1.8}$$

and

$$\begin{cases} \int \Psi_0^*(\boldsymbol{x}\,|\,E,\,\theta,\,\varphi)\Psi_0(\boldsymbol{x}\,|\,E',\,\theta',\,\varphi')\,\mathrm{d}\boldsymbol{x} = \delta(E-E')\delta(\theta-\theta')\,\mathrm{d}(\varphi-\varphi')\,, \\ \int_0^\infty \mathrm{d}E \int_0^\pi \mathrm{d}\theta \int_0^{2\pi} \mathrm{d}\varphi\, \Psi_0(\boldsymbol{x}\,|\,E,\,\theta,\,\varphi)\Psi_0^*(\boldsymbol{x}'\,|\,E,\,\theta,\,\varphi) = \delta(\boldsymbol{x}-\boldsymbol{x}')\,. \end{cases} \tag{1.9}$$

From the viewpoint of scattering problems the third set is most natural though use of the first set is conventional.

We shall assume that the spectrum of H is purely continuous and coincides with that of H_0. Of course, we shall have to specify boundary conditions on the eigenfunctions of H. For each boundary condition we shall introduce three sets of eigenfunctions analogous to those used for H_0.

Let us denote one set of the « outgoing » eigenfunctions of H by $\Psi_-(\boldsymbol{x}|\boldsymbol{p})$ where $\Psi_-(\boldsymbol{x}|\boldsymbol{p})$ satisfies the integral equation

$$\Psi_-(\boldsymbol{x}|\boldsymbol{p}) = \Psi_0(\boldsymbol{x}|\boldsymbol{p}) - \frac{1}{4\pi}\iint \frac{\exp[ip|\boldsymbol{x}-\boldsymbol{x}'|]}{|\boldsymbol{x}-\boldsymbol{x}'|} V(\boldsymbol{x}'|\boldsymbol{x}'')\Psi_-(\boldsymbol{x}''|\boldsymbol{p})\,d\boldsymbol{x}'\,d\boldsymbol{x}''. \tag{1.10}$$

We shall define the eigenfunctions $\Psi_-(\boldsymbol{x}|p,\theta,\varphi)$ and $\Psi_-(\boldsymbol{x}|E,\theta,\varphi)$ by

$$\begin{cases} \Psi_-(\boldsymbol{x}|p,\theta,\varphi) = p\sqrt{\sin\theta}\,\Psi_-(\boldsymbol{x}|\boldsymbol{p}), \\ \Psi_-(\boldsymbol{x}|E,\theta,\varphi) = \dfrac{(E)^{\frac{1}{4}}}{\sqrt{2}}\sqrt{\sin\theta}\,\Psi_-(\boldsymbol{x}|\boldsymbol{p}). \end{cases} \tag{1.11}$$

It can be shown that $\Psi_-(\boldsymbol{x}|p,\theta,\varphi)$ and $\Psi_-(\boldsymbol{x}|E,\theta,\varphi)$ satisfy the integral equation (1.10) when $\Psi_0(\boldsymbol{x}|\boldsymbol{p})$ is replaced by $\Psi_0(\boldsymbol{x}|p,\theta,\varphi)$ and $\Psi_0(\boldsymbol{x}|E,\theta,\varphi)$ respectively. The functions are all eigenfunctions of H with the eigenvalue $E=p^2$. They satisfy completeness and orthogonality relations identical to those satisfied by the corresponding eigenfunctions of H_0.

Similarly, we shall introduce « incoming » eigenfunctions of H denoted by

$$\Psi_+(\boldsymbol{x}|\boldsymbol{p}), \qquad \Psi_+(\boldsymbol{x}|p,\theta,\varphi), \qquad \Psi_+(\boldsymbol{x}|E,\theta,\varphi),$$

where

$$\Psi_+(\boldsymbol{x}|\boldsymbol{p}) = \Psi_0(\boldsymbol{x}|\boldsymbol{p}) - \frac{1}{4\pi}\iint \frac{\exp[-ip|\boldsymbol{x}-\boldsymbol{x}'|]}{|\boldsymbol{x}-\boldsymbol{x}'|} V(\boldsymbol{x}'|\boldsymbol{x}'')\Psi_+(\boldsymbol{x}''|\boldsymbol{p})\,d\boldsymbol{x}'\,d\boldsymbol{x}''. \tag{1.12}$$

Again $\Psi_+(\boldsymbol{x}|p,\theta,\varphi)$ and $\Psi_+(\boldsymbol{x}|E,\theta,\varphi)$ also satisfy the integral eq. (1.12) with $\Psi_0(\boldsymbol{x}|\boldsymbol{p})$ suitably replaced. The completeness and orthogonality relations satisfied by Ψ_0 are satisfied also by the various eigenfunctions Ψ_+.

Let us define the scattering amplitude $b_p(\lambda,\sigma|\lambda',\sigma')$ by

$$\lim_{r\to\infty}\Psi_-(\boldsymbol{x}|\boldsymbol{p}) = \Psi_0(\boldsymbol{x}|\boldsymbol{p}) - \frac{i}{p\sqrt{2\pi}}\frac{1}{\sqrt{\sin\lambda}\sqrt{\sin\theta}}\frac{\exp[ipr]}{r}\,b_p(\lambda,\sigma|\theta,\varphi). \tag{1.13}$$

In (1.13) $p=|\boldsymbol{p}|$, $r=|\boldsymbol{x}|$, θ, φ are the polar angles of the vector $\boldsymbol{p}$ while λ, σ are the polar angles of the vector $\boldsymbol{x}$. The somewhat odd normalization of the spherical wave is used to define $b_p(\theta,\varphi|\theta',\varphi')$ because with this normalization the scattering amplitude is essentially the scattering operator.

Although $b_p(\theta,\varphi|\theta',\varphi')$ was originally defined for positive p only we shall show later that the definition can be extended for negative values of p.

In fact

$$b_{-p}(\theta, \varphi | \theta', \varphi') = [b_p(\theta, \varphi | \theta' \varphi')]^* , \tag{1.14}$$

where the asterisk denotes the complex conjugate. Similarly, though the eigenfunctions $\Psi_0(\boldsymbol{x}|p, \theta, \varphi)$, $\Psi_\pm(\boldsymbol{x}\ p, \theta, \varphi)$ were defined only for $p > 0$, we have by continuing the definition of these functions to negative values of p:

$$\begin{cases} \Psi_0(\boldsymbol{x}|-p, \theta, \varphi) = -\Psi_0^*(\boldsymbol{x}|p, \theta, \varphi) , \\ \Psi_\pm(\boldsymbol{x}|-p, \theta, \varphi) = -\Psi_\pm^*(\boldsymbol{x}|p, \theta, \varphi) , \end{cases} \tag{1.15}$$

(The second equation follows from the integral equations for $\Psi_\pm$.)

We are now in a position to give the Gelfand-Levitan equation in three dimensions. Let us define

$$\Psi_0(r, \lambda, \sigma | p, \theta, \varphi) \equiv \Psi_0(\boldsymbol{x}|p, \theta, \varphi) , \tag{1.16}$$

$$\Omega(r, \lambda, \sigma | r', \lambda', \sigma') = \int_{-\infty}^{+\infty} \mathrm{d}p \int_0^{\pi/2} \mathrm{d}\theta \int_{\pi/2}^{\pi} \mathrm{d}\theta' \cdot \tag{1.17}$$

$$\cdot \int_0^{2\pi} \mathrm{d}\varphi \int_0^{2\pi} \mathrm{d}\varphi' \Psi_0(r, \lambda, \sigma | p, \theta, \varphi) \Psi_0^*(r', \lambda', \sigma' | p, \theta', \varphi') b_p(\theta, \varphi | \theta', \varphi') .$$

Furthermore let us require the functions of 6 variables $K(r, \lambda, \sigma\ r', \lambda', \sigma')$ be required to satisfy

$$K(r, \lambda, \sigma | r', \lambda', \sigma') = -\Omega(r, \lambda, \sigma | r', \lambda', \sigma') - \int_r^{\infty} r''^2 \mathrm{d}r'' \int_0^{\pi} \sin \lambda'' \, \mathrm{d}\lambda'' \int_0^{2\pi} \mathrm{d}\sigma'' \cdot \tag{1.18}$$

$$\cdot K(r, \lambda, \sigma | r'', \lambda'', \sigma'') \Omega(r'', \lambda'', \sigma'' | r', \lambda', \sigma') ,$$

for $r' \quad r$, then the potential $V(r|\lambda, \sigma; \lambda', \sigma')$ (see (1.3)) which will reproduce that part of the scattering amplitude which appears in the definition of Ω is given by

$$V(r|\lambda, \sigma; \lambda', \sigma') = -2 \frac{1}{r^2} \frac{\partial}{\partial r} r^2 K(r, \lambda, \sigma | r, \lambda', \sigma'). \tag{1.19}$$

Eq. (1.18) together with eq. (1.19) for the potential constitute the Gelfand-Levitan equations for the three-dimensional scattering problem.

As in the case of all Gelfand-Levitan equations for problems which involve degeneracy, the complete scattering operator is not needed to reconstruct the potential. In the case of three-dimensional scattering problem, only that part

of the scattering amplitude which corresponds to scattering in the positive z direction of waves traveling initially in the negative z direction—*i.e.* the back scattering on a hemisphere—is used to reconstruct the potential.

The quantities $K(r, \lambda, \sigma | r', \lambda', \sigma')$ can be used to construct eigenfunctions of H. Let $\Psi(\boldsymbol{x} | p, \theta, \varphi)$ be given by

$$(1.20) \qquad \Psi(\boldsymbol{x} | p, \theta, \varphi) \equiv \Psi(r, \lambda, \sigma | p, \theta, \varphi) = \Psi_0(r, \lambda, \sigma | p, \theta, \varphi) + \int_r^\infty r'^2 \, \mathrm{d}r' \int_0^\pi \sin \lambda' \, \mathrm{d}\lambda' \int_0^{2\pi} \mathrm{d}\sigma' \, K(r, \lambda, \sigma | r', \lambda', \sigma') \Psi_0(r', \lambda', \sigma' | p, \theta, \varphi) .$$

Then $\Psi(\boldsymbol{x} | p, \theta, \varphi)$ will be an eigenfunction of H corresponding to the eigenvalue $E = p^2$. The eigenfunction $\Psi(\boldsymbol{x} | p, \theta, \varphi)$ will satisfy the completeness relation

$$(1.21) \qquad \int_0^\infty \mathrm{d}p \int_0^\pi \mathrm{d}\theta \int_0^{2\pi} \mathrm{d}\varphi \, \Psi(\boldsymbol{x} | p, \theta, \varphi) \Psi^*(\boldsymbol{x}' | p, \theta, \varphi) +$$

$$+ \int_0^\infty \mathrm{d}p \int_{\pi/2}^{\pi/2} \mathrm{d}\theta \int_{\pi/2}^{\pi} \mathrm{d}\theta' \int_0^{2\pi} \mathrm{d}\varphi \int_0^{2\pi} \mathrm{d}\varphi' \, \Psi(\boldsymbol{x} | p, \theta, \varphi) b_p(\theta, \varphi | \theta', \varphi') \Psi^*(\boldsymbol{x}' | p, \theta', \varphi') +$$

$$+ \int_0^\infty \mathrm{d}p \int_{\pi/2}^{\pi} \mathrm{d}\theta \int_0^{\pi/2} \mathrm{d}\theta' \int_0^{2\pi} \mathrm{d}\varphi \int_0^{2\pi} \mathrm{d}\varphi' \, \Psi(\boldsymbol{x} | p, \theta, \varphi) b_p^*(\theta', \varphi' | \theta, \varphi) \Psi^*(\boldsymbol{x}' | p, \theta', \varphi') = \delta(\boldsymbol{x} - \boldsymbol{x}') .$$

2. – Asymptotic form for bundles of plane waves.

In later sections we shall use the method of reference [1] to construct the weight operator for use in the Gelfand-Levitan equation. But in order to find the weight operator we must indicate how $\Psi_0(\boldsymbol{x} | E, \theta, \varphi)$ behaves as $r = |\boldsymbol{x}| \to \infty$. We must, however, be more explicit as to the nature of the limit we wish to take. Actually we should like to find

$$\lim_{r \to \infty} \iiint \Psi_0(\boldsymbol{x} | E, \theta, \varphi) f(E, \theta, \varphi) \, \mathrm{d}E \, \mathrm{d}\theta \, \mathrm{d}\varphi ,$$

where $f(E, \theta, \varphi)$ is a suitably defined test function, for in this case

$$\iiint \Psi_0(\boldsymbol{x} | E, \theta, \varphi) f(E, \theta, \varphi) \, \mathrm{d}E \, \mathrm{d}\theta \, \mathrm{d}\varphi ,$$

could be considered as a function in Hilbert space. Actually, we need only

use test functions $g(\theta, \varphi)$ for integration over the angular variables θ, φ. Integrals of plane waves over the angular part are called « bundles of plane waves » (see ref. [3]). In evaluating

$$\lim_{r\to\infty} \int_0^{\pi} \mathrm{d}\theta \int_0^{2\pi} \mathrm{d}\varphi \, \Psi_0(\boldsymbol{x} \,|\, E, \theta, \varphi) g(\theta, \varphi) \,,$$

we shall use saddle-point techniques. For simplicity, however, we shall carry out the saddle-point evaluation in the sense of distributions. Our procedure will be based on the identity,

$$\lim_{\alpha\to\infty} \alpha^{\frac{1}{2}} \exp\left[\pm i\xi^2\alpha\right] = \pi^{\frac{1}{2}} \exp\left[\pm i\pi/4\right] \delta(\xi) \,, \tag{2.1}$$

First, let us write

$$\Psi_0(\boldsymbol{x} \,|\, E, \theta, \varphi) = \frac{(E)^{\frac{1}{4}}}{\sqrt{2}} \sqrt{\sin\theta} \exp\left[iprf(\theta, \varphi)\right] \,, \tag{2.2}$$

where

$$f(\theta, \varphi) = \cos\lambda\cos\theta + \sin\lambda\sin\theta\cos(\varphi - \sigma) \,. \tag{2.3}$$

In (2.3) λ and σ are the polar angles of $\boldsymbol{x}$. We shall want to find the values θ_0 and φ_0 such that $f_\theta(\theta_0, \varphi_0) = f_\varphi(\theta_0, \varphi_0) = 0$. Here f_θ and f_φ are the θ derivative and φ derivative of the function f.

Two sets of values θ_0, φ_0 are found. The first set is

$$\theta_0 = \lambda \,, \qquad \varphi_0 = \sigma \,, \tag{2.4}$$

while the second set is

$$\theta_0 = \pi - \lambda \,, \qquad \varphi_0 = \Sigma \,, \tag{2.4a}$$

where

$$\Sigma = \sigma + \pi \qquad \text{if } 0 < \sigma < \pi,$$
$$= \sigma - \pi \qquad \text{if } \pi < \sigma < 2\pi.$$

In the vicinity of the first set we have

$$f(\theta, \varphi) = 1 - \frac{(\theta - \lambda)^2}{2} - \sin^2\lambda \frac{(\varphi - \sigma)^2}{2} + F(\theta - \lambda, \varphi - \sigma) \,,$$

[3] K. O. FRIEDRICHS: *Seminar - Recent Developments in the Theory of Wave Propagation*, Section III-C, Institute for Mathematics and Mechanics of New York University (1949-1950).

where F is a function of its arguments such that $F(0, 0) = 0$. Hence, for values of φ and θ in the vicinity of φ_0 and θ_0 we may write

$$\Psi_0(\boldsymbol{x}\,|\,E, \theta, \varphi) = \frac{(E)^{\frac{1}{4}}}{\sqrt{2}} \frac{\sqrt{\sin\theta}}{(2\pi)^{\frac{3}{2}}} \Big\{ \exp[irp] \cdot \sqrt{\frac{2}{rp}} \sqrt{\frac{rp}{2}} \exp[-irp(\theta-\lambda)^2/2] \cdot$$

$$\cdot \sqrt{\frac{2}{rp}} \frac{1}{\sin\lambda} \sin\lambda \sqrt{\frac{rp}{2}} \cdot \exp[-ir(p/2)\sin^2\lambda(\varphi-\sigma)^2] \cdot \exp[irpF(\theta-\lambda, \varphi-\sigma)] \Big\} .$$

On using (2.1) we have

$$\lim_{r\to\infty} \Psi_0(\boldsymbol{x}\,|\,E, \theta, \varphi) = \frac{\sqrt{2}}{(2\pi)^{\frac{3}{2}}(E)^{\frac{1}{4}}} \frac{(-i\pi)}{r} \frac{\exp[irp]}{\sqrt{\sin\theta}} \delta(\theta-\lambda)\,\delta(\varphi-\sigma) .$$

Similarly in the vicinity of the second set of values of θ_0, φ_0

$$\lim_{r\to\infty} \Psi_0(\boldsymbol{x}\,|\,E, \theta, \varphi) = \frac{\sqrt{2}}{(2\pi)^{\frac{3}{2}}(E)^{\frac{1}{4}}} \frac{(i\pi)}{r} \frac{\exp[-irp]}{\sqrt{\sin\theta}} \delta(\theta-(\pi-\lambda))\,\delta(\varphi-\Sigma) .$$

Or we may write generally for the whole range of integration over the angular variables

$$\lim_{r\to\infty} \Psi_0(\boldsymbol{x}\,|\,E, \theta, p) = \frac{\sqrt{2}\,i\pi}{(E)^{\frac{1}{4}}(2\pi)^{\frac{3}{2}} r\sqrt{\sin\theta}} \big[-\exp[irp]\delta(\theta-\lambda)\,\delta(\varphi-\sigma) + \tag{2.5}$$

$$+ \exp[-irp]\delta(\theta-(\pi-\lambda))\,\delta(\varphi-\Sigma)\big] .$$

Hence, asymptotically a plane wave behaves like a sum of spherical waves.

3. – Triangular form of the K operators. Expression for the potential.

In deriving the Gelfand-Levitan equation for the three-dimensional problem, we shall follow closely the procedure for obtaining the Gelfand-Levitan equation for the one-dimensional problem which was used in Part III of reference [1]. Hence, it will be convenient to give the analogues of the various quantities which appear in the present paper with those of the one-dimensional problem.

The eigenfunctions $\Psi_{\pm}(\boldsymbol{x}\,|\,E, \theta, \varphi)$ and $\Psi(\boldsymbol{x}\,|\,E, \theta, \varphi)$ of the present paper correspond to $\langle x\,|\,E, a\rangle_{\pm}$ and $\langle x\,|\,E, a\rangle$ of the previous paper. The kernel

$$K(\boldsymbol{x}\,|\,\boldsymbol{x}') \equiv K(r, \lambda, \sigma\,|\,r', \lambda', \sigma)$$

corresponds to $\langle x\,|\,K\,|\,x'\rangle$; the kernels $\mu_{-E}^{-1}(\theta, \varphi\,|\,\theta', \varphi')$ and $\mu_{-E}^{*-1}(\theta, \varphi\,|\,\theta', \varphi')$ to $\langle a\,|\,\mu_{-}^{-1}(E)\,|\,a'\rangle$ and $\langle a\,|\,\mu_{-}^{*-1}(E)\,|\,a'\rangle$. The weight kernel $\omega_E(\theta, \varphi\,|\,\theta', \varphi')$ corre-

sponds to $\langle a|\omega_c(E)|a'\rangle$; the scattering operator $S_k(\theta, q\,|\theta', q')$ to $\langle a|S(E)|a'\rangle$; the kernel $\Omega(\boldsymbol{x}|\boldsymbol{x}') \equiv \Omega(r, \lambda, \sigma|r', \lambda', \sigma')$ to $\langle x|\Omega|x'\rangle$.

We shall now follow the procedure of Part III of reference [1] to obtain the expression for the potential and thereby verify that we have given the correct triangularization condition on the operator K. Accordingly we introduce the operators

$$\begin{cases} U = I + K \\ U_0 = I + K_0 \end{cases} \tag{3.1}$$

where K and K_0 are triangular operators in the x-representation; *i.e.*

$$\begin{cases} K(\boldsymbol{x}|\boldsymbol{x}') \equiv K(r, \lambda, \sigma|r', \lambda', \sigma') \equiv 0 \\ K_0(\boldsymbol{x}|\boldsymbol{x}') \equiv K_0(r, \lambda, \sigma|r', \lambda', \sigma') \equiv 0 \end{cases} \quad \text{for } r > r' \tag{3.2}$$

The operator which corresponds to the scattering potential is given by (cf. eq. (5.7) Part III, ref. [1]).

$$V = H - H_0 = UH_0U_0 - H_0UU_0 = (KH_0 - H_0K) + (KH_0 - H_0K)K_0 \tag{3.3}$$

or equivalently

$$V(\boldsymbol{x}|\boldsymbol{x}') = -\nabla'^2 K(\boldsymbol{x}|\boldsymbol{x}') + \nabla^2 K(\boldsymbol{x}|\boldsymbol{x}') - \int \dot{\nabla}''^2 K(\boldsymbol{x}|\boldsymbol{x}'')\cdot K_0(\boldsymbol{x}''|\boldsymbol{x}')\,\mathrm{d}\boldsymbol{x}'' + \tag{3.4}$$

$$+ \int \nabla^2 K(\boldsymbol{x}|\boldsymbol{x}'')\, K_0(\boldsymbol{x}''|\boldsymbol{x}')\,\mathrm{d}\boldsymbol{x}''$$

In (3.4) the primes on the Laplacian operators refer to the variables on which they act. A dot has been inserted in the first integral to indicate that the Laplacian acts on the first factor of the integral only. We shall have occasion to use this convention later. Also, we have used the Hermitian nature of the Laplacian operator. It will be convenient to indicate the triangular nature of K and K_0 operators explicitly by writing

$$\begin{cases} K(r, \lambda, \sigma|r', \lambda', \sigma') = \eta(r' - r)\, K(r, \lambda, \sigma|r', \lambda', \sigma') \\ K_0(r, \lambda, \sigma|r', \lambda', \sigma') = \eta(r' - r)\, K_0(r, \lambda, \sigma|r', \lambda', \sigma') \end{cases} \tag{3.5}$$

where

$$\begin{cases} \eta(x) = 0 & \text{if } x < 0. \\ \eta(x) = 1 & \text{if } x > 0. \end{cases} \tag{3.6}$$

On expressing (3.4) in terms of spherical co-ordinates and using (3.5) we find that $V(\boldsymbol{x}\,|\,\boldsymbol{x}')$ is the sum of two terms one of which has $\delta(r-r')$ as a factor and the other of which has $\eta(r'-r)$ as a factor. From the general theory, the scattering potential V *must* be Hermitian. Hence the coefficient of the $\eta(r'-r)$ is zero, since the term which has this factor cannot possibly be Hermitian. We are left with the terms that have the δ-function factor

$$V(\boldsymbol{x}\,|\,\boldsymbol{x}') = \delta(r-r')V(r\,|\,\lambda,\sigma;\,\lambda',\sigma')\,, \tag{3.7}$$

where

$$V(r\,|\,\lambda,\sigma;\,\lambda',\sigma') = -\frac{2}{r^2}\frac{\partial}{\partial r}\,r^2K(r,\lambda,\sigma\,|\,r,\lambda',\sigma')\,. \tag{3.8}$$

Hence our triangularity conditions assure us that the scattering potential is diagonal in the radial co-ordinate.

4. – The weight operator; the scattering operator; the Gelfan-Levitan equation.

In accordance with the general procedure we introduce the eigenfunctions of H, $\Psi(\boldsymbol{x}\,|\,E,\theta,\varphi)\equiv\Psi(r,\lambda,\sigma\,|\,E,\theta,\varphi)$ given by

$$\Psi(\boldsymbol{r},\lambda,\sigma\,|\,E,\theta,\varphi) = \Psi_0(r,\lambda,\sigma\,|\,E,\theta,\varphi) + \tag{4.1}$$
$$+\int_r^\infty r'^2\,\mathrm{d}r'\int_0^\pi \sin\lambda'\,\mathrm{d}\lambda'\int_0^{2\pi}\mathrm{d}\sigma'\,K(r,\lambda,\sigma\,|\,r',\lambda',\sigma')\,\Psi_0(r',\lambda',\sigma'\,|\,E,\theta,\varphi)\,.$$

These eigenfunctions will enable us to find the weight operator needed for the completeness relationship in terms of the scattering operator. Let us write

$$\int_0^\pi \mathrm{d}\theta\int_0^{2\pi}\mathrm{d}\varphi\,\Psi(\boldsymbol{x}\,|\,E,\theta,\varphi)\,\mu_{-E}^{-1}(\theta,\varphi\,|\,\theta',\varphi') = \Psi_-(\boldsymbol{x}\,|\,E,\theta',\varphi')\,. \tag{4.2}$$

We are required to find the functions $\mu_{-E}^{-1}(\theta,\varphi\,|\,\theta',\varphi')$ and $\mu_{-E}^{*-1}(\theta,\varphi\,|\,\theta',\varphi')$ where

$$\mu_{-E}^{*-1}(\theta,\varphi\,|\,\theta',\varphi') = [\mu_{-E}^{-1}(\theta',\varphi'\,|\,\theta,\varphi)]^*\,. \tag{4.3}$$

(The asterisk on the left-hand side arose from the notation of Hermitian adjoint, but that on the right-hand side is simply complex conjugate.) The weight operator is given by

$$\omega_E(\theta,\varphi\,|\,\theta',\varphi') = \int_0^\pi \mathrm{d}\theta''\int_0^{2\pi}\mathrm{d}\varphi''\,\mu_{-E}^{-1}(\theta,\varphi\,|\,\theta'',\varphi'')\mu_{-E}^{*-1}(\theta'',\varphi''\,|\,\theta',\varphi')\,. \tag{4.4}$$

From the triangularity conditions on K it is clear that

$$\lim_{r\to\infty} \Psi(\boldsymbol{x}\,|\,E,\theta,\varphi) - \Psi_0(\boldsymbol{x}\,|\,E,\theta,\varphi) = 0\,. \tag{4.5}$$

It is also possible to show

$$\lim_{r\to\infty} \Psi_{\pm}(\boldsymbol{x}\,|\,E,\theta,\varphi) = \Psi_0(\boldsymbol{x}\,|\,E,\theta,\varphi) - \\ - \frac{1}{4\pi}\frac{(2\pi)^{\frac{3}{2}}\sqrt{2}}{\sqrt{\sin\lambda}\,(E)^{\frac{1}{4}}}\frac{\exp[\pm ipr]}{r}\,T_{\pm E}(\lambda,\sigma\,|\,\theta,\varphi)\,, \tag{4.6}$$

where

$$T_{\pm E}(\theta,\varphi\,|\,\theta',\varphi') = \iint \Psi_0^*(\boldsymbol{x}\,|\,E,\theta,\varphi)\,V(\boldsymbol{x}\,|\,\boldsymbol{x}')\,\Psi_{\pm}(\boldsymbol{x}'\,|\,E,\theta,\varphi)\,\mathrm{d}\boldsymbol{x}\,\mathrm{d}\boldsymbol{x}'\,. \tag{4.7}$$

The importance of the function $T_{-E}(\theta,\varphi\,|\,\theta',\varphi')$ is that the scattering operator $S_E(\theta,\varphi\,|\,\theta',\varphi')$ is simply expressed in terms of it:

$$S_E(\theta,\varphi\,|\,\theta',\varphi') = \delta(\theta-\theta')\,\delta(\varphi-\varphi') - 2\pi i\,T_{-E}(\theta,\varphi\,|\,\theta',\varphi')\,. \tag{4.8}$$

The scattering operator $S_E(\theta,\varphi\,|\,\theta',\varphi')$ of course is the scattering amplitude for scattering in the direction θ, φ when the incident wave is in the direction θ', φ'. It is unitary in the sense

$$\begin{cases} \displaystyle\int_0^{\pi}\mathrm{d}\theta''\int_0^{2\pi}\mathrm{d}\varphi''\,S_E(\theta,\varphi\,|\,\theta'',\varphi'')[S_E(\theta',\varphi'\,|\,\theta'',\varphi'')]^* = \delta(\theta-\theta')\,\delta(\varphi-\varphi')\,, \\ \displaystyle\int_0^{\pi}\mathrm{d}\theta''\int_0^{2\pi}\mathrm{d}\varphi''\,[S_E(\theta'',\varphi''\,|\,\theta,\varphi)]^*\,S_E(\theta'',\varphi''\,|\,\theta',\varphi') = \delta(\theta-\theta')\,\delta(\varphi-\varphi')\,. \end{cases} \tag{4.9}$$

To find $\mu_{-E}^{-1}(\theta,\varphi\,|\,\theta',\varphi')$ we take the limit of (4.2) as $r\to\infty$. On using (2.5) and (4.6) we find as our equation for $\mu_{-E}^{-1}(\theta,\varphi\,|\,\theta',\varphi')$ after some cancellation of common factors

$$-\exp[irp]\mu_{-E}^{-1}(\lambda,\sigma\,|\,\theta',\varphi') + \exp[irp]\mu_{-E}^{-1}(\pi-\lambda,\Sigma\,|\,\theta',\varphi') = \\ = -\exp[irp]\,\delta(\theta'-\lambda)\,\delta(\varphi'-\sigma) + \exp[-irp]\,\delta(\theta'-(\pi-\lambda))\,\delta(\varphi'-\Sigma) + \\ + 2\pi i\exp[ipr]\,T_{-E}(\lambda,\sigma\,|\,\theta',\varphi')\,,$$

where Σ is defined below eq. (2.4a).

On equating coefficients of like exponentials we have

$$(4.10)\quad \begin{cases} \mu^{-1}_{-E}(\lambda, \sigma\,|\,\theta', \varphi') = \delta(\theta' - \lambda)\,\delta(\theta - \sigma) - 2\pi i\, T_{-E}(\lambda, \sigma\,|\,\theta', \varphi') = S_E(\lambda, \sigma\,|\,\theta', \varphi')\,, \\ \mu^{-1}_{-E}(\pi - \lambda, \Sigma\,|\,\theta', \varphi') = \delta(\theta' - (\pi - \lambda))\,\delta(\varphi' - \Sigma)\,. \end{cases}$$

Eq. (4.10) lead to

$$(4.11)\quad \begin{cases} \mu^{-1}_{-E}(\lambda, \sigma\,|\,\theta', \varphi') = S_E(\lambda, \sigma\,|\,\theta', \varphi')\,, & \left(0 \leqslant \lambda < \frac{\pi}{2}\right), \\ \mu^{-1}_{-E}(\lambda, \sigma\,|\,\theta', \varphi') = \delta(\lambda - \theta')\,\delta(\sigma - \varphi') & \left(\frac{\pi}{2} \leqslant \lambda \leqslant \pi\right), \end{cases}$$

or

$$(4.12)\quad \mu^{-1}_{-E}(\theta, \varphi\,|\,\theta', \varphi') = \eta\left(\frac{\pi}{2} - \theta\right) S_E(\theta, \varphi\,|\,\theta', \varphi') + \eta\left(\theta - \frac{\pi}{2}\right)\delta(\theta - \theta')\,\delta(\varphi - \varphi')\,.$$

Also

$$(4.13)\quad \mu^{*-1}_{-E}(\theta, \varphi\,|\,\theta', \varphi') = \eta\left(\frac{\pi}{2} - \theta'\right)[S_E(\theta', \varphi'\,|\,\theta, \varphi)]^* + \\ + \eta\left(\theta - \frac{\pi}{2}\right)\delta(\theta - \theta')\,\delta(\varphi - \varphi')\,.$$

The weight operator is given by

$$(4.14)\quad \omega_E(\theta, \varphi\,|\,\theta', \varphi') = \int_0^{\pi} \mathrm{d}\theta'' \int_0^{2\pi} \mathrm{d}\varphi''\, \mu^{-1}_{-E}(\theta, \varphi\,|\,\theta'', \varphi'')\, \mu^{*-1}_{-E}(\theta'', \varphi''\,|\,\theta', \varphi') = \\ = \delta(\theta - \theta') + \eta\left(\theta - \frac{\pi}{2}\right)\eta\left(\frac{\pi}{2} - \theta'\right)[S_E(\theta', \varphi'\,|\,\theta, \varphi)]^* + \\ + \eta\left(\frac{\pi}{2} - \theta\right)\eta\left(\theta' - \frac{\pi}{2}\right) S_E(\theta, \varphi\,|\,\theta', \varphi')\,.$$

In (4.14) we have used the unitary property of $S_E(\theta, \varphi\,|\,\theta', \varphi')$ (eq. (4.9)). Hence the kernel of the Gelfand-Levitan equation is

$$(4.15)\quad \Omega(\boldsymbol{x}\,|\,\boldsymbol{x}') = \int_0^{\infty} \mathrm{d}E \int_0^{\pi/2} \mathrm{d}\theta \int_{\pi/2}^{\pi} \mathrm{d}\theta' \int_0^{2\pi} \mathrm{d}\varphi \int_0^{2\pi} \mathrm{d}\varphi'\, \Psi_0(\boldsymbol{x}\,|\,E, \theta, \varphi)\, S_E(\theta, \varphi\,|\,\theta', \varphi') \cdot \\ \cdot \Psi_0^*(\boldsymbol{x}'\,|\,E, \theta', \varphi') + \int_0^{\infty} \mathrm{d}E \int_{\pi/2}^{\pi} \mathrm{d}\theta \int_0^{\pi/2} \mathrm{d}\theta' \int_0^{2\pi} \mathrm{d}\varphi \int_0^{2\pi} \mathrm{d}\varphi' \cdot \\ \cdot \Psi_0(\boldsymbol{x}\,|\,E, \theta, \varphi)[S_E(\theta', \varphi'\,|\,\theta, \varphi)]^* \Psi_0^*(\boldsymbol{x}'\,|\,E, \theta, \varphi)\,.$$

In principle, the expression (4.15) is all that is required to set up the Gelfand-Levitan equation (1.18). Eq. (1.18) follows from

$$K(\boldsymbol{x}\,|\,\boldsymbol{x}') = -\,\Omega(\boldsymbol{x}\,|\,\boldsymbol{x}') - \int K(\boldsymbol{x}\,|\,\boldsymbol{x}'')\,\Omega(\boldsymbol{x}''\,|\,\boldsymbol{x}')\,\mathrm{d}\boldsymbol{x}'' ,$$

when we use polar co-ordinates and the triangularity condition (3.2).

However, we wish to simplify the expression (4.15) for Ω. Toward this end we shall need more properties of the scattering operator and the eigenfunctions of H and H_0 introduced in Section **1**.

First of all we note

$$\Psi_0(\boldsymbol{x}\,|\,E, \pi-\theta, \Phi) = \Psi_0^*(\boldsymbol{x}\,|\,E, \theta, \varphi) , \tag{4.16}$$

where

$$\begin{cases} \Phi = \varphi + \pi & \text{if } 0 \leqslant \varphi < \pi , \\ \Phi = \varphi - \pi & \text{if } \pi \leqslant \varphi < 2\pi . \end{cases} \tag{4.16a}$$

Secondly we have

$$\begin{cases} \Psi_-(\boldsymbol{x}\,|\,E, \pi-\theta, \Phi) = \Psi_+^*(\boldsymbol{x}\,|\,E, \theta, \varphi) , \\ \Psi_+(\boldsymbol{x}\,|\,E, \pi-\theta, \Phi) = \Psi_-^*(\boldsymbol{x}\,|\,E, \theta, \varphi) . \end{cases} \tag{4.17}$$

These equations follow from the integral equations for $\Psi_\pm(\boldsymbol{x}\,|\,E, \theta, \varphi)$ and the reality condition on $V(\boldsymbol{x}\,|\,\boldsymbol{x}')$. Likewise

$$\begin{cases} \Psi_0(\boldsymbol{x}\,|\,p, \pi-\theta, \Phi) = \Psi_0^*(\boldsymbol{x}\,|\,p, \theta, \varphi) , \\ \Psi_\pm(\boldsymbol{x}\,|\,p, \pi-\theta, \Phi) = \Psi_\mp^*(\boldsymbol{x}\,|\,p, \theta, \varphi) . \end{cases} \tag{4.18}$$

We wish now to prove

$$S_E(\theta, \varphi\,|\,\theta', \varphi') = S_E(\pi-\theta', \Phi'\,|\,\pi-\theta, \Phi) , \tag{4.19}$$

where Φ' is the related to φ' as Φ is to φ (eq. (4.16*a*)).

Eq. (4.19) follows in part from the reciprocity theorem in the theory of the scattering operator which states

$$T_{-E}(\theta, \varphi\,|\,\theta', \varphi') = [T_{+E}(\theta', \varphi'\,|\,\theta, \varphi)]^* \tag{4.20}$$

(see *e.g.* ref. [4]).

The quantities $T_{\pm E}(\theta, \varphi\,|\,\theta', \varphi')$ are defined by eq. (4.6) and (4.7).

[4] H. E. MOSES: *Nuovo Cimento*, **1**, 103 (1955).

But on using (4.16) and (4.17)

$$T_{-E}(\theta, \varphi \,|\, \theta', \varphi') = [T_{+}(\theta', \varphi' \,|\, \theta, \varphi)]^* = \tag{4.21}$$

$$= \iint \Psi_0(\boldsymbol{x} \,|\, E, \theta', \varphi')\, V(\boldsymbol{x} \,|\, \boldsymbol{x}')\, \Psi_{+}^*(\boldsymbol{x}' \,|\, E, \theta, \varphi)\, \mathrm{d}\boldsymbol{x}\, \mathrm{d}\boldsymbol{x}' =$$

$$= \iint \Psi_0^*(\boldsymbol{x} \,|\, E, \pi - \theta', \Phi')\, V(\boldsymbol{x} \,|\, \boldsymbol{x}')\, \Psi_{-}(\boldsymbol{x}' \,|\, E, \pi - \theta, \Phi)\, \mathrm{d}\boldsymbol{x}\, \mathrm{d}\boldsymbol{x}' =$$

$$= T_{-E}(\pi - \theta', \Phi' \,|\, \pi - \theta, \Phi)\,,$$

and finally the use of (4.8) leads to the desired result (4.19).

On using (4.19) and (4.16) we find that our expression for $\Omega(\boldsymbol{x} \,|\, \boldsymbol{x}')$ becomes:

$$\Omega(\boldsymbol{x} \,|\, \boldsymbol{x}') = \int_0^{\infty} \mathrm{d}E \int_0^{\pi/2} \mathrm{d}\theta \int_{\pi/2}^{\pi} \mathrm{d}\theta' \int_0^{2\pi} \mathrm{d}\varphi \int_0^{2\pi} \mathrm{d}\varphi'\, \Psi_0(\boldsymbol{x} \,|\, E, \theta, \varphi) \cdot \tag{4.22}$$

$$\cdot S_E(\theta, \varphi \,|\, \theta', \varphi') \Psi_0^*(\boldsymbol{x}' \,|\, E, \theta', \varphi') + \int_0^{\infty} \mathrm{d}E \int_0^{\pi/2} \mathrm{d}\theta \int_{\pi/2}^{\pi} \mathrm{d}\theta' \int_0^{2\pi} \mathrm{d}\varphi \int_0^{2\pi} \mathrm{d}\varphi'\, \Psi_0^*(\boldsymbol{x} \,|\, E, \theta, \varphi) \cdot$$

$$\cdot [S_E(\theta, \varphi \,|\, \theta', \varphi')]^* \Psi_0(\boldsymbol{x}' \,|\, E, \theta', \varphi')\,.$$

Clearly $\Omega(\boldsymbol{x} \,|\, \boldsymbol{x}')$ is real. Hence the Gelfand-Levitan eq. (1.18) set up with this kernel has a real solution if the solution is unique. To get an even simpler representation of Ω we use the eigenfunctions $\Psi_0(\boldsymbol{x} \,|\, p, \theta, \varphi)$, $\Psi_{\pm}(\boldsymbol{x} \,|\, p, \theta, \varphi)$. First of all, it is clear that though Ψ_0 has been defined for positive p only, we have by continuing p to negative values

$$\Psi_0(\boldsymbol{x} \,|\, -p, \theta, \varphi) = -\Psi_0^*(\boldsymbol{x} \,|\, p, \theta, \varphi)\,. \tag{4.23}$$

Similarly, using the integral equation for $\Psi_{\pm}(\boldsymbol{x} \,|\, p, \theta, \varphi)$, we find

$$\Psi_{\pm}(\boldsymbol{x} \,|\, -p, \theta, \varphi) = -\Psi_{\pm}^*(\boldsymbol{x} \,|\, \boldsymbol{p}, \theta, \varphi)\,. \tag{4.24}$$

Let us now introduce the function $b_p(\theta, \varphi \,|\, \theta', \varphi')$ defined by

$$b_p(\theta, \varphi \,|\, \theta', \varphi') = S_E(\theta, \varphi \,|\, \theta', \varphi') \qquad (p = \sqrt{E}). \tag{4.15}$$

Now

$$\begin{cases} \Psi_0(\boldsymbol{x} \,|\, E, \theta, \varphi) = \dfrac{1}{\sqrt{2p}}\, \Psi_0(\boldsymbol{x} \,|\, p, \theta, \varphi)\,, \\ \Psi_{\pm}(\boldsymbol{x} \,|\, E, \theta, \varphi) = \dfrac{1}{\sqrt{2p}}\, \Psi_{\pm}(\boldsymbol{x} \,|\, p, \theta, \varphi)\,, \end{cases} \qquad (p > 0); \tag{4.26}$$

(see eq. (1.11)).

On using (4.7) and (4.8) we can express $b_p(\theta, \varphi | \theta', \varphi')$ in terms of $\Psi_0(\boldsymbol{x} | p, \theta, \varphi)$ and $\Psi_-(\boldsymbol{x} | p, \theta, \varphi)$

$$b_p(\theta, \varphi | \theta', \varphi') = \delta(\theta - \theta')\delta(\varphi - \varphi') - \\ - \frac{2\pi i}{2p} \iint \Psi_0^*(\boldsymbol{x} | p, \theta, \varphi) V(\boldsymbol{x} | \boldsymbol{x}') \Psi_-(\boldsymbol{x}' | p, \theta', \varphi') \, \mathrm{d}\boldsymbol{x} \mathrm{d}\boldsymbol{x}' . \tag{4.27}$$

If we continue to negative values of p we find (see eq. (1.15)),

$$b_{-p}(\theta, \varphi | \theta', \varphi') = [b_p(\theta, \varphi | \theta', \varphi')]^* . \tag{4.28}$$

We can now obtain our simple expression for $\Omega(\boldsymbol{x} | \boldsymbol{x}')$. We obtain

$$\Omega(\boldsymbol{x} | \boldsymbol{x}') = \int_{-\infty}^{+\infty} \mathrm{d}p \int_0^{\pi/2} \mathrm{d}\theta \int_{\pi/2}^{\pi} \mathrm{d}\theta' \int_0^{2\pi} \mathrm{d}\varphi \int_0^{2\pi} \mathrm{d}\varphi' \cdot \\ \cdot \Psi_0(\boldsymbol{x} | p, \theta, \varphi) b_p(\theta, \varphi | \theta', \varphi') \Psi_0^*(\boldsymbol{x}' | p, \theta', \varphi') . \tag{4.29}$$

5. – The completeness relationship.

In accordance with the general formalism of reference [1], the eigenfunctions of $H, \Psi(\boldsymbol{x} | E, \theta, \varphi)$ given by (4.1) must satisfy the completeness relation

$$\int_0^{\infty} \mathrm{d}E \int_0^{\pi} \mathrm{d}\theta \int_0^{\pi} \mathrm{d}\theta' \int_0^{2\pi} \mathrm{d}\varphi \int_0^{2\pi} \mathrm{d}\varphi' \Psi(\boldsymbol{x} | E, \theta, \varphi) \omega_E(\theta, \varphi | \theta', \varphi') \Psi^*(\boldsymbol{x}' | E, \theta', \varphi') = \delta(\boldsymbol{x} - \boldsymbol{x}') . \tag{5.1}$$

In terms of the eigenfunctions of H given by

$$\Psi(\boldsymbol{x} | p, \theta, \varphi) = \Psi_0(\boldsymbol{x} | p, \theta, \varphi) + \iint K(\boldsymbol{x} | \boldsymbol{x}') \Psi_0(\boldsymbol{x}' | p, \theta, \varphi) \, \mathrm{d}\boldsymbol{x}' = \\ = \sqrt{2p} \Psi(\boldsymbol{x} | E, \theta, \varphi) , \tag{5.2}$$

the completeness relation is:

$$\int_0^{\infty} \mathrm{d}p \int_0^{\pi} \mathrm{d}\theta \int_0^{2\pi} \mathrm{d}\varphi \, \Psi(\boldsymbol{x} | p, \theta, \varphi) \Psi^*(\boldsymbol{x}' | p, \theta, \varphi) + \\ + \int_0^{\infty} \mathrm{d}p \int_0^{\pi/2} \mathrm{d}\theta \int_{\pi/2}^{\pi} \mathrm{d}\theta' \int_0^{2\pi} \mathrm{d}\varphi \int_0^{2\pi} \mathrm{d}\varphi' \Psi(\boldsymbol{x} | p, \theta, \varphi) b_p(\theta, \varphi | \theta', \varphi') \Psi^*(\boldsymbol{x}' | p, \theta', \varphi') + \\ + \int_0^{\infty} \mathrm{d}p \int_{\pi/2}^{\pi} \mathrm{d}\theta \int_0^{\pi/2} \mathrm{d}\theta' \int_0^{2\pi} \mathrm{d}\varphi \int_0^{2\pi} \mathrm{d}\varphi' \Psi(\boldsymbol{x} | p, \theta, \varphi) b_p(\theta', \varphi' | \theta, \varphi)]^* \Psi^*(\boldsymbol{x}' | \theta', \varphi') = \delta(\boldsymbol{x} - \boldsymbol{x}') . \tag{5.3}$$

Since $K(\boldsymbol{x}|\boldsymbol{x}')$ is real, we obtain on using (4.18), (4.23) and (5.2)

$$(5.4)\qquad \begin{cases} \Psi(\overset{*}{\boldsymbol{x}}|-p,\theta,\varphi) = -\Psi^*(\boldsymbol{x}|p,\theta,\varphi)\,, \\ \Psi(\boldsymbol{x}|p,\pi-\theta,\Phi) = \Psi^*(\boldsymbol{x}|p,\theta,\varphi)\,, \end{cases}$$

(Φ defined previously).

Using this result together with the relations for $b_p(\theta,q\,|\theta',q')$ obtainable from (4.19), (4.25), and (4.28) we have the somewhat simpler form of the completeness relation

$$(5.5)\qquad \int_0^\infty \mathrm{d}p \int_0^\pi \mathrm{d}\theta \int_0^{2\pi} \mathrm{d}\varphi\, \Psi(\boldsymbol{x}|p,\theta,\varphi)\Psi^*(\boldsymbol{x}'|p,\theta,\varphi) +$$

$$+\int_{-\infty}^{+\infty} \mathrm{d}p \int_0^{\pi/2} \mathrm{d}\theta \int_{\pi/2}^{\pi} \mathrm{d}\theta' \int_0^{2\pi} \mathrm{d}\varphi \int_0^{2\pi} \mathrm{d}\varphi'\, \Psi(\boldsymbol{x}|p,\theta,q) b_p(\theta,q\,|\theta',\varphi')\Psi^*(\boldsymbol{x}'|p,\theta',q') - \delta(\boldsymbol{x}-\boldsymbol{x}')\,.$$

RIASSUNTO (*)

Introduciamo una equazione di Gelfand-Levitan che permette di calcolare i potenziali di scattering da una parte dell'ampiezza di scattering nei problemi di scattering tridimensionale. L'equazione di Gelfand-Levitan introdotta, è una generalizzazione della equazione di Gelfand-Levitan unidimensionale di Kay e Moses. La parte richiesta dell'ampiezza di scattering è l'analogo del coefficiente di riflessione del caso unidimensionale. Il potenziale ottenuto è più generale di quello generalmente assunto nel problema di scattering tridimensionale, in quanto è diagonale nella variabile radiale ma è un operatore integrale reale nelle variabili angolari. Il potenziale puramente locale (cioè, il potenziale diagonale sia nella variabile radiale che in quelle angolari) risulta essere un caso speciale. In questo lavoro noi supponiamo che l'Hamiltoniano perturbato abbia uno spettro puramente continuo che coincide con quello dell'Hamiltoniano non perturbato. Il caso in cui vi siano anche autovalori puntuali si omette allo scopo di presentare le idee principali senza inutili complicazioni. Deriveremo l'equazione di Gelfand-Levitan dal metodo di Gelfand-Levitan più generalizzato da Kay e Moses. Questo formalismo garantisce già che il potenziale ottenuto riprodurrà il coefficiente di riflessione e che l'equazione è corretta. In un lavoro successivo, comunque, dimostreremo, con un formalismo elementare che non fa alcun uso della tecnica generale di Gelfand-Levitan, che l'equazione di Gelfand-Levitan, che deriviamo, è corretta; questa procedura ha il vantaggio di convincere immediatamente che l'equazione è quella giusta.

(*) *Traduzione a cura della Redazione.*

Teoria generale della radiazione di Čerenkov.

G. Zin

Facoltà di Scienze dell'Università - Torino

(ricevuto il 31 Luglio 1961)

Riassunto. — Si istituisce la teoria della radiazione di Čerenkov emessa da una carica in moto vario. Lo sviluppo di tale teoria è stato reso possibile dall'introduzione di un nuovo metodo di determinazione del campo elettromagnetico generato da una carica in moto, metodo di portata quanto mai generale. Il lavoro consta di una breve introduzione e di tre capitoli. Nel primo capitolo si introducono nell'elettromagnetismo i due punti di vista corrispondenti al lagrangiano e all'euleriano della dinamica dei fluidi. La formulazione maxwelliana dell'elettromagnetismo appartiene al punto di vista euleriano. Del campo elettromagnetico generato da una corrente di convezione si possono dare due diverse rappresentazioni integrali, corrispondenti ai due diversi punti di vista. Dalla uguaglianza dei valori forniti dalle due rappresentazioni integrali si ottengono relazioni integrali, nelle quali figurano i potenziali e i campi generati dall'elemento di carica in moto. L'arbitrarietà della corrente di convezione permette di scegliere questa in modo da rendere le equazioni integrali facilmente risolubili. Si perviene così a un teorema il quale fornisce le trasformate di Fourier, rispetto al tempo, dei potenziali e campi generati da una carica elementare in moto. Tale teorema è quanto mai generale, valendo senza limite alcuno per la velocità e l'accelerazione della carica, e qualunque sia il mezzo, omogeneo o non omogeneo, conduttore o non conduttore, isotropo o anisotropo, dispersivo o non dispersivo. Evidentemente il problema che ora si pone è quello dell'antitrasformazione delle espressioni che così si ottengono. Un elegante procedimento viene a tale scopo istituito e viene illustrato in una serie di applicazioni nel corso dei capitoli secondo e terzo. I mezzi considerati nei Cap. II e III sono dielettrici isotropi, omogenei, riempienti tutto lo spazio, potendo essi tuttavia essere dispersivi o non dispersivi. Nel Cap. II si considera il moto rettilineo e uniforme della carica. Nel caso della velocità v della carica maggiore di c/n (c=velocità della luce nel vuoto, n=indice di rifrazione del mezzo) e del dielettrico non dispersivo si ottiene la soluzione di Tamm. Questa viene esaminata da un punto di vista fisico. Il verso dei campi vi appare in contrasto con le leggi dell'elettromagnetismo e con il principio di conservazione dell'energia. Una discussione della questione mette in evidenza che la causa è da ascriversi al fatto che il

dielettrico non dispersivo è un limite di casi più aderenti alla realtà fisica. Funzioni che in un dielettrico dispersivo sono finite diventano infinite in un dielettrico non dispersivo. Per metterle in evidenza in tale secondo caso si rende necessario forzare il procedimento di derivazione. Il problema della determinazione del campo elettromagnetico viene allora ripreso, usando nuove regole di derivazione (che vengono tuttavia giustificate). Balza allora evidente l'esistenza sul fronte d'onda di campi di intensità infinita, dei quali l'algoritmo introdotto consente di determinare la direzione e il verso. Tali campi sono di gran lunga più importanti di quelli esistenti posteriormente al fronte d'onda e descritti dalla rappresentazione di Tamm. In prossimità del fronte d'onda i campi elettrico e magnetico della soluzione di Tamm sono paralleli, ma opposti, ai campi impulsivi, rispettivamente elettrico e magnetico, esistenti sul fronte d'onda. Con l'introduzione di questi ultimi scompaiono le incongruenze menzionate. Il Cap. III è destinato allo studio del moto vario. Se la traiettoria C della carica è la curva di equazioni parametriche $x=x(\theta)$, $y=y(\theta)$, $z=z(\theta)$ $(-\infty<\theta<+\infty)$e se la carica percorre la curva C con la legge del moto $\theta=t$, il problema della determinazione del campo elettromagnetico in un punto $P(x, y, z)$ è dominato dal comportamento della funzione τ della variabile θ così definita

$$\tau = \theta + \frac{n}{c}\sqrt{[(x - x(\theta)]^2 + [y - y(\theta)]^2 + [z \quad z(\theta)]^2} = \theta + \frac{n}{c}r(\theta) ,$$

essendo $r(\theta)$ la distanza del punto $P(x, y, z)$ dal punto $(x(\theta), y(\theta), z(\theta))$ della curva C. Se la velocità v della carica è sempre minore di c/n, la funzione $\tau(\theta)$ è sempre crescente. Se la velocità v della carica supera lungo tutta o lungo un tratto della traiettoria il valore c/n, la funzione $\tau(\theta)$ ammette almeno un punto di minimo. Il caso che corrisponde alle ordinarie manifestazioni della radiazione di Čerenkov è quello in cui $\tau(\theta)$ ha un solo minimo. I diversi problemi vengono così classificati secondo il comportamento della funzione $\tau(\theta)$. Alle variabili θ e τ si danno rispettivamente i nomi di variabile di partenza (o di emissione) e di variabile di arrivo (o di ricezione). In conseguenza dell'impostazione euleriana dell'elettromagnetismo di Maxwell l'applicazione del teorema generale stabilito al Cap. I conduce ad esprimere le F-trasformate dei potenziali e dei campi mediante integrali nei quali la variabile d'integrazione è la variabile di partenza. Il metodo di antitrasformazione che viene qui introdotto consiste nel fare assumere alle dette rappresentazioni integrali l'aspetto formale di F-trasformate manipolando opportunamente le funzioni integrande. Si constata che lo scopo viene raggiunto mediante una sostituzione di variabile: basta che le F-trasformate siano espresse da integrali nei quali la variabile di integrazione è la variabile di arrivo. Si studia dapprima il caso in cui $\tau(\theta)$ è sempre crescente. Ciò costituisce un interessante esame del nuovo metodo, perchè esso viene così applicato a un problema noto e di cui si conoscono i risultati. In seguito si passa a studiare il caso di $\tau(\theta)$ con un solo minimo. Nessuna difficoltà sorge per quanto riguarda la trattazione dei potenziali scalare e vettore. Si determinano le equazioni del fronte d'onda. Questo risulta ancora costruibile mediante il principio di Huyghens. Per quanto riguarda i campi si danno due rappresentazioni integrali delle F-trasformate rispetto alla

variabile di arrivo. Tali rappresentazioni mettono entrambe in evidenza l'effetto dell'accelerazione. Una di esse è costruita mediante integrali convergenti ed è particolarmente utile nello studio dei problemi energetici e di altri problemi interessanti la radiazione di Čerenkov nei mezzi dispersivi. L'altra è una rappresentazione simbolica, ricavata con il procedimento di derivazione esposto al Cap. II e utile per la determinazione dei campi nei mezzi non dispersivi. In un mezzo non dispersivo il fronte d'onda risulta ancora dominato dai campi impulsivi. Questi dipendono dalla velocità e non dall'accelerazione. Come nel moto rettilineo e uniforme, anche nel moto vario si manifesta sul fronte d'onda la brusca inversione del campo elettromagnetico. Nella regione posteriore al fronte d'onda si stende un campo elettromagnetico che si può scindere in due componenti, una dovuta alla velocità e l'altra dovuta all'accelerazione. La componente dovuta all'accelerazione segue una legge di distribuzione nello spazio ben diversa dalla componente dovuta alla velocità. Chiude il Cap. III, più che altro per illustrare le possibilità offerte dal metodo, una rapida trattazione del caso in cui la funzione $\tau(\theta)$ ha un numero qualunque di massimi e minimi. Il presente scritto è stato dedicato esclusivamente alla esposizione di metodi e alla descrizione del campo elettromagnetico generato da una carica in moto. I problemi energetici relativi alla radiazione di Čerenkov, come pure l'esame quantitativo dell'influenza dell'accelerazione nelle esperienze costituirà l'oggetto di un prossimo scritto dal titolo *L'energia della radiazione di Čerenkov*.

1. – Introduzione.

1·1. – Un metodo per la determinazione del campo elettromagnetico generato da una carica puntiforme in moto consiste nel partire dalle note espressioni integrali che forniscono i potenziali scalare e vettore generati da una distribuzione di corrente di convezione. Si deducono poi le espressioni particolari alle quali tali integrali danno luogo nel caso in cui tutta la carica esistente nel mezzo si riduce a una carica concentrata nell'intorno di un punto mobile. Si giunge così ai potenziali di Lienard e Wiechert. Da questi il campo elettromagnetico si ricava mediante le relazioni di noto significato

$$\mathscr{E} = -\operatorname{grad}\varphi - \frac{1}{c}\frac{\partial \mathscr{A}}{\partial t}, \qquad \mathscr{H} = \frac{1}{\mu}\operatorname{rot}\mathscr{A}.$$

È questo il metodo più antico. Lo si trova riportato in molti trattati classici di elettromagnetismo.

In seguito Sommerfeld, ispirandosi a certe relazioni introdotte dalla relatività e riprendendo una precedente idea di Herglotz (*), concepiva un altro

(*) Per una bibliografia sul metodo di Sommerfeld si veda: W. Pauli: *Teoria della relatività* (ed. it.) (Torino, 1958), pp. 137-140; J. A. Stratton: *Teoria dell'elettromagnetismo* (ed. it.) (Torino, 1952), p. 653.

metodo di determinazione dei potenziali e dei campi generati da una carica mobile e puntiforme. SOMMERFELD considera nel suo metodo anche valori immaginari del tempo e ricorre ad integrazioni nel piano complesso di tale variabile.

La deduzione dei campi dai potenziali di Lienard e Wiechert comporta una fastidiosa esecuzione di derivate di funzioni implicitamente definite. Il metodo di Sommerfeld non è evidentemente altrettanto elementare, ma conduce al risultato in modo più agevole.

Entrambi tali metodi sono applicabili nel caso del moto della carica nel vuoto o in un dielettrico perfetto, non dispersivo. Essi valgono per il moto comunque vario della carica e sono necessariamente soggetti alla limitazione che la velocità di questa sia sempre minore della velocità c/n della luce nel mezzo ($c =$ velocità della luce nel vuoto, $n =$ indice di rifrazione del mezzo).

1'2. – Nel 1937 FRANK e TAMM esponevano una teoria atta a descrivere il campo elettromagnetico generato da una carica in moto rettilineo e uniforme, in un dielettrico omogeneo e dispersivo, con velocità maggiore di c/n. Essi dimostravano che in tali condizioni la carica irradia e determinavano l'espressione dell'energia irradiata dalla carica per unità di lunghezza del percorso. Tale teoria forniva un'interpretazione di esperienze condotte da ČERENKOV, il quale poi in esperienze successive confermava quantitativamente la bontà della teoria di Frank e Tamm (*).

Nel 1939 TAMM pubblicava un'altra trattazione del fenomeno. Mentre il primitivo lavoro di FRANK e TAMM considerava mezzi dispersivi e i campi elettrici e magnetici vi erano rappresentati tramite le loro trasformate di Fourier (e quindi mediante rappresentazioni integrali), nel lavoro del 1939 TAMM considerava anche il dielettrico non dispersivo. In tal caso egli riusciva a liberarsi delle rappresentazioni integrali pervenendo a una semplicissima descrizione analitica del campo elettromagnetico generato dalla carica in moto (tale descrizione sarà tuttavia, nel corso del presente lavoro, riscontrata incompleta).

In seguito intorno alla radiazione di Čerenkov fioriva una vasta letteratura, che al giorno d'oggi va assumendo proporzioni notevoli. Tuttavia in tutte le trattazioni teoriche si è sempre considerato il caso del moto rettilineo e uniforme della carica, per cui a tutt'oggi nessuna precisa idea si ha dell'influenza che la decelerazione della carica esercita sulla radiazione di Čerenkov. D'altronde in un dielettrico solido o liquido un elettrone perde un'energia dell'ordine di alcuni MeV per cm.

(*) Per la bibliografia relativa all'effetto Čerenkov si veda J. V. JELLEY: *Čerenkov Radiation* (London, 1958).

1'3. – Con il presente lavoro si intende esporre un metodo di grande generalità per la determinazione del campo elettromagnetico generato da una carica in moto, metodo valido qualunque sia il mezzo e qualunque sia la velocità e l'accelerazione della carica. Tale metodo sarà poi applicato allo studio della radiazione di Čerenkov emessa da una carica in moto vario.

Il presente scritto è destinato esclusivamente all'esposizione del metodo e alla descrizione del campo elettromagnetico generato da una carica elementare in moto. I problemi energetici relativi alla radiazione di Čerenkov come pure l'aspetto quantitativo di fenomeni interessanti l'esperienza saranno considerati in altro scritto dal titolo *L'energia della radiazione di Čerenkov* di prossima pubblicazione.

Capitolo Primo

INTRODUZIONE NELL'ELETTROMAGNETISMO DEI PUNTI DI VISTA LAGRANGIANO ED EULERIANO DELLA DINAMICA DEI FLUIDI

2. – Formula fondamentali. Introduzione della rappresentazione attuale del campo elettromagnetico.

2'1. – Le equazioni dell'elettromagnetismo relative a un mezzo omogeneo di costante dielettrica ε e permeabilità magnetica μ notoriamente sono:

$$\text{(1)} \qquad \operatorname{rot}\mathscr{E} + \frac{\mu}{c}\frac{\partial \mathscr{H}}{\partial t} = 0\,, \qquad \operatorname{div}\mathscr{H} = 0\,,$$

$$\text{(2)} \qquad \operatorname{rot}\mathscr{H} - \frac{\varepsilon}{c}\frac{\partial \mathscr{E}}{\partial t} = \frac{4\pi}{c}\boldsymbol{j}\,, \qquad \operatorname{div}\mathscr{E} = \frac{4\pi\varrho}{\varepsilon}\,.$$

Esse ammettono gli integrali:

$$\text{(3)} \qquad \mathscr{E} = -\operatorname{grad}\varphi - \frac{1}{c}\frac{\partial \mathscr{A}}{\partial t}\,, \qquad \mathscr{H} = \frac{1}{\mu}\operatorname{rot}\mathscr{A}\,,$$

dove notoriamente è

$$\text{(4)} \qquad \begin{cases} \mathscr{A}(x,y,z,t) = \dfrac{\mu}{c}\displaystyle\int \frac{\boldsymbol{j}(\xi,\eta,\zeta,t-nr/c)}{r}\,\mathrm{d}S\,, \\ \varphi(x,y,z,t) = \dfrac{1}{\varepsilon}\displaystyle\int \frac{\varrho(\xi,\eta,\zeta,t-nr/c)}{r}\,\mathrm{d}S\,, \end{cases} \qquad n = \sqrt{\varepsilon\mu}\,.$$

Gli integrali si intendono estesi a tutto lo spazio. È inoltre

$$r = \sqrt{(x-\xi)^2 + (y-\eta)^2 + (z-\zeta)^2},$$

mentre dS è l'elemento di volume avente il centro nel punto di coordinate ξ, η, ζ, punto che costituisce la variabile d'integrazione.

I potenziali (4) vengono spesso denominati potenziali ritardati di Kirchhoff.

Dalle (2) discende la nota equazione di continuità (conservazione della carica)

$$\operatorname{div} \boldsymbol{j} = -\frac{\partial \varrho}{\partial t}. \tag{5}$$

È superfluo avvertire che tutte le correnti che vengono considerate nel presente scritto sono correnti di convezione o di Lorentz, per cui il rapporto $\boldsymbol{j}/\varrho$ ha il significato di *velocità della carica*.

2'2. – Notoriamente dalle (4) e (3) si può dedurre il campo elettromagnetico generato dal movimento di una carica elettrica e puntiforme q. Nel caso in cui il mezzo sia il vuoto, tale campo ammette i noti potenziali ritardati di Lienard e Wiechert (*):

$$\varphi = \frac{q}{s}, \qquad \mathscr{A} = \frac{q}{c}\frac{\boldsymbol{v}}{s}, \tag{6}$$

essendosi posto

$$s = r - \frac{\boldsymbol{v}\cdot\boldsymbol{r}}{c}. \tag{7}$$

In tali relazioni φ e $\mathscr{A}$ sono i potenziali scalare e vettore in un punto P all'istante t, $\boldsymbol{r}$ è il segmento che va dal punto P' al punto P, essendo P' il punto in cui si trova la carica all'istante t' legato a t dalla relazione

$$t - t' = \frac{r}{c}, \tag{8}$$

mentre il vettore $\boldsymbol{v}$ denota la velocità della carica al detto istante t'.

Inoltre, con le stesse convenzioni sul significato dei simboli, i campi elettrico $\mathscr{E}$ e magnetico $\mathscr{H}$ generati dalla carica q sono forniti dalle note espres-

(*) Quantunque la deduzione delle (6) e (9) sia riportata in molti trattati di elettromagnetismo, tuttavia il metodo generale che viene qui esposto permetterà di ritrovarle, anzi permetterà di stabilire formule generali, di cui le (6) e (9) sono casi particolari.

sioni:

$$(9)\qquad \begin{cases} \dfrac{\mathscr{E}}{q} = \dfrac{1-\beta^2}{s^3}\left(\boldsymbol{r} - \dfrac{r\boldsymbol{v}}{c}\right) + \dfrac{1}{s^3 c^2}\boldsymbol{r}\wedge\left[\left(\boldsymbol{r} - \dfrac{r}{c}\boldsymbol{v}\right)\wedge\dot{\boldsymbol{v}}\right], \\ \mathscr{H} = \dfrac{\boldsymbol{r}}{r}\wedge\mathscr{E}, \qquad \beta = \dfrac{v}{c}, \end{cases}$$

dove $\dot{\boldsymbol{v}}$ denota l'accelerazione della carica all'istante t'.

2'3. – Nel caso del moto rettilineo e uniforme della carica q le (6) e (9) possono essere opportunamente trasformate. Siano pertanto P il punto in cui si vuole conoscere il campo elettromagnetico all'istante t, Q il punto in cui si trova la carica q al medesimo istante t, P' il punto in cui si trova la carica q all'istante t' definito dalla (8) (vedasi annessa figura). Poichè la carica è supposta muoversi con velocità costante $\boldsymbol{v}$, è

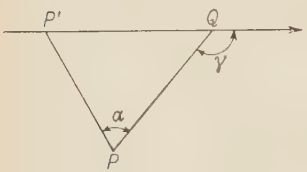

Fig. 1.

$$\boldsymbol{P'Q} = (t-t')\boldsymbol{v} = \frac{r}{c}\boldsymbol{v}, \qquad \boldsymbol{P'P} = \boldsymbol{r},$$

e quindi

$$\boldsymbol{r} - \frac{r}{c}\boldsymbol{v} = \boldsymbol{P'P} + \boldsymbol{QP'} = \boldsymbol{QP}.$$

Da questa moltiplicando scalarmente per $\boldsymbol{r}$ si ottiene ancora

$$r^2 - \frac{\boldsymbol{r}\cdot\boldsymbol{v}}{c}r = \boldsymbol{r}\cdot\boldsymbol{QP} \qquad \text{ossia} \qquad s = \frac{\boldsymbol{r}}{r}\cdot\boldsymbol{QP}.$$

È ora (vedasi figura)

$$\frac{\boldsymbol{r}}{r}\cdot\boldsymbol{QP} = QP\cos\alpha,$$

essendo α l'angolo formato dai vettori $\boldsymbol{PP'}$ e $\boldsymbol{PQ}$. Ancora, designando con γ l'angolo formato dal vettore $\boldsymbol{QP}$ con la velocità $\boldsymbol{v}$, per il teorema dei seni si ottiene:

$$\frac{r}{\sin\gamma} = \frac{P'Q}{\sin\alpha},$$

da cui, essendo per quanto visto sopra $P'Q = (r/c)v$,

$$\sin\alpha = \frac{v}{c}\sin\gamma = \beta\sin\gamma.$$

La precedente espressione di s può perciò essere così sostituita:

$$s = QP\cos\alpha = QP\sqrt{1-\beta^2\sin^2\gamma}.$$

Le espressioni (6) dei potenziali diventano allora:

$$(10) \qquad \mathcal{A} = \frac{q}{c}\frac{\boldsymbol{v}}{QP\sqrt{1-\beta^2\sin^2\gamma}}, \qquad \varphi = \frac{q}{QP\sqrt{1-\beta^2\sin^2\gamma}},$$

mentre l'espressione (9) del campo elettrico (si osservi che ora è $\dot{\boldsymbol{v}} = 0$ e si tenga presente l'espressione sopra scritta di $\boldsymbol{QP}$) può essere sostituita con la seguente altra:

$$(11) \qquad \mathcal{E} = q\frac{1-\beta^2}{(1-\beta^2\sin^2\gamma)^{\frac{3}{2}}}\frac{\boldsymbol{QP}}{QP^3}.$$

Tale espressione mostra che quando la carica è in moto rettilineo uniforme il campo elettrico da essa generato in un punto P ha sempre la direzione della retta passante per la carica e per il punto P.

Poichè sopra si è visto essere $\boldsymbol{r} = (r/c)\boldsymbol{v} + \boldsymbol{QP}$, l'espressione del campo magnetico, cioè di $(\boldsymbol{r}/r)\wedge\mathcal{E}$, dà luogo al prodotto vettoriale $(\boldsymbol{r}/r)\wedge\boldsymbol{QP}$, che può essere sostituito con $(\boldsymbol{v}/c)\wedge\boldsymbol{QP}$ e si ha

$$(12) \qquad \mathcal{H} = \frac{\boldsymbol{v}}{c}\wedge\mathcal{E}.$$

Si osservi che tutte le grandezze simboleggiate nelle formule (10), (11) e (12) si riferiscono allo stesso istante t in cui si considera il campo elettromagnetico in P. A una tale rappresentazione, per distinguerla dalle rappresentazioni anticipate e ritardate, si darà il nome di *rappresentazione attuale.*

3. – Due diversi procedimenti per calcolare il campo elettromagnetico generato da una corrente di Lorentz.

Alla luce di un esempio semplicissimo, forse del più semplice che si possa pensare, saranno ora illustrati due diversi procedimenti di calcolo del campo elettromagnetico generato da una corrente di Lorentz.

Si consideri una retta orientata x percorsa da una corrente costante I, dovuta a una distribuzione uniforme di carica elettrica, di densità lineica ϱ_l, spostantesi con velocità v. È così

$$I = \varrho_l v.$$

Il calcolo dei campi elettrico e magnetico generati in un punto P dello spazio dalla predetta distribuzione mobile di carica elettrica può essere effettuato in due modi concettualmente diversi.

Primo procedimento. – Esso consiste nel determinare l'integrale delle equazioni dell'elettromagnetismo corrispondente al particolare problema in oggetto. Dato il caso estremamente semplice, si può abbreviare il calcolo ricorrendo a qualche nota proposizione deducibile dalle equazioni generali dell'elettromagnetismo, quali la legge di Biot e Savart relativa al campo magnetico e il teorema del flusso del campo elettrico. Dalla legge di Biot e Savart si ha:

$$\mathscr{H} = \frac{2I}{c}\frac{\boldsymbol{i}\wedge\boldsymbol{R}}{R^2},$$

dove $\boldsymbol{i}$ è un vettore unitario, parallelo ed equiorientato all'asse x. Tale formula esprime il campo magnetico in un punto P a distanza R dalla retta x. Si è posto $\boldsymbol{R} = \boldsymbol{OP}$, essendo O il piede della perpendicolare all'asse x passante per P. Osservando che è $I = \varrho_l v$ e ponendo $v\boldsymbol{i} = \boldsymbol{v}$, la precedente può anche essere così trascritta

$$\mathscr{H} = \frac{2\varrho_l}{c}\frac{\boldsymbol{v}\wedge\boldsymbol{R}}{R^2}. \tag{13}$$

Per quanto riguarda il campo elettrico, il flusso di questo uscente dalla superficie laterale di un cilindro di raggio R, di altezza h (molto grande) e avente l'asse sulla retta x, è $2\pi Rh\mathscr{E}$. Esso vale notoriamente 4π volte la carica totale $\varrho_l h$ contenuta nel cilindro. Perciò

$$\mathscr{E} = 2\varrho_l\frac{\boldsymbol{R}}{R^2}. \tag{14}$$

Tale formula fornisce il campo elettrico in un punto P a distanza R dalla retta x.

Secondo procedimento. – Esso consiste nel considerare il campo elettromagnetico generato dalla predetta distribuzione di carica mobile come somma di tanti campi elettromagnetici elementari dovuti alle singole cariche $\varrho_l \mathrm{d}x$ viaggianti con velocità $\boldsymbol{v}$. Tale procedimento è concettualmente diverso dal primo in quanto che esso considera elementi cinematici che al primo sono del tutto estranei. Il calcolo del campo elettromagnetico sarà ora condotto ricorrendo alla rappresentazione attuale dei campi, introdotta al n. 2'3 precedente. Si osservi che, a differenza del primo, tale secondo procedimento presuppone la limitazione

$$v < c.$$

Il piede O della perpendicolare all'asse x passante per P sia l'origine delle ascisse. Sia x l'ascissa di un punto generico Q dell'asse x. Allora, per la (11), la carica $\varrho_l \mathrm{d}x$ avente il centro in Q genera nel punto P all'istante t un campo

elettrico

$$d\mathcal{E} = \frac{\varrho_l \, dx(1-\beta^2)}{(1-\beta^2 \sin^2\gamma')^{\frac{3}{2}}} \frac{\boldsymbol{QP}}{QP^3} .$$

Ma, ricordando il significato di $\sin\gamma$, è

$$\sin\gamma = \frac{R}{PQ} ,$$

e quindi

$$d\mathcal{E} = \frac{\varrho_l \, dx(1-\beta^2)}{(PQ^2 - \beta^2 R^2)^{\frac{3}{2}}} \boldsymbol{QP} = \frac{\varrho_l \, dx(1-\beta^2)}{[(1-\beta^2)R^2 + x^2]^{\frac{3}{2}}} (\boldsymbol{R} - x\boldsymbol{i}) .$$

Poichè mutando x in $-x$ la componente del vettore $d\mathcal{E}$ parallela all'asse x cambia di segno, basta limitare l'integrazione alla sola componente normale. Allora, introducendo le posizioni

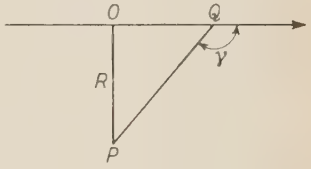

Fig. 2.

$$a = R\sqrt{1-\beta^2}, \qquad x = a\lambda ,$$

dove, per l'ipotesi $v < c$, il valore di a risulta reale e positivo, si ha

$$\mathcal{E} = \varrho_l(1-\beta^2)\boldsymbol{R}\int_{-\infty}^{+\infty} \frac{dx}{(a^2+x^2)^{\frac{3}{2}}} = \varrho_l \frac{1-\beta^2}{a^2} \boldsymbol{R}\int_{-\infty}^{+\infty} \frac{d\lambda}{(1+\lambda^2)^{\frac{3}{2}}} = \frac{\varrho_l}{R^2}\boldsymbol{R}\int_{-\infty}^{+\infty} \frac{d\lambda}{(1+\lambda^2)^{\frac{3}{2}}} .$$

Con la sostituzione $\lambda = \sinh u$, per cui $1+\lambda^2 = \cosh^2 u$, $d\lambda = \cosh u \, du$, si ottiene

$$\int_{-\infty}^{+\infty} \frac{d\lambda}{(1+\lambda^2)^{\frac{3}{2}}} = \int_{-\infty}^{+\infty} \frac{du}{\cosh^2 u} = [\operatorname{tgh} u]_{-\infty}^{+\infty} = 2 ,$$

per cui

$$\mathcal{E} = \frac{2\varrho_l}{R^2}\boldsymbol{R} . \tag{15}$$

che coincide con la (14).

Per calcolare il campo magnetico in P basta ricorrere alla (12). Ma questa, a motivo della costanza del vettore $\boldsymbol{v}$ lungo tutta la retta, ci dice che per ottenere il campo magnetico in P basta eseguire il prodotto $(\boldsymbol{v}\wedge\mathcal{E})/c$; così che dalla (15) subito si ricava

$$\mathcal{H} = \frac{2\varrho_l}{cR^2}\boldsymbol{v}\wedge\boldsymbol{R} , \tag{16}$$

che coincide con la (13).

Concludendo: Il primo procedimento sussiste qualunque sia la velocità v delle cariche. Il secondo procedimento è applicabile soltanto se è $v < c$. Nel comune intervallo $v < c$ di applicabilità i due procedimenti portano allo stesso risultato.

4. – Considerazioni sui due metodi precedenti. Introduzione nell'elettromagnetismo dei due punti di vista corrispondenti all'euleriano e al lagrangiano della dinamica dei fluidi.

4'1. – I due procedimenti di calcolo usati al numero precedente si ispirano a due diverse concezioni che corrispondono ai due differenti punti di vista, euleriano e lagrangiano della dinamica dei fluidi.

Secondo il punto di vista euleriano il comportamento di un fluido viene descritto mediante un certo numero di grandezze, quali la velocità, la pressione, la densità, la temperatura, etc., che sono funzioni del punto dello spazio, oltre che del tempo. Lo stato del fluido a un certo istante è pertanto interpretabile come lo stato, a quell'istante, dei singoli elementi dello spazio occupato dal fluido, stato definito dalle predette funzioni.

Invece il punto di vista lagrangiano investe in pieno l'aspetto cinematico del fluido, il quale viene considerato un insieme di particelle che si muovono mantenendo ciascuna la propria individualità. Secondo il punto di vista lagrangiano descrivere il comportamento del fluido significa essere in possesso della legge del moto di ogni singola particella.

4'2. – Anche nell'elettromagnetismo si possono introdurre due differenti punti di vista, corrispondenti a quelli di Eulero e di Lagrange della dinamica dei fluidi. Ciò, beninteso, fin che ci si limiti a considerare correnti di convezione, dette anche di Lorentz. Il primo consiste nello stabilire le relazioni tra campo elettromagnetico e corrente quando questa, intesa come un fluido, venga descritta secondo il punto di vista euleriano; ossia quando la corrente sia definita mediante le funzioni ϱ e $\boldsymbol{j}$. Il secondo consiste nello stabilire le relazioni tra campo elettromagnetico e corrente, quando questa sia descritta secondo il punto di vista di Lagrange, cioè quando siano note le leggi del moto delle singole cariche elementari.

Le equazioni di Maxwell esprimono le leggi dell'elettromagnetismo secondo il primo punto di vista. Infatti esse si fondano sulla descrizione euleriana della corrente. Questa vi è rappresentata mediante le funzioni $\boldsymbol{j}$ e ϱ del punto (x, y, z) dello spazio e del tempo t.

Nessuna limitazione impongono le equazioni dell'elettromagnetismo al modulo del vettore $\boldsymbol{j}/\varrho$. Ciò risulta particolarmente evidente nell'integrazione di Kirchhoff. Infatti le operazioni (4) e (3) secondo le quali dalla densità di cor-

rente $\boldsymbol{j}$ e dalla densità di carica ϱ si ricavano i campi elettrico e magnetico sono lineari rispetto a $\boldsymbol{j}$ e ϱ. Le operazioni da eseguirsi su $\boldsymbol{j}$ e ϱ, indicate dalle (4) e (3), non presuppongono pertanto limitazione alcuna per il modulo j/ϱ. Nemmeno la (5), da cui le funzioni $\boldsymbol{j}$ e ϱ sono legate, è tale da subordinare il rapporto j/ϱ a particolari restrizioni.

Il primo procedimento di calcolo esposto al numero precedente costituisce un esempio in tal senso. Esso, come si è visto, sussiste qualunque sia il rapporto I/ϱ_l.

43. – Per rappresentare il campo elettromagnetico con il metodo corrispondente alla descrizione lagrangiana della corrente è necessario ricavare dalle funzioni $\boldsymbol{j}(x, y, z, t)$ e $\varrho(x, y, z, t)$ la legge del moto delle singole cariche elementari, tenendo presente che nel caso della corrente di convezione o di Lorentz la velocità $\boldsymbol{v}(x, y, z, t)$ della carica nel punto (x, y, z) all'istante t è definita dalla relazione

$$\boldsymbol{v}(x, y, z, t) = \frac{\boldsymbol{j}(x, y, z, t)}{\varrho(x, y, z, t)}.$$

Mediante le formule che forniscono i potenziali e i campi generati da una carica elementare in moto si possono allora ottenere i potenziali e i campi generati da tutto il fluido, integrando rispetto a tutte le particelle in moto.

5. – Idea del metodo di calcolo del campo elettromagnetico generato da una carica in moto.

Il metodo che viene qui introdotto per calcolare il campo elettromagnetico generato da una carica elettrica elementare in moto consiste nel rappresentare i potenziali e i campi generati da una corrente di convezione ricorrendo una volta alla descrizione lagrangiana della corrente e una seconda volta alla descrizione euleriana. Si ottengono così due diverse formulazioni integrali dei potenziali e dei campi. Evidentemente nella prima formulazione intervengono i potenziali e i campi generati dall'elemento di carica in moto, potenziali e campi che sono incogniti. Per cui uguagliando le espressioni integrali corrispondenti alle due diverse descrizioni si ottengono equazioni integrali le cui incognite sono appunto i potenziali e i campi generati dall'elemento di carica in moto. Le equazioni possono essere rese molto semplici, ai fini del problema risolutivo che esse pongono, mediante una scelta opportuna della corrente di convezione.

Evidentemente tale metodo offre possibilità alquanto estese, potendo esso essere applicato tanto se il mezzo in cui si muove la carica è dielettrico perfetto o conduttore, isotropo o anisotropo, dispersivo o non dispersivo, omogeneo o non omogeneo. Inoltre il metodo consente di studiare i campi gene-

rati non solo dalle cariche in moto rettilineo e uniforme, ma anche in moto vario e senza limitazione alcuna per quanto riguarda la loro velocità rispetto a quella della luce nel mezzo in cui la carica si muove, consentendo così la trattazione di molti problemi interessanti l'effetto Čerenkov fino ad oggi insoluti

6. – Un teorema sul campo elettromagnetico generato da una carica in moto rettilineo e uniforme in un mezzo qualunque.

6'1. – Una carica puntiforme q percorra l'asse x con velocità costante v e secondo la legge $x = vt$. Scelto un punto P non appartenente all'asse x siano $\varphi(P, t)$, $\mathscr{A}(P, t)$, $\mathscr{E}(P, t)$, $\mathscr{H}(P, t)$ rispettivamente il potenziale scalare il potenziale vettore, il campo elettrico ed il campo magnetico presenti in P all'istante t e dovuti al moto della carica. È tuttavia opportuno sostituire in essi il tempo t con x/v. Si ottengono così quattro funzioni $\varphi(P, x/v)$, $\mathscr{A}(P, x/v)$, $\mathscr{E}(P, x/v)$, $\mathscr{H}(P, x/v)$ le quali esprimono i potenziali e i campi generati dalla carica q e *presenti in P nello stesso istante in cui la carica assume l'ascissa x*. Con tale accorgimento le nuove espressioni dei potenziali e dei campi sono utilizzabili anche nel caso di cariche che si trovano all'istante $t = 0$ in un punto diverso dall'origine, cioè che si muovono con la legge del moto $x = vt - \text{costante}$.

Si consideri ora una distribuzione Σ di cariche elettriche lungo l'asse x tutte procedenti con la stessa velocità costante v. Sia $\varrho_l(x, t)$ la densità lineica delle cariche elettriche nel punto x all'istante t. Allora, in forza dei concetti e simboli or ora introdotti, i potenziali scalare $\varphi_L(P, t)$, vettore $\mathscr{A}_L(P, t)$, campo elettrico $\mathscr{E}_L(P, t)$ ed il campo magnetico $\mathscr{H}_L(P, t)$, generati in P all'istante dalla distribuzione Σ di cariche elettriche, sono:

$$\varphi_L(P, t) = \frac{1}{q}\int_{-\infty}^{+\infty} \varrho_l(x, t) q \left(P, \frac{x}{v}\right) \mathrm{d}x, \qquad \mathscr{A}_L(P, t) = \frac{1}{q}\int_{-\infty}^{+\infty} \varrho_l(x, t)\, \mathscr{A}\left(P, \frac{x}{v}\right) \mathrm{d}x,$$

$$\mathscr{E}_L(P, t) = \frac{1}{q}\int_{-\infty}^{+\infty} \varrho_l(x, t) \mathscr{E}\left(P, \frac{x}{v}\right) \mathrm{d}x, \qquad \mathscr{H}_L(P, t) = \frac{1}{q}\int_{-\infty}^{+\infty} \varrho_l(x, t)\, \mathscr{H}\left(P, \frac{x}{v}\right) \mathrm{d}x.$$

Evidentemente tale rappresentazione dei potenziali e dei campi corrisponde al punto di vista lagrangiano.

Si osservi ora che la densità lineica $\varrho_l(x, t)$ della carica e l'intensità $I(x, t)$ della corrente che percorre l'asse x sono legate dalla relazione

$$I(x, t) = v\, \varrho_l(x, t)$$

e inoltre che le funzioni $I(x, t)$ e $\varrho_l(x, t)$ devono soddisfare all'equazione

conservazione della carica

$$\frac{\partial I}{\partial x} = -\frac{\partial \varrho_l}{\partial t} .$$

Da questa, per la precedente si ricava

$$\frac{\partial \varrho_l}{\partial x} + \frac{1}{v}\frac{\partial \varrho_l}{\partial t} = 0 .$$

Tale equazione è soddisfatta per $\varrho_l(x, t) = F(x - vt)$ con F funzione arbitraria. Si scelga pertanto (*)

$$\varrho_l(x, t) = \frac{q}{v}\exp\left[-i\omega\left(\frac{x}{v} - t\right)\right],$$

con ω costante arbitraria. Si ha così

$$I(x, t) = q\exp\left[-i\omega\left(\frac{x}{v} - t\right)\right].$$

Con una tale scelta della densità $\varrho_l(x, t)$ e facendo $t = 0$, dalle precedenti espressioni dei potenziali e dei campi si deduce:

$$\varphi_L(P, 0) = \int_{-\infty}^{+\infty}\exp\left[-i\omega\frac{x}{r}\right] q\left(P, \frac{x}{r}\right)\frac{\mathrm{d}x}{r}, \qquad \mathcal{A}_L(P, 0) = \int_{\infty}^{+\infty}\exp\left[-i\omega\frac{x}{r}\right]\mathcal{A}\left(P, \frac{x}{r}\right)\frac{\mathrm{d}x}{r},$$

$$\mathcal{E}_L(P, 0) = \int_{-\infty}^{+\infty}\exp\left[-i\omega\frac{x}{r}\right]\mathcal{E}\left(P, \frac{x}{r}\right)\frac{\mathrm{d}x}{r}, \qquad \mathcal{H}_L(P, 0) = \int_{\infty}^{+\infty}\exp\left[-i\omega\frac{x}{r}\right]\mathcal{H}\left(P, \frac{x}{r}\right)\frac{\mathrm{d}x}{r}.$$

Effettuando sotto il segno degli integrali la sostituzione formale $x = vt$ si ottiene

$$\varphi_L(P, 0) = \int_{-\infty}^{+\infty}\exp\left[-i\omega t\right]\varphi(P, t)\,\mathrm{d}t, \qquad \mathcal{A}_L(P, 0) = \int_{\infty}^{+\infty}\exp\left[-i\omega t\right]\mathcal{A}(P, t)\,\mathrm{d}t,$$

$$\mathcal{E}_L(P, 0) = \int_{-\infty}^{+\infty}\exp\left[-i\omega t\right]\mathcal{E}(P, t)\,\mathrm{d}t, \qquad \mathcal{H}_L(P, 0) = \int_{-\infty}^{+\infty}\exp\left[-i\omega t\right]\mathcal{H}(P, t)\,\mathrm{d}t.$$

(*) L'introduzione di una funzione complessa ha il solo scopo di consentire la trattazione simultanea dei due casi reali

$$\varrho_l(x, t) = \frac{q}{v}\cos\omega\left(\frac{x}{v} - t\right) \qquad \text{e} \qquad \varrho_l(x, t) = \frac{q}{v}\sin\omega\left(\frac{x}{v} - t\right).$$

Si osservi che gli integrali ora scritti altro non sono che le trasformate di Fourier (fatte rispetto al tempo) delle funzioni $q(P,t)$, $\mathscr{A}(P,t)$, $\mathscr{E}(P,t)$, $\mathscr{H}(P,t)$. Per cui si può enunciare il seguente teorema:

Una carica puntiforme q percorra l'asse x con la legge del moto $x = vt$, essendo v costante. Allora le trasformate di Fourier (*)

$$(17)\qquad \begin{cases} \int_{-\infty}^{+\infty} \exp[-i\omega t]\,\varphi(P,t)\,dt & \int_{-\infty}^{+\infty} \exp[-i\omega t]\,\mathscr{A}(P,t)\,dt\,, \\ \int_{-\infty}^{+\infty} \exp[-i\omega t]\,\mathscr{E}(P,t)\,dt & \int_{-\infty}^{+\infty} \exp[-i\omega t]\,\mathscr{H}(P,t)\,dt\,, \end{cases}$$

dei potenziali e dei campi generati dalla detta carica in un punto P sono uguali ai corrispondenti potenziali e campi generati in P all'istante $t = 0$ da una corrente di convezione che percorra l'asse x con intensità (**)

$$(18)\qquad I(x,t) = q \exp\left[-i\omega\left(\frac{x}{v} - t\right)\right],$$

e con densità lineica di carica distribuita

$$(19)\qquad \varrho_l(x,t) = \frac{q}{v} \exp -\left[i\omega\left(\frac{x}{v} - t\right)\right] .$$

6'2. – Evidentemente tale teorema ha una portata generale, potendo esso essere applicato non solo al caso in cui il mezzo sia un dielettrico perfetto, non dispersivo, omogeneo e isotropo, ma al caso più generale in cui il mezzo sia non omogeneo, dispersivo, conduttore, anisotropo. Si osservi poi che il teorema è particolarmente adatto per il caso in cui il mezzo è dispersivo, in quanto che

(*) Ben s'intende quando queste esistono. Così, nel caso del moto di una carica con velocità maggiore di c/n in un dielettrico perfetto, omogeneo, non dispersivo, esistono le trasformate di Fourier dei potenziali, ma non quelle dei campi. Ciò perchè gli integrali che dovrebbero rappresentare queste ultime risultano divergenti. Tale fatto condizionerà i procedimenti di calcolo di cui ai Cap. II e III. Quando invece si considera uno schema più aderente alla realtà, cioè un mezzo dispersivo ed assorbente, allora esistono evidentemente anche le trasformate dei campi, sempre che sia $v < c$.

(**) Per rimediare alla disomogeneità dimensionale che si riscontra nelle (18) e (19) basterebbe considerare una corrente e una densità di carica uguali ai secondi membri delle (18) e (19) moltiplicati per ω. Si dovrebbero poi considerare i potenziali e campi generati da tali nuove corrente e carica. Essi, all'istante $t = 0$, sarebbero uguali alle trasformate (17) moltiplicate per ω. Evidentemente si tratta di una complicazione che si è preferito evitare.

lo studio del campo elettromagnetico generato da una particella in moto è ricondotto a quello del campo generato da una corrente dipendente dal tempo con legge armonica; ciò che rende possibile la costruzione della soluzione anche quando le costanti ε e μ dipendono dalla frequenza.

Con il teorema enunciato il calcolo del campo elettromagnetico generato da una carica elementare in moto è ricondotto a un'antitrasformazione di Fourier;

$$(20)\quad \begin{cases} q(P,t) = \dfrac{1}{2\pi}\displaystyle\int_{-\infty}^{+\infty} q_L(P,0)\exp[i\omega t]\,\mathrm{d}\omega\,, & \mathscr{A}(P,t) = \dfrac{1}{2\pi}\displaystyle\int_{-\infty}^{+\infty} \mathscr{A}_L(P,0)\exp[i\omega t]\,\mathrm{d}\omega\,. \\ \mathscr{E}(P,t) = \dfrac{1}{2\pi}\displaystyle\int_{-\infty}^{+\infty} \mathscr{E}_L(P,0)\exp[i\omega t]\,\mathrm{d}\omega\,, & \mathscr{H}(P,t) = \dfrac{1}{2\pi}\displaystyle\int_{-\infty}^{+\infty} \mathscr{H}_L(P,0)\exp[i\omega t]\,\mathrm{d}\omega\,. \end{cases}$$

Esistono tuttavia casi particolari in cui il problema può essere risolto operando un opportuno cambiamento di variabile sotto il segno degli integrali che esprimono i potenziali e i campi generati dalla corrente (18) e dalla carica (19), in modo da fare assumere a tali integrali l'aspetto di trasformate di Fourier. Il problema viene allora immediatamente risolto dall'osservazione che per l'uguaglianza di due trasformate di Fourier è necessaria e sufficiente l'uguaglianza delle funzioni trasformande. Di tali casi semplici saranno dati esempi in seguito (*).

7. – Un teorema generale nel caso della carica in moto comunque vario in un mezzo qualunque.

7'1. – Ci si propone ora di estendere il teorema precedente al caso in cui la carica q percorre una curva C con velocità comunque variabile.

(*) Si tenga presente che secondo taluni autori per trasformata di Fourier di una funzione $f(t)$ si intende non già l'integrale

$$\int_{-\infty}^{+\infty} \exp[-i\omega t] f(t)\,\mathrm{d}t\,,$$

ma il prodotto

$$\frac{1}{\sqrt{2\pi}} \int_{-\infty}^{+\infty} \exp[-i\omega t] f(t)\,\mathrm{d}t\,.$$

Ove si volesse adottare tale definizione, bisognerebbe modificare il teorema precedente moltiplicando per $1/\sqrt{2\pi}$ le (17) e i secondi membri delle (18) e (19); bisognerebbe poi sostituire il coefficiente $1/2\pi$ che figura nelle (20) con $1/\sqrt{2\pi}$.

Sia C la curva di equazioni parametriche

$$x = x(\theta)\,, \qquad y = y(\theta)\,, \qquad z = z(\theta) \qquad -\infty < \theta < +\infty. \tag{21}$$

Sia $v(\theta)$ la funzione definita in ogni punto di C dalla relazione

$$v(\theta) = \sqrt{\left(\frac{dx}{d\theta}\right)^2 + \left(\frac{dy}{d\theta}\right)^2 + \left(\frac{dz}{d\theta}\right)^2}. \tag{22}$$

Una carica puntiforme q percorra la curva C con la legge del moto (*)

$$\theta = t\,. \tag{23}$$

I potenziali scalare e vettore, i campi elettrico e magnetico generati all'istante t in un punto P dello spazio dalla detta carica in moto siano rispettivamente $\varphi(P, t)$, $\mathscr{A}(P, t)$, $\mathscr{E}(P, t)$, $\mathscr{H}(P, t)$. Evidentemente un'altra carica q la quale si muovesse su C con la legge del moto

$$\theta = t + t_0 \tag{24}$$

genererebbe in P i potenziali $\varphi(P, t+t_0)$, $\mathscr{A}(P, t+t_0)$ e i campi $\mathscr{E}(P, t+t_0)$, $\mathscr{H}(P, t+t_0)$. Per eliminare la costante t_0 conviene in tali espressioni sostituire θ al posto di $t+t_0$. Si ottengono così le nuove espressioni $\varphi(P, \theta)$, $\mathscr{A}(P, \theta)$ $\mathscr{E}(P, \theta)$, $\mathscr{H}(P, \theta)$, le quali esprimono i potenziali e i campi generati da una carica q moventesi su C con una legge del tipo (24) e *presenti in P nello stesso istante in cui la detta carica occupa il punto θ di C*. Si osservi che ogni carica che si muova su C con la legge del moto (24) ha nel punto θ la velocità $v(\theta)$ definita dalla (22), qualunque sia la costante t_0.

Si consideri ora una distribuzione Σ di cariche elettriche su C, tutte in moto nel senso crescente del parametro θ. La carica elementare di Σ presente

(*) Con θ si intende un parametro spaziale. Esso consente di individuare ogni punto della curva C mediante il corrispondente valore di θ. Tale punto è evidentemente il punto di coordinate $x(\theta)$, $y(\theta)$, $z(\theta)$, che viene brevemente chiamato il punto θ di C. Invece t è un parametro temporale. Il diverso carattere dei due parametri non va mai confuso, anche se il particolare moto della carica puntiforme che qui si considera è retto dalla legge $\theta = t$, il che equivale a considerare una carica puntiforme movente con la legge $x=x(t)$, $y=y(t)$, $z=z(t)$. Infatti nel seguito si renderà utile l'introduzione di grandezze sia variabili lungo C e sia variabili nel tempo. Tali funzioni del posto e del tempo saranno funzioni di θ e di t. Da ciò deriva la necessità di non lasciarsi trarre in inganno dalla (23) e di mantenere ben distinte nella mente le diverse parti dei due parametri θ e t. Il parametro θ può essere anche pensato come una coordinata lagrangiana. Al lettore non sfuggirà che il successo del metodo è in parte dovuto all'opportuna introduzione e scelta della coordinata lagrangiana θ.

nel punto θ abbia ivi velocità $v(\theta)$. Pertanto ogni carica elementare di Σ segue una legge del moto di tipo (24).

Sia $\sigma(\theta, t)\,\mathrm{d}\theta$ la quantità delle cariche di Σ presenti all'istante t sull'arco $(\theta, \theta+\mathrm{d}\theta)$ di C. Per quanto detto sopra i potenziali scalare $\varphi_L(P, t)$, vettore $\mathscr{A}_L(P, t)$, i campi elettrico $\mathscr{E}_L(P, t)$, magnetico $\mathscr{H}_L(P, t)$ presenti in P all'istante t e dovuti a tutte le cariche di Σ sono

$$(25)\qquad \begin{cases} \varphi_L(P, t) = \dfrac{1}{q}\displaystyle\int_{-\infty}^{+\infty}\sigma(\theta, t)\,\varphi(P, \theta)\,\mathrm{d}\theta\,, & \mathscr{A}_L(P, t) = \dfrac{1}{q}\displaystyle\int_{-\infty}^{+\infty}\sigma(\theta, t)\mathscr{A}(P, \theta)\,\mathrm{d}\theta \\ \mathscr{E}_L(P, t) = \dfrac{1}{q}\displaystyle\int_{-\infty}^{+\infty}\sigma(\theta, t)\mathscr{E}(P, \theta)\,\mathrm{d}\theta\,, & \mathscr{H}_L(P, t) = \dfrac{1}{q}\displaystyle\int_{-\infty}^{+\infty}\sigma(\theta, t)\mathscr{H}(P, \theta)\,\mathrm{d}\theta\,. \end{cases}$$

La funzione $\sigma(\theta, t)$ non può tuttavia essere scelta ad arbitrio. Detto $\mathrm{d}s$ un arco elementare di C, dalla (22) si ha $\mathrm{d}s/\mathrm{d}\theta = v(\theta)$. Perciò si può scrivere $\sigma(\theta, t)\,\mathrm{d}\theta = (\sigma(\theta, t)/v(\theta))\,\mathrm{d}s$. Tale espressione mostra che la densità di carica $\varrho_l(\theta, t)$ per unità di lunghezza vale

$$\varrho_l(\theta, t) = \frac{\sigma(\theta, t)}{v(\theta)}\,.$$

La corrente $I(\theta, t)$ che percorre la curva C è allora $\varrho_l(\theta, t)\,v(\theta)$ ossia

$$I(\theta, t) = \sigma(\theta, t)\,.$$

La condizione di conservazione della carica impone la condizione (s = arco di C):

$$\frac{\partial I(\theta, t)}{\partial s} = -\frac{\partial \varrho_l(\theta, t)}{\partial t}\,.$$

Ma è

$$\frac{\partial I(\theta, t)}{\partial s} = \frac{\partial \sigma(\theta, t)}{\partial \theta}\frac{\mathrm{d}\theta}{\mathrm{d}s} = \frac{1}{v(\theta)}\frac{\partial \sigma(\theta, t)}{\partial \theta}\,,$$

$$\frac{\partial \varrho_l(\theta, t)}{\partial t} = \frac{1}{v(\theta)}\frac{\partial \sigma(\theta, t)}{\partial t}$$

per cui l'equazione di continuità diventa

$$\frac{\partial \sigma}{\partial \theta} + \frac{\partial \sigma}{\partial t} = 0\,.$$

Questa è soddisfatta per $\sigma(\theta, t) = F(\theta - t)$, con F funzione arbitraria. Si può pertanto porre

$$\sigma(\theta, t) = q \exp[-i\omega(\theta - t)]$$

con ω costante arbitraria. Ciò comporta

$$\varrho_l(\theta, t) = \frac{q}{v(\theta)} \exp[-i\omega(\theta - t)], \qquad I(\theta, t) = q \exp[-i\omega(\theta - t)].$$

Con una tale scelta della funzione $\sigma(\theta, t)$ le relazioni (25), quando in esse sia fatto $t = 0$, diventano

$$q_L(P, 0) = \int_{-\infty}^{+\infty} \exp[-i\omega\theta]\, q(P, \theta)\, d\theta, \qquad \mathscr{A}_L(P, 0) = \int_{-\infty}^{+\infty} \exp[-i\omega\theta]\, \mathscr{A}(P, \theta)\, d\theta,$$

$$\mathscr{E}_L(P, 0) = \int_{-\infty}^{+\infty} \exp[-i\omega\theta]\, \mathscr{E}(P, \theta)\, d\theta, \qquad \mathscr{H}_L(P, 0) = \int_{-\infty}^{+\infty} \exp[-i\omega\theta]\, \mathscr{H}(P, \theta)\, d\theta.$$

Ma gli integrali a secondo membro ora scritti sono le trasformate di Fourier delle funzioni $q(P, \theta)$, $\mathscr{A}(P, \theta)$, $\mathscr{E}(P, \theta)$, $\mathscr{H}(P, \theta)$, per cui si ha il teorema:

Sia C una curva di equazioni parametriche

$$x = x(\theta), \qquad y = y(\theta), \qquad z = z(\theta).$$

Una carica puntiforme q percorra la curva C con la legge del moto $\theta = t$. Allora le trasformate di Fourier

$$(26) \qquad \begin{cases} \displaystyle\int_{-\infty}^{+\infty} \exp[-i\omega t]\, \varphi(P, t)\, dt, & \displaystyle\int_{-\infty}^{+\infty} \exp[-i\omega t]\, \mathscr{A}(P, t)\, dt, \\ \displaystyle\int_{-\infty}^{+\infty} \exp[-i\omega t]\, \mathscr{E}(P, t)\, dt, & \displaystyle\int_{-\infty}^{+\infty} \exp[-i\omega t]\, \mathscr{H}(P, t)\, dt, \end{cases}$$

dei potenziali $q(P, t)$, $\mathscr{A}(P, t)$ e dei campi $\mathscr{E}(P, t)$, $\mathscr{H}(P, t)$ generati dalla detta carica in un punto P sono uguali ai corrispondenti potenziali e campi generati in P all'istante $t = 0$ da una corrente di convezione che percorre la curva C con intensità

$$(27) \qquad I(\theta, t) = q \exp[-i\omega(\theta - t)],$$

e con densità di carica per unità di lunghezza

$$(28)\qquad \varrho_l(\theta, t) = \frac{q}{v(\theta)} \exp\left[-i\omega(\theta - t)\right] \qquad \left[v(\theta) = \sqrt{\left(\frac{\mathrm{d}x}{\mathrm{d}\theta}\right)^2 + \left(\frac{\mathrm{d}y}{\mathrm{d}\theta}\right)^2 + \left(\frac{\mathrm{d}z}{\mathrm{d}\theta}\right)^2}\right].$$

7·2 Si osservi che la corrente e la densità di carica di cui si parla nel teorema dipendono dal tempo con legge armonica, ciò che rende il teorema stesso particolarmente adatto allo studio dei campi elettromagnetici generati dalle cariche in moto nei mezzi dispersivi.

La validità del teorema è evidentemente generale, potendo esso essere applicato al caso in cui la carica si muova in un mezzo qualunque, omogeneo o non omogeneo, purchè soddisfacente al principio di sovrapposizione.

Con il teorema precedente il calcolo dei potenziali $q(P, t)$ e $\mathscr{A}(P, t)$ e dei campi $\mathscr{E}(P, t)$ e $\mathscr{H}(P, t)$ generati da una carica q in moto vario viene ricondotto a un'antitrasformazione di Fourier. Si ha infatti:

$$(29)\qquad \begin{cases} q(P, t) = \dfrac{1}{2\pi}\displaystyle\int_{-\infty}^{+\infty} q_L(P, 0) \exp\left[i\omega t\right]\mathrm{d}\omega\,, & \mathscr{A}(P, t) = \dfrac{1}{2\pi}\displaystyle\int_{-\infty}^{+\infty} \mathscr{A}_L(P, 0) \exp\left[i\omega t\right]\mathrm{d}\omega, \\ \mathscr{E}(P, t) = \dfrac{1}{2\pi}\displaystyle\int_{-\infty}^{+\infty} \mathscr{E}_L(P, 0) \exp\left[i\omega t\right]\mathrm{d}\omega\,, & \mathscr{H}(P, t) = \dfrac{1}{2\pi}\displaystyle\int_{-\infty}^{+\infty} \mathscr{H}_L(P, 0) \exp\left[i\omega t\right]\mathrm{d}\omega\,. \end{cases}$$

Come nel problema relativo al moto rettilineo e uniforme, esistono anche in quello del moto vario della carica casi particolari in cui l'antitrasformazione di Fourier può essere eseguita, mediante il procedimento già spiegato al precedente n. **6**. Di tali casi semplici saranno dati esempi al Capitolo III.

I due teoremi stabiliti riconducono il problema del calcolo del campo elettromagnetico generato da una carica puntiforme in moto a un ordinario problema di elettromagnetismo, consistente nel calcolare il campo elettromagnetico assegnate che siano l'intensità e la densità di carica di una corrente stazionaria.

7·3. – Che i teoremi stabiliti si informino all'idea generale esposta al n. **5** è manifesto. Infatti il filo conduttore della dimostrazione del teorema precedente passa attraverso le (25). In queste i secondi membri rappresentano la descrizione dei potenziali e dei campi secondo il punto di vista lagrangiano. Ma i primi membri possono essere calcolati integrando le equazioni dell'elettromagnetismo, che sono formulate secondo il punto di vista euleriano. Le (25) diventano così equazioni integrali nelle incognite $q(P, t)$, $\mathscr{A}(P, t)$, $\mathscr{E}(P, t)$, $\mathscr{H}(P, t)$. Tali equazioni integrali sono state poi rese facilmente risolubili (me-

diante un'antitrasformazione di Fourier) con l'opportuna scelta della corrente di Lorentz definita dalle (27) e (28) e facendo inoltre nelle dette equazioni $t = 0$.

8. – Moto periodico della carica.

Se la curva C è chiusa e il moto della carica è periodico è opportuno rappresentare la curva mediante funzioni periodiche del parametro θ ponendo ancora

$$x = x(\theta)\,, \qquad y = y(\theta)\,, \qquad z = z(\theta) \qquad\qquad -\infty < \theta < +\infty$$

le funzioni $x(\theta)$, $y(\theta)$, $z(\theta)$ essendo periodiche con periodo T

$$x(\theta) = x(\theta + T)\,, \qquad y(\theta) = y(\theta + T)\,, \qquad z(\theta) = z(\theta + T)\,. \tag{30}$$

La carica q percorrerà la curva C ancora con la legge del moto

$$\theta = t\,.$$

In tal caso il campo elettromagnetico generato da q in un punto $P(x, y, z)$ sarà una funzione periodica del tempo t con periodo T. In questo caso esso non deve più essere rappresentato mediante integrali di Fourier, ma mediante serie di Fourier. La dimostrazione si svolge come nel caso del precedente n. **7**, introducendo tuttavia l'ulteriore condizione $I(\theta, t) = I(\theta + T, t)$, $\varrho_l(\theta, t) = \varrho_l(\theta + T, t)$, a motivo della (30). Ciò obbliga nelle (27) e (28) ad attribuire alla pulsazione ω soltanto i valori $\omega = n\Omega$ con n intero, positivo, nullo o negativo ($\Omega = 2\pi/T$).

I potenziali scalare $\Phi_n(P, 0)$ e vettore $\boldsymbol{A}_n(P, 0)$, i campi elettrico $\boldsymbol{E}_n(P, 0)$ e magnetico $\boldsymbol{H}_n(P, 0)$ generati in un punto P all'istante $t = 0$ da una corrente che percorre la curva C con intensità $q \exp|-in\Omega(\theta - t)|$ e con densità lineica $(q/r(\theta)) \exp[-in\Omega(\theta - t)]$ di carica elettrica sono allora legati alle grandezze $\varphi(P, t)$, $\mathscr{A}(P, t)$, $\mathscr{E}(P, t)$ e $\mathscr{H}(P, t)$ dalle relazioni

$$\Phi_n(P, 0) = \int_0^T \exp[-in\Omega t]\,\varphi(P, t)\,\mathrm{d}t\,, \ \ldots,\ \boldsymbol{H}_n(P, t) = \int_0^T \exp[-in\Omega t]\,\mathscr{H}(P, t)\,\mathrm{d}t\,, \tag{31}$$

per cui i potenziali e campi $\varphi(P, t)$, $\mathscr{A}(P, t)$, $\mathscr{E}(P, t)$, $\mathscr{H}(P, t)$ generati in P all'istante t dal moto della carica q sono forniti dalle serie

$$\varphi(P, t) = \frac{1}{T} \sum_{n=-\infty}^{n=+\infty} \Phi_n(P, 0) \exp[in\Omega t],\ \ldots,\ \mathscr{H}(P, t) = \tag{32}$$

$$= \frac{1}{T} \sum_{n=-\infty}^{n=+\infty} \boldsymbol{H}_n(P, 0) \exp[in\Omega t]\,.$$

Capitolo Secondo

CAMPO ELETTROMAGNETICO DI UNA CARICA IN MOTO RETTILINEO UNIFORME

9. – Trasformazione di integrali. Mezzo dispersivo.

9'1. – Nel capitolo seguente si studieranno i campi generati da una carica nel caso del moto più generale di essa. Evidentemente tale studio comprende anche quello relativo al moto rettilineo e uniforme. Tuttavia si è ritenuto opportuno trattare a parte tale particolare caso, perchè quando il moto della carica è rettilineo e uniforme è possibile condurre la trattazione analitica in modo da sfociare nelle rappresentazioni attuali dei potenziali e dei campi, secondo la via che sarà percorsa nel presente capitolo.

Il caso che viene qui considerato è quello di una carica q che si muove in un dielettrico omogeneo e isotropo, perfettamente isolante. La carica si intende muoversi sull'asse x con la legge del moto $x = vt$, in modo da poter direttamente applicare il teorema del n. 6. Le relazioni che saranno stabilite nel presente numero valgono anche se il dielettrico è dispersivo, cioè se ε, μ, n sono funzioni della pulsazione ω ($\omega = 2\pi\nu$, essendo ν la frequenza).

I potenziali scalare $\varphi_L(P, t)$ e vettore $\mathscr{A}_L(P, t)$ generati all'istante t in un punto $P(x, y, z)$ da una corrente di convezione che percorra l'asse x con intensità $I(x, t)$ e con densità lineica $\varrho_l(x, t)$ di carica distribuita sono forniti dalle (4) del Cap. I:

$$\varphi_L(P, t) = \frac{1}{\varepsilon}\int_{-\infty}^{+\infty} \frac{\varrho_l(\xi, t - nr/c)}{r}\,\mathrm{d}\xi\,, \qquad \mathscr{A}_L(P, t) = \frac{\mu}{c}\int_{-\infty}^{+\infty} \frac{I(\xi, t - nr/c)\boldsymbol{i}}{r}\,\mathrm{d}\xi\,,$$

con $n = \sqrt{\varepsilon\mu}$, $r = \sqrt{(\xi - x)^2 + y^2 + z^2}$, $\boldsymbol{i}$ = versore dell'asse x.

Facendo, in base al citato teorema del n. 6,

$$I(x, t) = q \exp\left[-i\omega\left(\frac{x}{v} - t\right)\right], \qquad \varrho_l(x, t) = \frac{q}{v}\exp\left[-i\omega\left(\frac{x}{v} - t\right)\right],$$

si ha

$$\text{(33)} \qquad \begin{cases} \varphi_L(P, t) = \dfrac{q}{v\varepsilon}\displaystyle\int_{-\infty}^{+\infty} \frac{1}{r}\exp\left[-i\omega\left(\frac{\xi}{v} - t + \frac{nr}{c}\right)\right]\mathrm{d}\xi, \\ \mathscr{A}_L(P, t) = \dfrac{q\mu\boldsymbol{i}}{c}\displaystyle\int_{-\infty}^{+\infty} \frac{1}{r}\exp\left[-i\omega\left(\frac{\xi}{v} - t + \frac{nr}{c}\right)\right]\mathrm{d}\xi\,, \end{cases}$$

4127

Si osservi che è

$$\mathscr{A}_L(P,t) = \frac{n^2 v \boldsymbol{i}}{c}\,\varphi_L(P,t)\,. \tag{34}$$

I campi elettrico $\mathscr{E}_L(P,t)$ e magnetico $\mathscr{H}_L(P,t)$ si ricavano dai precedenti potenziali mediante le (3) del Cap. I:

$$\mathscr{E}_L = -\operatorname{grad}\varphi_L - \frac{1}{c}\frac{\partial \mathscr{A}_L}{\partial t}\,, \qquad \mathscr{H} = \frac{1}{\mu}\operatorname{rot}\mathscr{A}_L\,.$$

Per la (34) è allora

$$\mathscr{E}_L = -\operatorname{grad}\varphi_L - \frac{n^2 v \boldsymbol{i}}{c^2}\frac{\partial \varphi_L}{\partial t}\,, \qquad \mathscr{H}_L = \frac{\varepsilon v}{c}\operatorname{grad}\varphi_L \wedge \boldsymbol{i}\,.$$

Moltiplicando esternamente la prima di queste per il vettore $-(\varepsilon v/c)\boldsymbol{i}$ ed osservando che è $\boldsymbol{i}\wedge\boldsymbol{i} = 0$, si ha:

$$-\frac{\varepsilon v}{c}\,\mathscr{E}_L \wedge \boldsymbol{i} = \frac{\varepsilon v}{c}\operatorname{grad}\varphi_L \wedge \boldsymbol{i}\,,$$

e confrontando tale risultato con la seconda

$$\mathscr{H}_L(P,t) = \frac{\varepsilon v}{c}\,\boldsymbol{i}\wedge\mathscr{E}_L(P,t)\,. \tag{35}$$

In seguito, per semplificare le espressioni, si useranno le posizioni

$$a = \sqrt{1 - \frac{n^2 v^2}{c^2}}\,, \qquad \varrho = \sqrt{x^2 + y^2}\,. \tag{36}$$

In conseguenza della prima si scriverà $a^2 = 1 - (n^2 v^2/c^2)$ quando è $v < c/n$ e $a^2 = (n^2 v^2/c^2) - 1$ quando è $v > c/n$. In conseguenza della seconda si può scrivere $r = \sqrt{(\xi - x)^2 + \varrho^2}$.

9'2. – *Si supponga ora* $v < c/n(\omega)$.

La funzione $(\xi/v) + (nr/c)$ della variabile ξ è allora sempre crescente in tutto l'intervallo $-\infty < \xi < +\infty$. Infatti la sua derivata rispetto a ξ è

$$\frac{1}{v} + \frac{n}{c}\,\frac{\xi - x}{r}\,,$$

e questa è sempre positiva, perchè è sempre $|(\xi - x)/r| < 1$. Si può pertanto

nell'integrale che fornisce $\varphi_L(P, t)$ effettuare la sostituzione di variabile

$$\frac{\xi}{v} + \frac{nr}{c} = \tau \,, \tag{37}$$

mantenendo invariati i limiti $-\infty$ e $+\infty$ di integrazione. Differenziando si ottiene

$$\frac{\mathrm{d}\xi}{r}\lambda = \mathrm{d}\tau \,, \tag{38}$$

essendosi posto

$$\frac{r}{v} + \frac{n}{c}(\xi - x) = \lambda \,. \tag{39}$$

La (37) può essere anche così scritta

$$\frac{\xi - x}{v} + \frac{nr}{c} = \tau - \frac{x}{v} \,. \tag{40}$$

Quadrando i due membri delle (39) e (40) e poi sottraendo l'una dall'altra le due equazioni così ottenute si ottiene:

$$\lambda^2 - \left(\tau - \frac{x}{v}\right)^2 = \frac{1}{v^2}\left[r^2 - (\xi - x)^2\right] - \frac{n^2}{c^2}\left[r^2 - (\xi - x)^2\right] = \left[\frac{1}{v^2} - \frac{n^2}{c^2}\right](y^2 + z^2) \,,$$

da cui

$$\lambda = \sqrt{\left(\tau - \frac{x}{v}\right)^2 + \left(\frac{1}{v^2} - \frac{n^2}{c^2}\right)(y^2 + z^2)} = \frac{1}{v}\sqrt{(x - v\tau)^2 + a^2\varrho^2} \,, \tag{41}$$

e quindi per la (38)

$$\frac{\mathrm{d}\xi}{r} = \frac{\mathrm{d}\tau}{\lambda} = \frac{v\,\mathrm{d}\tau}{\sqrt{(x - v\tau)^2 + a^2\varrho^2}} \,.$$

Le posizioni fatte e le relazioni stabilite consentono di trasformare la (33) nella seguente:

$$\varphi_L(P, t) = \frac{q}{\varepsilon}\int_{-\infty}^{+\infty} \frac{\exp\left[-i\omega(\tau - t)\right]\mathrm{d}\tau}{\sqrt{(x - v\tau)^2 + a^2\varrho^2}} \,. \tag{42}$$

Da questa in particolare si ha:

$$\varphi_L(P, 0) = \frac{q}{\varepsilon}\int_{-\infty}^{+\infty} \frac{\exp\left[-i\omega\tau\right]\mathrm{d}\tau}{\sqrt{(x - v\tau)^2 + a^2\varrho^2}} \,. \tag{43}$$

9·3. – *Si supponga ora* $v > c/n(\omega)$.

La funzione $(\xi/v)+(nr/c)$ della variabile ξ ammette allora un minimo in corrispondenza della radice dell'equazione (condizione di annullamento della derivata):

$$\frac{1}{v} + \frac{n}{c}\frac{\xi - x}{r} = 0 .$$

Osservato che il valore di $\xi - x$ che soddisfa a tale equazione è negativo, da essa si ricava

$$(\xi - x)^2 = \frac{c^2 r^2}{n^2 v^2} = \frac{c^2}{n^2 v^2}(\xi - x)^2 = \frac{c^2}{n^2 v^2}\varrho^2 .$$

Da questa moltiplicando tutti i termini per $n^2 v^2 / c^2$ si ottiene

$$\left(\frac{n^2 v^2}{c^2} - 1\right)(\xi - x)^2 = \varrho^2 ,$$

per cui

$$\xi = x - \frac{\varrho}{a} . \tag{44}$$

In corrispondenza di tale valore di ξ, che in seguito sarà indicato con ξ_0, la funzione $(\xi/v)+(nr/c)$ assume il seguente valore minimo t_0:

$$t_0 = \frac{x}{v} - \frac{\varrho}{av} + \frac{n}{c}\sqrt{\frac{\varrho^2}{a^2} + \varrho^2} = \frac{x}{v} - \frac{\varrho}{av} + \frac{n^2 \varrho v}{c^2 a} ,$$

ossia

$$t_0 = \frac{x}{v} + \frac{a\varrho}{v} . \tag{45}$$

Ciò premesso, l'integrale a secondo membro della (33) può essere così scomposto:

$$\int_{-\infty}^{+\infty} \frac{1}{r} \exp\left[-i\omega\left(\frac{\xi}{v} + \frac{nr}{c} - t\right)\right] \mathrm{d}\xi = \int_{-\infty}^{\xi_0} \ldots \mathrm{d}\xi + \int_{\xi_0}^{+\infty} \ldots \mathrm{d}\xi . \tag{46}$$

Nell'intervallo $(\xi_0, +\infty)$ la funzione $(\xi/v)+(nr/c)$ è crescente da t_0 a $+\infty$. Si può pertanto integrare come precedentemente per sostituzione di variabile, ponendo ancora

$$\frac{\xi}{v} + \frac{nr}{c} = \tau .$$

Operando come in precedenza (formula (37) e seguenti), si ottiene allora

$$\int_{\xi_0}^{+\infty} \frac{1}{r} \exp\left[-i\omega\left(\frac{\xi}{v} + \frac{nr}{c} - t\right)\right] \mathrm{d}\xi = \int_{t_0}^{+\infty} \frac{\exp\left[-i\omega(\tau - t)\right] v \,\mathrm{d}\tau}{\sqrt{(x - v\tau)^2 - a^2\varrho^2}} .$$

Invece nell'intervallo $(-\infty, \xi_0)$ la funzione $(\xi/v)+(nr/c)$ della variabile ξ è decrescente da $+\infty$ a t_0. Si può ancora integrare per sostituzione con la solita posizione

$$\frac{\xi}{v} + \frac{nr}{c} = \tau ,$$

e procedendo come sopra. Tuttavia, quando in conformità con le (38) e (39) si ponga $\mathrm{d}\xi/r = \mathrm{d}\tau/\lambda$, si riscontra che nel caso attuale è $\lambda < 0$. Di ciò si dovrà tener conto nella successiva operazione di estrazione della radice e in luogo della (41) scrivere

$$\lambda = -\frac{1}{v}\sqrt{(x - v\tau)^2 - a^2\varrho^2} .$$

Si ha così

$$\frac{\mathrm{d}\xi}{r} = -\frac{v\,\mathrm{d}\tau}{\sqrt{(x - v\tau)^2 - a^2\varrho^2}} ,$$

e quindi

$$\int_{-\infty}^{\xi_0} \frac{1}{r} \exp\left[-i\omega\left(\frac{\xi}{v} + \frac{nr}{c} - t\right)\right] \mathrm{d}\xi = -\int_{+\infty}^{t_0} \frac{\exp\left[-i\omega(\tau - t)\right] v \,\mathrm{d}\tau}{\sqrt{(x - v\tau)^2 - a^2\varrho^2}} = \int_{t_0}^{+\infty} \frac{\exp\left[-i\omega(\tau - t)\right] v \,\mathrm{d}\tau}{\sqrt{(x - v\tau)^2 - a^2\varrho^2}}$$

La scomposizione introdotta con la (46) e i risultati ora conseguiti permettono di scrivere

$$\varphi_L(P, t) = \frac{2q}{\varepsilon} \int_{t_0}^{+\infty} \frac{\exp\left[-i\omega(\tau - t)\right] \mathrm{d}\tau}{\sqrt{(x - v\tau)^2 - a^2\varrho^2}} . \tag{47}$$

Questa, ai fini del teorema del n. 6, contiene l'importante caso particolare

$$\varphi_L(P, 0) = \frac{2q}{\varepsilon} \int_{t_0}^{+\infty} \frac{\exp\left[-i\omega\tau\right] \mathrm{d}\tau}{\sqrt{(x - v\tau)^2 - a^2\varrho^2}} . \tag{48}$$

10. – Moto della carica in un dielettrico non dispersivo, nel caso $v < c/n$

Si supponga ora che il dielettrico sia non dispersivo, cioè che i parametri ε, μ e quindi anche l'indice di rifrazione n non dipendano dalla frequenza.

Per il teorema del n. 6 il potenziale scalare $\varphi_L(P, 0)$ calcolato al numero precedente (relazione (43)) è la trasformata di Fourier

$$\int_{-\infty}^{+\infty} \exp[-i\omega t]\varphi(P, t)\,dt\,,$$

del potenziale scalare generato in P dalla carica q. Sostituendo formalmente nella (43), valida nel caso $v < c/n$ qui considerato, il simbolo τ con il simbolo t si ha allora:

$$\int_{-\infty}^{+\infty} \frac{q \exp[-i\omega t]\,dt}{\varepsilon\sqrt{(x - vt)^2 + a^2\varrho^2}} = \int_{-\infty}^{+\infty} \exp[-i\omega t]\varphi(P, t)\,dt\,.$$

Si osservi che gli integrali che figurano ai due membri di tale relazione rappresentano entrambi trasformate di Fourier. L'uguaglianza di queste implica l'uguaglianza delle funzioni trasformande. Si ha così

$$\varphi(P, t) = \frac{q}{\varepsilon}\frac{1}{\sqrt{(x - vt)^2 + a^2\varrho^2}}\,. \tag{49}$$

In forza della (34) è ancora

$$\mathscr{A}_L(P, 0) = \frac{\varepsilon\mu v\boldsymbol{i}}{c}\,\varphi_L(P, 0)\,.$$

Questa, sempre per il teorema del n. 6, equivale alla seguente altra

$$\int_{-\infty}^{+\infty} \exp[-i\omega t]\mathscr{A}(P, t)\,dt = \int_{-\infty}^{+\infty} \exp[-i\omega t]\,\frac{\varepsilon\mu v\boldsymbol{i}}{c}\,\varphi(P, t)\,dt\,.$$

Dall'uguaglianza di tali trasformate si ha allora

$$\mathscr{A}(P, t) = \frac{\varepsilon\mu v\boldsymbol{i}}{c}\,\varphi(P, t)\,. \tag{50}$$

Con ciò anche il potenziale vettore $\mathscr{A}(P, t)$ generato in P dalla carica q è calcolato.

I campi elettrico $\mathscr{E}(P, t)$ e magnetico $\mathscr{H}(P, t)$ generati in P dalla carica puntiforme q possono essere ricavati dai potenziali $\varphi(P, t)$ e $\mathscr{A}(P, t)$ ora calcolati mediante le solite relazioni

$$\mathscr{E} = -\operatorname{grad}\varphi - \frac{1}{c}\frac{\partial\mathscr{A}}{\partial t}\,, \qquad \mathscr{H} = \frac{1}{\mu}\operatorname{rot}\mathscr{A}\,,$$

Si ha così:

$$\mathscr{E}(P, t) = \frac{q}{\varepsilon} \frac{(x - vt)\boldsymbol{i} + a^2(y\boldsymbol{j} + z\boldsymbol{k}) - (\varepsilon\mu v^2/c^2)(x - vt)\boldsymbol{i}}{[(x - vt)^2 + a^2\varrho^2]^{\frac{3}{2}}},$$

dove $\boldsymbol{i}$, $\boldsymbol{j}$, $\boldsymbol{k}$ sono i versori degli assi x, y, z rispettivamente. Semplificando si ha poi:

$$\mathscr{E}(P, t) = \frac{qa^2}{\varepsilon} \frac{(x - vt)\boldsymbol{i} + y\boldsymbol{j} + z\boldsymbol{k}}{[(x - vt)^2 + a^2\varrho^2]^{\frac{3}{2}}}. \tag{51}$$

La (35), per il teorema del n. 6, dà luogo alla seguente:

$$\int_{-\infty}^{+\infty} \exp[-i\omega t]\mathscr{H}(P, t)\,dt = \int_{-\infty}^{+\infty} \exp[-i\omega t] \frac{\varepsilon v}{c} \boldsymbol{i} \wedge \mathscr{E}(P, t)\,dt .$$

Dall'uguaglianza fra tali trasformate di Fourier discende l'uguaglianza fra le funzioni trasformande, ossia

$$\mathscr{H}(P, t) = \frac{\varepsilon}{c} \boldsymbol{v} \wedge \mathscr{E}(P, t), \qquad (\boldsymbol{v} = v\boldsymbol{i}). \tag{52}$$

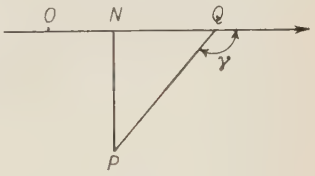

Fig. 3.

Allo scopo di rendere più espressiva la soluzione stabilita, sia O l'origine degli assi, Q la posizione della carica all'istante t, N il piede della perpendicolare condotta da P all'asse x. Sia inoltre γ l'angolo formato dal vettore $\boldsymbol{QP}$ con l'asse x. È perciò $\boldsymbol{ON} = x\boldsymbol{i}$, $\boldsymbol{OQ} = vt\boldsymbol{i}$, $(x - vt)i = \boldsymbol{QN}$, $y\boldsymbol{j} + z\boldsymbol{k} = \boldsymbol{NP}$, $(x - vt)\boldsymbol{i} + y\boldsymbol{j} + z\boldsymbol{k} = \boldsymbol{QP}$. Con tali posizioni si ha:

$$\varphi(P, t) = \frac{q}{\varepsilon} \frac{1}{\sqrt{QP^2 - n^2\beta^2\varrho^2}}, \qquad \left(\beta = \frac{v}{c}\right),$$

o anche, essendo $\varrho = NP = QP \sin\gamma$,

$$\varphi(P, t) = \frac{q}{\varepsilon} \frac{1}{\sqrt{1 - n^2\beta^2 \sin^2\gamma}} \frac{1}{QP}. \tag{53}$$

Inoltre la (51) diventa

$$\mathscr{E}(P, t) = \frac{qa^2}{\varepsilon} \frac{1}{(1 - n^2\beta^2 \sin^2\gamma)^{\frac{3}{2}}} \frac{\boldsymbol{QP}}{QP^3}. \tag{54}$$

Le (53) e (54), unitamente alle (50) e (52), forniscono una rappresentazione attuale dei potenziali e dei campi, nel senso spiegato al n. 2. Esse costituiscono un'estensione delle (11) e (12) del n. 2, le quali valgono per una carica q moventesi nel vuoto.

11. – Moto della carica in un dielettrico non dispersivo con $v > c/n$

Sempre per il teorema del n. 6 il potenziale scalare $q_L(P, 0)$ calcolato al n. 9 è la trasformata di Fourier

$$\int_{-\infty}^{+\infty} \exp[-i\omega t]\varphi(P, t)\,\mathrm{d}t\,,$$

del potenziale scalare $q(P, t)$ generato in P dalla carica puntiforme q. Evidentemente nel caso $v > c/n$ qui considerato si ricorrerà alla (48). Sostituendo formalmente in questa τ con t si ha allora

$$\int_{t_0}^{+\infty} \frac{2q \exp[-i\omega t]\,\mathrm{d}t}{\varepsilon\sqrt{(x - vt)^2 - a^2\varrho^2}} = \int_{-\infty}^{+\infty} \exp[-i\omega t]\varphi(P, t)\,\mathrm{d}t\,.$$

Si osservi che l'integrale a primo membro è la trasformata di Fourier di una funzione nulla nell'intervallo $-\infty < t < t_0$ e uguale a

$$\frac{2q}{\varepsilon\sqrt{(x - vt)^2 - a^2\varrho^2}}$$

nell'intervallo $t_0 < t < +\infty$. L'uguaglianza delle funzioni trasformande implica perciò

$$(55)\qquad \begin{cases} \varphi(P, t) = 0\,, & \text{per } t < t_0, \qquad \left(t_0 = \dfrac{x}{v} + \dfrac{a\varrho}{v}\right), \\ \varphi(P, t) = \dfrac{2q}{\varepsilon\sqrt{(x - vt)^2 - a^2\varrho^2}}\,, & \text{per } t > t_0\,. \end{cases}$$

Con lo stesso ragionamento esposto al numero precedente si ottiene

$$(56)\qquad \mathscr{A}(P, t) = \frac{\varepsilon\mu v\boldsymbol{i}}{c}\varphi(P, t)\,.$$

Le operazioni che consentono di ricavare i campi dai potenziali sono le solite:

$$\mathscr{E} = -\operatorname{grad}\varphi - \frac{1}{c}\frac{\partial\mathscr{A}}{\partial t}\,, \qquad \mathscr{H} = \frac{1}{\mu}\operatorname{rot}\mathscr{A}\,.$$

Si ha così:

$$(57)\qquad \mathscr{E}(P, t) = 0\,, \qquad \mathscr{H}(P, t) = 0 \qquad \text{per } t < t_0,$$

mentre per $t > t_0$ si ottiene

$$\mathscr{E}(P, t) = \frac{2q}{\varepsilon} \frac{(x - vt)\boldsymbol{i} - a^2(y\boldsymbol{j} + z\boldsymbol{k})}{[(x - vt)^2 - a^2\varrho^2]^{\frac{3}{2}}} - \frac{\varepsilon\mu v\boldsymbol{i}}{c^2} \frac{2q}{\varepsilon} \frac{(x - vt)v}{[(x - vt)^2 - a^2\varrho^2]^{\frac{3}{2}}},$$

ossia, ricordando che per $v > c/n$, è $a^2 = (n^2v^2/c^2) - 1$,

$$\mathscr{E}(P, t) = -\frac{2qa^2}{\varepsilon} \frac{(x - vt)\boldsymbol{i} + y\boldsymbol{j} + z\boldsymbol{k}}{[(x - vt)^2 - a^2\varrho^2]^{\frac{3}{2}}}. \qquad (t > t_0). \tag{58}$$

Per il campo magnetico si ha poi (*)

$$\mathscr{H}(P, t) = \frac{1}{\mu} \operatorname{rot} \mathscr{A}(P, t) = \frac{\varepsilon v}{c} \operatorname{rot} \varphi(P, t)\boldsymbol{i} = \frac{\varepsilon v}{c} \operatorname{grad} \varphi(P, t) \wedge \boldsymbol{i} =$$

$$= \frac{2qv}{c} \boldsymbol{i} \wedge \frac{(x - vt)\boldsymbol{i} - a^2(y\boldsymbol{j} + z\boldsymbol{k})}{[(x - vt)^2 - a^2\varrho^2]^{\frac{3}{2}}},$$

da cui per l'annullamento dei prodotti $\boldsymbol{i} \wedge \boldsymbol{i}$ e per la (58)

$$\mathscr{H}(P, t) = \frac{\varepsilon}{c} \boldsymbol{v} \wedge \mathscr{E}(P, t), \qquad (t \text{ qualunque}). \tag{59}$$

La soluzione costituita dalle (57), (58) e (59) coincide con la soluzione di Tamm per i mezzi non dispersivi (**). Alle (58) e (59) si può dare un aspetto più espressivo rifacendoci alla figura annessa al numero precedente. Si ha così

$$\varphi(P, t) = \frac{2q}{\varepsilon} \frac{1}{\sqrt{1 - n^2\beta^2 \sin^2\gamma}} \frac{1}{QP}, \qquad (t > t_0), \tag{60}$$

$$\mathscr{E}(P, t) = -\frac{2qa^2}{\varepsilon} \frac{1}{(1 - n^2\beta^2 \sin^2\gamma)^{\frac{3}{2}}} \frac{\boldsymbol{QP}}{QP^3}. \qquad (t > t_0). \tag{61}$$

(*) Il ragionamento con il quale è stata ricavata la (52) del paragrafo precedente non può qui essere ripetuto, anche se la (52) e la (59) sono formalmente identiche. Ciò perchè nel caso $v > c/n$ non esiste la trasformata di Fourier del campo elettrico $\mathscr{E}(P, t)$, a motivo della rapidità con cui tale campo diventa infinito in prossimità del fronte d'onda.

(**) Tale soluzione trovasi riportata nella citata opera di J. V. Jelley, pp. 23 e 24. Ivi si trova n^2 al posto della nostra ε, perchè quella soluzione vale per $\mu = 1$. Le altre differenze dalla nostra soluzione sono puramente formali (diverso simbolismo, quale ad es. asse z al posto dell'asse x e uso di coordinate cilindriche). È questa la soluzione di Tamm apparsa nel 1939, cioè due anni dopo il lavoro in collaborazione con I. M. Frank.

Confrontando tale espressione con la (54) del numero precedente si constata che il campo elettrico ha sempre la direzione della retta passante per la carica e per il punto P, con la differenza che il vettore $q\mathcal{E}(P, t)$ è diretto dalla carica al punto P nel caso $v < c/n$, mentre è diretto in senso contrario nel caso $v > c/n$. Corrispondente inversione di senso vale per il campo magnetico.

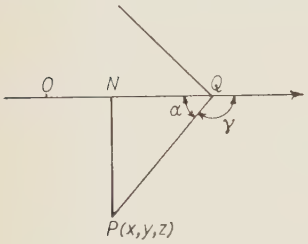

Fig. 4.

La comprensione di certe caratteristiche strutturali della soluzione, come ad esempio, del coefficiente 2 che figura nelle (60) e (61), può essere fornita soltanto dallo studio del campo elettromagnetico generato con moto vario dalla carica.

In quanto al significato dell'istante t_0, esso è chiarito dalla figura qui accanto. Poichè in figura è $ON = x$ e poichè è $t_0 = (x/v) + (a\varrho/v)$, la carica all'istante t_0 si trova in un punto Q di ascissa vt_0 ossia $x + a\varrho$, tale cioè che è $NQ = a\varrho = aNP$. Il campo elettromagnetico generato dalla carica è perciò limitato da una superficie di discontinuità, a forma conica, costituente il fronte d'onda. Il semiangolo α di apertura del cono è definito dalla relazione

$$\operatorname{tg}\alpha = \frac{NP}{NQ} = \frac{1}{a} = \frac{1}{\sqrt{\beta^2 n^2 - 1}} = \frac{c/nv}{\sqrt{1 - c^2/n^2 v^2}}, \qquad \text{ossia } \sin\alpha = \frac{c}{nv}.$$

La regione del mezzo anteriore a tale superficie conica risulta all'istante t_0 non ancora interessata dal campo elettromagnetico generato dalla carica, il quale al detto istante interessa soltanto la regione posteriore (*). Sul fronte d'onda i campi elettrico e magnetico sono infiniti, come appare dalle (61), e (59), osservando che in tal caso è $\sin\gamma = \sin\alpha = c/nv$ e quindi $1 - n^2(v^2/c^2)\cdot\sin^2\gamma = 0$.

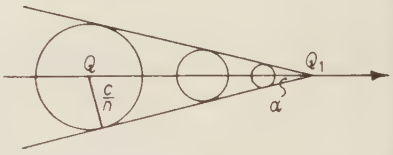

Fig. 5.

La forma del fronte d'onda è notoriamente interpretabile mediante il principio di Huyghens. Si pensi una carica in moto rettilineo uniforme con velocità v. Essa all'istante t si trovi in Q, all'istante $t+1$ in Q_1. È così $QQ_1 = v$. Evidentemente da Q esce all'istante t un'onda sferica (mezzo isotropo), la quale all'istante $t+1$ ha raggio c/n. Analogamente in tutti gli altri punti del segmento QQ_1 prendono origine onde sferiche quando essi vengono via via interessati dalla carica. Per conoscere il fronte dell'onda all'istante $t+1$ basta determinare l'inviluppo di tutte le onde sferiche così generate. Evidentemente

(*) In prossimità del fronte d'onda il vettore di Poynting risulta normale a questo e diretto verso la regione anteriore, come si può facilmente constatare mediante le (59) e (61).

tale inviluppo è una superficie conica uscente da Q_1 e tangente alla superficie sferica considerata di centro Q e raggio c/n. Il semiangolo α di apertura del cono è allora definito dalla relazione $\sin\alpha = c/nv$.

12. – Critica della soluzione di Tamm.

12·1. – Come appare dalle (58) e (61) la soluzione di Tamm presenta un campo elettrico tale che il prodotto $q\mathcal{E}(P, t)$ risulta diretto verso la carica. Invece quando è $r < c/n$ il vettore $q\mathcal{E}(P, t)$ è diretto dalla carica all'infinito, come appare dalla (54). Ancora il campo magnetico fornito dalla soluzione di Tamm ha senso contrario, come risulta dalla (59), a quello previsto dalla regola del cavatappi.

Tali considerazioni pongono interrogativi e problemi:

a) Non si comprende infatti come in tali condizioni il flusso del vettore spostamento elettrico uscente da una superficie chiusa contenente la carica q possa essere dello stesso segno della carica q.

b) Ove la carica q avesse dimensioni piccole, ma non nulle, le azioni esercitate dalle varie parti elementari di q sulle altre parti della stessa carica q darebbero luogo a una forza risultante cospirante con la velocità. Poichè, come è stato dimostrato da Frank e Tamm, quando la carica q ha una velocità maggiore di c/n essa irradia, ne verrebbe di conseguenza che la carica q irradierebbe e nello stesso tempo sarebbe accelerata dal proprio stesso campo, contrariamente al principio di conservazione dell'energia.

c) Poichè le linee di flusso del campo magnetico hanno verso contrario a quello previsto dalle note regole sui campi magnetici generati dalle correnti, una carica q che attraversasse con velocità $v > c/n$ un dielettrico immerso in un forte campo magnetostatico dovrebbe essere da questo deviata in senso contrario a quello previsto dalla legge della forza di Lorentz.

12·2. – Le cause delle incongruenze che derivano dalla soluzione di Tamm vanno ricercate nelle operazioni che portano dai potenziali ai campi. I potenziali sono forniti dalle espressioni (55) e (56)

$$(62)\qquad \begin{cases} \varphi(P, t) = 0\,, & \text{per } t < t_0, \\ \varphi(P, t) = \dfrac{2q}{\varepsilon\sqrt{(x - vt)^2 - a^2\varrho^2}}\,, & \text{per } t > t_0, \end{cases}$$

$$(63)\qquad \mathcal{A}(P, t) = \frac{\varepsilon\mu v\boldsymbol{i}}{c}\,\varphi(P, t)\,.$$

Da questi si passa ai campi mediante operazioni di derivazione, essendo

$$(64)\qquad \mathcal{E} = -\operatorname{grad}\varphi - \frac{1}{c}\frac{\partial\mathcal{A}}{\partial t}\,, \qquad \mathcal{H} = \frac{1}{\mu}\operatorname{rot}\mathcal{A}\,.$$

Ma i potenziali non sono derivabili dappertutto, a causa della superficie di discontinuità costituente il fronte d'onda. Anteriormente al fronte d'onda i potenziali sono nulli. Posteriormente al fronte d'onda e nelle sue immediate vicinanze essi sono infiniti. Tali valori infiniti sono tuttavia da attribuirsi al fatto che il dielettrico è stato supposto non dispersivo.

Si consideri infatti un dielettrico dispersivo D_ω, caratterizzato da un certo indice di rifrazione $n(\omega)$. Sarà tuttavia bene considerare tale sistema da un punto di vista matematico, cioè come un sistema che possa essere fatto tendere a un dielettrico non dispersivo D. Nel caso del sistema dispersivo D_ω i potenziali in un punto P non salteranno bruscamente, ad un certo istante t_0, da un valore nullo a un valore infinito, ma essi varieranno con continuità, portandosi in un tempo breve sì, ma finito, da un valore quasi nullo a un valore massimo, per poi ridiscendere con un andamento che, per t convenientemente maggiore di t_0, può considerarsi descritto dalle (62) e (63) con buona approssimazione. Pertanto nel caso del dielettrico dispersivo D_ω i potenziali sono sempre funzioni continue e derivabili rispetto al tempo t.

Ciò del resto è legato a un altro fatto. I potenziali presenti a un certo istante nel dielettrico dispersivo D_ω non ammettono un fronte d'onda costituito da una superficie conica di discontinuità, come nel dielettrico D. In D_ω il fronte d'onda interesserà, *grosso modo*, una regione R del dielettrico compresa fra due superfici coniche S_1 (anteriore) e S_2 (posteriore), aventi entrambe il vertice sulla carica q e angoli di apertura leggermente diversi. Se si procede lungo una retta r normale a tale fronte d'onda, attraversandolo dalla parte anteriore alla parte posteriore, si avranno potenziali quasi nulli prima di giungere su S_1 e potenziali rapidamente crescenti fra S_1 e S_2; questi raggiungeranno i loro massimi valori su S_2, per poi discendere, nell'interno di S_2, con un andamento descritto con buona approssimazione dalle (62) e (63). È allora evidente che nel caso del dielettrico dispersivo D_ω i potenziali ammettono derivate rispetto a x, y, z in ogni punto dello spazio, salvo che dove si trova la carica puntiforme q. Perciò, nel caso del dielettrico dispersivo D_ω, le operazioni (64) sono eseguibili in qualunque punto dello spazio (salvo che in q) e in qualunque istante.

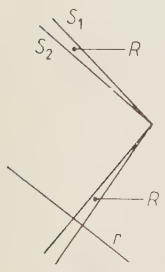

Fig. 6.

Quando il dielettrico D_ω tende al dielettrico non dispersivo D_ω i campi elettrico e magnetico presenti nei punti di D_ω esterni alla regione R tendono alla soluzione di Tamm. Ma la soluzione di Tamm non mette in evidenza quanto avviene nella regione R per $D_\omega \to D$. Allorchè D_ω tende a D le due superfici coniche S_1 e S_2 tendono l'una all'altra; i valori massimi (*) dei poten-

(*) Tali valori massimi si intendono in valore assoluto se si tratta del potenziale scalare, in modulo se si tratta del potenziale vettore.

ziali su S_2 aumentano, le derivate dei potenziali nei punti di R tendono all'infinito. Sorgono così dei termini impulsivi che non figurano nella rappresentazione di Tamm. Si tratta pertanto di costruire un opportuno algoritmo il quale permetta di esaminare i campi impulsivi che sorgono sul fronte d'onda, sia per comprendere il modo in cui essi tendono all'infinito per $D_m \to D$ e sia per studiarne la direzione e il verso.

13. – Funzioni impulsive destre e sinistre.

13'1. – Secondo il simbolismo corrente la funzione unitaria di Heaviside $1(t)$ così definita

$$1(t) = 0 \quad \text{per } t < 0\,, \qquad 1(t) = 1 \quad \text{per } t > 0$$

ammette per derivata la funzione impulsiva di Giorgi, rappresentata ordinariamente mediante il simbolo $\delta(t)$ di Dirac

$$\frac{\mathrm{d}1(t)}{\mathrm{d}t} = \delta(t)\,. \tag{65}$$

Notoriamente è $\delta(t) = 0$ per $t < 0$, $\delta(t) = 0$ per $t > 0$, $\int_{-\infty}^{+\infty} \delta(t)\,\mathrm{d}t = 1$. Se $f(t)$ è una funzione continua in $-\infty < t < +\infty$ si ha $\int_{-\infty}^{+\infty} f(t)\,\delta(t) = f(0)$. Tale integrale non è più definito se in $t = 0$ la $f(t)$ è discontinua, ad esempio, se la $f(t)$ ammette una discontinuità di prima specie. È allora opportuno introdurre due altre funzioni impulsive, $\delta^+(t)$ e $\delta^-(t)$, simbolicamente così definite

$$\delta^-(t) = 0\,, \quad \text{per } t < 0 \text{ e per } t > 0, \qquad \int_{-\infty}^{0} \delta^-(t)\,\mathrm{d}t = 1\,, \qquad \int_{0}^{+\infty} \delta^-(t)\,\mathrm{d}t = 0\,,$$

$$\delta^+(t) = 0\,, \quad \text{per } t < 0 \text{ e per } t > 0, \qquad \int_{-\infty}^{0} \delta^+(t)\,\mathrm{d}t = 0\,, \qquad \int_{0}^{+\infty} \delta^+(t)\,\mathrm{d}t = 1\,.$$

Il significato di tali definizioni è evidente. La funzione $\delta(t)$, agli effetti dell'integrazione, può considerarsi come il limite di una successione di funzioni $f_n(t)$ $(n = 1, 2, \ldots)$ simmetriche $(f_n(t) = f_n(-t))$, mai negative $(f_n(t) \geqslant 0)$, soddisfacenti alle condizioni

$$\int_{-\infty}^{+\infty} f_n(t)\,\mathrm{d}t = 1\,, \qquad \lim_{n\to\infty} \int_{-\eta}^{+\eta} f_n(t)\,\mathrm{d}t = 1\,,$$

($\eta > 0$, costante arbitrariamente piccola).

Invece il simbolo $\delta^-(t)$ denota il limite di una successione di funzioni $g_n(t)$ $(n = 1, 2, \ldots)$ soddisfacenti alle condizioni $g_n(t) = 0$ per $t > 0$, $g_n(t) > 0$ per $t < 0$,

$$\int_{-\infty}^{0} g_n(t)\,\mathrm{d}t = 1\,, \qquad \lim_{n\to\infty} \int_{-\eta}^{0} g_n(t)\,\mathrm{d}t = 1\,.$$

Analogamente $\delta^+(t)$ è il limite di una successione di funzioni $h_n(t)$ $(n = 1, 2, \ldots)$ soddisfacenti alle condizioni $h_n(t) = 0$ per $t < 0$, $h_n(t) \geqslant 0$ per $t > 0$,

$$\int_{0}^{+\infty} h_n(t)\,\mathrm{d}t = 1\,, \qquad \lim_{n\to\infty} \int_{0}^{+\eta} h_n(t)\,\mathrm{d}t = 1\,,$$

I due simboli $\delta^-(t)$ e $\delta^+(t)$ si chiameranno rispettivamente *funzione impulsiva sinistra* e *funzione impulsiva destra*.

Evidentemente se una funzione $f(t)$ ammette in $t = 0$ il limite $\lim_{t\to 0^-} f(t) = f(0^-)$ si ha

$$\int_{-\infty}^{+\infty} f(t)\,\delta^-(t)\,\mathrm{d}t = f(0^-)\,. \tag{66}$$

Si ha invece

$$\int_{-\infty}^{+\infty} f(t)\,\delta^+(t)\,\mathrm{d}t = f(0^+)\,, \tag{67}$$

se $f(t)$ ammette in $t = 0$ il limite destro.

13'2. – Sia una funzione $f(t)$ definita in $-\infty < t < +\infty$ ed ivi, ad esempio, assolutamente continua. Se allora alla funzione $1(t)\,f(t)$ si applica la regola della derivazione di un prodotto si ottiene

$$\frac{\mathrm{d}}{\mathrm{d}t}\left(1(t)f(t)\right) = 1(t)\,\frac{\mathrm{d}f(t)}{\mathrm{d}t} + f(t)\,\delta(t)\,. \tag{68}$$

Se ora si integrano i due membri in un intervallo (a, b) con $a < 0$ e $b > 0$, si ottengono risultati uguali. Ma se la $f(t)$ ammette in $t = 0$ una discontinuità di prima specie, l'integrazione dei due membri della (68) porta a risultati uguali se la funzione $\delta(t)$ che figura a secondo membro viene sostituita con la $\delta^+(t)$. Si ha infatti

$$\int_a^b \frac{\mathrm{d}}{\mathrm{d}t}\left(1(t)f(t)\right)\mathrm{d}t = f(b)\,, \qquad \int_a^b 1(t)\,\frac{\mathrm{d}f(t)}{\mathrm{d}t}\,\mathrm{d}t = f(b) - f(0^+)\,, \qquad \int_a^b f(t)\,\delta^+(t) = f(0^+)\,.$$

Appare da ciò come, allo scopo di rendere possibile l'operazione $(\mathrm{d}/\mathrm{d}t)\,(1(t)\,f(t))$ anche per funzioni discontinue in $t=0$, purchè ivi dotate di limite destro, si rende opportuno porre

$$\frac{\mathrm{d}\,1(t)}{\mathrm{d}t} = \delta^+(t)\,. \tag{69}$$

La regola

$$\frac{\mathrm{d}}{\mathrm{d}t}\big(1(t)f(t)\big) = 1(t)\,\frac{\mathrm{d}f(t)}{\mathrm{d}t} + f(t)\,\delta^+(t)\,, \tag{70}$$

è allora applicabile a funzioni $f(t)$ di andamento molto generale, come ad es. al caso in cui la $f(t)$ sia in $t=0$ dotata di limite destro. Per il resto essa potrà essere assolutamente continua per $t>0$ e ad andamento qualunque per $t<0$.

13'3. – Sia ora $f(t)$ una funzione di andamento qualsivoglia per $t<0$, assolutamente continua in ogni intervallo $\eta \leqslant t < -\infty$ (η costante arbitraria maggiore di zero) e inoltre soddisfacente alla condizione $\lim_{t\to 0^+} f(t) = +\infty$.

Si costruisca allora una successione di funzioni tagliate $f_n(t)$ $(n=1, 2, 3, \ldots)$ definite nel seguente modo:

sia $f_n(t) = f(t)$ per $t<0$;

sia $f_n(t) = f(t)$ in ogni punto $t>0$ in cui è $f(t)<n$;

sia $f_n(t) = n$ in ogni punto $t>0$ in cui è $f(t)\geqslant n$.

Per il fatto che è $\lim_{t\to 0^+} f(t) = +\infty$, ogni funzione $f_n(t)$ è assolutamente continua nell'intervallo $t>0$ ed è in $t=0$ dotata di limite destro. A ciascuna di esse si può allora applicare la (70). Si ha così

$$\frac{\mathrm{d}}{\mathrm{d}t}\big(1(t)f_n(t)\big) = 1(t)\,\frac{\mathrm{d}f_n}{\mathrm{d}t} + f_n(t)\,\delta^+(t)\,, \qquad (n=1, 2, 3, \ldots). \tag{71}$$

L'insieme delle infinite relazioni ora scritte sarà indicato mediante la notazione simbolica

$$\frac{\mathrm{d}}{\mathrm{d}t}\big(1(t)f(t)\big) = f(t)\,\delta^+(t) + 1(t)\,\frac{\mathrm{d}f}{\mathrm{d}t}\,, \tag{72}$$

alla quale viene così attribuito un senso anche se la funzione $f(t)$ che in essa figura è infinita positiva in 0^+.

Mutando la $f(t)$ nella $-f(t)$ si ottiene l'estensione al caso in cui la funzione tenda in 0^+ al limite $-\infty$. Sostituendo poi la variabile t con la $-t$

si ottiene l'estensione della (72) al caso in cui la funzione sia infinita positiva o infinita negativa in 0^-.

Le estensioni fatte in questo paragrafo si rendono necessarie per dare un senso al simbolismo che sarà in seguito usato. Tutto si riduce, per quanto riguarda il simbolismo, a sostituire l'usuale relazione (65) con la (69) (*).

14. – Nuova rappresentazione dei campi nel caso del dielettrico non dispersivo.

I potenziali (62) e (63) possono essere così rappresentati

$$(73) \qquad \varphi(P,t) = \frac{2q1(t-t_0)}{\varepsilon\sqrt{(x-vt)^2 - a^2\varrho^2}}, \qquad \mathscr{A}(P,t) = \frac{\varepsilon\mu v i}{c}\varphi(P,t),$$

dove è

$$t_0 = \frac{x}{v} + \frac{a\varrho}{v}.$$

I campi elettrico $\mathscr{E}(P,t)$ e magnetico $\mathscr{H}(P,t)$ saranno ora ricavati dalle (73) attraverso le relazioni

$$\mathscr{E} = -\operatorname{grad}\varphi - \frac{1}{c}\frac{\partial\mathscr{A}}{\partial t}, \qquad \mathscr{H} = \frac{1}{\mu}\operatorname{rot}\mathscr{A},$$

(*) Si faccia attenzione ad evitare equivoci del genere del seguente:

$$\frac{\mathrm{d}}{\mathrm{d}t}[1(t)]^2 = 2\frac{\mathrm{d}}{\mathrm{d}t}1(t) = 2\delta^+(t).$$

Per essere $[1(t)]^2 = 1(t)$, tale risultato è in contrasto con la (69).

A rigore si dovrebbero usare due diversi simboli per esprimere le derivate di una funzione. Il simbolo $\mathrm{d}/\mathrm{d}t$ dovrebbe operare soltanto nei punti di una funzione $f(t)$ nei quali essa ammette derivata nel senso classico del termine. Nei punti in cui tale derivata non esiste si farà uso della convenzione $\mathrm{d}f(t)/\mathrm{d}t = 0$. Un altro simbolo, ad es. $\mathrm{D}/\mathrm{D}t$, dovrebbe invece essere usato per indicare non solo la derivata ordinaria, ma anche la derivata eseguita nei punti di discontinuità della funzione. In un punto della $f(t)$ in cui esiste la derivata ordinaria è allora $\mathrm{d}f(t)/\mathrm{d}t = \mathrm{D}f(t)/\mathrm{D}t$. Ma, per le convenzioni precedenti, è $\mathrm{D}1(t)/\mathrm{D}t = \delta^+(t)$; $\mathrm{d}1(t)/\mathrm{d}t = 0$. La regola (72) sarà allora così scritta

$$\frac{\mathrm{D}}{\mathrm{D}t}(1(t)f(t)) = 1(t)\frac{\mathrm{d}f(t)}{\mathrm{d}t} + f(t)\delta^+(t).$$

Con tale regola si ha

$$\frac{\mathrm{D}}{\mathrm{D}t}[1(t)]^2 = 1(t)\frac{\mathrm{d}1(t)}{\mathrm{d}t} + 1(t)\delta^+(t) = 1(t)\delta^+(t) = \delta^+(t).$$

Ci esimiamo tuttavia dall'introdurre ulteriori precisazioni e sviluppi dato l'uso limitato che sarà qui fatto dell'algoritmo introdotto.

e facendo uso della (72). Si ha intanto

$$\mathscr{E}(P,t) = \left(-\operatorname{grad} - \frac{\varepsilon\mu v\boldsymbol{i}}{c^2}\frac{\partial}{\partial t}\right)\frac{2q1(t-t_0)}{\varepsilon\sqrt{(x-vt)^2-a^2\varrho^2}}, \tag{74}$$

$$\mathscr{H}(P,t) = -\frac{\varepsilon v\boldsymbol{i}}{c}\wedge\operatorname{grad}\frac{2q1(t-t_0)}{\varepsilon\sqrt{(x-vt)^2-a^2\varrho^2}}. \tag{75}$$

Si osservi ora che è

$$\frac{\partial}{\partial t}1(t-t_0) = \delta^+(t-t_0),$$

$$\operatorname{grad}1(t-t_0) = \frac{\mathrm{d}1(t-t_0)}{\mathrm{d}(t-t_0)}\operatorname{grad}(t-t_0) = -\delta^+(t-t_0)\operatorname{grad}t_0,$$

$$\operatorname{grad}t_0 = \frac{1}{v}\left(\boldsymbol{i}+\frac{a}{\varrho}(y\boldsymbol{j}+z\boldsymbol{k})\right),$$

e quindi

$$\operatorname{grad}1(t-t_0) = -\frac{1}{v}\left(\boldsymbol{i}+\frac{ay}{\varrho}\boldsymbol{j}+\frac{az}{\varrho}\boldsymbol{k}\right)\delta^+(t-t_0).$$

In seguito, per semplicità, si farà uso della posizione

$$R = \sqrt{(x-vt)^2-a^2\varrho^2}.$$

In corrispondenza dei due termini che figurano al secondo membro della (72) è opportuno scindere la soluzione in due parti, ponendo

$$\mathscr{E}(P,t) = \mathscr{E}^{(0)}(P,t)+\mathscr{E}^{(i)}(P,t), \quad \mathscr{H}(P,t) = \mathscr{H}^{(0)}(P,t)+\mathscr{H}^{(i)}(P,t), \tag{76}$$

con

$$\mathscr{E}^{(0)}(P,t) = 1(t-t_0)\left(-\operatorname{grad} - \frac{\varepsilon\mu v\boldsymbol{i}}{c^2}\frac{\partial}{\partial t}\right)\frac{2q}{\varepsilon R},$$

$$\mathscr{H}^{(0)}(P,t) = -1(t-t_0)\frac{v\boldsymbol{i}}{c}\wedge\operatorname{grad}\frac{2q}{R},$$

$$\mathscr{E}^{(i)}(P,t) = \frac{2q}{\varepsilon R}\left(-\operatorname{grad} - \frac{\varepsilon\mu v\boldsymbol{i}}{c^2}\frac{\partial}{\partial t}\right)1(t-t_0) =$$

$$\frac{2q}{\varepsilon R}\left(\frac{\boldsymbol{i}}{r} + \frac{ay}{\varrho r}\boldsymbol{j} + \frac{az}{\varrho r}\boldsymbol{k} - \frac{\varepsilon\mu v\boldsymbol{i}}{c^2}\right)\delta^+(t-t_0).$$

È ora $a^2 = (n^2v^2/c^2) - 1$, per $v > c/n$ e quindi

$$\frac{\boldsymbol{i}}{v} - \frac{\varepsilon\mu v\boldsymbol{i}}{c^2} = \frac{\boldsymbol{i}}{v}\left(1 - \frac{n^2v^2}{c^2}\right) = -\frac{a^2\boldsymbol{i}}{v},$$

per cui

$$\mathscr{E}^{(i)}(P, t) = \frac{2q}{\varepsilon vR}\left(-a^2\boldsymbol{i} + \frac{ay}{\varrho}\boldsymbol{j} + \frac{az}{\varrho}\boldsymbol{k}\right)\delta^+(t - t_0)\,. \tag{77}$$

Si porrà ancora

$$\mathscr{H}^{(i)}(P, t) = -\frac{2qv\boldsymbol{i}}{cR} \wedge \operatorname{grad} 1(t - t_0) = \tag{78}$$

$$= \frac{2q\boldsymbol{i}}{cR} \wedge \left(\boldsymbol{i} + \frac{ay}{\varrho}\boldsymbol{j} + \frac{az}{\varrho}\boldsymbol{k}\right)\delta^+(t - t_0) = \frac{\varepsilon\boldsymbol{v}}{c} \wedge \mathscr{E}^{(i)}(P, t)\,.$$

Evidentemente i campi $\mathscr{E}^{(0)}(P, t)$ e $\mathscr{H}^{(0)}(P, t)$ sono quelli relativi alla soluzione di Tamm e forniti dai secondi membri delle (58) e (59). Per queste e per le espressioni dei campi impulsivi ora scritte le (76) danno luogo alle seguenti

$$\mathscr{E}(P, t) = -\frac{2qa^2}{\varepsilon R^3}\left[(x - vt)\boldsymbol{i} + y\boldsymbol{j} + z\boldsymbol{k}\right]1(t - t_0) + \tag{79}$$

$$+ \frac{2q}{\varepsilon vR}\left(-a^2\boldsymbol{i} + \frac{ay}{\varrho}\boldsymbol{j} + \frac{az}{\varrho}\boldsymbol{k}\right)\delta^+(t - t_0)\,,$$

$$\mathscr{H}(P, t) = \frac{\varepsilon\boldsymbol{v}}{c} \wedge \mathscr{E}(P, t)\,. \tag{80}$$

È ora interessante esaminare la direzione e il verso dei campi impulsivi $\mathscr{E}^{(i)}$ e $\mathscr{H}^{(i)}$. Si osservi che per valori di t che cadono nell'intorno destro di t_0 l'espressione $(2/\varepsilon vR)\,\delta^+(t - t_0)$ è positiva (cioè indica la tendenza a un limite infinito positivo). Pertanto in un punto $P(x, y, z)$ del fronte d'onda la direzione e il verso del vettore $q\mathscr{E}^{(i)}(P, t)$ sono, per la (77), quelli del vettore $-a^2\boldsymbol{i} + (ay/\varrho)\boldsymbol{j} + (az/\varrho)\boldsymbol{k}$. Ora tale vettore ha proiezione sull'asse x contraria alla velocità $\boldsymbol{v}$ della carica. Inoltre, essendo $\sqrt{(a^2y^2/\varrho^2) + (a^2z^2/\varrho^2)} = a$, il vettore considerato forma con la velocità $\boldsymbol{v}$ della carica un angolo il cui seno è

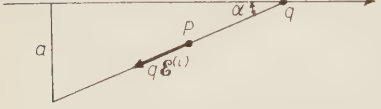

Fig. 7.

$$\frac{a}{\sqrt{a^2 + a^4}} = \frac{1}{\sqrt{1 + a^2}} = \frac{1}{\sqrt{n^2v^2/c^2}} = \frac{c}{nv}\,.$$

Ora questo è proprio l'angolo di semi apertura del cono la cui superficie costituisce il fronte d'onda.

Con ciò appare chiaramente il meccanismo della radiazione di Čerenkov. In un punto P del fronte d'onda è presente un campo elettrico impulsivo $\mathcal{E}^{(i)}$ (nella figura a lato i versi dei campi si riferiscono a una carica $q > 0$). Posteriormente al fronte d'onda è presente un campo elettrico $\mathcal{E}^{(0)}$ di valore finito. Tuttavia nelle immediate vicinanze del punto P tale campo $\mathcal{E}^{(0)}$ tende a diventare parallelo a $\mathcal{E}^{(i)}$, di verso opposto a $\mathcal{E}^{(i)}$ e di modulo infinito.

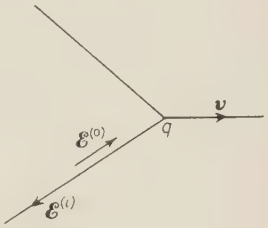

Fig. 8.

Analogo discorso si può fare per il campo magnetico, dato che per la (78) il campo magnetico impulsivo $\mathcal{H}^{(i)}$ presente sul fronte d'onda ha senso conforme alla regola del cavatappi.

Si osservi che il vettore di Poynting formato con i campi impulsivi $\mathcal{E}^{(i)}$ e $\mathcal{H}^{(i)}$ è normale al fronte d'onda e diretto secondo il verso di avanzamento di esso. Tale direzione e verso caratterizzano pure il vettore di Poynting costruito sui campi $\mathcal{E}^{(0)}$ e $\mathcal{H}^{(0)}$ in prossimità del fronte d'onda.

La nuova rappresentazione della radiazione di Čerenkov a cui si è testè pervenuti è esente dalle critiche formulate al n. **12** a motivo delle direzioni e dei versi dei campi impulsivi. In particolare il campo elettrico impulsivo $\mathcal{E}^{(i)}$ esercita una reazione frenante sulla carica che irradia. Poichè tale effetto deve prevalere sull'effetto acceleratore del campo $\mathcal{E}^{(0)}$, si comprende come i campi impulsivi siano di gran lunga più importanti dei campi $\mathcal{E}^{(0)}$ e $\mathcal{H}^{(0)}$ che intervengono nella rappresentazione di Tamm. Indubbiamente l'energia irradiata dalla particella è prevalentemente dovuta ai campi impulsivi e quindi concentrata per la maggior parte sul fronte d'onda.

Capitolo Terzo

CAMPO ELETTROMAGNETICO GENERATO DA UNA CARICA IN MOTO VARIO

15. – Rappresentazioni integrali delle trasformate di Fourier rispetto alla variabile di partenza. Caso generale. Mezzo dispersivo.

Il caso che viene trattato nel presente capitolo riguarda una carica puntiforme q moventesi di moto vario in un dielettrico omogeneo e isotropo, perfettamente isolante.

Per utilizzare direttamente il teorema del n. **7** si considererà una carica q percorrente la curva C di equazioni parametriche

$$x = x(\theta)\,, \quad y = y(\theta)\,, \quad z = z(\theta)\,, \qquad -\infty < \theta < +\infty \tag{81}$$

con la legge del moto

$$\theta = t\,. \tag{82}$$

I potenziali scalare $\varphi_L(P, t)$ e vettore $\mathscr{A}_L(P, t)$ generati in un punto $P(x, y, z)$ all'istante t da una corrente di convezione percorrente la curva C con intensità $I(\theta, t)$ e con densità lineica $\varrho_l(\theta, t)$ di carica elettrica sono ottenibili mediante le (4) del n. 2,

$$\varphi_L(P, t) = \frac{1}{\varepsilon}\int_{-\infty}^{+\infty} \frac{\varrho_l(\theta,\, t - nr/c)}{r}\, r(\theta)\,\mathrm{d}\theta\,, \qquad \mathscr{A}_L(P, t) = \frac{\mu}{c}\int_{-\infty}^{+\infty} \frac{I(\theta,\, t - nr/c)}{r}\, \boldsymbol{v}(\theta)\,\mathrm{d}\theta\,,$$

dove $\boldsymbol{v}(\theta)\,\mathrm{d}\theta$ è l'elemento della curva C e $r(\theta)\,\mathrm{d}\theta$ la sua lunghezza

$$\boldsymbol{v}(\theta) = \frac{\mathrm{d}x(\theta)}{\mathrm{d}\theta}\,\boldsymbol{i} + \frac{\mathrm{d}y(\theta)}{\mathrm{d}\theta}\,\boldsymbol{j} + \frac{\mathrm{d}z(\theta)}{\mathrm{d}\theta}\,\boldsymbol{k}\,, \qquad r(\theta) = \sqrt{\left(\frac{\mathrm{d}x(\theta)}{\mathrm{d}\theta}\right)^2 + \left(\frac{\mathrm{d}y(\theta)}{\mathrm{d}\theta}\right)^2 + \left(\frac{\mathrm{d}z(\theta)}{\mathrm{d}\theta}\right)^2}\,.$$

Si è inoltre posto

$$\boldsymbol{r} = (x - x(\theta))\,\boldsymbol{i} + (y - y(\theta))\,\boldsymbol{j} + (z - z(\theta))\,\boldsymbol{k}\,,$$
$$r = \sqrt{(x - x(\theta))^2 + (y - y(\theta))^2 + (z - z(\theta))^2}\,,$$

Il vettore $\boldsymbol{r}$ è perciò il segmento che va dal punto θ di C al punto $P(x, y, z)$.

Ponendo ora, conformemente al teorema del n. 7,

$$I(\theta, t) = q\exp\left[-i\omega(\theta - t)\right], \qquad \varrho_l(\theta, t) = \frac{q}{r(\theta)}\exp\left[-i\omega(\theta - t)\right],$$

dalle precedenti si ha

$$\begin{cases} \varphi_L(P, t) = \dfrac{q}{\varepsilon}\displaystyle\int_{-\infty}^{+\infty} \exp\left[-i\omega\left(\theta - t + \frac{nr}{c}\right)\right]\frac{\mathrm{d}\theta}{r}\,, \\[2ex] \mathscr{A}_L(P, t) = \dfrac{q\mu}{c}\displaystyle\int_{-\infty}^{+\infty} \exp\left[-i\omega\left(\theta - t + \frac{nr}{c}\right)\right]\frac{\boldsymbol{v}\,\mathrm{d}\theta}{r}\,. \end{cases} \tag{83}$$

Da queste mediante le relazioni (3) del n. 2

$$\mathscr{E} = -\operatorname{grad}\varphi - \frac{1}{c}\frac{\partial\mathscr{A}}{\partial t}\,, \qquad \mathscr{H} = \frac{1}{\mu}\operatorname{rot}\mathscr{A}\,,$$

si deducono i campi elettrico $\mathcal{E}_L(P,t)$ e magnetico $\mathcal{H}_L(P,t)$. Si osservi a tale scopo che è

$$\operatorname{grad}\frac{\exp\left[-i\omega(\vartheta-nr/c)\right]}{r} = -\exp\left[-i\omega\left(\vartheta-\frac{nr}{c}\right)\right]\left(\frac{1}{r}-\frac{i\omega n}{c}\right)\frac{\boldsymbol{r}}{r^2},$$

e quindi

$$\mathcal{E}_L(P,t)=\frac{q}{\varepsilon}\int_{-\infty}^{-\infty}\exp\left[-i\omega\left(\vartheta-t-\frac{nr}{c}\right)\right]\cdot$$

$$\cdot\left(\frac{1}{r}-\frac{i\omega n}{c}\right)\frac{\boldsymbol{r}}{r^2}\,d\vartheta-\frac{qi\omega\mu}{c^2}\int_{-\infty}^{+\infty}\exp\left[-i\omega\left(\vartheta-t-\frac{nr}{c}\right)\right]\boldsymbol{v}(\vartheta)\,d\vartheta,$$

ossia

$$\mathcal{E}_L(P,t)=q\int_{-\infty}^{-\infty}\exp\left[-i\omega\left(\vartheta-t-\frac{nr}{c}\right)\right]\left(\frac{1}{r}-\frac{i\omega n}{c}\right)\frac{\boldsymbol{r}}{cr^2}-\frac{i\omega q}{c^2r}\boldsymbol{v}\,d\vartheta. \tag{84}$$

È poi

$$\operatorname{rot}\frac{\exp\left[-i\omega\left(\vartheta-nr/c\right)\right]}{r}\boldsymbol{v}(\vartheta)=\operatorname{grad}\frac{\exp\left[-i\omega(\vartheta-nr/c)\right]}{r}\wedge\boldsymbol{v}(\vartheta).$$

Utilizzando allora la precedente espressione del gradiente si può scrivere

$$\mathcal{H}_L(P,t)=-\frac{q}{c}\int_{-\infty}^{+\infty}\exp\left[-i\omega\left(\vartheta-t-\frac{nr}{c}\right)\right]\left(\frac{1}{r}-\frac{i\omega n}{c}\right)\frac{\boldsymbol{r}}{r^2}\wedge\boldsymbol{v}\,d\vartheta. \tag{85}$$

La variabile ϑ sarà anche chiamata *variabile di emissione* o *variabile di partenza*. I secondi membri delle (83), (84) e (85) sono perciò rappresentazioni integrali rispetto alla variabile di emissione (o di partenza), in quanto che la variabile di integrazione che in essi figura è la variabile ϑ. Per il teorema del n. 7 essi forniscono, quando vi si faccia $t=0$, le trasformate di Fourier dei potenziali e campi generati dalla carica puntiforme q.

16. – Rappresentazioni integrali delle trasformate di Fourier rispetto alla variabile di arrivo. Caso $\tau(\vartheta)$ sempre crescente. Mezzo dispersivo.

16·1. – Nel presente numero e in altri successivi si daranno nuove rappresentazioni delle trasformate di Fourier dei potenziali e dei campi generati dalla carica q, pure valide nel caso in cui il mezzo sia dispersivo.

Si consideri la funzione $\tau(\theta)$ della variabile θ così definita

$$\tau = \theta + \frac{nr(\theta)}{c} = \theta + \frac{n}{c}\sqrt{[x - x(\theta)]^2 + [y - y(\theta)]^2 + [z - z(\theta)]^2}\,, \tag{86}$$

dove con n si intende il valore dell'indice di rifrazione del mezzo relativo alla pulsazione ω che figura nelle (83), (84) e (85). Il caso che verrà trattato nel presente numero è quello in cui la funzione $\tau(\theta)$ è sempre crescente in tutto l'intervallo $-\infty < \theta < +\infty$, soddisfacendo inoltre alle condizioni $\lim_{\theta\to+\infty}\tau = +\infty$ $\lim_{\theta\to-\infty}\tau = -\infty$. Il significato fisico di tali condizioni è chiarito dalle considerazioni seguenti.

Si ammetta che l'estremo superiore dei valori assunti dalla velocità $v(\theta)$ della carica in $-\infty < \theta < +\infty$ sia minore di c/n. Dalla (86) si ha

$$\frac{d\tau}{d\theta} = 1 + \frac{n}{c}\frac{dr(\theta)}{d\theta} = 1 - \frac{n}{c}\frac{\boldsymbol{r}(\theta)\cdot\boldsymbol{v}(\theta)}{r(\theta)}\,. \tag{86'}$$

Per l'ipotesi formulata sull'estremo superiore della velocità $v(\theta)$ esiste un numero $\eta > 0$ per cui si ha $v(\theta) < (c/n) - \eta$. Essendo allora $\boldsymbol{r}(\theta)\,\boldsymbol{v}(\theta)/r(\theta) < v(\theta)$ consegue $d\tau/d\theta > \eta n/c$. Pertanto la funzione τ della variabile θ non solo è sempre crescente, ma al variare di θ da $-\infty$ a $+\infty$ varia essa pure da $-\infty$ a $+\infty$. Si può anche scrivere

$$\frac{d\theta}{d\tau} = \frac{1}{1 - \dfrac{n}{c}\dfrac{\boldsymbol{r}(\theta)\cdot\boldsymbol{v}(\theta)}{r(\theta)}}\,. \tag{87}$$

in quanto che dall'ipotesi che τ sia funzione sempre crescente di θ segue che θ può a sua volta considerarsi funzione di τ, crescente da $-\infty$ a $+\infty$ al variare di τ da $-\infty$ a $+\infty$.

La nuova variabile τ, di cui θ è funzione tramite la (86), si chiamerà *variabile di ricezione* o *di arrivo*. Nei seguenti numeri si stabiliranno rappresentazioni integrali nelle quali la variabile d'integrazione è la variabile di arrivo τ.

16'2. *Trasformate dei potenziali.* – Dalle (83) per la (86) si ha

$$q_L(P, 0) = \frac{q}{\varepsilon}\int_{-\infty}^{+\infty}\exp\left[-i\omega\tau\right]\frac{1}{r(\theta)}\frac{d\theta}{d\tau}\,d\tau\,,$$

ossia, per la (87),

$$q_L(P, 0) = \int_{-\infty}^{+\infty}\exp\left[-i\omega\tau\right]\frac{q/\varepsilon}{r(\theta) - (n/c)\,\boldsymbol{r}(\theta)\cdot\boldsymbol{v}(\theta)]}\,d\tau\,. \tag{88}$$

Analogamente

$$\mathcal{A}_L(P,0)=\int_{-\infty}^{+\infty}\exp\left[-i\omega\tau\right]\frac{(q\mu/c)\boldsymbol{v}(\theta)}{r(\theta)-(n/c)\boldsymbol{r}(\theta)\cdot\boldsymbol{v}(\theta)}\,\mathrm{d}\tau\,. \tag{89}$$

16·3. *Trasformate dei campi.* – Anche negli integrali (84) e (85) si può procedere alla sostituzione della variabile θ con la variabile τ come nel caso precedente. Si ha così

$$\mathcal{E}_L(P,0)=q\int_{-\infty}^{+\infty}\exp\left[-i\omega\tau\right]\left[\left(\frac{1}{r}+\frac{i\omega n}{c}\right)\frac{\boldsymbol{r}}{\varepsilon r}-\frac{i\omega\mu}{c^2}\,\boldsymbol{v}\right]\frac{1}{r-(n/c)(\boldsymbol{r}\cdot\boldsymbol{v})}\,\mathrm{d}\tau=$$

$$=q\int_{-\infty}^{+\infty}\exp\left[-i\omega\tau\right]\frac{\boldsymbol{r}}{\varepsilon r^2}\frac{1}{r-(n/c)(\boldsymbol{r}\cdot\boldsymbol{v})}\,\mathrm{d}\tau+q\int_{-\infty}^{+\infty}\exp\left[-i\omega\tau\right]i\omega\,\frac{(n/c)(\boldsymbol{r}/\varepsilon r)-(\mu/c^2)\boldsymbol{v}}{r-(n/c)(\boldsymbol{r}\cdot\boldsymbol{v})}\,\mathrm{d}\tau\,,$$

dove le grandezze r, $\boldsymbol{r}$ e $\boldsymbol{v}$ che figurano sotto tali integrali sono tutte funzioni di θ, considerate in corrispondenza del particolare valore di θ legato a τ dalla (86). È ora opportuno trasformare l'ultimo integrale scritto mediante integrazione per parti al fine di far sparire il fattore $i\omega$. Posto allora

$$\boldsymbol{g}=\frac{n}{c\varepsilon}\frac{\boldsymbol{r}}{r}-\frac{\mu}{c^2}\,\boldsymbol{v}\,,\qquad s=r-\frac{n}{c}\,\boldsymbol{r}\cdot\boldsymbol{v}\,, \tag{90}$$

si può effettuare la seguente trasformazione

$$\mathcal{E}_L(P,0)=q\int_{-\infty}^{+\infty}\exp\left[-i\omega\tau\right]\frac{\boldsymbol{r}}{\varepsilon s r^2}\,\mathrm{d}\tau- \tag{91}$$

$$-q\left|\exp\left[-i\omega\tau\right]\frac{\boldsymbol{g}}{s}\right|_{-\infty}^{+\infty}+q\int_{-\infty}^{+\infty}\exp\left[-i\omega\tau\right]\frac{\mathrm{d}}{\mathrm{d}\tau}\left(\frac{\boldsymbol{g}}{s}\right)\mathrm{d}\tau\,.$$

Si ammetterà ora che per $\theta=-\infty$ e per $\theta=+\infty$ (tali valori corrispondono ai valori $-\infty$ e $+\infty$ di τ) la carica q sia infinitamente lontana dal punto $P(x,y,z)$. È perciò $\left[\exp\left[-i\omega\tau\right](\boldsymbol{g}/s)\right]_{-\infty}^{+\infty}=0$. Si ha così

$$\mathcal{E}_L(P,0)=q\int_{-\infty}^{+\infty}\exp\left[-i\omega\tau\right]\left|\frac{\boldsymbol{r}}{\varepsilon r^2 s}+\frac{\mathrm{d}}{\mathrm{d}\tau}\left(\frac{\boldsymbol{g}}{s}\right)\right|\mathrm{d}\tau\,. \tag{92}$$

Con le posizioni precedentemente introdotte la (87) diventa

$$\frac{\mathrm{d}\theta}{\mathrm{d}\tau} = \frac{r}{s}. \tag{93}$$

Si ha così

$$\frac{\boldsymbol{r}}{\varepsilon r^2 s} \cdot \frac{\mathrm{d}}{\mathrm{d}\tau}\left(\frac{\boldsymbol{g}}{s}\right) = \frac{\boldsymbol{r}}{\varepsilon r^2 s} \cdot \frac{r}{s}\,\frac{s(\mathrm{d}\boldsymbol{g}/\mathrm{d}\theta) - \boldsymbol{g}(\mathrm{d}s/\mathrm{d}\theta)}{s^2} = \frac{1}{s^3}\left[rs\frac{\mathrm{d}\boldsymbol{g}}{\mathrm{d}\theta} - r\boldsymbol{g}\frac{\mathrm{d}s}{\mathrm{d}\theta} + \frac{s^2\boldsymbol{r}}{\varepsilon r^2}\right],$$

e quindi

$$\boldsymbol{\mathcal{E}}_L(P,0) = \int_{-\infty}^{+\infty} \exp\left[-i\omega\tau\right] \frac{q}{s^3}\left[rs\frac{\mathrm{d}\boldsymbol{g}}{\mathrm{d}\theta} - r\boldsymbol{g}\frac{\mathrm{d}s}{\mathrm{d}\theta} + \frac{s^2\boldsymbol{r}}{\varepsilon r^2}\right]\mathrm{d}\tau\,.$$

È ora (si tenga presente che è $\mathrm{d}\boldsymbol{r}/\mathrm{d}\theta = -\boldsymbol{v}$, $\mathrm{d}\boldsymbol{v}/\mathrm{d}\theta = \dot{\boldsymbol{v}}$, $\mathrm{d}r/\mathrm{d}\theta = -(\boldsymbol{r}\cdot\boldsymbol{v})/r$)

$$\frac{\mathrm{d}\boldsymbol{g}}{\mathrm{d}\theta} = -\frac{n}{c\varepsilon}\frac{\boldsymbol{v}}{r} + \frac{n}{c\varepsilon}\frac{(\boldsymbol{r}\cdot\boldsymbol{v})\boldsymbol{r}}{r^3} - \frac{\mu}{c^2}\dot{\boldsymbol{v}}\,,$$

$$\frac{\mathrm{d}s}{\mathrm{d}\theta} = -\frac{\boldsymbol{r}\cdot\boldsymbol{v}}{r} + \frac{n}{c}v^2 - \frac{n}{c}\boldsymbol{r}\cdot\dot{\boldsymbol{v}}\,,$$

$$s^2 = r^2 + \frac{n^2}{c^2}(\boldsymbol{r}\cdot\boldsymbol{v})^2 - \frac{2n}{c}r(\boldsymbol{r}\cdot\boldsymbol{v})\,,$$

e quindi

$$rs\frac{\mathrm{d}\boldsymbol{g}}{\mathrm{d}\theta} - r\boldsymbol{g}\frac{\mathrm{d}s}{\mathrm{d}\theta} + \frac{s^2\boldsymbol{r}}{\varepsilon r^2} = -\left(r^2 - \frac{n}{c}r(\boldsymbol{r}\cdot\boldsymbol{v})\right)\left(-\frac{n}{c\varepsilon}\frac{\boldsymbol{v}}{r} + \frac{n}{c\varepsilon}\frac{(\boldsymbol{r}\cdot\boldsymbol{v})\boldsymbol{r}}{r^3} - \frac{\mu}{c^2}\dot{\boldsymbol{v}}\right)$$

$$\left(\frac{n}{c\varepsilon}\boldsymbol{r} + \frac{\mu}{c^2}r\boldsymbol{v}\right)\left(-\frac{\boldsymbol{r}\cdot\boldsymbol{v}}{r} + \frac{n}{c}v^2 - \frac{n}{c}\boldsymbol{r}\cdot\dot{\boldsymbol{v}}\right) - \left(r^2 - \frac{n^2}{c^2}(\boldsymbol{r}\cdot\boldsymbol{v})^2 - \frac{2n}{c}r(\boldsymbol{r}\cdot\boldsymbol{v})\right)\frac{\boldsymbol{r}}{\varepsilon r^2}.$$

Sviluppando l'espressione a secondo membro ed eliminando i termini che si presentano con segno opposto si ottiene

$$rs\frac{\mathrm{d}\boldsymbol{g}}{\mathrm{d}\theta} - r\boldsymbol{g}\frac{\mathrm{d}s}{\mathrm{d}\theta} + \frac{s^2\boldsymbol{r}}{\varepsilon r^2} = -\frac{n}{c\varepsilon}r\boldsymbol{v} - \frac{\mu}{c^2}r^2\dot{\boldsymbol{v}} + \frac{n\mu}{c^3}r(\boldsymbol{r}\cdot\boldsymbol{v})\dot{\boldsymbol{v}} -$$

$$\frac{n^2}{c^2\varepsilon}v^2\boldsymbol{r} + \frac{n^2}{c^2\varepsilon}(\boldsymbol{r}\cdot\dot{\boldsymbol{v}})\boldsymbol{r} + \frac{\mu n}{c^3}rv^2\boldsymbol{v} - \frac{\mu n}{c^3}r(\boldsymbol{r}\cdot\dot{\boldsymbol{v}})\boldsymbol{v} + \frac{\boldsymbol{r}}{\varepsilon} =$$

$$= \frac{1}{\varepsilon}\left(1 - \frac{n^2v^2}{c^2}\right)\left(\boldsymbol{r} - \frac{nr\boldsymbol{v}}{c}\right) + \frac{\mu}{c^2}\boldsymbol{r}\wedge\left|\left(\boldsymbol{r} - \frac{nr\boldsymbol{v}}{c}\right)\wedge\dot{\boldsymbol{v}}\right|. \tag{94}$$

Si ha così

$$(95)\qquad \mathscr{E}_L(P,0) = -\int_{-\infty}^{+\infty} \exp[-i\omega\tau]\,\frac{q}{s^3}\left\{\frac{1}{\varepsilon}\left(1-\frac{n^2v^2}{c^2}\right)\left(\boldsymbol{r}-\frac{nr\boldsymbol{v}}{c}\right)+\frac{\mu}{c^2}\,\boldsymbol{r}\wedge\left[\left(\boldsymbol{r}-\frac{nr}{c}\,\boldsymbol{v}\right)\wedge\dot{\boldsymbol{v}}\right]\right\}\mathrm{d}\tau\,.$$

Per quanto riguarda l'integrale (85), con procedimento analogo si trova

$$\mathscr{H}_L(P,0) = -\frac{q}{c}\int_{-\infty}^{+\infty}\exp[-i\omega\tau]\left(\frac{1}{r}+\frac{i\omega n}{c}\right)\frac{\boldsymbol{r}}{r^2}\wedge\boldsymbol{v}\,\frac{r}{s}\,\mathrm{d}\tau =$$

$$= -\frac{q}{c}\int_{-\infty}^{+\infty}\exp[-i\omega\tau]\,\frac{\boldsymbol{r}}{sr^2}\wedge\boldsymbol{v}\,\mathrm{d}\tau - \frac{q}{c}\int_{-\infty}^{+\infty}\exp[-i\omega\tau]\,\frac{i\omega n\boldsymbol{r}}{csr}\wedge\boldsymbol{v}\,\mathrm{d}\tau =$$

$$= -\frac{q}{c}\int_{-\infty}^{+\infty}\exp[-i\omega\tau]\,\frac{\boldsymbol{r}}{sr^2}\wedge\boldsymbol{v}\,\mathrm{d}\tau + \frac{q}{c}\left[\exp[-i\omega\tau]\,\frac{n\boldsymbol{r}}{csr}\wedge\boldsymbol{v}\right]_{-\infty}^{+\infty} -$$

$$-\frac{q}{c}\int_{-\infty}^{+\infty}\exp[-i\omega\tau]\,\frac{\mathrm{d}}{\mathrm{d}\tau}\left(\frac{n\boldsymbol{r}\wedge\boldsymbol{v}}{csr}\right)\mathrm{d}\tau = -\frac{q}{c}\int_{-\infty}^{+\infty}\exp[-i\omega\tau]\left(\frac{\boldsymbol{r}\wedge\boldsymbol{v}}{sr^2}+\frac{r}{s}\,\frac{\mathrm{d}}{\mathrm{d}\theta}\,\frac{n\boldsymbol{r}\wedge\boldsymbol{v}}{csr}\right)\mathrm{d}\tau -$$

$$= \int_{-\infty}^{+\infty}\exp[-i\omega\tau]\,\frac{q}{c}\left(\frac{\boldsymbol{v}}{sr^2}+\frac{r}{s}\,\frac{\mathrm{d}}{\mathrm{d}\theta}\,\frac{n\boldsymbol{v}}{csr}\right)\wedge\boldsymbol{r}\,\mathrm{d}\tau\,,$$

l'ultimo passaggio essendo dovuto al fatto che è $\mathrm{d}\boldsymbol{r}/\mathrm{d}\theta = -\boldsymbol{v}$ e $\boldsymbol{v}\wedge\boldsymbol{v}=0$. È ora

$$\frac{\boldsymbol{v}}{sr^2}+\frac{r}{s}\,\frac{\mathrm{d}}{\mathrm{d}\theta}\,\frac{n\boldsymbol{v}}{csr} = \frac{\boldsymbol{v}s^2}{s^3r^2}+\frac{r}{s}\,\frac{n\dot{\boldsymbol{v}}csr - nc\boldsymbol{v}(\mathrm{d}/\mathrm{d}\theta)(sr)}{c^2s^2r^2} = \frac{1}{s^3r}\left(s^2\,\frac{\boldsymbol{v}}{r}+s\,\frac{nr\dot{\boldsymbol{v}}}{c}-\frac{\mathrm{d}(sr)}{\mathrm{d}\theta}\,\frac{n\boldsymbol{v}}{c}\right).$$

Da questa, mediante le espressioni di s e di s^2 sopra introdotte ed osservando che è

$$\frac{\mathrm{d}(sr)}{\mathrm{d}\theta} = \frac{\mathrm{d}}{\mathrm{d}\theta}\left(r^2-\frac{n}{c}\,r\boldsymbol{r}\cdot\boldsymbol{v}\right) = -2\boldsymbol{r}\cdot\boldsymbol{v}+\frac{n}{c}\,\frac{(\boldsymbol{r}\cdot\boldsymbol{v})^2}{r}+\frac{n}{c}\,rv^2-\frac{n}{c}\,r\boldsymbol{r}\cdot\dot{\boldsymbol{v}}\,,$$

si deduce

$$\frac{\boldsymbol{v}}{sr^2}+\frac{r}{s}\,\frac{\mathrm{d}}{\mathrm{d}\theta}\,\frac{n\boldsymbol{v}}{csr} = \frac{1}{s^3r}\left|r\boldsymbol{v}-\frac{n}{c}\,r^2\dot{\boldsymbol{v}}-\frac{n^2}{c^2}\,(\boldsymbol{r}\cdot\boldsymbol{v})r\dot{\boldsymbol{v}}-\frac{n^2}{c^2}\,rv^2\boldsymbol{v}+\frac{n^2}{c^2}\,r(\boldsymbol{r}\cdot\dot{\boldsymbol{v}})\boldsymbol{v}\right|,$$

o anche

$$\frac{\boldsymbol{v}}{sr^2}+\frac{r}{s}\frac{\mathrm{d}}{\mathrm{d}\theta}\frac{n\boldsymbol{v}}{csr}=\frac{1}{s^3}\left|\left(1-\frac{n^2v^2}{c^2}\right)\boldsymbol{v}+\frac{n^2}{c^2}\boldsymbol{r}\wedge(\boldsymbol{v}\wedge\dot{\boldsymbol{v}})+\frac{n}{c}r\dot{\boldsymbol{v}}\right|. \tag{96}$$

L'ultimo integrale scritto diventa così

$$\mathscr{H}_L(P,0)=\int_{-\infty}^{+\infty}\exp\left[-i\omega\tau\right]\frac{q}{cs^3}\left|\left(1-\frac{n^2v^2}{c^2}\right)\boldsymbol{v}+\frac{n^2}{c^2}\boldsymbol{r}\wedge(\boldsymbol{v}\wedge\dot{\boldsymbol{v}})+\frac{n}{c}r\dot{\boldsymbol{v}}\right|\wedge\boldsymbol{r}\,\mathrm{d}\tau\,. \tag{97}$$

Questo può essere posto anche sotto la forma

$$\mathscr{H}_L(P,0)= \tag{98}$$

$$=\int_{-\infty}^{+\infty}\exp\left[-i\omega\tau\right]\sqrt{\frac{\varepsilon}{\mu}}\frac{\boldsymbol{r}}{r}\wedge\frac{q}{s^3}\left\{\frac{1}{\varepsilon}\left(1-\frac{n^2v^2}{c^2}\right)\left(\boldsymbol{r}-\frac{nr\boldsymbol{v}}{c}\right)+\frac{\mu}{c^2}\boldsymbol{r}\quad\left|\left(\boldsymbol{r}-\frac{nr}{c}\boldsymbol{v}\right)\quad\dot{\boldsymbol{v}}\right|\right\}\mathrm{d}\tau\,.$$

come si può facilmente verificare sviluppando le funzioni integrande.

17. – Potenziali e campi generati dalla carica in un mezzo non dispersivo nel caso in cui $\tau(\theta)$ è sempre crescente.

17'1. – I parametri ε, μ e perciò n siano ora supposti indipendenti da ω.

Nell'integrale (88) si sostituisca *formalmente* il simbolo τ con il simbolo t, il simbolo θ con t'. Evidentemente, per la (86), t' risulta funzione di t attraverso la relazione

$$t=t'+\frac{n}{c}\sqrt{[x-x(t')]^2+[y-y(t')]^2+[z-z(t')]^2}\,. \tag{99}$$

Si ha così

$$q_L(P,0)=\int_{-\infty}^{+\infty}\exp\left[-i\omega t\right]\frac{q/\varepsilon}{r(t')-(n/c)\boldsymbol{r}(t')\cdot\boldsymbol{v}(t')}\,\mathrm{d}t\,.$$

Evidentemente tale espressione è la trasformata di Fourier della funzione

$$\frac{q/\varepsilon}{r(t')-(n/c)\,\boldsymbol{r}(t')\cdot\boldsymbol{v}(t')}\,,$$

della variabile t. D'altra parte il teorema del n. **7** assicura che $q_L(P,0)$ è la trasformata di Fourier del potenziale scalare $q(P,t)$ generato in P all'istante t

dalla carica q, moventesi secondo la legge (81) e (82). Si ha così

$$(100) \qquad \varphi(P,t) = \frac{q}{\varepsilon}\,\frac{1}{r(t') - (n/c)\boldsymbol{r}(t')\cdot\boldsymbol{v}(t')}\,,$$

essendo t' deducibile da t mediante la (99).

Analogamente la (89) e il teorema del n. **7** forniscono

$$(101) \qquad \mathscr{A}(P,t) = \frac{q\mu}{c}\,\frac{\boldsymbol{v}(t')}{r(t') - (n/c)\boldsymbol{r}(t')\cdot\boldsymbol{v}(t')}\,,$$

essendo $\mathscr{A}(P,t)$ il potenziale vettore generato in P all'istante t dalla carica puntiforme q.

Si sono così ritrovati i ben noti potenziali di Lienard e Wiechert. Notoriamente essi vengono spesso indicati con i simboli

$$\varphi(P,t) = \frac{q}{\varepsilon}\,\frac{1}{r - (n/c)\boldsymbol{r}\cdot\boldsymbol{v}}\Big|_{t-(nr/c)}, \qquad \mathscr{A}(P,t) = \frac{q\mu}{c}\,\frac{\boldsymbol{v}}{r - (n/c)\boldsymbol{r}\cdot\boldsymbol{v}}\Big|_{t-(nr/c)}.$$

17. – Anche negli integrali (95) e (97), se si sostituisce formalmente τ con t e θ con t', si ottengono due trasformate di Fourier di funzioni della variabile t. D'altronde esse, per il teorema del n. **7** sono le trasformate di Fourier di $\mathscr{E}(P,t)$ e di $\mathscr{H}(P,t)$ rispettivamente. È perciò

$$(102) \qquad \mathscr{E}(P,t) = \frac{q}{s^3}\left\{\frac{1}{\varepsilon}\left(1 - \frac{n^2v^2}{c^2}\right)\left(\boldsymbol{r} - \frac{nr\boldsymbol{v}}{c}\right) + \frac{\mu}{c^2}\boldsymbol{r}\wedge\left[\left(\boldsymbol{r} - \frac{nr}{c}\boldsymbol{v}\right)\wedge\dot{\boldsymbol{v}}\right]\right\},$$

$$(103) \qquad \mathscr{H}(P,t) = \frac{q}{cs^3}\left[\left(1 - \frac{n^2v^2}{c^2}\right)\boldsymbol{v} + \frac{n^2}{c^2}\boldsymbol{r}\wedge(\boldsymbol{v}\wedge\dot{\boldsymbol{v}}) + \frac{n}{c}r\dot{\boldsymbol{v}}\right]\wedge\boldsymbol{r}\,,$$

dove $\boldsymbol{v}$ e $\dot{\boldsymbol{v}}$ sono rispettivamente la velocità e l'accelerazione della carica all'istante t' legato a t dalla (99). Analogamente $\boldsymbol{r}$ è il segmento (di lunghezza r) che va dalla posizione occupata dalla carica in tale istante t' al punto P, mentre s è la grandezza definita dalla (90).

Le (102) e (103) costituiscono un'estensione delle (9) a un dielettrico omogeneo e non dispersivo qualunque e ad esse si riducono nel caso del vuoto ($\varepsilon = 1$, $\mu = 1$, $n = 1$).

Con analoghe considerazioni dalle (97) e (98) si deduce che i campi elettrico $\mathscr{E}(P,t)$ e magnetico $\mathscr{H}(P,t)$ generati dalla carica puntiforme q all'istante t in un punto P sono legati dalla relazione

$$(104) \qquad \mathscr{H}(P,t) = \sqrt{\frac{\varepsilon}{\mu}}\,\frac{\boldsymbol{r}}{r}\wedge\mathscr{E}(P,t)\,.$$

18. – Rappresentazioni integrali delle trasformate di Fourier rispetto alla variabile di arrivo. Caso $\tau(\theta)$ con un solo minimo. Mezzo dispersivo.

18'1. – Nel presente numero saranno stabilite rappresentazioni integrali delle trasformate $q_L(P,0)$, $\mathscr{A}_L(P,0)$, $\mathscr{E}_L(P,0)$, $\mathscr{H}_L(P,0)$ rispetto alla variabile di arrivo τ, valide nel caso del mezzo dispersivo e sotto l'ipotesi che la funzione $\tau(\theta)$ definita dalla (86) ammetta nell'intervallo $-\infty < \theta < -\infty$ uno ed un solo punto di minimo, risultando sempre decrescente alla sinistra di esso e sempre crescente a destra e soddisfacendo inoltre alle condizioni

$$\lim_{\theta\to-\infty}\tau = \lim_{\theta\to+\infty}\tau(\theta) = +\infty\,.$$

Evidentemente si pone in primo luogo la questione se esistano moti per i quali la funzione $\tau(\theta)$ gode di siffatte proprietà. Anche limitando lo studio al caso delle traiettorie rettilinee, l'esistenza di tali moti è assicurata dal seguente teorema:

Se la carica percorre una retta da un estremo all'altro con velocità mai crescente e se inizialmente questa è maggiore di c n (precisamente se è $\lim_{\theta\to-\infty} v(\theta) > c/n(\omega)$*) allora la funzione* $\tau(\theta)$ *ammette, qualunque sia il punto* $P(x, y, z)$*, uno ed un solo punto di minimo, risultando alla sinistra di questo sempre decrescente, alla destra sempre crescente e soddisfacendo inoltre alle condizioni* $\lim_{\theta\to-\infty}\tau = \lim_{\theta\to+\infty}\tau = -\infty$.

Sia γ l'angolo formato dal segmento $\boldsymbol{r}$ e dalla velocità $\boldsymbol{v}(\theta)$. La (86') può allora anche scriversi

$$\frac{\mathrm{d}\tau}{\mathrm{d}\theta} = 1 - \frac{n}{c}v(\theta)\cos\gamma\,.$$

Sia N il piede della perpendicolare condotta da P alla retta percorsa dalla carica. Sia θ_N il valore di θ corrispondente al punto N. Nell'intervallo $-\infty < \theta \leqslant \theta_N$ l'angolo γ varia, sempre crescendo da 0 a $\pi/2$. Pertanto in $-\infty < \theta < \theta_N$ la funzione $v(\theta)$ è mai crescente e positiva, la funzione $\cos\gamma$ è sempre decrescente e pure positiva, quindi $1 - (n/c)v(\theta)\cos\gamma$ risulta in $-\infty < \theta \leqslant \theta_N$ sempre crescente. Oltre a tale proprietà, la derivata $\mathrm{d}\tau/\mathrm{d}\theta$ gode anche delle seguenti altre: *a*) poichè nel punto $\theta = \theta_N$ è $\gamma = \pi/2$, ivi è $\mathrm{d}\tau/\mathrm{d}\theta = 1$; *b*) è inoltre $\lim_{\theta\to-\infty}\cos\gamma = 1$, $\lim_{\theta\to-\infty} v(\theta) > c/n$ e quindi $\lim_{\theta\to-\infty}\mathrm{d}\tau/\mathrm{d}\theta < 0$. Perciò nell'intervallo $-\infty < \theta < \theta_N$ la funzione $\mathrm{d}\tau/\mathrm{d}\theta$ cresce sempre passando con continuità (*) da valori negativi al valore 1. Esiste quindi in tale intervallo

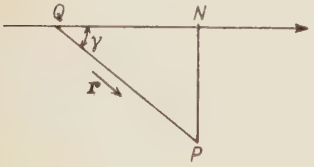

Fig. 9.

(*) Le funzioni $x(\theta)$, $y(\theta)$, $z(\theta)$ che figurano nelle (81) sono supposte dotate delle derivate prime e seconde almeno (nelle formule che esprimono il campo elettromagnetico generato da una carica in moto vario interviene l'accelerazione). Tuttavia per la dimostrazione del teorema qui in oggetto sarebbe sufficiente l'esistenza e continuità delle derivate prime.

uno ed un solo punto in cui la derivata $d\tau/d\theta$ si annulla. Esso è un punto di minimo della funzione $\tau(\theta)$ perchè la derivata $d\tau/d\theta$ è negativa a sinistra del detto punto e positiva a destra.

Nell'intervallo $\theta_N < \theta < +\infty$ è $\cos\gamma < 0$ e quindi $d\tau/d\theta > 1$. La funzione $\tau(\theta)$ è perciò sempre crescente in tale intervallo ed è inoltre $\lim_{\theta\to+\infty} \tau = +\infty$.

Poichè, come sopra si è visto, è $\lim_{\theta\to-\infty} d\tau/d\theta < 0$, si può trovare un $\eta > 0$ e ancora un valore θ_M tale che per $\theta < \theta_M$ sia sempre $d\tau/d\theta < -\eta$, per cui è $\lim_{\theta\to-\infty} \tau = +\infty$.

Il teorema risulta così dimostrato. Incidentalmente si è visto che il minimo in questione cade nella semiretta $-\infty < \theta < \theta_N$; che alla sinistra del punto di minimo la funzione $\tau(\theta)$ è sempre decrescente ($d\tau/d\theta < 0$) e che a destra di esso è sempre crescente ($d\tau/d\theta > 0$). c. v. d.

L'ipotesi contenuta nel teorema di una velocità $v(\theta)$ mai crescente non costituisce, dal punto di vista fisico, una limitazione, a motivo del frenamento che la particella subisce da parte della materia (perdita di energia di alcuni MeV per cm nel caso di un ordinario dielettrico liquido o solido). Il moto della particella in un tale mezzo non può essere accelerato nemmeno mediante un campo elettrostatico, perchè, per supplire alla perdita di energia della particella, l'intensità di tale campo dovrebbe superare di gran lunga la rigidità dielettrica del materiale isolante in cui la particella si muove.

Lo studio di certi moti curvilinei della carica con velocità maggiore di c/n su tutta o parte della traiettoria metterebbe in evidenza anche funzioni $\tau(\theta)$ dall'andamento piuttosto complicato, caratterizzate da più massimi e minimi in numero eventualmente dipendente dal punto $P(x, y, z)$. E ciò anche nell'ipotesi restrittiva della velocità sempre decrescente. Ma i moti che danno luogo a siffatti complicati andamenti della funzione $\tau(\theta)$ non sembrano essere di grande interesse fisico. Essi comunque saranno considerati al n. **21**. Tuttavia dal teorema ora stabilito appare chiaro che il problema centrale della fisica delle particelle ad alta velocità moventisi nei dielettrici densi è quello relativo al caso in cui la funzione $\tau(\theta)$ ha un solo minimo. Con lo studio di tale problema si perviene alla descrizione della radiazione di Čerenkov emessa dalle cariche in moto vario, facendo così un altro passo avanti rispetto alle teorie di Frank e Tamm, le quali si limitano al caso ideale del moto rettilineo e uniforme. Evidentemente la nuova descrizione è più aderente alla realtà, perchè la radiazione di Čerenkov nella pratica sperimentazione è sempre emessa da particelle in moto ritardato.

18˙3. *Trasformate dei potenziali.* – Attribuite pertanto alla funzione $\tau(\theta)$ le proprietà elencate al precedente n. **18**˙1, sia τ_0 il minimo valore assunto dalla funzione $\tau(\theta)$ nell'intervallo $-\infty < \theta < +\infty$ e sia θ_0 il valore di θ ad esso corrispondente. È perciò $\tau_0 = \tau(\theta_0)$. Quando la relazione che definisce la fun-

zione τ della variabile θ

$$\tau = \theta + \frac{nr(\theta)}{c}, \tag{105}$$

venga riguardata come un'equazione nell'incognita θ, essa non ammette alcuna radice se è $\tau < \tau_0$, ammette invece due radici se è $\tau > \tau_0$. Di tali radici si indicherà con θ' quella minore di θ_0, con θ'' quella maggiore. Le radici θ' e θ'' risultano pertanto così definite ($\tau \geqslant \tau_0$)

$$\tau = \theta' + \frac{n}{c}\sqrt{[x - x(\theta')]^2 + [y - y(\theta')]^2 + [z - z(\theta')]^2}, \qquad \theta' \leqslant \theta_0 \tag{106}$$

$$\tau = \theta'' + \frac{n}{c}\sqrt{[x - x(\theta'')]^2 + [y - y(\theta'')]^2 + [z - z(\theta'')]^2}. \qquad \theta'' \geqslant \theta_0 \tag{107}$$

A lor volta tali relazioni permettono di definire θ' e θ'' quali funzioni di τ in tutto l'intervallo $\tau_0 \leqslant \tau < +\infty$. Al variare di τ da τ_0 a $+\infty$ la funzione θ'' varia da θ_0 a $+\infty$ sempre crescendo, mentre θ' varia da θ_0 a $-\infty$ sempre decrescendo. Si ha dalle (106) e (107), in armonia con la (86'),

$$\frac{d\tau}{d\theta'} = 1 - \frac{n}{c}\frac{\boldsymbol{r}(\theta')\cdot\boldsymbol{v}(\theta')}{r(\theta')}, \qquad \frac{d\tau}{d\theta''} = 1 - \frac{n}{c}\frac{\boldsymbol{r}(\theta'')\cdot\boldsymbol{v}(\theta'')}{r(\theta'')}, \tag{108}$$

e da queste

$$\frac{d\theta'}{d\tau} = \frac{1}{1 - (n/c)[\boldsymbol{r}(\theta')\cdot\boldsymbol{v}(\theta')]/r(\theta')}, \qquad \frac{d\theta''}{d\tau} = \frac{1}{1 - (n/c)[\boldsymbol{r}(\theta'')\cdot\boldsymbol{v}(\theta'')]/r(\theta'')}. \tag{109}$$

Si ricorra ora alle (83), le quali sono valide senza limitazione alcuna, per quanto riguarda la velocità della carica. Si ha

$$\varphi_L(P, 0) = \frac{q}{\varepsilon}\int_{\theta_0}^{+\infty} \frac{\exp\left[-i\omega\left(\theta + nr(\theta)/c\right)\right]}{r(\theta)}\, d\theta, \tag{110}$$

$$\boldsymbol{A}_L(P, 0) = \frac{q\mu}{c}\int_{\theta_0}^{+\infty} \frac{\exp\left[-i\omega\left(\theta + nr(\theta)/c\right)\right]}{r(\theta)}\, \boldsymbol{v}(\theta)\, d\theta. \tag{111}$$

Ci si limiti, per semplicità, a considerare soltanto la seconda. Si può allora

introdurre la seguente scomposizione

$$\mathscr{A}_L(P,0) = \frac{q\mu}{c}\int_{-\infty}^{\theta_0} \frac{\exp\left[-i\omega\left(\theta' + nr(\theta')/c\right)\right]}{r(\theta')}\,\boldsymbol{v}(\theta')\,\mathrm{d}\theta' + \\ + \frac{q\mu}{c}\int_{\theta_0}^{+\infty} \frac{\exp\left[-i\omega\left(\theta'' + nr(\theta'')/c\right)\right]}{r(\theta'')}\,\boldsymbol{v}(\theta'')\,\mathrm{d}\theta'' .$$

Per le proprietà di cui godono θ' e θ'' quando esse vengano pensate funzioni di τ, entrambe le integrazioni possono essere eseguite rispetto alla variabile τ. Per le (106) e (107) si ha allora

$$\mathscr{A}_L(P,0) = \frac{q\mu}{c}\int_{+\infty}^{\tau_0} \frac{\exp\left[-i\omega\tau\right]}{r(\theta')}\,\boldsymbol{v}(\theta')\,\frac{\mathrm{d}\theta'}{\mathrm{d}\tau}\,\mathrm{d}\tau + \frac{q\mu}{c}\int_{\tau_0}^{+\infty} \frac{\exp\left[-i\omega\tau\right]}{r(\theta'')}\,\boldsymbol{v}(\theta'')\,\frac{\mathrm{d}\theta''}{\mathrm{d}\tau}\,\mathrm{d}\tau ,$$

e per le (109)

$$\mathscr{A}_L(P,0) = \frac{q\mu}{c}\int_{+\infty}^{\tau_0} \frac{\exp\left[-i\omega\tau\right]\boldsymbol{v}(\theta')}{r(\theta') - (n/c)\boldsymbol{r}(\theta')\cdot\boldsymbol{v}(\theta')}\,\mathrm{d}\tau + \frac{q\mu}{c}\int_{\tau_0}^{+\infty} \frac{\exp\left[-i\omega\tau\right]\boldsymbol{v}(\theta'')}{r(\theta'') - (n/c)\boldsymbol{r}(\theta'')\cdot\boldsymbol{v}(\theta'')}\,\mathrm{d}\tau ,$$

ossia

$$\mathscr{A}_L(P,0) = \\ = \int_{\tau_0}^{+\infty} \exp\left[-i\omega\tau\right]\frac{q\mu}{c}\left(\frac{\boldsymbol{v}(\theta'')}{r(\theta'') - (n/c)\boldsymbol{r}(\theta'')\cdot\boldsymbol{v}(\theta'')} - \frac{\boldsymbol{v}(\theta')}{r(\theta') - (n/c)\boldsymbol{r}(\theta')\cdot\boldsymbol{v}(\theta')}\right)\mathrm{d}\tau . \tag{112}$$

Analogamente dalla (83) si otterrebbe ancora

$$\varphi_L(P,0) = \\ = \int_{\tau_0}^{+\infty} \exp\left[-i\omega\tau\right]\frac{q}{\varepsilon}\left(\frac{1}{r(\theta'') - (n/c)\boldsymbol{r}(\theta'')\cdot\boldsymbol{v}(\theta'')} - \frac{1}{r(\theta') - (n/c)\boldsymbol{r}(\theta')\cdot\boldsymbol{v}(\theta')}\right)\mathrm{d}\tau . \tag{113}$$

18·4. *Trasformate dei campi.* – Allo scopo di esprimere le trasformate dei campi rispetto alla variabile di arrivo si rende opportuno semplificare le notazioni scrivendo r_1, $\boldsymbol{r}_1$, v_1, $\boldsymbol{v}_1$, $\dot{\boldsymbol{v}}_1$ al posto di $r(\theta')$, $\boldsymbol{r}(\theta')$, $v(\theta')$, $\boldsymbol{v}(\theta')$, $\dot{\boldsymbol{v}}(\theta')$ rispettivamente e scrivendo r_2, $\boldsymbol{r}_2$, v_2, etc., al posto di $r(\theta'')$, $\boldsymbol{r}(\theta'')$, $v(\theta'')$, etc., rispettivamente. Oltre a ciò, in armonia con le (90), si porrà

$$s_1 = r_1 - \frac{n}{c}\boldsymbol{r}_1\cdot\boldsymbol{v}_1 , \qquad s_2 = r_2 - \frac{n}{c}\boldsymbol{r}_2\cdot\boldsymbol{v}_2 , \tag{114}$$

$$g_1 = \frac{n}{c\varepsilon}\frac{\boldsymbol{r}_1}{r_1} - \frac{\mu}{c^2}\boldsymbol{v}_1 , \qquad g_2 = \frac{n}{c\varepsilon}\frac{\boldsymbol{r}_2}{r_2} - \frac{\mu}{c^2}\boldsymbol{v}_2 . \tag{115}$$

Dalla (84), spezzando l'intervallo di integrazione nei due tratti $-\infty < \theta < \theta_0$ e $\theta_0 < \theta < +\infty$ si ha allora

$$\mathcal{E}_L(P,0) = q\int_{-\infty}^{\theta_0} \exp\left[-i\omega\left(\theta' + \frac{nr_1}{c}\right)\right]\left[\left(\frac{1}{r_1} + \frac{i\omega n}{c}\right)\frac{\boldsymbol{r}_1}{\varepsilon r_1^2} - \frac{i\omega\mu}{c^2 r_1}\boldsymbol{v}_1\right] d\theta' +$$

$$+ q\int_{\theta_0}^{+\infty} \exp\left[-i\omega\left(\theta'' + \frac{nr_2}{c}\right)\right]\left[\left(\frac{1}{r_2} + \frac{i\omega n}{c}\right)\frac{\boldsymbol{r}_2}{\varepsilon r_2^2} - \frac{i\omega\mu}{c^2 r_2}\boldsymbol{v}_2\right] d\theta'' .$$

Si può ora in tali espressioni sostituire le integrazioni rispetto alle variabili θ' e θ'' mediante integrazioni rispetto alla variabile τ. Per le (109) è

$$\frac{d\theta'}{d\tau} = \frac{r_1}{s_1}, \qquad \frac{d\theta''}{d\tau} = \frac{r_2}{s_2}. \tag{116}$$

Si ha così

$$\mathcal{E}_L(P,0) = \sum_{h=1}^{h=2} (-1)^h q \int_{\tau_0}^{+\infty} \exp\left[-i\omega\tau\right]\left[\left(\frac{1}{r_h} + \frac{i\omega n}{c}\right)\frac{\boldsymbol{r}_h}{\varepsilon r_h^2} - \frac{i\omega\mu}{c^2 r_h}\boldsymbol{v}_h\right]\frac{r_h}{s_h} d\tau .$$

Si osservi che per $\theta = \theta_0$, cioè per $\tau = \tau_0$, è $s_h = 0$ in forza della condizione $(d\tau/d\theta)_{\theta=\theta_0} = 0$ relativa al punto di minimo. Ciò nonostante gli integrali ora scritti sono convergenti.

Si può anche scrivere

$$\mathcal{E}_L(P,0) = \tag{117}$$

$$= \sum_{h=1}^{h=2} (-1)^h q \int_{\tau_0}^{+\infty} \exp\left[-i\omega\tau\right] \frac{\boldsymbol{r}_h}{\varepsilon s_h r_h^2} d\tau + \sum_{h=1}^{h=2} (-1)^h q i\omega \int_{\tau_0}^{+\infty} \exp\left[-i\omega\tau\right] \frac{g_h}{s_h} d\tau .$$

Allo scopo di eliminare il fattore $i\omega$ è bene trasformare l'ultimo integrale mediante integrazione per parti. Per conservare la convergenza dei nuovi integrali, per primitiva della funzione $i\omega \exp[-i\omega\tau]$ si assumerà la funzione $-\exp[-i\omega\tau] + \exp[-i\omega\tau_0]$. Questa si annulla per $\tau = \tau_0$, risultando nell'intorno destro di τ_0 infinitesima dell'ordine di $\tau - \tau_0$, cioè infinitesima di ordine superiore a s_h, per cui è $\lim_{\tau \to \tau_0} (\exp[-i\omega\tau] - \exp[-i\omega\tau_0]) g_h/s_h = 0$. Inoltre ammettendo che per $\theta = \pm\infty$ la carica sia a distanza infinita, si ha

$$\lim_{\tau \to +\infty} (\exp[-i\omega\tau] - \exp[-i\omega\tau_0])(g_h/s_h) = 0.$$

Si ha così

$$\int_{\tau_0}^{+\infty} i\omega \exp[-i\omega\tau]\frac{g_h}{s_h}\,d\tau = -\left[(\exp[-i\omega\tau]-\exp[-i\omega\tau_0])\frac{g_h}{s_h}\right]_{\tau_0}^{+\infty} +$$

$$+\int_{\tau_0}^{+\infty}(\exp[-i\omega\tau]-\exp[-i\omega\tau_0])\,d\left(\frac{g_h}{s_h}\right) = \int_{\tau_0}^{+\infty}(\exp[-i\omega\tau]-\exp[-i\omega\tau_0])\frac{d}{d\tau}\left(\frac{g_h}{s_h}\right)d\tau,$$

e quindi

$$\mathscr{E}_L(P,0) = \sum_{h=1}^{h=2}(-1)^h q\int_{\tau_0}^{+\infty}\exp[-i\omega\tau]\frac{\boldsymbol{r}_h}{\varepsilon s_h r_h^2}\,d\tau +$$

$$+\sum_{h=1}^{h=2}(-1)^h q\int_{\tau_0}^{+\infty}(\exp[-i\omega\tau]-\exp[-i\omega\tau_0])\frac{d}{d\tau}\left(\frac{g_h}{s_h}\right)d\tau,$$

o anche

$$\mathscr{E}_L(P,0) = q\sum_{h=1}^{h=2}(-1)^h\int_{\tau_0}^{+\infty}(\exp[-i\omega\tau]-\exp[-i\omega\tau_0])\left[\frac{d}{d\tau}\left(\frac{g_h}{s_h}\right)+\frac{\boldsymbol{r}_h}{\varepsilon s_h r_h^2}\right]d\tau +$$

$$+ q\exp[i\omega\tau_0]\sum_{h=1}^{h=2}(-1)^h\int_{\tau_0}^{+\infty}\frac{\boldsymbol{r}_h}{\varepsilon s_h r_h^2}\,d\tau.$$

Provvisoriamente e per pura semplicità di calcolo si sostituiscano i simboli θ' e θ'' con θ_1 e θ_2 rispettivamente. Si ha così dalle (116)

$$\frac{d\theta_h}{d\tau} = \frac{r_h}{s_h},$$

e quindi

$$\frac{d}{d\tau}\left(\frac{g_h}{s_h}\right) = \frac{d\theta_h}{d\tau}\frac{d}{d\theta_h}\left(\frac{g_h}{s_h}\right) = \frac{r_h}{s_h}\frac{s_h(dg_h/d\theta_h)-g_h(ds_h/d\theta_h)}{s_h^2},$$

per cui

$$\frac{d}{d\tau}\left(\frac{g_h}{s_h}\right)+\frac{\boldsymbol{r}_h}{\varepsilon s_h r_h^2} = \frac{1}{s_h^3}\left(r_h s_h\frac{dg_h}{d\theta_h}-r_h g_h\frac{ds_h}{d\theta_h}+\frac{s_h^2\boldsymbol{r}_h}{\varepsilon r_h^2}\right). \tag{118}$$

Ora l'espressione a secondo membro racchiusa fra parentesi può desumersi dalla (94). Si ha così

$$r_h s_h\frac{dg_h}{d\theta_h}-r_h g_h\frac{ds_h}{d\theta_h}+\frac{s_h^2\boldsymbol{r}_h}{\varepsilon r_h^2} = \frac{1}{\varepsilon}\left(1-\frac{n^2v_h^2}{c^2}\right)\left(\boldsymbol{r}_h-\frac{nr_h\boldsymbol{v}_h}{c}\right)+ \tag{119}$$

$$+\frac{\mu}{c^2}\boldsymbol{r}_h\wedge\left[\left(\boldsymbol{r}_h-\frac{nr_h}{v}\boldsymbol{v}_h\right)\wedge\dot{\boldsymbol{v}}_h\right].$$

L'espressione di $\mathscr{E}_L(P, 0)$ diventa così

$$(120)\qquad \mathscr{E}_L(P,0) = q\sum_{h=1}^{h=2}(-1)^h\int_{\tau_0}^{+\infty}\frac{\exp[-i\omega\tau]-\exp[-i\omega\tau_0]}{s_h^3}\cdot$$
$$\cdot\left\{\frac{1}{\varepsilon}\left(1-\frac{n^2v_h^2}{c^2}\right)\left(\boldsymbol{r}_h-\frac{nr_h\boldsymbol{v}_h}{c}\right)+\frac{\mu}{c^2}\boldsymbol{r}_h\wedge\left[\left(\boldsymbol{r}_h-\frac{nr_h}{c}\boldsymbol{v}_h\right)\wedge\dot{\boldsymbol{v}}_h\right]\right\}\mathrm{d}\tau -$$
$$+\,q\sum_{h=1}^{h=2}\exp[i\omega\tau_0](-1)^h\int_{\tau_0}^{+\infty}\frac{\boldsymbol{r}_h}{\varepsilon s_h r_h^2}\mathrm{d}\tau.$$

L'espressione di $\mathscr{H}_L(P, 0)$ fornita dalla (85) sarà ora trattata in modo del tutto analogo. Si ha così

$$(121)\qquad \mathscr{H}_L(P,0) = -\frac{q}{c}\int_{-\infty}^{+\infty}\exp\left[-i\omega\left(\theta+\frac{nr}{r}\right)\right]\left(\frac{1}{r}+\frac{i\omega n}{c}\right)\frac{\boldsymbol{r}}{r^2}\cdot\boldsymbol{v}\,\mathrm{d}\theta =$$
$$= -\frac{q}{c}\int_{+\infty}^{\tau_1}\exp[-i\omega\tau]\left(\frac{1}{r_1}+\frac{i\omega n}{c}\right)\frac{\boldsymbol{r}_1}{r_1^2}\wedge\boldsymbol{v}_1\frac{\mathrm{d}\theta'}{\mathrm{d}\tau}\mathrm{d}\tau -$$
$$-\frac{q}{c}\int_{\tau_0}^{+\infty}\exp[-i\omega\tau]\left(\frac{1}{r_2}+\frac{i\omega n}{c}\right)\frac{\boldsymbol{r}_2}{r_2^2}\wedge\boldsymbol{v}_2\frac{\mathrm{d}\theta''}{\mathrm{d}\tau}\mathrm{d}\tau =$$
$$= -\frac{q}{c}\sum_{h=1}^{h=2}(-1)^h\int_{\tau_0}^{+\infty}\exp[-i\omega\tau]\left(\frac{1}{r_h}+\frac{i\omega n}{c}\right)\frac{\boldsymbol{r}_h}{r_h s_h}\wedge\boldsymbol{v}_h\,\mathrm{d}\tau\,.$$

Anche qui si farà sparire il fattore $i\omega$ mediante un'integrazione per parti, scegliendo quale primitiva di $-i\omega\exp[-i\omega\tau]$ la funzione $\exp[-i\omega\tau] - -\exp[-i\omega\tau_0]$ al fine di conservare, come nel caso precedente, la convergenza degli integrali. Si ha pertanto

$$\int_{\tau_0}^{+\infty}\exp[-i\omega\tau]\frac{i\omega n}{c}\frac{\boldsymbol{r}_h}{r_h s_h}\wedge\boldsymbol{v}_h\,\mathrm{d}\tau = -\frac{1}{i}\left(\exp[-i\omega\tau]-\exp[-i\omega\tau_0]\right)\frac{n\boldsymbol{r}_h}{cr_h s_h}\wedge\boldsymbol{v}_h\Big|_{\tau_0}^{+\infty} +$$
$$+\int_{\tau_0}^{+\infty}\left(\exp[-i\omega\tau]-\exp[-i\omega\tau_0]\right)\frac{\mathrm{d}}{\mathrm{d}\tau}\left(\frac{n\boldsymbol{r}_h}{cr_h s_h}\wedge\boldsymbol{v}_h\right)\mathrm{d}\tau\,.$$

In seguito all'annullamento del termine $[....]_{\tau_0}^{+\infty}$ si può così scrivere

$$\mathscr{H}_L(P,0) = -\frac{q}{c}\sum_{h=1}^{h=2}(-1)^h\int_{\tau_0}^{+\infty}\exp\left[-i\omega\tau\right]\frac{\boldsymbol{r}_h\wedge\boldsymbol{v}_h}{r_h^2 s_h}\,\mathrm{d}\tau -$$

$$-\frac{q}{c}\sum_{h=1}^{h=2}(-1)^h\int_{\tau_0}^{+\infty}\left(\exp\left[-i\omega\tau\right]-\exp\left[-i\omega\tau_0\right]\right)\frac{r_h}{s_h}\frac{\mathrm{d}}{\mathrm{d}\theta_h}\left(\frac{n\boldsymbol{r}_h\wedge\boldsymbol{v}_h}{cr_h s_h}\right)\mathrm{d}\tau =$$

$$= -\frac{q}{c}\sum_{h=1}^{h=2}(-1)^h\exp\left[-i\omega\tau_0\right]\int_{\tau_0}^{+\infty}\frac{\boldsymbol{r}_h\wedge\boldsymbol{v}_h}{r_h^2 s_h}\,\mathrm{d}\tau -$$

$$-\frac{q}{c}\sum_{h=1}^{h=2}(-1)^h\int_{\tau_0}^{+\infty}\left(\exp\left[-i\omega\tau\right]-\exp\left[-i\omega\tau_0\right]\right)\left[\frac{\boldsymbol{r}_h\wedge\boldsymbol{v}_h}{r_h^2 s_h}+\frac{r_h}{s_h}\frac{\mathrm{d}}{\mathrm{d}\theta_h}\left(\frac{n\boldsymbol{r}_h\wedge\boldsymbol{v}_h}{cr_h s_h}\right)\right]\mathrm{d}\tau\,.$$

Quest'ultima espressione, per il fatto che è $\mathrm{d}\boldsymbol{r}_h/\mathrm{d}\theta_h = -\boldsymbol{v}_h$ e $\boldsymbol{v}_h\wedge\boldsymbol{v}_h = 0$, può essere trasformata nella seguente

$$\mathscr{H}_L(P,0) = \frac{q}{c}\sum_{h=1}^{h=2}(-1)^h\exp\left[-i\omega\tau_0\right]\int_{\tau_0}^{+\infty}\frac{\boldsymbol{v}_h\wedge\boldsymbol{r}_h}{r_h^2 s_h}\,\mathrm{d}\tau +$$

$$+\frac{q}{c}\sum_{h=1}^{h=2}(-1)^h\int_{\tau_0}^{+\infty}\left(\exp\left[-i\omega\tau\right]-\exp\left[-i\omega\tau_0\right]\right)\left[\frac{\boldsymbol{v}_h}{r_h^2 s_h}+\frac{r_h}{s_h}\frac{\mathrm{d}}{\mathrm{d}\theta_h}\left(\frac{n\boldsymbol{v}_h}{cr_h s_h}\right)\right]\wedge\boldsymbol{r}_h\,\mathrm{d}\tau\,.$$

Da questa, ricorrendo alla (96), si ha infine

$$\text{(122)}\qquad \mathscr{H}_L(P,0) = \frac{q}{c}\sum_{h=1}^{h=2}(-1)^h\exp\left[-i\omega\tau_0\right]\int_{\tau_0}^{+\infty}\frac{\boldsymbol{v}_h\wedge\boldsymbol{r}_h}{r_h^2 s_h}\,\mathrm{d}\tau + \frac{q}{c}\sum_{h=1}^{h=2}(-1)^h\cdot$$

$$\cdot\int_{\tau_0}^{+\infty}\frac{\exp\left[-i\omega\tau\right]-\exp\left[-i\omega\tau_0\right]}{s_h^3}\left[\left(1-\frac{n^2v_h^2}{c^2}\right)\boldsymbol{v}_h+\frac{n^2}{c^2}\boldsymbol{r}_h\wedge(\boldsymbol{v}_h\wedge\dot{\boldsymbol{v}}_h)+\frac{n}{c}r_h\dot{\boldsymbol{v}}_h\right]\wedge\boldsymbol{r}_h\,\mathrm{d}\tau\,.$$

Le (120) e (122) sono particolarmente utili nello studio dei vari aspetti della radiazione di Čerenkov emessa da una carica puntiforme q in moto vario. Esse infatti esprimono le trasformate di Fourier dei campi $\mathscr{E}(P,t)$ e $\mathscr{H}(P,t)$ generati dalla carica q mediante integrali convergenti, mettendo in evidenza l'influenza dell'accelerazione.

18'5. *Espressioni simboliche delle trasformate dei campi.* – Mediante un procedimento che utilizza le regole di derivazione introdotte al n. **13**, saranno ora stabilite rappresentazioni simboliche delle trasformate $\mathscr{E}_L(P,0)$ e $\mathscr{H}_L(P,0)$ dei campi.

Le funzioni che nella (117) figurano sotto i segni di integrazione risultano definite nell'intervallo $(\tau_0, +\infty)$ della variabile τ. Sarà tuttavia bene estendere la loro definizione anche all'intervallo $-\infty < \tau < \tau_0$, attribuendo ad esse un valore (ad esempio, il valore zero) anche in tale intervallo, affinchè il prodotto di esse per la funzione $1(\tau-\tau_0)$ abbia un senso in tutto l'intervallo $-\infty<\tau<+\infty$ della variabile τ. La (117) può pertanto essere posta anche sotto la seguente altra forma

$$\mathscr{E}_L(P,0)=\sum_{h=1}^{h=2}(-1)^h q\int_{\infty}^{+\infty}\exp[-i\omega\tau]1(\tau-\tau_0)\frac{\boldsymbol{r}_h}{\varepsilon s_h r_h^2}\,\mathrm{d}\tau+$$
$$+\sum_{h=1}^{h=2}(-1)^h q\int_{-\infty}^{+\infty}\exp[-i\omega\tau]i\omega\frac{g_h}{s_h}1(\tau-\tau_0)\,\mathrm{d}\tau\,.$$

Si può ora trasformare l'ultimo integrale mediante integrazione per parti, nel seguente modo

$$\int_{-\infty}^{+\infty}\exp[-i\omega\tau]i\omega\frac{g_h}{s_h}1(\tau-\tau_0)\,\mathrm{d}\tau=-\left[\exp[-i\omega\tau]\frac{g_h}{s_h}1(\tau-\tau_0)\right]_{-\infty}^{+\infty}+$$
$$-\int_{-\infty}^{+\infty}\exp[-i\omega\tau]\frac{\mathrm{d}}{\mathrm{d}\tau}\left[\frac{g_h}{s_h}1(\tau-\tau_0)\right]\mathrm{d}\tau=\int_{-\infty}^{+\infty}\exp[-i\omega\tau]\frac{\mathrm{d}}{\mathrm{d}\tau}\left[\frac{g_h}{s_h}1(\tau-\tau_1)\right]\mathrm{d}\tau=$$
$$=\int_{-\infty}^{+\infty}\exp[-i\omega\tau]\left[1(\tau-\tau_0)\frac{\mathrm{d}}{\mathrm{d}\tau}\left(\frac{g_h}{s_h}\right)+\frac{g_h}{s_h}\delta^+(\tau-\tau_0)\right]\mathrm{d}\tau\,.$$

La precedente expressione di $\mathscr{E}_L(P,0)$ diventa così

$$\mathscr{E}_L(P,0)=\sum_{h=1}^{h=2}(-1)^h q\int_{-\infty}^{+\infty}\exp[-i\omega\tau]\left[\frac{\mathrm{d}}{\mathrm{d}\tau}\left(\frac{g_h}{s_h}\right)+\frac{\boldsymbol{r}_h}{\varepsilon s_h r_h^2}\right]1(\tau-\tau_0)\,\mathrm{d}\tau+$$
$$+\sum_{h=1}^{h=2}(-1)^h q\int_{\infty}^{+\infty}\exp[-i\omega\tau]\frac{g_h}{s_h}\delta^+(\tau-\tau_0)\,\mathrm{d}\tau\,.$$

Per le (118) e (119) questa dà luogo alla seguente altra

$$\mathscr{E}_L(P,0)=\sum_{h=1}^{h=2}(-1)^h q\int_{\tau_0}^{+\infty}\exp[-i\omega\tau]\cdot \tag{123}$$
$$\cdot\frac{1}{s_h^3}\left\{\frac{1}{\varepsilon}\left(1-\frac{n^2v_h^2}{c^2}\right)\left(\boldsymbol{r}_h-\frac{nr_h\boldsymbol{v}_h}{c}\right)+\frac{\mu}{c^2}\boldsymbol{r}_h\wedge\left[\left(\boldsymbol{r}_h-\frac{nr_h\boldsymbol{v}_h}{c}\right)\wedge\dot{\boldsymbol{v}}_h\right]\right\}\mathrm{d}\tau\,\cdot$$
$$+\sum_{h=1}^{h=2}(-1)^h q\int_{-\infty}^{+\infty}\exp[-i\omega\tau]\frac{1}{s_h}\left(\frac{n}{c\varepsilon}\frac{\boldsymbol{r}_h}{r_h}-\frac{\mu}{c^2}\boldsymbol{v}_h\right)\delta^+(\tau-\tau_0)\,\mathrm{d}\tau\,.$$

Analoga rappresentazione si può dare per $\mathscr{H}_L(P, 0)$. Muovendo dall'ultimo membro della (121) si ottiene

$$\mathscr{H}_L(P, 0) = -\frac{q}{c}\sum_{h=1}^{h=2}(-1)^h\int_{-\infty}^{+\infty}\exp[-i\omega\tau]\,\frac{\boldsymbol{r}_h\wedge\boldsymbol{v}_h}{r_h^2 s_h}\,1(\tau-\tau_0)\,\mathrm{d}\tau -$$

$$-\frac{q}{c}\sum_{h=1}^{h=2}(-1)^h\int_{-\infty}^{+\infty}\exp[-i\omega\tau]\,i\omega\,\frac{n\boldsymbol{r}_h\wedge\boldsymbol{v}_h}{cr_h s_h}\,1(\tau-\tau_0)\,\mathrm{d}\tau\,.$$

Mediante integrazione per parti l'ultimo integrale diventa

$$\int_{-\infty}^{+\infty}\exp[-i\omega\tau]\,i\omega\,\frac{n\boldsymbol{r}_h\wedge\boldsymbol{v}_h}{cr_h s_h}\,1(\tau-\tau_0)\,\mathrm{d}\tau = -\left[\exp[-i\omega\tau]\,\frac{n\boldsymbol{r}_h\wedge\boldsymbol{v}_h}{cr_h s_h}\,1(\tau-\tau_0)\right]_{\infty}^{+\infty} +$$

$$+\int_{-\infty}^{+\infty}\exp[-i\omega\tau]\,\frac{\mathrm{d}}{\mathrm{d}\tau}\left(\frac{n\boldsymbol{r}_h\wedge\boldsymbol{v}_h}{cr_h s_h}\,1(\tau-\tau_0)\right)\mathrm{d}\tau =$$

$$=\int_{-\infty}^{+\infty}\exp[-i\omega\tau]\,\frac{\boldsymbol{r}_h\boldsymbol{r}_h}{s_h}\wedge\frac{\mathrm{d}}{\mathrm{d}\theta_h}\left(\frac{n\boldsymbol{v}_h}{cr_h s_h}\right)1(\tau-\tau_0)\,\mathrm{d}\tau+\int_{-\infty}^{+\infty}\exp[-i\omega\tau]\,\frac{n\boldsymbol{r}_h\wedge\boldsymbol{v}_h}{cr_h s_h}\,\delta^+(\tau-\tau_0)\mathrm{d}\tau\,.$$

L'espressione di $\mathscr{H}_L(P, 0)$ diventa così

$$\mathscr{H}_L(P, 0) = \frac{q}{c}\sum_{h=1}^{h=2}(-1)^h\int_{\tau_0}^{+\infty}\exp[-i\omega\tau]\left[\frac{\boldsymbol{v}_h}{r_h^2 s_h}+\frac{\boldsymbol{r}_h}{s_h}\frac{\mathrm{d}}{\mathrm{d}\theta_h}\left(\frac{n\boldsymbol{v}_h}{cr_h s_h}\right)\right]\wedge\boldsymbol{r}_h\,\mathrm{d}\tau +$$

$$+\frac{q}{c}\sum_{h=1}^{h=2}(-1)^h\int_{-\infty}^{+\infty}\exp[-i\omega\tau]\,\frac{n\boldsymbol{v}_h\wedge\boldsymbol{r}_h}{cr_h s_h}\,\delta^+(\tau-\tau_0)\,\mathrm{d}\tau\,.$$

Ricorrendo alla (96) si ha infine

$$\mathscr{H}_L(P, 0) = \frac{q}{c}\sum_{h=1}^{h=2}(-1)^h\int_{-\infty}^{+\infty}\exp[-i\omega\tau]\,\frac{n\boldsymbol{v}_h\wedge\boldsymbol{r}_h}{cr_h s_h}\,\delta^+(\tau-\tau_0)\,\mathrm{d}\tau + \tag{124}$$

$$-\frac{q}{c}\sum_{h=1}^{h=2}(-1)^h\int_{\tau_0}^{+\infty}\exp[-i\omega\tau]\,\frac{1}{s_h^3}\left[\left(1-\frac{n^2v_h^2}{c^2}\right)\boldsymbol{v}_h+\frac{n^2}{c^2}\,\boldsymbol{r}_h\wedge(\boldsymbol{v}_h\wedge\dot{\boldsymbol{v}}_h)+\frac{n}{c}\,r_h\dot{\boldsymbol{v}}_h\right]\wedge\boldsymbol{r}_h\,\mathrm{d}\tau\,.$$

Delle trasformate di Fourier dei campi $\mathscr{E}(P, t)$ e $\mathscr{H}(P, t)$ generati in un punto P all'istante t dalla carica q si sono ottenute con le (123) e (124) rap-

presentazioni simboliche rispetto alla variabile di arrivo. Esse saranno utilizzate al n. **20** nella determinazione dei campi $\mathscr{E}(P, t)$ e $\mathscr{H}(P, t)$ generati dalla carica q in un mezzo non dispersivo.

19. – Potenziali in un mezzo non dispersivo. Caso $\tau(\theta)$ con un solo minimo. Il fronte d'onda.

19'1. – Si consideri ora il caso di un mezzo non dispersivo. Pertanto negli integrali (112) e (113) i parametri ε, μ, n non dipendono dalla pulsazione ω. Si cambi ora nome alle variabili τ, θ', θ'' che figurano in tali integrali, chiamando τ con t, θ' con t', θ'' con t''. Si ha così

$$(125)\qquad \mathscr{A}_L(P, 0) = \int_{\tau_0}^{+\infty} \exp[-i\omega t]\, \frac{q\mu}{c} \left(\frac{\boldsymbol{v}(t'')}{r(t'') - (n/c)\boldsymbol{r}(t'')\cdot\boldsymbol{v}(t'')} - \frac{\boldsymbol{v}(t')}{r(t') - (n/c)\boldsymbol{r}(t')\cdot\boldsymbol{v}(t')} \right) dt\,.$$

Manifestamente, per le (106) e (107) i valori di t' e di t'' si desumono dal valore di t mediante le equazioni e le limitazioni

$$(126)\qquad t = t' + \frac{n}{c}\sqrt{[(x - x(t'))]^2 + [y - y(t')]^2 + [z - z(t')]^2}\,, \qquad t' \leqslant \theta_0\,.$$

$$(127)\qquad t = t'' + \frac{n}{c}\sqrt{[(x - x(t''))]^2 + [y - y(t'')]^2 + [z - z(t'')]^2}. \qquad t'' \geqslant \theta_0\,.$$

Per il teorema del n. **7** $\mathscr{A}_L(P, 0)$ è la trasformata di Fourier del potenziale vettore $\mathscr{A}(P, t)$ generato in P all'istante t dalla carica q. D'altronde la (125) mostra anche che $\mathscr{A}_L(P, 0)$ è la trasformata di Fourier di una funzione *della variabile* t la quale per $t < \tau_0$ è nulla e per $t > \tau_0$ vale

$$\frac{q\mu}{c} \left(\frac{\boldsymbol{v}(t'')}{r(t'') - (n/c)\boldsymbol{r}(t'')\cdot\boldsymbol{v}(t'')} - \frac{\boldsymbol{v}(t')}{r(t') - (n/c)\boldsymbol{r}(t')\cdot\boldsymbol{v}(t')} \right).$$

L'uguaglianza delle due trasformate implica l'uguaglianza fra le funzioni trasformande. Si ha così

$$(128)\qquad \mathscr{A}(P, t) = 0\,, \qquad \text{per } t < \tau_0,$$

$$(129)\qquad \mathscr{A}(P, t) = \frac{q\mu}{c} \left(\frac{\boldsymbol{v}(t'')}{r(t'') - (n/c)\boldsymbol{r}(t'')\cdot\boldsymbol{v}(t'')} - \frac{\boldsymbol{v}(t')}{r(t') - (n/c)\boldsymbol{r}(t')\cdot\boldsymbol{v}(t')} \right), \quad \text{per } t > \tau_0,$$

dove i valori t' e t'' si ricavano da quelli di t mediante le equazioni e limitazioni (126) e (127).

Con lo stesso procedimento dalla (113) si deduce

$$\varphi(P, t) = 0 , \qquad \text{per } t < \tau_0, \tag{130}$$

$$\varphi(P, t) = \frac{q}{\varepsilon}\left(\frac{1}{r(t'') - (n/c)\boldsymbol{r}(t'')\cdot\boldsymbol{v}(t'')} - \frac{1}{r(t') - (n/c)\boldsymbol{r}(t')\cdot\boldsymbol{v}(t')}\right), \qquad \text{per } t > \tau_0, \tag{131}$$

essendo $\varphi(P, t)$ il potenziale scalare causato in P all'istante t dalla carica q.

19˙2. – I campi elettrico $\mathscr{E}(P, t)$ e magnetico $\mathscr{H}(P, t)$ si potrebbero ora ottenere, limitatamente al mezzo non dispersivo qui considerato, moltiplicando i secondi membri delle (129) e (131) per $1(t - t_0)$ ed effettuando sulle espressioni così ottenute le operazioni

$$\mathscr{E} = -\operatorname{grad}\varphi - \frac{1}{c}\frac{\partial \mathscr{A}}{\partial t} , \qquad \mathscr{H} = \frac{1}{\mu}\operatorname{rot}\mathscr{A} , \tag{132}$$

facendo uso della regola (72). Ma tale procedimento porterebbe all'esecuzione di fastidiose derivate di funzioni implicitamente definite. È molto più comodo dedurre i campi dalle rappresentazioni simboliche delle loro trasformate di Fourier, come sarà fatto al numero successivo.

19˙3. *Equazione del fronte d'onda.* – Dalle soluzioni stabilite appare che il campo elettromagnetico generato dalla carica q è, in un punto $P(x, y, z)$ del mezzo, nullo per $t < \tau_0$ e non nullo per $t > \tau_0$. Da ciò discende l'esistenza di un fronte d'onda.

Per stabilire l'equazione del fronte d'onda all'istante τ_0 si ricordi che τ_0 è il minimo valore assunto dalla funzione $\tau(\theta)$ relativa al punto $P(x, y, z)$. Si hanno così le equazioni

$$\frac{\mathrm{d}\tau(\theta)}{\mathrm{d}\theta} = 0 , \qquad \tau(\theta) = \tau_0 . \tag{133}$$

Da queste, eliminando θ, si ottiene un'equazione fra le variabili x, y, z che rappresenta il fronte d'onda all'istante τ_0.

19˙4. *Fronte d'onda e principio di Huyghens.* – Il significato geometrico delle (133) è subito messo in evidenza. Per essere $\tau_0 = \theta + (nr(\theta)/c)$, in corrispondenza di ogni punto θ della traiettoria C si costruisca una superficie sferica di raggio $(c/n)(\tau_0 - \theta)$ e centro nel detto punto θ. Sia S l'inviluppo di tutte tali superficie sferiche. Si vede subito che S è il fronte d'onda relativo all'istante τ_0. Infatti scelti sulla traiettoria C due punti θ_0 e θ_1 infinitamente vicini si considerino le rispettive superfici sferiche Σ_0 e Σ_1 costruite con il criterio dianzi

enunciato. Esse cioè abbiano centri in θ_0 e θ_1 e raggi

$$\frac{c}{n}(\tau_0 - \theta_0) \quad \text{e} \quad \frac{c}{n}(\tau_0 - \theta_1),$$

rispettivamente. Sia γ la circonferenza di intersezione di Σ_0 con Σ_1 e sia $P(x, y, z)$ un punto di γ. Evidentemente $P(x, y, z)$ è punto appartenente all'inviluppo S.

La funzione $\tau(\theta)$ relativa al punto $P(x, y, z)$ di γ ha nei punti θ_0 e θ_1 i seguenti valori

$$\tau(\theta_0) = \theta_0 + \frac{nr(\theta_0)}{c}, \qquad \tau(\theta_1) = \theta_1 + \frac{nr(\theta_1)}{c}. \tag{134}$$

Ma la superficie Σ_0 ha raggio $(c/n)(\tau_0 - \theta_0)$, per cui è

$$\tau(\theta_0) = \theta_0 + \frac{n}{c}\left[\frac{c}{n}(\tau_0 - \theta_0)\right] = \tau_0.$$

Analogamente, essendo $(c/n)(\tau_0 - \theta_1)$ il raggio di Σ_1, si ha

$$\tau(\theta_1) = \theta_1 + \frac{n}{c}\left[\frac{c}{n}(\tau_0 - \theta_1)\right] = \tau_0.$$

È cioè $\tau(\theta_0) = \tau(\theta_1)$, ossia

$$\frac{\tau(\theta_0) - \tau(\theta_1)}{\theta_0 - \theta_1} = \left(\frac{d\tau}{d\theta}\right)_{\theta=\theta_0} = 0.$$

Questa e la prima delle (134) mostrano che nel punto $P(x, y, z)$ di γ le due equazioni (133) possono essere soddisfatte attribuendo a θ un comune valore θ_0. Perciò (*) il punto $P(x, y, z)$ della circonferenza γ (e quindi qualunque punto dell'inviluppo S) appartiene al fronte d'onda presente nel mezzo all'istante τ_0.

Dalla possibilità ora emersa di identificare il fronte d'onda con la superficie inviluppo S risulta manifesto che il fronte d'onda ubbidisce al principio di Huyghens anche nel caso del moto vario della carica.

195. – Dalla possibilità di costruire il fronte d'onda ricorrendo al principio di Huyghens e dalla dimostrazione ora esposta discende che il raggio $\boldsymbol{r}$ che unisce il punto θ_0 di C (in corrispondenza del quale la funzione $\tau(\theta)$ relativa

(*) Se alle variabili x, y, z che figurano nelle (133) si sostituiscono i valori x_0, y_0, z_0, le (133) diventano due equazioni nell'incognita θ. Se esse ammettono una radice comune $\theta = \theta_0$, allora il punto (x_0, y_0, z_0) appartiene al fronte d'onda relativo all'istante τ_0.

al punto $P(x, y, z)$ ammette il minimo valore) con il punto $P(x, y, z)$ è normale al fronte d'onda passante per $P(x, y, z)$. Infatti esso congiunge il punto θ_0 della traiettoria C, che è centro di una superficie sferica Σ_0 tangente all'inviluppo S, con un punto di tangenza di S e Σ_0.

19'6. – Anzichè costruire una famiglia di superfici sferiche per poi determinarne l'inviluppo, il fronte d'onda può, dal punto di vista geometrico, essere ricavato con procedimento più semplice, osservando che la condizione $\mathrm{d}\tau/\mathrm{d}\theta = 0$ equivale alla seguente (n. **16**)

$$1 - \frac{n}{c}\frac{\boldsymbol{r}(\theta)\cdot\boldsymbol{v}(\theta)}{r(\theta)} = 0 ,$$

alla quale si può dare il seguente altro aspetto

$$\frac{\boldsymbol{r}(\theta)}{r(\theta)}\cdot\frac{\boldsymbol{v}(\theta)}{v(\theta)} = \frac{c}{nv(\theta)} . \tag{135}$$

Si scelga allora una semiretta uscente da un punto arbitrario θ di C e ivi formante con la curva C un angolo di coseno $c/nv(\theta)$. Si scelga poi sulla semiretta un punto P a distanza $(c/n)(\tau_0 - \theta)$ dal punto θ di C, cioè dall'estremo della semiretta stessa. Evidentemente il raggio $\boldsymbol{r}$ che unisce il punto θ di C con il punto P così definito soddisfa alla (135) e alla condizione $\tau_0 = \theta + (nr/c)$, cioè a entrambe le (133). Perciò il detto punto P appartiene al fronte d'onda esistente nel mezzo all'istante τ_0.

Per quanto visto al n. **19**'5 la semiretta interseca normalmente il fronte d'onda all'istante τ_0. Se si fosse scelto sulla semiretta un punto P, a distanza $(c/n)(\tau_1 - \theta)$ dall'estremo, si sarebbe pure trovato un punto del fronte d'onda esistente nel mezzo all'istante τ_1 e la semiretta sarebbe stata all'istante τ_1 normale anche a tale fronte d'onda (evidentemente si presuppone $\tau_0 > \theta$, $\tau_1 > \theta$). Segue che *se una semiretta uscente da un punto della traiettoria è a un certo istante normale al fronte d'onda, essa permane normale al fronte d'onda anche negli istanti successivi.*

Ai nn. 1 e 2 del presente paragrafo si è considerato un particolare punto $P(x, y, z)$. Le considerazioni colà svolte presuppongono che la funzione $\tau(\theta)$ relativa a tale particolare punto $P(x, y, z)$ goda di certe proprietà, quale, tra l'altro, quella di possedere un solo minimo. Invece nei nn. successivi, essendosi considerato un fronte d'onda il quale evolvendo nel tempo interessa tutti i punti del mezzo, si presuppone che le predette proprietà della funzione $\tau(\theta)$ sussistano comunque si scelga il punto $P(x, y, z)$ fuori della curva C.

19'7. – Si consideri ora la radiazione di Čerenkov emessa da una particella animata di moto vario. In un punto $P(x, y, z)$ di osservazione il fronte d'onda

si presenta normale alla semiretta uscente da un punto θ_0 della traiettoria. Tale semiretta forma con la velocità della particella nel detto punto θ_0 un angolo il cui coseno è $c/nv(\theta_0)$, come si è visto al precedente n. **19**'6, cioè un angolo che non dipende dall'accelerazione ma soltanto dalla velocità della particella. Pertanto la normale al fronte d'onda in $P(x, y, z)$ è la stessa che si avrebbe nel caso di una particella che si muovesse di moto rettilineo e uniforme e che passasse per il punto θ_0 con velocità costante $\boldsymbol{v}(\theta_0)$. Tanto nel caso del moto rettilineo e uniforme quanto nel caso del moto vario la direzione della normale al fronte d'onda è indicativa della velocità della particella all'istante di emissione.

Si tenga presente che tale conclusione si riferisce a un dielettrico non dispersivo, omogeneo ed infinitamente esteso, cioè occupante l'intero spazio.

20. – Campi in un dielettrico non dispersivo. Caso $\tau(\theta)$ con un solo minimo.

20'1. – Si consideri ancora il caso del mezzo non dispersivo. Negli integrali ai secondi membri delle (123) e (124) si mutino formalmente le variabili τ, θ' e θ'', in t, t' e t'' rispettivamente; essi allora acquistano l'aspetto di trasformate di Fourier di funzioni *della variabile* t. D'altra parte $\mathscr{E}_L(P, 0)$ e $\mathscr{H}_L(P, 0)$ sono per il teorema del n. **7** le trasformate di $\mathscr{E}(P, t)$ e $\mathscr{H}(P, t)$. Si deduce così

$$(136)\quad \mathscr{E}(P,t) = q\sum_{h=1}^{h=2}(-1)^h\frac{1}{s_h^3}\left\{\frac{1}{\varepsilon}\left(1-\frac{n^2v_h^2}{c^2}\right)\left(\boldsymbol{r}_h-\frac{nr_h\boldsymbol{v}_h}{c}\right)+\right.$$
$$\left.+\frac{\mu}{c^2}\boldsymbol{r}_h\wedge\left[\left(\boldsymbol{r}_h-\frac{nr_h\boldsymbol{v}_h}{c}\right)\wedge\dot{\boldsymbol{v}}_h\right]\right\}1(t-\tau_0)+q\sum_{h=1}^{h=2}(-1)^h\frac{1}{s_h}\left(\frac{n}{c\varepsilon}\frac{\boldsymbol{r}_h}{r_h}-\frac{\mu}{c^2}\boldsymbol{v}_h\right)\delta^{-1}(t-\tau_0)\,,$$

$$(137)\quad \mathscr{H}(P,t) = \frac{q}{c}\sum_{h=1}^{h=2}(-1)^h\frac{1}{s_h^3}\left[\left(1-\frac{n^2v_h^2}{c^2}\right)\boldsymbol{v}_h+\frac{n^2}{c^2}\boldsymbol{r}_h\wedge(\boldsymbol{v}_h\wedge\dot{\boldsymbol{v}}_h)+\frac{n}{c}r_h\dot{\boldsymbol{v}}_h\right]\wedge\boldsymbol{r}_h\cdot$$
$$\cdot 1(t-\tau_0)+\frac{q}{c}\sum_{h=1}^{h=2}(-1)^h\frac{n\boldsymbol{v}_h\wedge\boldsymbol{r}_h}{cr_hs_h}\delta^{+}(t-\tau_0)\,.$$

Evidentemente in tale rappresentazione si possono distinguere i termini simbolici relativi ai campi impulsivi presenti sul fronte d'onda, dagli altri termini che descrivono il campo elettromagnetico posteriormente al fronte d'onda. Si porrà pertanto

$$(138)\quad \mathscr{E}(P,t)=\mathscr{E}^{(0)}(P,t)+\mathscr{E}^{(i)}(P,t)\,,\qquad \mathscr{H}(P,t)=\mathscr{H}^{(0)}(P,t)+\mathscr{H}^{(i)}(P,t)\,,$$

con

$$\mathscr{E}^{(0)}(P,t)=\mathscr{E}_1^{(0)}(P,t)+\mathscr{E}_2^{(0)}(P,t)\,,\qquad \mathscr{H}^{(0)}(P,t)=\mathscr{H}_1^{(0)}(P,t)+\mathscr{H}_2^{(0)}(P,t)\,,$$
$$\mathscr{E}^{(i)}(P,t)=\mathscr{E}_1^{(i)}(P,t)+\mathscr{E}_2^{(i)}(P,t)\,,\qquad \mathscr{H}^{(i)}(P,t)=\mathscr{H}_1^{(i)}(P,t)+\mathscr{H}_2^{(i)}(P,t)\,,$$

essendo

$$\mathscr{E}_h^{(0)}(P,t) = q\frac{(-1)^h}{s_h^3}\left\{\frac{1}{\varepsilon}\left(1-\frac{n^2v_h^2}{c^2}\right)\left(\boldsymbol{r}_h-\frac{nr_h\boldsymbol{v}_h}{c}\right)+\frac{\mu}{c^2}\boldsymbol{r}_h\wedge\left[\left(\boldsymbol{r}_h-\frac{nr_h\boldsymbol{v}_h}{c}\right)\wedge\dot{\boldsymbol{v}}_h\right]\right\}1(t-\tau_0),$$

$$\mathscr{H}_h^{(0)}(P,t) = \frac{q}{c}\frac{(-1)^h}{s_h^3}\left[\left(1-\frac{n^2v^2}{c^2}\right)\boldsymbol{v}_h+\frac{n^2}{c^2}\boldsymbol{r}_h\wedge(\boldsymbol{v}_h\wedge\dot{\boldsymbol{v}}_h)+\frac{n}{c}r_h\dot{\boldsymbol{v}}_h\right]\wedge\boldsymbol{r}_h1(t-\tau_0)\,,$$

$$\mathscr{E}_h^{(i)}(P,t) = q\frac{(-1)^h}{s_h}\left(\frac{n}{c\varepsilon}\frac{\boldsymbol{r}_h}{r_h}-\frac{\mu}{c}\boldsymbol{v}_h\right)\delta^+(t-\tau_0)\,,$$

$$\mathscr{H}_h^{(i)}(P,t) = \frac{q}{c}(-1)^h\frac{n\boldsymbol{v}_h\wedge\boldsymbol{r}_h}{cr_hs_h}\delta^+(t-\tau_0)\,.$$

In tali espressioni le notazioni r_1, $\boldsymbol{r}_1$, $\boldsymbol{v}_1$, $\dot{\boldsymbol{v}}_1$, s_1 sono abbreviazioni delle notazioni più complete $r_1(t')$, $\boldsymbol{r}_1(t')$, $\boldsymbol{v}_1(t')$, ..., dove t' è deducibile da t mediante le (126). Il vettore $\boldsymbol{r}_1$ è il segmento che va dalla posizione occupata dalla carica q all'istante t' verso il punto $P(x, y, z)$. Analogamente $\boldsymbol{r}_2$ è il segmento orientato il cui primo estremo è la posizione occupata dalla carica q all'istante t'' e il cui secondo estremo è il punto $P(x, y, z)$, l'istante t'' risultando definito dalle (127). Evidentemente r_2, $\boldsymbol{r}_2$, ..., $\dot{\boldsymbol{v}}_2$, ... sono notazioni abbreviate in sostituzione di $r(t'')$, $\boldsymbol{r}(t'')$, ..., $\dot{\boldsymbol{v}}(t'')$, ... Come è facile verificare, sussiste la seguente relazione

$$\mathscr{H}^{(0)}(P,t) = \sqrt{\frac{\varepsilon}{\mu}}\sum_{h=1}^{h=2}\frac{\boldsymbol{r}_h}{r_h}\wedge\mathscr{E}_h^{(0)}(P,t)\,, \tag{139}$$

che è la corrispondente della (104).

Il lettore può facilmente constatare, magari usando uno schema di calcolo analogo a quello del n. 2, che quando il moto della carica q è rettilineo e uniforme si ha (*)

$$\mathscr{E}_1^{(0)}(P,t) = \mathscr{E}_2^{(0)}(P,t)\,, \qquad \mathscr{H}_1^{(0)}(P,t) = \mathscr{H}_2^{(0)}(P,t)\,.$$

Ciò spiega la provenienza del coefficiente 2 che figura nelle espressioni dei campi stabilite al Cap. II e relative al moto rettilineo e uniforme.

202. *I campi impulsivi.* – Sul fronte d'onda sono presenti i campi impulsivi $\mathscr{E}^{(i)}$ e $\mathscr{H}^{(i)}$, come già nel caso del moto rettilineo e uniforme con velocità $v > c/n$. Nelle espressioni di $\mathscr{E}_h^{(i)}$ e di $\mathscr{H}_h^{(i)}$, conseguite al precedente n. 1, figurano i simboli s_h $(h = 1, 2)$. A proposito di questi, si ricordi che s_1 sta per $s(\theta')$ con $\theta' < \theta_0$ e che s_2 sta per $s(\theta'')$ con $\theta'' > \theta_0$. Poichè (relazione (86′)) è

(*) Del resto tale concordanza sarà incidentalmente riscontrata nel successivo scritto *Energia della radiazione di Čerenkov.*

$d\tau/d\theta = s/r$ e poichè in $\theta - \theta_0$ la funzione $\tau(\theta)$ ammette un minimo, si ha $(d\tau/d\theta)_{\theta-\theta_0} = 0$, ossia $s(\theta_0) = 0$. Dall'essere $\tau(\theta)$ sempre decrescente a sinistra del punto di minimo e sempre crescente a destra si ha $s(\theta) < 0$ per $\theta < \theta_0$, $s(\theta) > 0$ per $\theta > \theta_0$, ossia $s_1 < 0$, $s_2 > 0$.

I due coefficienti $(-1)^h/s_h$ relativi ai valori $h = 1$ e $h = 2$ hanno perciò entrambi segno positivo, cosicchè ciascuno dei due termini simbolici $(-1)^h/s_h \cdot \delta^+(t - \tau_0)$ indica la tendenza a un limite infinito positivo.

Ne segue che i due vettori elettrici $\mathcal{E}_h^{(1)}(P, t)$ $(h = 1, 2)$ hanno entrambi la direzione e il verso del vettore

$$q\left(\frac{n}{c\varepsilon}\frac{\boldsymbol{r}(\theta_0)}{r(\theta_0)} - \frac{\mu}{c^2}\boldsymbol{v}(\theta_0)\right). \tag{140}$$

Ora tale vettore è normale al raggio $\boldsymbol{r}(\theta_0)$ e quindi tangenziale al fronte d'onda (n. **19**5), come risulta dal fatto che è

$$q\left(\frac{n}{c\varepsilon}\frac{\boldsymbol{r}(\theta_0)}{r(\theta_0)} - \frac{\mu}{c^2}\boldsymbol{v}(\theta_0)\right)\cdot\boldsymbol{r}(\theta_0) = \frac{nq}{c\varepsilon}\left(r(\theta_0) - \frac{n}{c}\boldsymbol{r}(\theta_0)\cdot\boldsymbol{v}(\theta_0)\right) = \frac{nq}{c\varepsilon}s(\theta_0) = 0\,. \tag{141}$$

Pertanto il campo elettrico impulsivo $\mathcal{E}^{(1)}(P, t)$, somma dei due vettori $\mathcal{E}_h^{(1)}(P, t)$ $(h = 1, 2)$ risulta diretto come il vettore (140) e quindi tangenziale al fronte d'onda

Analogamente i due vettori $\mathcal{H}_h^{(1)}(P, t)$ $(h = 1, 2)$ hanno entrambi la direzione e il verso del vettore

$$q\boldsymbol{v}(\theta_0)\wedge\boldsymbol{r}(\theta_0)\,, \tag{142}$$

perchè i coefficienti $(-1)^h(n/c^2 r_h s_h)\,\delta^+(t - \tau_0)$ denotano entrambi la tendenza a limiti infiniti positivi. Perciò pure il campo magnetico impulsivo $\mathcal{H}^{(1)}(P, t)$ è tangenziale al fronte d'onda. Anzi uno sguardo alle (142) e (140) permette di affermare che il campo magnetico impulsivo $\mathcal{H}^{(1)}(P, t)$ è diretto come il vettore

$$\boldsymbol{r}(\theta_0)\wedge\mathcal{E}^{(1)}(P, t)\,. \tag{143}$$

Pertanto esso è normale al campo elettrico $\mathcal{E}^{(1)}$ e il vettore di Poynting $(c/4\pi)\mathcal{E}^{(1)}\wedge\mathcal{H}^{(1)}$ relativo ai campi impulsivi è normale al fronte d'onda e rivolto verso la regione a questo anteriore.

203. *I campi nella regione posteriore al fronte d'onda.* – In tale regione sono presenti il campo elettrico $\mathcal{E}^{(0)}(P, t)$ e il campo magnetico $\mathcal{H}^{(0)}(P, t)$. Nelle espressioni analitiche di tali campi figurano pure termini dipendenti dall'accelerazione. In prossimità del fronte d'onda i campi $\mathcal{E}^{(0)}$ e $\mathcal{H}^{(0)}$ diventano infiniti.

Lo studio dei campi $\mathscr{E}^{(0)}$ e $\mathscr{H}^{(0)}$ in prossimità del fronte d'onda si manifesta particolarmente interessante. Si incominci dal campo $\mathscr{E}^{(0)}$.

Anzitutto si osservi che, per quanto visto al precedente n. 20˙2, i coefficienti $(-1)^h/s_h^3$ sono entrambi positivi. In quanto poi ai termini

$$\frac{\mu}{c^2}\boldsymbol{r}_h \wedge \left[\left(\boldsymbol{r}_h - \frac{n r_h \boldsymbol{v}_h}{c}\right) \wedge \dot{\boldsymbol{v}}_h\right],$$

che figurano nelle espressioni di $\mathscr{E}_h^{(0)}$ date al n. 20˙1, si osservi che per lo studio in prossimità del fronte d'onda si possono assumere le approssimazioni $\boldsymbol{r}_1 = \boldsymbol{r}_2 = \boldsymbol{r}(\theta_0)$, $\boldsymbol{v}_1 = \boldsymbol{v}_2 = \boldsymbol{v}(\theta_0)$, $\dot{\boldsymbol{v}}_1 = \dot{\boldsymbol{v}}_2 = \dot{\boldsymbol{v}}(\theta_0)$. Tenendo allora presenti i risultati (141), si può scrivere

$$\frac{\mu}{c^2}\boldsymbol{r}_h \wedge \left[\left(\boldsymbol{r}_h - \frac{n r_h \boldsymbol{v}_h}{c}\right) \wedge \dot{\boldsymbol{v}}_h\right] = \frac{\mu}{c^2}\left[\boldsymbol{r}(\theta_0)\cdot\dot{\boldsymbol{v}}(\theta_0)\right]\left[\boldsymbol{r}(\theta_0) - \frac{n\, r(\theta_0)\boldsymbol{v}(\theta_0)}{c}\right].$$

Pertanto il campo $\mathscr{E}^{(0)}$ è in prossimità del fronte d'onda diretto come il vettore

$$q\left[\frac{1}{\varepsilon}\left(1 - \frac{n^2 v^2(\theta_0)}{c^2}\right) + \frac{\mu}{c^2}\boldsymbol{r}(\theta_0)\cdot\dot{\boldsymbol{v}}(\theta_0)\right]\left(\boldsymbol{r}(\theta_0) - \frac{n r(\theta_0)\boldsymbol{v}(\theta_0)}{c}\right).$$

Dal confronto di tale espressione con la (140) risulta che in prossimità del rfonte d'onda il campo elettrico $\mathscr{E}^{(0)}$ ha la stessa direzione del campo impulsivo $\mathscr{E}^{(i)}$. Per decidere se tali campi abbiano anche lo stesso verso o versi opposti si rende necessario esaminare il segno del coefficiente

$$\frac{1}{\varepsilon}\left(1 - \frac{n^2 v^2(\theta_0)}{c^2}\right) + \frac{\mu}{c^2}\boldsymbol{r}(\theta_0)\cdot\dot{\boldsymbol{v}}(\theta_0),$$

o, ciò che è lo stesso, il segno dell'espressione

$$1 - \frac{n^2 v^2(\theta_0)}{c^2} + \frac{n^2}{c^2}\boldsymbol{r}(\theta_0)\cdot\dot{\boldsymbol{v}}(\theta_0). \tag{144}$$

Si osservi a tale proposito che dal n. 16˙3, si ha

$$\frac{\mathrm{d}s}{\mathrm{d}\theta} = -\frac{\boldsymbol{r}\cdot\boldsymbol{v}}{r} + \frac{n}{c}v^2 - \frac{n}{c}\boldsymbol{r}\cdot\dot{\boldsymbol{v}},$$

e che tale relazione, per il fatto che è $s = r - (n/c)\boldsymbol{r}\cdot\boldsymbol{v}$, può essere anche così scritta

$$-\frac{n}{c}\frac{\mathrm{d}s}{\mathrm{d}\theta} = -\frac{s}{r} + 1 - \frac{n^2 v^2}{c^2} + \frac{n^2}{c^2}\boldsymbol{r}\cdot\dot{\boldsymbol{v}}. \tag{145}$$

Ma, come si è visto al precedente n. 20'2, nel punto $\theta = \theta_0$ è $s = 0$; per $\theta < \theta_0$ è $s < 0$; per $\theta > \theta_0$ è $s > 0$; quindi $[ds/d\theta]_{\theta=\theta_0} > 0$. Dalla (145) si deduce così

$$\left[1 - \frac{n^2 r^2}{c^2} + \frac{n^2}{c^2} \boldsymbol{r} \cdot \dot{\boldsymbol{v}}\right]_{\theta=\theta_0} = -\frac{n}{c}\left[\frac{ds}{d\theta}\right]_{\theta=\theta_0} < 0 .$$

Le ipotesi formulate sul comportamento della funzione $\tau(\theta)$ hanno perciò come consequenza che l'espressione (144) è sempre negativa. Consegue che in prossimità del fronte d'onda il campo elettrico $\mathcal{E}^{(0)}(P, t)$ è parallelo e di verso opposto al campo impulsivo $\mathcal{E}^{(1)}(P, t)$.

L'approssimazione $\boldsymbol{r}_1 = \boldsymbol{r}_2 = \boldsymbol{r}(\theta_0)$ valida in prossimità del fronte d'onda consente di dare alla (139) la forma

$$\mathcal{H}^{(0)}(P, t) = \sqrt{\frac{\varepsilon}{\mu}} \frac{\boldsymbol{r}(\theta_0)}{r(\theta_0)} \wedge \mathcal{E}^{(0)}(P, t) . \tag{146}$$

Dalle cose ora dette e dal confronto di tale relazione con la (143) si deduce che il campo magntico $\mathcal{H}^{(0)}(P, t)$ è, in prossimità del fronte d'onda, parallelo e di verso opposto al campo magnetico impulsivo $\mathcal{H}^{(1)}(P, t)$. Segue che il vettore di Poynting $(c/4\pi)\mathcal{E}^{(0)} \wedge \mathcal{H}^{(0)}$ relativo ai campi $\mathcal{E}^{(0)}$ e $\mathcal{H}^{(0)}$ è, nelle immediate vicinanze del fronte d'onda, normale a questo e rivolto verso la regione anteriore al fronte stesso.

Secondo le espressioni date al n. 20'1 il campo elettrico $\mathcal{E}^{(0)}$ può essere scomposto nella somma di due componenti, una *componente di velocità*

$$q \sum_{h=1}^{h=2} \frac{(-1)^h}{s_h^3} \frac{1}{\varepsilon}\left(1 - \frac{n^2 v_h^2}{c^2}\right)\left(\boldsymbol{r}_h - \frac{n r_h \boldsymbol{v}_h}{c}\right) 1(t - \tau_0) , \tag{147}$$

e una *componente di accelerazione*

$$q \sum_{h=1}^{h=2} \frac{(-1)^h}{s_h^3} \frac{\mu}{c^2} \boldsymbol{r}_h \wedge \left[\left(\boldsymbol{r}_h - \frac{n r_h \boldsymbol{v}_h}{c}\right) \wedge \dot{\boldsymbol{v}}_h\right] 1(t - \tau_0) , \tag{148}$$

Analoga scomposizione si può introdurre per il campo magnetico (*). Poichè dall'analisi precedente risulta che le due componenti elettriche (147) e (148) hanno in prossimità del fronte d'onda la stessa direzione, ci si può chiedere

(*) Nel caso dell'analoga scomposizione relativa a velocità minori di c/n si usano le denominazioni di « campo di velocità » e « campo di accelerazione ». Noi preferiamo le denominazioni « componente di velocità » e « componente di accelerazione » perchè il « campo elettrico di velocità » e il « campo magnetico di velocità » costituiscono un campo elettromagnetico (cioè soddisfano alle equazioni dell'elettromagnetismo) soltanto nel caso della velocità costante.

quale di esse prevalga. Quando si riesamini il semplice calcolo precedente si trova che il rapporto tra la componente elettrica di accelerazione e la componente elettrica di velocità si può desumere dai termini che figurano nell'espressione (144) e che tale rapporto vale

$$\frac{n^2}{c^2}\left(\frac{\boldsymbol{r}\cdot\dot{\boldsymbol{v}}}{1-n^2v^2/c^2}\right)_{\theta=\theta_0}. \tag{149}$$

Poichè la (146) sussiste separatamente per le componenti di velocità e per le componenti di accelerazione, la (149) esprime pure il rapporto, in prossimità del fronte d'onda, fra la componente magnetica di accelerazione e la componente magnetica di velocità.

Nel caso particolare di un moto rettilineo e ritardato della particella, $\boldsymbol{v}(\theta)$ e $\dot{\boldsymbol{v}}(\theta)$ hanno la stessa direzione, se pur versi opposti. Inoltre, per quanto visto al n. **19**'6, nel punto $\theta=\theta_0$ l'angolo fra $\boldsymbol{r}(\theta_0)$ e $\boldsymbol{v}(\theta_0)$ ha il coseno di valore $c/nv(\theta_0)$. Detta allora ϱ la distanza del punto $P(x, y, z)$ di osservazione dalla traiettoria, è

$$\varrho = r(\theta_0)\sqrt{1-\frac{c^2}{n^2v^2(\theta_0)}},$$

e quindi

$$\boldsymbol{r}(\theta_0)\cdot\dot{\boldsymbol{v}}(\theta_0) = \varrho\,\frac{\dot{v}(\theta_0)}{\sqrt{1-c^2/n^2v^2(\theta_0)}}\,\frac{c}{nv(\theta_0)} = \varrho\,\frac{\dot{v}(\theta_0)}{\sqrt{(n^2v^2(\theta_0)/c^2)-1}},$$

per cui il rapporto (149) assume, in tale caso particolare, l'espressione

$$-\varrho\left|\frac{n^2\dot{v}/c^2}{(n^2v^2/c^2-1)^{\frac{3}{2}}}\right|_{\theta\ \theta_0}. \tag{150}$$

Si consideri un elettrone il quale si muova in un dielettrico di indice di rifrazione $n=1.33$, perdendo l'energia di 2 MeV per cm. Nel punto $\theta=\theta_0$ l'energia dell'elettrone sia di 500 keV. Un facile calcolo mostra allora che ivi è $v^2/c^2=0.75$ e $\dot{v}/c^2=-\frac{1}{2}$ cm^{-1}. Il rapporto (150) vale allora 4.6 ϱ. Pertanto in un punto che si trovi in prossimità del fronte d'onda e a una distanza $\varrho=0{,}2$ cm dalla traiettoria la componente di accelerazione uguaglia la componente di velocità. A distanze maggiori prevale la componente di accelerazione, a distanze minori quella di velocità.

21. – Il moto più generale della carica in un mezzo dispersivo.

21'1. – Più che altro, allo scopo di illustrare le possibilità del metodo esposto nel presente lavoro si considererà ora, se pur brevemente, il caso in cui la

funzione $\tau(\theta)$ ammette un numero qualunque di massimi e di minimi (dielettrico omogeneo, isotropo, dispersivo).

Siano $\theta_0, \theta_2, \ldots, \theta_{2n}$ i punti di minimo della funzione $\tau(\theta)$ e siano $\theta_1, \theta_3, \ldots, \theta_{2n-1}$ i punti di massimo, risultando inoltre

$$\theta_h < \theta_{h+1} \qquad (h = 0, \ldots, 2n-1).$$

Sia inoltre $\tau_h = \tau(\theta_h)$. Per semplicità si ponga

$$\theta_{-1} = -\infty\,, \quad \theta_{2n+1} = +\infty\,, \quad \tau_{-1} = +\infty\,, \quad \tau_{2n+1} = +\infty\,.$$

Si ammetteranno le condizioni

$$\tau_h < \tau_{h+1} \qquad \text{se } h \text{ è pari} \qquad (h = 0, 2, \ldots, 2n)$$

$$\tau_h > \tau_{h+1} \qquad \text{se } h \text{ è dispari} \quad (h = -1, 1, \ldots, 2n-1).$$

Si ammetterà ancora che la funzione $\tau(\theta)$ sia nell'intervallo $\theta_h \leqslant \theta \leqslant \theta_{h+1}$ sempre crescente da τ_h a τ_{h+1} se h è pari ($h = 0, 2, \ldots, 2n$), sia sempre decrescente da τ_h a τ_{h+1} se h è dispari ($h = -1, 1, 3, \ldots, 2n-1$).

Nell'intervallo $\theta_h \leqslant \theta \leqslant \theta_{h+1}$ la funzione $\tau(\theta)$ può pertanto essere invertita, cioè si può introdurre una funzione $\theta^{(h)}$ così definita

$$\tau = \tau(\theta^{(h)}) \qquad \theta_h \leqslant \theta^{(h)} \leqslant \theta_{h+1} \qquad (h = -1, 0, 1, \ldots, 2n).$$

Tali relazioni definiscono una funzione $\theta^{(h)}$ di τ nell'intervallo $\tau_h \leqslant \tau \leqslant \tau_{h-1}$ se h è pari, nell'intervallo $\tau_{h+1} \leqslant \tau \leqslant \tau_h$ se h è dispari (*).

Per semplicità si useranno le notazioni

$$r(\theta^{(h)}) = r_h\,, \qquad \boldsymbol{r}(\theta^{(h)}) = \boldsymbol{r}_h\,, \qquad \boldsymbol{v}(\theta^{(h)}) = \boldsymbol{v}_h\,.$$

L'espressione (83) di $\varphi_L(P, 0)$ può allora essere così scomposta

$$\varphi_L(P,0) = \frac{q}{\varepsilon}\int_{-\infty}^{+\infty} \exp\left[-i\omega\left(\theta + \frac{n\,r(\theta)}{c}\right)\right]\frac{1}{r(\theta)}\,\mathrm{d}\theta =$$

$$= \frac{q}{\varepsilon}\sum_{h=1}^{h=2n}\int_{\theta_h}^{\theta_{h+1}} \exp\left[-i\omega\left(\theta^{(h)} + \frac{n\,r(\theta^{(h)})}{c}\right)\right]\frac{1}{r(\theta^{(h)})}\,\mathrm{d}\theta^{(h)}\,.$$

(*) Il fatto di aver indicato il limite $+\infty$ di $\tau(\theta)$ per $\theta \to -\infty$ con il simbolo τ_{-1} offre simultaneamente la trattazione del caso in cui il limite di $\tau(\theta)$ per $\theta \to -\infty$ è finito.

Si osservi che nel problema qui considerato il primo punto di annullamento della derivata $\mathrm{d}\tau/\mathrm{d}\theta$ è il punto $\theta = \theta_0$, dove si è supposto l'esistenza di un minimo. Evidentemente con lievi modifiche si può anche considerare il caso in cui il primo punto di annullamento della derivata $\mathrm{d}\tau/\mathrm{d}\theta$ sia un massimo.

È ora, in analogia con le (109),

$$\frac{\mathrm{d}\theta^{(h)}}{\mathrm{d}\tau} = \frac{1}{1 - (n/c)(\boldsymbol{r}_h \cdot \boldsymbol{v}_h)/r_h},$$

e quindi

$$(151)\quad \varphi_L(P,0) = \frac{q}{\varepsilon}\sum_{h=0}^{h=n}\int_{\tau_{2h}}^{\tau_{2h+1}} \frac{\exp[-i\omega\tau]}{r_{2h} - (n/c)(\boldsymbol{r}_{2h}\cdot\boldsymbol{v}_{2h})}\,\mathrm{d}\tau - \frac{q}{\varepsilon}\sum_{h=0}^{h=n}\int_{\tau_{2h}}^{\tau_{2h-1}} \frac{\exp[-i\omega\tau]\,\mathrm{d}\tau}{r_{2h-1} - (n/c)(\boldsymbol{r}_{2h-1}\cdot\boldsymbol{v}_{2h-1})}.$$

Per quanto riguarda il potenziale vettore $\mathscr{A}_L(P,0)$, procedendo analogamente si trova

$$(152)\quad \mathscr{A}_L(P,0) = \frac{q\mu}{c}\sum_{h=0}^{h=n}\int_{\tau_{2h}}^{\tau_{2h+1}} \frac{\exp[-i\omega\tau]\boldsymbol{v}_{2h}}{r_{2h} - (n/c)(\boldsymbol{r}_{2h}\cdot\boldsymbol{v}_{2h})}\,\mathrm{d}\tau - \frac{q\mu}{c}\sum_{h=0}^{h=n}\int_{\tau_{2h}}^{\tau_{2h-1}} \frac{\exp[-i\omega\tau]\boldsymbol{v}_{2h-1}\,\mathrm{d}\tau}{r_{2h-1} - (n/c)(\boldsymbol{r}_{2h-1}\cdot\boldsymbol{v}_{2h-1})}.$$

Da quanto ora detto, appare chiara, senza bisogno di ulteriormente insistere, la via da seguire per dare a $\mathscr{E}_L(P,0)$ e a $\mathscr{H}_L(P,0)$ la struttura di rappresentazioni integrali rispetto alla variabile di arrivo, sia convergenti e sia simboliche, secondo il senso che conforma il n. **18**.

22. – Il moto più generale della carica in un mezzo non dispersivo.

Considerando un mezzo non dispersivo, si sostituiscano nella (151) le variabili τ con t e $\theta^{(h)}$ con $t^{(h)}$. Allora l'espressione

$$(153)\qquad \int_{\tau_{2h}}^{\tau_{2h+1}} \frac{\exp[-i\omega t]\,\mathrm{d}t}{r(t^{(2h)}) - (n/c)\boldsymbol{r}(t^{(2h)})\cdot\boldsymbol{v}(t^{(2h)})},$$

è la trasformata di Fourier di una funzione della variabile t nulla sia per $t < \tau_{2h}$ e sia per $t > \tau_{2h+1}$ ed uguale a

$$(154)\qquad \frac{1}{r(t^{(2h)}) - (n/c)\boldsymbol{r}(t^{(2h)})\cdot\boldsymbol{v}(t^{(2h)})}, \qquad \text{per } \tau_{2h} < t < \tau_{2h+1},$$

essendo $t^{(2h)}$ funzione di t definita dalle relazioni

$$t = \tau(t^{(2h)}) \qquad \theta_{2h} \leqslant t^{(2h)} \leqslant \theta_{2h+1}.$$

Attribuendo valori nulli all'espressione (154) allorchè t cade esternamente all'intervallo (τ_{2h}, τ_{2h+1}), si può anche dire che la (153) è la trasformata di Fourier della funzione

$$\frac{1}{r_{2h} - (n/c)(\boldsymbol{r}_{2h} \cdot \boldsymbol{v}_{2h})} 1(t - \tau_{2h}) 1(\tau_{2h+1} - t) ,$$

dove questa volta r_{2h}, $\boldsymbol{r}_{2h}$ e $\boldsymbol{v}_{2h}$ stanno per $r(t^{(2h)})$, $\boldsymbol{r}(t^{(2h)})$, $\boldsymbol{v}(t^{(2h)})$. Analogo discorso si può fare per gli integrali estesi all'intervallo (τ_{2h}, τ_{2h-1}) della variabile τ. L'antitrasformazione dei due membri della (153) fornisce perciò

$$(155) \quad \varphi(P,t) = \frac{q}{\varepsilon} \sum_{h=0}^{h=n} \frac{1}{r_{2h} - (n/c)(\boldsymbol{r}_{2h} \cdot \boldsymbol{v}_{2h})} 1(t - \tau_{2h}) 1(\tau_{2h+1} - t) - \\ - \frac{q}{\varepsilon} \sum_{h=0}^{h=n} \frac{1}{r_{2h-1} - (n/c)(\boldsymbol{r}_{2h-1} \cdot \boldsymbol{v}_{2h-1})} 1(t - \tau_{2h}) 1(\tau_{2h-1} - t) .$$

Analogamente si ha

$$(156) \quad \mathscr{A}(P, t) = \frac{q\mu}{c} \sum_{h=0}^{h=n} \frac{\boldsymbol{v}_{2h}}{r_{2h} - (n/c)(\boldsymbol{r}_{2h} \cdot \boldsymbol{v}_{2h})} 1(t - \tau_{2h}) 1(\tau_{2h+1} - t) - \\ - \frac{q\mu}{c} \sum_{h=0}^{h=n} \frac{\boldsymbol{v}_{2h-1}}{r_{2h-1} - (n/c)(\boldsymbol{r}_{2h-1} \cdot \boldsymbol{v}_{2h-1})} 1(t - \tau_{2h}) 1(\tau_{2h-1} - t) ,$$

dove, come si ripete, sono state usate le notazioni

$$r_i = r(t^{(i)}) , \qquad \boldsymbol{r}_i = \boldsymbol{r}(t^{(i)}) , \qquad \boldsymbol{v}_i = \boldsymbol{v}(t^{(i)}) ,$$

essendo t_i la radice dell'equazione

$$t = \tau(t^{(i)}) \qquad \theta_i \leqslant t^{(i)} \leqslant \theta_{i+1} \qquad (i = -1, 0, ..., 2n)$$

Dalle espressioni ora stabilite dei potenziali si possono ricavare i campi $\mathscr{E}(P, t)$ e $\mathscr{H}(P, t)$ mediante le relazioni

$$\mathscr{E} = - \operatorname{grad} \varphi - \frac{1}{c} \frac{\mathrm{d}\mathscr{A}}{\mathrm{d}t} , \qquad \mathscr{H} = \frac{1}{\mu} \operatorname{rot} \mathscr{A} ,$$

e mediante le regole di derivazione esposte al Cap. II, al fine di mettere in evidenza i campi impulsivi. I campi $\mathscr{E}(P, t)$ e $\mathscr{H}(P, t)$ si possono anche ricavare dalle espressioni simboliche delle trasformate alle quali si è alluso alla fine del numero precedente.

Nel caso generale qui considerato il campo elettromagnetico generato dalla carica ammette più fronti d'onda, come appare evidente da un semplice esame delle (155) e (156).

SUMMARY

The Author treats the theory of the Čerenkov radiation emitted by a charge in random motion. The development of this theory has been made possible by the introduction of a new method of the determination of the magnetic field produced by a charge in motion, which has a quite general purport. The paper consists of a short introduction and of three chapters. In the first chapter the wievpoints are introduced corresponding to the Lagrangian and the Eulerian of the dynamics of fluids. The Maxwellian formulation of electromagnetism pertains to the Eulerian wievpoint. One can give two different integral representations of the electromagnetic field generated by a convection current, corresponding to the two different wievpoints. From the equality of the values obtained by the two integral representations one obtains integral relations in which the potentials and fields generated by the moving charge element appear. The arbitrariness of the convection current allows one to choose it so to make the integral equations easily solvable. One obtains in this way a theorem which furnishes the Fourier time transforms of the potentials and fields generated by a moving elementary charge. This theorem is quite general as it applies without any limit for the velocity and acceleration of the charge, and for any medium, omogeneous or not, conducting or not, isotropic or anisotropic, dispersive or not. Obviously the problem now is to antitransform the expressions thus obtained. For this purpose a procedure is established and it is illustrated by a number of applications in chapters II and III. The media there considered are isotropic, homogeneous dielectrics, filling up the whole space; they may however be dispersive or not. In chap. II the uniform rectilinear motion of the charge is considered. In the case where the dielectric is not dispersive and the velocity v of the charge is higher than c/n (c=velocity of light in vacuum, n=refraction index of the medium), one obtains Tamm's solution. This solution is discussed from a physical point of view. The directions of the fields appear there to disagree with the laws of the electrodynamics and with the principle of energy conservation. The discussion points out how the disagreement is due to the fact that the non-dispersive dielectric is a limit of more realistic cases. Functions that are finite in a dispersive dielectric become infinite in a non-dispersive one. In order to make them evident in the latter case, it becomes necessary to stretch the differentiation procedure. Then the problem of determining the electromagnetic field is reconsidered, by using new differentiation rules (which are justified). Thus it becomes evident how they exist on the wave front fields of infinite intensity, of which our algorithm allows to determine the direction. These fields are much more important than those existing behind the wave front, described by Tamm's representation. Near the wave front the electric and magnetic fields of Tamm's solution are parallel, but with opposite direction, to the impulsive electric and magnetic fields existing on the wave front.

By introducing the latter ones the disagreements disappear. In chap. III the variable motion is studied. If the trajectory C of the charge is a curve of parametric equations $x=x(\theta)$, $y=y(\theta)$, $z=z(\theta)$ $(-\infty<\theta<+\infty)$ and if the charge covers the curve C with the law of the motion $\theta = t$, the problem of determining the electromagnetic field in a point $P(x, y, z)$ is dominated by the behaviour of the function τ of the variable θ, thus defined:

$$\tau = \theta + \frac{n}{c}\sqrt{[(x - x(\theta)]^2 + [y - y(\theta)]^2 + [z - z(\theta)]^2} = \theta + \frac{n}{c} r(\theta) ,$$

where $r(\theta)$ is the distance of the point $P(x, y, z)$ from the point $(x(\theta), y(\theta), z(\theta))$ of the curve C. If the velocity v of the charge is always lower than c/n, the function $\tau(\theta)$ is always increasing. If v is higher than c/n along the whole or a part of the trajectory, the function $\tau(\theta)$ has at least one point of minimum. In the case of the conventional Čerenkov radiation, $\tau(\theta)$ has only one minimum. The different problems are thus classified according to the behavior of the function $\tau(\theta)$. The variables θ and τ are given respectively the names of start variable and arrival variable. As a consequence of the eulerian definition of Maxwell's electrodynamics, the application of the general theorem established in chap. I leads to express the F-transforms of the potentials and fields by means of integrals where the integration variable is the start variable. The inverse transformation method here introduced consists in giving the formal appearance of F-transforms to these integral representations, by handling the integrands in a suitable way. The purpose is achieved by a substitution of the variable: it is sufficient to express the F-transforms with integrals where the integration variable is the arrival variable. The case where $\tau(\theta)$ is always increasing is examined first. This is an interesting trial of the new method, because it is applied to a known problem with known solutions. Afterwards the case where $\tau(\theta)$ has only one minimum is studied. No difficulty arises in treating the scalar and vector potentials. The equations of the wave front are determined. It is still possible to construct the wave front by Huyghens' principle. As far as the fields are concerned, two integral representations of the F-transforms with respect to the arrival variable are given. Both representations make evident the effect of the acceleration. One of them, made of convergent integrals, is specially suitable to study energetic problems and other problems concerning the Čerenkov radiation in dispersive media. The other one is a symbolic representation, obtained with the differentiation procedure developed in chap. II, and useful for determining the fields in non-dispersive media. In a non-dispersive medium the wave front is still dominated by the impulsive fields. These fields depend on the velocity, but not on the acceleration. As in the uniform rectilinear motion, also in the variable motion the electromagnetic field shows a sharp inversion on the wave front. In the region behind the wave front the electromagnetic field may be divided in two components, one due to the velocity and the other one to the acceleration. The distribution in space of the two components is very different. Chap. III ends with a brief treatment of the case where $\tau(\theta)$ has any number of maxima and minima, in order to illustrate the possibilities of the method. The present paper has been devoted only to an exposition of methods and the description of the electromagnetic field generated by a moving charge. The energy problems concerning the Čerenkov radiation, and the quantitative discussion of the effect of the acceleration in the experiments, will be the object of another paper with the title *The energy of the Čerenkov radiation.*

IL NUOVO CIMENTO · Vol. XXII, N. 4 16 Novembre 1961

Static Gravitational Fields in General Relativity.

A. A. Evett

Department of Physics, University of Arizona - Tucson, Ariz.

(ricevuto il 17 Agosto 1961)

Summary. — Static gravitational fields are defined in terms of the existence of a set of observers mutually « at rest » with respect to each observer's Fermi coordinate frame. The Fermi co-ordinate frame is chosen because it is the only « non-rotating » frame for an observer. It is shown that this definition is equivalent to the usual one, and the time-reversibility of static fields is derived from the new definition. Application of Fermi cylindrical co-ordinates to an axially symmetric static field is discussed.

1. – Introduction.

The usual definition or criterion for a static gravitational field is that a set of co-ordinates can be found such that the metric tensor (1) has $g_{\alpha 4} = 0$ and none of the g_{ij} dependent on x^4. This is purely a mathematical requirement which is supposed to be applicable to physical situations in which all the matter is « at rest » in some sense. The stipulation for the g_{ij} to be independent of x^4, sometimes referred to as the condition for a *stationary* gravitational field, is easy to establish on the basis that the universe should « appear the same » to an observer at all times in order to qualify as a member of the « static » category. However, the physical basis for setting $g_{\alpha 4} = 0$ is more obscure. A common approach is to appeal to a time-reversal hypothesis (2). But a justification as to why a physical situation qualifying as static should necessarily imply time reversibility has not been presented, except in the nega-

(1) The timelike co-ordinate is taken to be x^4, with $g_{44} < 0$. Latin indices have the range 1, 2, 3, 4 while Greek indices take the values 1, 2, 3. The symbolism and nomenclature are chosen to agree with that used in J. L. Synge: *Relativity: The General Theory* (Amsterdam, 1960). In the following, this reference will be denoted reference I.

(2) G. Y. Rainich: *Mathematics of Relativity* (New York, 1950), p. 151. See also reference I, pp. 309 ff.

tive sense of not leading to contradictions or inconsistencies in situations where such arguments have been applied. The purpose of this note is to give an alternate definition of static gravitational fields and to show that it leads to the same form for the metric tensor as does the time reversal hypothesis.

2. – Definition of a static field.

Consider the world line C_1 of an observer. Construct Fermi co-ordinates ([3]) using C_1 as the base line. In this way we assign co-ordinates to space-time. Lines of constant x^1, x^2, x^3 form a collection of world lines. The utilization of a reference frame based on Fermi-Walker transport of an orthogonal tetrad is motivated by the fact that such a frame is the only one which gives the observer with world line C_1 a physical basis for claiming his frame to be « non-rotating » ([4]). Next we require the metric tensor to be independent of the proper time τ of the observer C_1. This merely indicates that the static field must satisfy the stationary condition in a « non-rotating » frame from C_1's viewpoint. To complete the definition of a static field we require that each observer at constant x^1, x^2, x^3 should find that the other observers also have fixed positions with respect to his « non-rotating » Fermi co-ordinate frame and the metric tensor time-independent in his frame. In other words, we define a static field to be one in which there exists a set of privileged world lines, filling all space-time in the region of interest, such that the metric tensor is time-independent and the space co-ordinates of the world lines are constant relative to the Fermi frame constructed on any of the world lines. Such a field would certainly have the physical justification from the viewpoint of this privileged set of observers for the connotation of « static ».

Actually we could have imposed a much weaker set of requirements on our static field and the derivation to follow uses only this weaker set. However, the consequences of the weaker set are such as to make valid the stated stronger requirements.

3. – Derivation of the metric form.

It is convenient for analytical purposes to make a slight modification in the Fermi co-ordinates used in reference ([1]). Let τ be the proper time of the observer with world line C_1. Consider an event P in space-time, and construct a geodesic orthogonal to C_1 to the event P, as shown in Fig. 1. Let ϱ be the measure along the geodesic from O to P. Next construct an infinitesimal spherical 2-surface in the 3-space of constant τ around the point O on C_1 and

([3]) Reference I, pp. 83 ff.
([4]) Reference I, pp. 123 ff.

let θ and φ be the usual spherical polar angle co-ordinates on this sphere, the angles being measured with respect to the Fermi-transported orthogonal triad in the 3-space. If the geodesic to P cuts through the infinitesimal sphere at angle co-ordinates θ, φ then assign to the point P the co-ordinates $(x^1, x^2, x^3, x^4) \rightarrow (\varrho, \theta, \varphi, \tau)$. We are in effect using « polar » Fermi co-ordinates in contrast to « cartesian » Fermi co-ordinates. Using the well-known properties of deviation vectors between adjacent geodesics [5] and the geometric properties of the Fermi co-ordinates, one can establish that the metric tensor in these co-ordinates must have $g_{1k} = \delta_{1k}$. Therefore the metric form is

$$(\mathrm{d}\varrho)^2 + g_{22}(\mathrm{d}\theta)^2 + 2g_{23}\,\mathrm{d}\theta\,\mathrm{d}\varphi + g_{33}(\mathrm{d}\varphi)^2 + 2g_{24}\,\mathrm{d}\theta\,\mathrm{d}\tau + 2g_{34}\,\mathrm{d}\varphi\,\mathrm{d}\tau + g_{44}(\mathrm{d}\tau)^2 .$$

Also, as $\varrho \rightarrow 0$, then $g_{24} \rightarrow 0$, $g_{34} \rightarrow 0$, $g_{44} \rightarrow -1$.

The next step is to determine what happens to the above metric form when the gravitational field is static and C_1 is the world line of one of the privileged observers. First of all, the stationary condition forces the g_{ij} to be independent of τ.

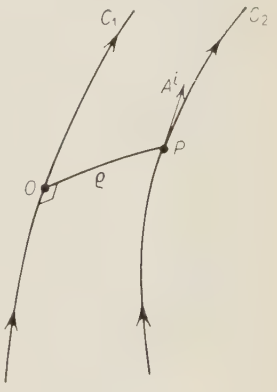

Fig. 1.

Suppose event P in Fig. 1 has co-ordinates $(\varrho, \theta, \varphi, \tau)$ and C_2 is the world line made up of events all with the same ϱ, θ, φ. The second part of our definition of a static field means that the displacement vector from P to an event on a neighboring world line, with slightly different ϱ, θ, φ, must undergo Fermi-Walker transport as it moves along C_2. So consider a neighboring world line with space co-ordinates $\varrho, \theta + \mathrm{d}\theta, \varphi$. The displacement vector between C_2 and this neighboring world line has components $\lambda^i = (0, \mathrm{d}\theta, 0, 0)$. The unit tangent vector to C_2 has components $A^i = (0, 0, 0, 1/\sqrt{-g_{44}})$. Along C_2, $\mathrm{d}s = \sqrt{-g_{44}}\,\mathrm{d}\tau$. The mathematical conditions for λ^i to undergo Fermi-Walker transport along C_2 is that $\delta\lambda^i/\delta s = A^i\lambda^j(\delta A_j/\delta s) - (\delta A^i/\delta s)\lambda^j A_j$, For the metric form established above, this reduces to

$$g_{44}\Gamma^i_{24} = \delta^i_4 \Gamma^m_{24} g_{m4} + \Gamma^i_{44} g_{24} . \tag{1}$$

Similarly, if we consider a displacement vector $(0, 0, \mathrm{d}\varphi, 0)$ and require it to undergo Fermi-Walker transport along C_2, we find

$$g_{44}\Gamma^i_{34} = \delta^i_4 \Gamma^m_{34} g_{m4} + \Gamma^i_{44} g_{34} . \tag{2}$$

[5] Reference I, p. 21.

Eight equations are included in (1) and (2). However, we need to use only two of them, because the solution of these two satisfies the rest of the equations identically. Let $i = 1$ in (1). This gives $g_{44}\Gamma^1_{24} = \Gamma^{11}_{44} g_{24}$, and for the co-ordinates being used this is equivalent to $g_{11}\,\partial g_{24}/\partial\varrho = g_{24}\,\partial g_{44}/\partial\varrho$. Integrating partially with respect to ϱ yields $g_{24} = f(\theta, \varphi) g_{44}$. But $g_{24} \to 0$, and $g_{44} \to -1$ as $\varrho \to 0$ for all θ, φ. Therefore $f(\theta, \varphi) = 0$, and consequently $g_{24} = 0$. A similar analysis applied to the $i = 1$ equation in (2) shows $g_{34} = 0$.

So we have established that, in Fermi polar co-ordinates, our definition of a static gravitational field implies $g_{\alpha 4} = 0$ and the metric form is

$$(\mathrm{d}\varrho)^2 + g_{22}(\mathrm{d}\theta)^2 + g_{33}(\mathrm{d}\varphi)^2 + g_{44}(\mathrm{d}\tau)^2 + 2g_{23}\,\mathrm{d}\theta\,\mathrm{d}\varphi\,. \tag{3}$$

Various modifications of the Fermi co-ordinates are useful for particular situations involving static gravitational fields. The polar form above would be most appropriate for spherically symmetric static fields, in which case the form in (3) can be further simplified. A modification appropriate to an axially symmetric static field will be discussed next. This modification amounts to a change in co-ordinates from Fermi polar to what we shall call Fermi cylindrical co-ordinates. Rather than search for the analytical transformation equations between these two co-ordinate systems, it is simpler to start afresh with a new geometrical construction.

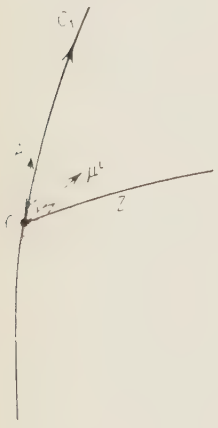

Fig. 2.

Again, we consider the world line C_1 of one of the privileged observers as shown in Fig. 2. At the event corresponding to the proper time τ on this observer's world line, draw an orthogonal geodesic out from the world line and let z be the measure along this geodesic. Select a vector μ^i at O orthogonal to both the world line (whose tangent unit vector we call A^i) and the z-line. Now transport parallely the vectors A^i and μ^i along the geodesic z-line. For static fields the parallely transported A' will be the unit tangent vector of the world line of the privileged observer passing through that event. At each value of z draw all the geodesics that are perpendicular to A' and the z-line. Let the measure along each of these geodesics be σ, and denote the angle between the σ-geodesic and μ^i on the z-line by ψ. Label events by co-ordinates $(\bar{x}^1, \bar{x}^2, \bar{x}^3, \bar{x}^4) \to (z, \sigma, \psi, \tau)$. The reference vector μ^i and the geodesic z-line are moved by Fermi transport along C_1. For a given τ, the totality of points in the 3-space z, σ, ψ is the same as the totality of points in the 3-space ϱ, θ, φ corresponding to the use of Fermi polar co-ordinates. Using the geometric properties of our construction along with the previously established property that the τ-lines are ortho-

gonal to the ϱ, θ, φ (or z, σ, ψ) 3-space, the metric form must be

$$\bar{g}_{11}(\mathrm{d}z)^2 + (\mathrm{d}\sigma)^2 + \bar{g}_{33}(\mathrm{d}\psi)^2 + \bar{g}_{44}(\mathrm{d}\tau)^2 + 2\bar{g}_{13}\,\mathrm{d}z\,\mathrm{d}\psi\,. \tag{4}$$

The metric form (4) applies to any static field. If the physical situation is such that complete axial symmetry holds about the z-line, then $\bar{g}_{13} = 0$ and the $\bar{g}_{ij}$ are functions of z and σ only.

4. – Discussion.

Nowhere in the definition of the static gravitational fields was a statement made concerning the relative motion of the matter producing the gravitational field. A reasonable expectation for a static field is that the matter be « at rest » to our set of privileged observers; *i.e.*, each privileged observer should find the space co-ordinates of all the matter to be unchanging with respect to his « non-rotating » Fermi reference frame. It will now be shown that this property is indeed satisfied for static gravitational fields whose origin arises solely from a matter distribution with no contribution from other sources such as an electromagnetic field.

In the absence of fields other than matter fields, the unit tangent vector to the world lines of the matter is the unit time-like eigenvector of the Einstein tensor G_{ij}. For the static situation with g_{ij} independent of x^4 and $g_{34} = 0$, one can easily verify that $G_{34} = 0$. The unit tangent vector to the privileged world lines has components $A^i = (0, 0, 0, 1/\sqrt{-g_{44}})$. Then $G_{ij}A^j = (G_{44}/g_{44})g_{ij}A^j$. So A^i is an eigenvector of G_{ij} with eigenvalue G_{44}/g_{44}, and therefore the matter world lines and the privileged observers' world lines everywhere coincide. Of course, in regions free of matter there is no meaning associated with the direction of the matter world lines.

If there are other fields besides matter fields contributing to the stress-energy tensor, then our definition of a static field would not necessarily imply that the matter was at rest to the privileged observers.

RIASSUNTO (*)

I campi gravitazionali statici sono definiti con riferimento all'esistenza di un gruppo di osservatori reciprocamente in quiete rispetto al sistema di coordinate di Fermi di ciascun osservatore. Si è scelto il sistema di coordinate di Fermi perchè è il solo « non-rotante » per un osservatore. Si mostra che questa definizione è equivalente a quella usuale, e dalla nuova definizione si deriva l'invertibilità rispetto al tempo dei campi statici. Si discute l'applicazione delle coordinate cilindriche di Fermi ad un campo statico con simmetria assiale.

(*) *Traduzione a cura della Redazione.*

Multipole Magnetic Field Configurations for Stable Plasma Confinement (*).

T. Ohkawa (**) and W. D. Kerst

John Jay Hopkins Laboratory for Pure and Applied Science, General Atomic Division of General Dynamics Corporation - San Diego, Cal.

(ricevuto il 18 Agosto 1961)

Summary. — A method of eliminating plasma leakage by connecting cusps with a magnetic field bridge has been described by Tuck [1]. Here we discuss a multipole configuration employing this idea but with no circumferential (B_z) field. High β plasma is confined with no free plasma surface in the usual cusp model sense. The stability diagram for such configurations can be obtained with the pressure of the plasma as a parameter. Generally this condition on the structure can be stated as $(B_2/B_1)^2 > r/d$ where r is the radius of the current carrying rods which produce the multipole field, $2d$ is the distance between a rod and the conducting wall (bridge width), and B_2 and B_1 are the maximum and minimum fields along the wall surface. Approximations resulting from the magnetohydrodynamic treatment are considered. Some practical questions are mentioned and it is shown that in a sample case one expect confinement time of $\sim 10^{-2}$ s for a plasma temperature of 10^4 eV.

1. – Introduction.

The method of stabilizing the pinch, which suffers sausage and kink instabilities, by applying the magnetic field parallel to the discharge tube turns out to be fairly effective and in fact in some cases the pinch may be stable. However, the stability of the pinch depends critically on the influence of the plasma on the magnetic field distribution. Especially the existence of the sin-

(*) Research on controlled thermonuclear reactions is a joint program carried out by General Atomic and the Texas Atomic Energy Research Foundation.

(**) On leave from the University of Tokyo.

gular surface makes the plasma sensitive to magnetic field errors [1] and difficult to stabilize.

If one considers an alternative method, namely, stabilization of the plasma without the usual axial field, it becomes clear that conductors are required in the plasma. Many of these configurations have been discussed by GRAD [2] and by BRAGINSKII and KADOMTSEV [3]. The very important suggestion made by TUCK [1] of connecting the cusps to each other around the conductor to eliminate plasma leakage by containing all lines of force may be simplified and leads to multipole configurations shown in Fig. 1. Since the magnetic field decreases rapidly towards the center, most of the plasma has β nearly one, although there are no cusps or discreet surfaces [5]. We thus have an equilibrium position for diamagnetic plasma at any plasma density. For pinches such an equilibrium position is not created by the vacuum magnetic field but it depends on proper plasma current distribution and persistence.

We shall consider the equilibrium and the stability of the plasma in this configuration using the hydromagnetic approximation. The deviation from this approximation will be discussed later.

2. – Hydromagnetic equilibria.

Although we have in mind toroidal and linear configurations we shall neglect toroidal effects since they are small with high multipole numbers, and we shall assume the structure is straight in the z direction. The set of equations for equilibrium of the plasma is given by

$$[\mathrm{curl}\,\boldsymbol{B}]\times\boldsymbol{B} = \nabla\boldsymbol{p}\,, \tag{2.1}$$

$$\mathrm{div}\,\boldsymbol{B} = 0\,. \tag{2.2}$$

From eq. (2.2) it is convenient to use a flux function, ψ, defined by

$$B_r = (1/r)\,\partial\psi/\partial\theta\,, \tag{2.3}$$

$$B_\theta = -\,\partial\psi/\partial r\,. \tag{2.4}$$

[1] D. W. KERST: *Bull. Am. Phys. Soc.*, **4**, 352 (1959) and **5**, 352 (1960); T. OHKAWA and D. W. KERST: *Bull. Am. Phys. Soc.*, **6**, 290 (1961).

[2] J. BERKOWITZ, K. O. FRIEDRICHS, H. GOERTZEL, H. GRAD, J. KILLEEN and E. RUBIN: *Proc. Sec. U. N. Int. Conf. Peaceful Uses of Atomic Energy*, vol. **31** (1959), p. 171.

[3] S. I. BRAGINSKII and B. B. KADOMTSEV: *Plasma Physics and the Problem of Controlled Nuclear Reactions*, vol. **3** (London, 1922), p. 356.

[4] J. L. TUCK: *Nature*, **187**, 863 (1960).

[5] T. OHKAWA and D. W. KERST: *Phys. Rev. Lett.*, **7**, 41 (1961).

Then eq. (2.1) yields

$$p = p(\psi) \tag{2.5}$$

and

$$\partial^2\psi/\partial r^2 + (1/r)\,\partial\psi/\partial r + (1/r^2)\,\partial^2\psi/\partial\theta^2 + \mathrm{d}p(\psi)/\mathrm{d}\psi = 0\,. \tag{2.6}$$

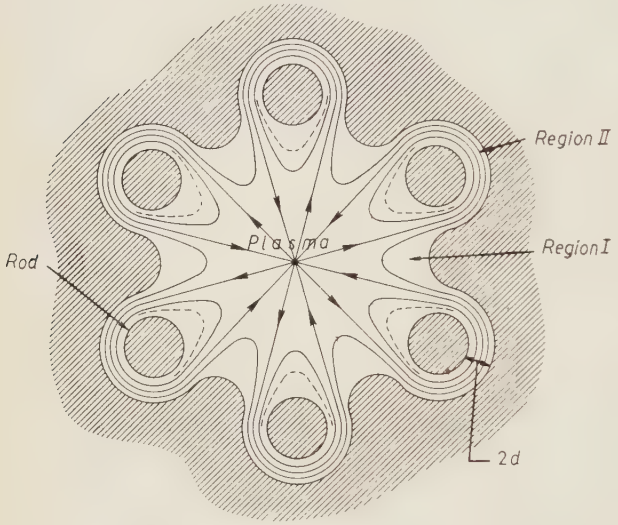

Fig. 1. – Cross-section of the multipole configuration.

Near the wall and the rod, the field is very strong and β is low. Therefore, the field distribution is only slightly modified by the presence of the plasma and in that region it is almost a vacuum field. In the central region we may approximate the pressure distribution by

$$\begin{cases} (\mathrm{d}/\mathrm{d}\psi)\,p(\psi) = -\,a\psi \\ \text{or} \\ p(\psi) = p_0 - (a/2)\psi^2\,. \end{cases} \tag{2.7}$$

This assumption gives a pure multipole solution for ψ from eq. (2.6) and thus neglects higher harmonics of the multipole. This may be considered as a power expansion of p in ψ near the center. Then ψ and p are given by

$$\psi = I_m(ar)\cos m\theta\,, \tag{2.8}$$

$$p = p_0 - (a/2)I_m^2(ar)\cos^2 m\theta\,, \tag{2.9}$$

where I_m is the modified Bessel function. The vacuum field ψ_0 is given by

$$\psi_0 \propto r^m \cos m\theta \tag{2.10}$$

and the effect of the pressure is to push the flux lines outward as shown by the broken lines in Fig. 1 and Fig. 2.

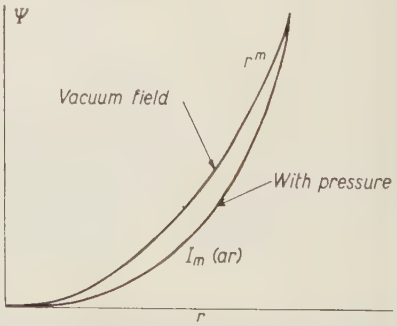

Fig. 2. Magnetic flux as a function of radius with or without plasma pressure.

3. – Hydromagnetic stability.

The part of the plasma which faces the rod in Fig. 1 is clearly stable since the surface is concave. The outer plasma surface in region II is convex and in region I, it is concave. These regions are connected through flux lines and have the same pressure along the flux line. By making the magnetic field in region II much stronger than the field in region I, the contribution to the instability may be made as small as we like and the overall effect can be stability. However, the possibility of a displacement of the flux lines in such a way that the plasma is not disturbed in the stabilizing region I but is disturbed in the unstabilizing region II leaves the question of the stability open. This kind of displacement requires bending of the flux line and the stability depends on which effects dominate.

We shall calculate the stability criteria by using the energy principle for these cases.

For a plasma configuration which is two-dimensional, *i.e.*, no dependence of all quantities on the third direction and no magnetic field component in that direction, the energy integral for the stability calculation has been worked out by the Princeton group [6].

Here we shall trace their method.

We choose the co-ordinate system consisting of (ψ, χ, z), where z is in the perpendicular direction to the plane, $\psi =$ constant defines a flux line on the plane, and χ is chosen so that (ψ, χ, z) makes the orthogonal set of co-ordinates. The line element $\mathrm{d}s$ and the volume element $\mathrm{d}\tau$ are given by

$$\mathrm{d}s^2 = (1/B^2)(\mathrm{d}\psi)^2 + J^2B^2(\mathrm{d}\chi)^2 + \mathrm{d}z^2 , \tag{3.1}$$

$$\mathrm{d}\tau = J\,\mathrm{d}\psi\,\mathrm{d}\chi\,\mathrm{d}z . \tag{3.2}$$

where B is the magnetic field strength and J is the volume of unit $(\mathrm{d}\psi)(\mathrm{d}\chi)(\mathrm{d}z)$.

The pressure balance equation is given by

$$\mathrm{d}p(\psi)/\mathrm{d}\psi = -(1/J)(\partial/\partial\psi)(JB^2) , \tag{3.3}$$

where p, the pressure of the plasma, is a function of ψ only, since the pressure is constant along a flux line in the hydromagnetic approximation.

The energy integral for small disturbance

$$\xi = (\xi_\psi, \xi_\chi, \xi_z)$$

[6] I. B. Bernstein, E. A. Frieman, M. D. Kruskal and R. M. Kulsrud: *Proc. Roy. Soc.*, A **244**, 17 (1958).

is given by

$$\delta w = \frac{1}{2}\int \mathrm{d}\psi\,\mathrm{d}\chi\,\mathrm{d}z\, J\,[\boldsymbol{Q}^2 - \boldsymbol{j}\cdot(\boldsymbol{Q}\times\boldsymbol{\xi}) + \gamma p(\nabla\cdot\boldsymbol{\xi})^2 + (\nabla\cdot\boldsymbol{\xi})(\boldsymbol{\xi}\cdot\nabla p)\,, \tag{3.4}$$

where $\boldsymbol{Q} = \boldsymbol{\nabla}\times(\boldsymbol{\xi}\times\boldsymbol{B})$.

Since all equilibrium quantities are independent of z it is convenient to expand ξ in Fourier series in z,

$$\left|\begin{array}{l} \xi_\psi = \sum_{k=0} 1/B\,X_k \left\{\begin{matrix}\cos\\ \sin\end{matrix}\right\} kz\,, \\ \xi_z = \sum_{k=1} 1/k\;Y_k \left\{\begin{matrix}\sin\\ -\cos\end{matrix}\right\} kz + \xi_z^{(0)}\,, \\ \xi_\chi = \sum_{k=0} B\,Z_k \left\{\begin{matrix}\cos\\ \sin\end{matrix}\right\} kz, \end{array}\right. \tag{3.5}$$

The absence of B_z separates cos and sin modes and only one of the modes needs to be considered. By using (3.5) in (3.4) and performing the integral over z, we obtain

$$\delta w = \sum_k \delta w_k\,, \tag{3.6}$$

$$\begin{aligned}\delta w_k = (\pi/2)\int \mathrm{d}\chi\,\mathrm{d}\psi\big\{&1/(B^2J)(\partial X_k/\partial\chi)^2 + (1/k^2)(1/J)(\partial Y_k/\partial\chi)^2 + \\ &+ B^2J(\partial X_k/\partial\psi + Y_k)^2 + p'JX_k(\partial X_k/\partial\chi + Y_k) + \\ &+ \gamma p/J[(\partial/\partial\psi)(JX_k) + JY_k + \partial Z_k/\partial\chi]^2 + p'X_k(J\,\partial X_k/\partial\psi + X_k\,\partial J/\partial\psi + JY_k)\big\}\,,\end{aligned} \tag{3.7}$$

where the prime denotes the derivative with respect to ψ. It is clear that $k\to\infty$ modes (shortest wave length) are the worst modes from (3.7). By putting $k=\infty$ and dropping the suffixes, (3.7) becomes

$$\begin{aligned}\delta w = (\pi/2)\int \mathrm{d}\psi\,\mathrm{d}\chi J\big\{&(1/J^2B^2)(\partial X/\partial\psi)^2 + p'X^2\partial(\ell nJ)/\partial\psi - p'^2X^2/B^2 + \\ &+ \big(1/[B^{-2} + (\gamma p)^{-1}]\big)[X\,\partial(\ell nJ)/\partial\psi + (1/J)\,\partial Z/\partial\chi - p'X/B^2]^2 + \\ &+ (B^2+\gamma p)[Y + \partial X/\partial\psi + X\big(p' + \gamma p\,\partial(\ell nJ)/\partial\psi + (\gamma p/J)(\partial Z/\partial\chi)\big)/(B^2+\gamma p)]^2\big\}\,.\end{aligned} \tag{3.8}$$

Since Y is contained only in the last term, W is minimized with respect to Y by making the last term vanish. Then we obtain

$$\begin{aligned}\delta w = \left(\frac{\pi}{2}\right)\int \mathrm{d}\psi\,\mathrm{d}\chi\cdot \\ \cdot\left\{\left(\frac{1}{B^2J}\right)\left(\frac{\partial X}{\partial\chi}\right)^2 + (p')DX^2J\cdot\left[\frac{J}{B^2 + (\gamma p)^{-1}}\right]XD + \left(\frac{1}{J}\right)\left|\frac{\partial Z}{\partial\chi}\right|^2\right\}\,,\end{aligned} \tag{3.9}$$

where

$$D = \partial(\ell n J)/\partial\psi - (1/B^2)p' = -(1/B^2)\,\partial(p + 1/2\,B^2)/\partial\psi\,. \tag{3.10}$$

Note that the only term which could be negative is $(p')DJX^2$. The sign of $(p')D$ depends on the sign of the curvature of the flux line towards higher pressure sides. In (3.9) there is no $(\partial X/\partial\psi)$ or $(\partial Z/\partial\psi)$ term and δw may be written as

$$\delta w = \int \mathrm{d}\psi\,\delta W(\psi)\,. \tag{3.11}$$

This means that if we consider the stability of a flux line separately and if all the flux satisfy the stability condition,

$$\delta W(\psi) > 0\,, \tag{3.12}$$

the plasma will be stable. $\delta W(\psi)$ is given by

$$\delta W(\psi) = \frac{\pi}{2}\int \mathrm{d}\chi \left\{\left(\frac{1}{B^2 J}\right)\left(\frac{\partial X}{\partial\chi}\right)^2 - p' J D X^2 - J^{-1}\underbrace{(XD + J^{-1}\partial Z/\partial\chi)^2}_{(B^{-2} + (\gamma P)^{-1})}\right\}. \tag{3.13}$$

From (3.13) we may obtain Euler's equation for X and Z. However, we shall consider only the sufficient conditions for stability here. We define S by

$$S = \int \mathrm{d}\chi\,\{(1/B^2 J)(\partial X/\partial\chi)^2 + p' D J X^2\}\,, \tag{3.14}$$

then stability is obtained when

$$S > 0\,. \tag{3.15}$$

This is equivalent to neglecting the compressibility which would provide still more stability.

The integral, $\int JD\,\mathrm{d}\chi$, may be written as

$$\int JD\,\mathrm{d}\chi = (\partial/\partial\psi)\int \mathrm{d}s/B - p'\int \mathrm{d}s/B^3\,, \tag{3.16}$$

where $\mathrm{d}\psi\int \mathrm{d}s/B$ is the volume occupied by a flux tube $\mathrm{d}\psi$. At the lower pressure limit the stability criterion becomes $(\partial/\partial\psi)\int \mathrm{d}s/B > 0$ and this agrees with the Rosenbluth-Longmire criterion for flute instability.

We shall assume that the flux lines consist of arcs to apply the above criteria to the present configurations, Fig. 3. Then we have

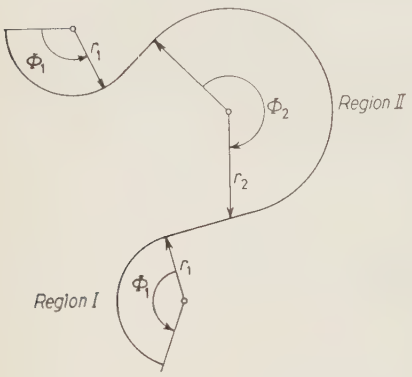

Fig. 3. – Geometry of flux lines for stability calculation.

$$\text{(3.17)} \qquad \begin{cases} \mathrm{d}\chi = \mathrm{d}\varphi\,, \\ J \;\; = r/B(r)\,, \\ \mathrm{d}\psi(r)/\mathrm{d}r = \pm\, B(r)\,. \end{cases}$$

The sign of the last equation depends on whether ψ increases with radius or decreases.

By using (3.17), we have

$$\text{(3.18)} \qquad JD = \pm\, 2/B^2$$

and S is given by

$$\text{(3.19)} \qquad S = (1/rB)\int \mathrm{d}\varphi(\partial X/\partial\varphi)^2 + (\mathrm{d}p/\mathrm{d}r)(2/B^3)\int X^2\,\mathrm{d}\varphi\,.$$

We shall approximate the configuration shown in Fig. 1 by two arcs connected by a straight line as shown in Fig. 3.

First we shall consider a uniform X which is independent of φ, or $\xi_\psi \propto (1/B)$.

Then S is given by

$$\text{(3.20)} \qquad S = (\mathrm{d}p/\mathrm{d}r_1)(2/B_1^3)X^2\varphi_1 + (\mathrm{d}p\mathrm{d}r_2)(2/B_2^3)\,X^2\varphi_2$$

and we have the relation

$$\text{(3.21)} \qquad (\mathrm{d}p/\mathrm{d}r_1) = -\,(\mathrm{d}p/\mathrm{d}r_2)\,B_1/B_2 > 0\,.$$

Hence the stability condition becomes

$$\varphi_1/B_1^2 - \varphi_2/B_2^2 > 0$$

or

$$\text{(3.22)} \qquad (B_2/B_1)^2 > \varphi_2/\varphi_1\,.$$

If we define β by

$$\text{(3.23)} \qquad \beta \equiv 2p_0/B^2\,,$$

where p_0 is the maximum plasma pressure then (3.22) becomes

$$\beta_2 < \varphi_1/\varphi_2 \,. \tag{3.24}$$

This case may not be the worst mode. If X is zero in the region I, the stabilizing effects of the region I disappear and stability must come from the $(\partial X/\partial q)^2$ term or physically from bending the flux lines. Therefore we shall assume

$$\begin{cases} X = 0 & \text{in region I} \\ X = X(\varphi) & \text{in region II} \end{cases}$$

as the worst case.

Then S is given by

$$S = (1/rB_2)\int \mathrm{d}q\,(\partial X/\partial q)^2 + (\mathrm{d}p/\mathrm{d}r_2)(2/B_2^3)\int X^2\mathrm{d}q \,, \tag{3.25}$$

and the stability condition becomes

$$|r_2(\mathrm{d}p/\mathrm{d}r_2)| < B_2^2 F/2 \,, \tag{3.26}$$

where F is the form factor and is given by

$$F = \left|\int_0^{\varphi_2} (\partial X/\partial\varphi)^2\,\mathrm{d}\varphi\right| \Big/ \int_0^{\varphi_2} X^2\,\mathrm{d}q \,. \tag{3.27}$$

F is apparently the smallest with

$$X \approx |X| \sin(\pi\varphi/\varphi_2)$$

and is given by

$$F = (\pi/\varphi_2)^2 \,. \tag{3.28}$$

The pressure gradient is given approximately by

$$|\mathrm{d}p/\mathrm{d}r_2| \approx p_0/d_2 \,, \tag{3.29}$$

where d_2 is the thickness of the plasma in region II.

From (3.23), (3.26), (3.28), and (3.29), we obtain

$$\beta_2 < (d_2/r_2)(\pi/\varphi_2)^2 \quad \text{or} \quad (B_1/B_2)^2 < (d_2/r_2)(\pi/\varphi_2)^2 \,. \tag{3.30}$$

Now we minimize S with respect to X to show that these two modes are actually the worst modes [6].

By defining ζ

$$\zeta = \int_0^\chi J B^2 \,\mathrm{d}\chi \,, \tag{3.31}$$

S is given by

$$S = \oint \left\{ \left(\frac{\partial X}{\partial \zeta} \right)^2 + \frac{p' D}{B^2} X^2 \right\} \mathrm{d}\zeta \,. \tag{3.32}$$

With the normalization

$$H = \oint X^2 \mathrm{d}\zeta = 1 \,, \tag{3.33}$$

we obtain Euler's equation of (3.32)

$$\partial^2 X/\partial \zeta^2 + [\Lambda - p' D/B^2] X = 0 \,, \tag{3.34}$$

where $\Lambda = S/H$.

Since all the coefficients are periodic in ζ, this is Hill's equation and the solution is given by

$$X = \exp[i\sigma\zeta] g(\zeta) + \exp[-i\sigma\zeta] g^*(\zeta) \,, \tag{3.35}$$

where $g(\zeta)$ and $g^*(\zeta)$ are periodic functions and σ is the characteristic exponent.

Then the stability condition is that, if the lowest of the eigenvalues, Λ, of eq. (3.34) which gives the periodic solution is positive, the plasma is stable. This condition may be calculated by finding the characteristic exponent of the equation

$$\partial^2 X/\partial \zeta^2 - (p' D/B^2) X = 0 \,. \tag{3.36}$$

The characteristic exponent of this equation is either real or imaginary, depending on the quantities $-p' D/B^2$ and $-p' D/B^2 - (-p' D/B^2)$ as shown in Fig. 1. It is apparent that, if eq. (3.36) is in the region on the left side of

curve I, the eigenvalues S of eq. (3.34) are all positive. By using the smooth approximation (7), the curve I is given approximately by

$$\left\langle \left[\int \{ - p' D/B^2 - \langle p' D/B^2 \rangle \} \, \mathrm{d}\zeta \right]^2 \right\rangle = \langle p' D/B^2 \rangle \,, \tag{3.37}$$

where

$$p' D/B^2\rangle = \left[\oint (p' D/B^2) \, \mathrm{d}\zeta \right] \Big/ \oint \mathrm{d}\zeta \,.$$

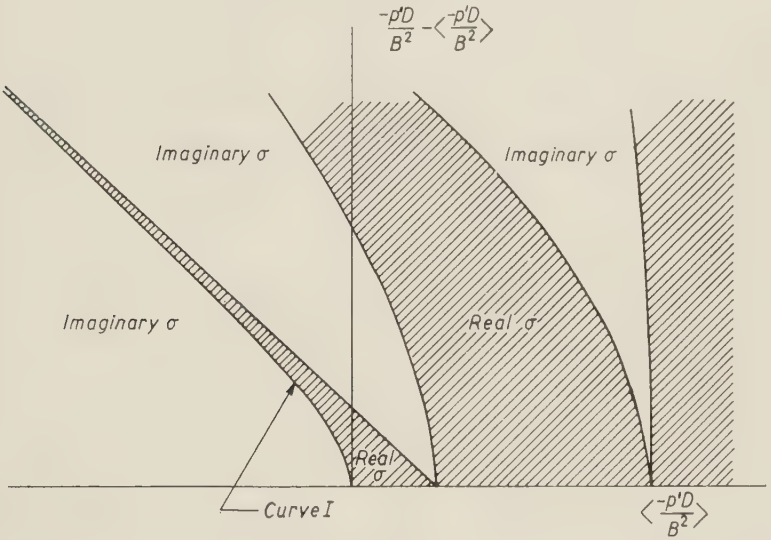

Fig. 4. – Regions of real and imaginary characteristic exponent for Hill's equation.

We shall calculate the stability criteria by dividing the flux lines into two sections and by assuming the flux lines consist of arcs in each section as before. Then the coefficient of eq. (3.36) is a constant in a section and it is convenient to use the matrix method to calculate the characteristic exponent (8).

For the case of Fig. 3, we obtain

$$\cos\sigma = \cosh \left| \frac{2p'r_1}{B_1} \right|^{\frac{1}{2}} \varphi_1 \cos \left| \frac{2p'r_2}{B_2} \right|^{\frac{1}{2}} \varphi_2 + \tag{3.38}$$

$$+ 1/2 \, (B_1^3 B_2^3 r_1 r_2)^{\frac{1}{2}} \left| \frac{1}{B_1^3 r_1} - \frac{1}{B_2^3 r_2} \right| \sinh \left| \frac{2p'r_1}{B_1} \right|^{\frac{1}{2}} \varphi_1 \sin \left| \frac{2p'r_2}{B_2} \right|^{\frac{1}{2}} \varphi_2 \,,$$

where the arc end effects have been neglected.

(7) K. R. Symon, D. W. Kerst, L. W. Jones, L. J. Laslett and K. M. Terwilliger: *Phys. Rev.*, **103**, 1837 (1956).

(8) D. K. Green and E. D. Courant: *Hand. d. Phys.*, vol. **44** (1959), p. 302.

For Λ to be positive σ for (3.36) must be imaginary, so the stability criterion is given by

$$|\cos\sigma| \geq 1 \tag{3.39}$$

with the condition that this represents the left side of the curve I.

Fig. 5 shows the schematic stability diagram. The operating point of a given configuration on the diagram is near the origin with a vanishingly small plasma pressure. As the pressure is increased, the point moves along a line away from the origin until it hits the stability limit as indicated in the diagram. Near the origin, $\cos\sigma$ is given approximately

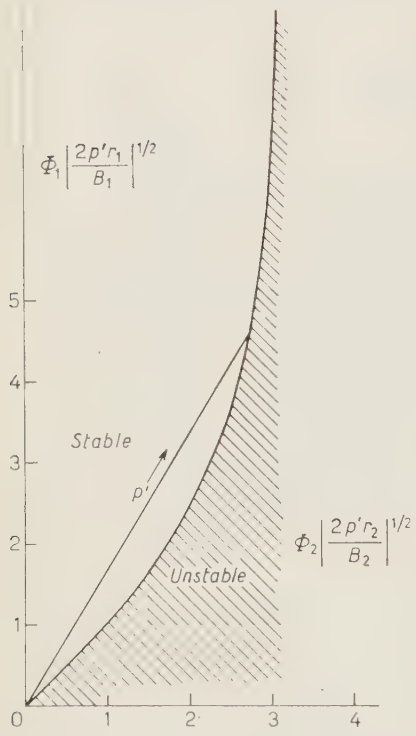

Fig. 5. – Stability diagram calculated from eq. (3.38).

$$\cos\sigma \approx 1 + \left(\frac{2|p'|}{B_1^2}\varphi_1 - \frac{2|p'|}{B_2^2}\varphi_2\right)(r_1\varphi_1 B_1 + r_2\varphi_2 B_2)\,, \tag{3.40}$$

and stability is obtained if

$$\varphi_1/B_1^2 - \varphi_2/B_2^2 > 0\,. \tag{3.41}$$

This is identical with eq. (3.22).

Further from the origin, the boundary line may be calculated approximately by assuming $B_2 \gg B_1$, giving

$$\mathrm{tg}\,|2p'r_2/B_2|^{\frac{1}{2}}\varphi_2 \approx -(B_1^3 r_2/B_2^3 r_1)^{\frac{1}{2}} \approx 0, \tag{3.42}$$

or simply

$$|2p'r_2/B_2|^{\frac{1}{2}}\varphi_2 \approx \pi\,. \tag{3.43}$$

This agrees with eq. (3.26) with stability when $|2p'r_2/B_2| < (\pi/\varphi_2)^2$.

When the flux lines have the straight part between two sections, $\cos\sigma$ is given by

$$\cos\sigma = \cos\sigma_0 + B_s\ell_s\left|\frac{2p'}{B_1^3 r_1}\right|^{\frac{1}{2}}\sinh\left|\frac{2p'r_1}{B_1}\right|^{\frac{1}{2}}\varphi_1\cos\left|\frac{2p'r_2}{B_2}\right|^{\frac{1}{2}}\varphi_2 - \tag{3.44}$$

$$-\left|\frac{2p'}{B_2^3 r_2}\right|^{\frac{1}{2}}\sin\left|\frac{2p'r_2}{B_2}\right|^{\frac{1}{2}}\varphi_2\cosh\left|\frac{2p'r_1}{B_1}\right|^{\frac{1}{2}}\varphi_1\Bigg|\,,$$

where B_s and ℓ_s are the magnetic field and the length of the straight part respectively, and $\cos\sigma_0$ is $\cos\sigma$ with $\ell_s = 0$.

The main effects of the straight section is to make the stable region a little smaller by displacing the boundary line near

$$\varphi_2 |2p' r_2/B_2|^{\frac{1}{2}} \approx \pi \quad \text{to the left} .$$

The plasma is sufficiently stable, if the conditions (3.24) and (3.30) are satisfied. It must be noted that the presence of the current carrying rod is essential for satisfying these conditions, and the required proportions of the structure necessary for stability are prescribed.

4. – Diffusion.

We shall assume diffusion across the field is very slow and use the simple formula given by SPITZER in terms of our orthogonal ψ and χ co-ordinates,

$$\left| \begin{array}{l} v_\psi = -(\eta/B^2)(\nabla p)_\psi , \\ \quad = -(\eta/B) p' . \end{array} \right. \tag{4.1}$$

This indicates the time to diffuse from one flux line to the next line is the same anywhere along the pair of flux lines, no matter what the distance is between the flux lines. In the steady state, the particle flux across the flux lines must be constant throughout the volume and we have

$$\oint n v_\psi J B \, \mathrm{d}\chi = \text{independent of } \psi , \tag{4.2}$$

where this integral is over the flux loop.

By using (4.1) in (4.2) and by assuming isothermal plasma, we obtain

$$(\mathrm{d}/\mathrm{d}\psi)(n^2[\psi])\, V(\psi) = \text{constant} < 0 , \tag{4.3}$$

where $V(\psi) = \int J \, \mathrm{d}\chi = \int \mathrm{d}s/B$ is the volume of a flux tube. To know the actual field and pressure distribution, we have to solve eq. (2.6) and eq. (4.3), simultaneously. However, eq. (4.3) tells us qualitatively what the pressure distribution may be. By differentiating (4.3), we have

$$(\mathrm{d}^2/\mathrm{d}\psi)(n^2) \propto (1/V^2)\, \mathrm{d}V/\mathrm{d}\psi . \tag{4.4}$$

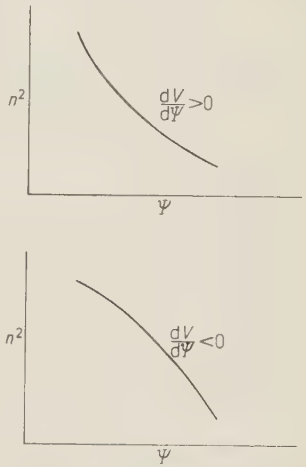

Fig. 6. - The distribution of particle density for different variations of the volume of a magnetic flux tube.

If $\mathrm{d}V/\mathrm{d}\psi > 0$, n^2 decreases slowly with ψ and if $\mathrm{d}V/\mathrm{d}\psi < 0$, n^2 decreases rapidly as shown in Fig. 6.

The total number of particles N in unit length in the z direction is given by

$$N = \int_0^{\psi_m} n(\psi t)\, V(\psi)\, \mathrm{d}\psi \,. \tag{4.5}$$

The decay of N due to the diffusion is given by (4.2)

$$\mathrm{d}N/\mathrm{d}t = -\eta kTn(\partial n/\partial\psi)V(\psi) = \text{independent of } \psi \,, \tag{4.6}$$

where $\int J\,\mathrm{d}\chi = V(\psi)$.
From eq. (4.5), eq. (4.6) becomes

$$\mathrm{d}/\mathrm{d}t \int_0^{\psi_m} \mathrm{d}\psi/(\mathrm{d}n/\mathrm{d}\psi) = -\eta kT \,. \tag{4.7}$$

Then using $\mathrm{d}n/\mathrm{d}\psi \sim n/\psi$ the containment time τ is given approximately by

$$\tau \approx (\psi_m)^2/\eta P_0 \,, \tag{4.8}$$

where ψ_m is half of the magnetic flux around the rod and p_0 is the maximum plasma pressure. This simple relation we see is generally true for containment time for various field shapes without B_z. By using

$$P_0 \approx B_1^2/2 \,, \tag{4.9}$$

$$\psi_m \approx B_2 d \,, \tag{4.10}$$

where B_2 and B_1 are the field around the rod and the minimum field along a flux line respectively and $2d$ is the distance between the rod and the wall we obtain

$$\left\{ \begin{array}{l} \tau = (2/\eta)\, \mathrm{d}^2 B_2^2/B_1^2 \\ \text{or} \\ \tau = 10^{-7}\, T\ (\mathrm{eV})^{\frac{3}{2}}\, \mathrm{d}^2 (B_2^2/B_1^2) \,. \end{array} \right. \tag{4.11}$$

As example take $T = 10^5$ eV, $2d = 10$ cm, $(B_2/B_1)^2 = 10$, which gives $\tau = 700$ s; and for $T = 100$ eV, $2d = 2$ cm, $(B_2/B_1)^2 = 10$, $\tau = 10^{-3}$ s. These times are conveniently long.

5. – Low-density plasma.

We shall consider the multipole configuration as a confining field for a low-density plasma where collisions are not frequent.

Since the magnetic field near the center is small, we assume that the electrons and the ions may move freely and the velocity distributions are spherically symmetric. As they move outwards, they will be trapped by the flux lines and will be reflected back towards the central region by the mirror action.

We shall estimate the density and the pressure in the strong field region.

The change of the distribution function along a flux line is to be considered. Since the orbital magnetic moment μ is an adiabatic invariant of the motion, the steady state distribution function is only a function of $\mu = m(v^2 - v_\parallel^2)/2B(s)$,

$$f(v, v_\parallel, s) = f\big(v, m(v^2 - v_\parallel^2)/B(s)\big)\,, \tag{5.1}$$

where s is taken along the flux line, and v is the velocity of the particle and is considered constant. Then the density and the pressure are given by

$$n(s) = \int f\big(m(v^2 - v_\parallel^2)/B(s)\big)\,\mathrm{d}v_\parallel\,, \tag{5.2}$$

$$p_{\left\{\begin{smallmatrix}\parallel\\ \perp\end{smallmatrix}\right\}}(s) = \int f[m(v^2 - v_\parallel^2)/B(s)] \left\{\begin{smallmatrix} v_\parallel^2 \\ v^2 - v_\parallel^2 \end{smallmatrix}\right\} \mathrm{d}v_\parallel\,. \tag{5.3}$$

From (5.2) and (5.3) one can easily show that, if the distribution function f is symmetric in velocity space at s_1, f is also symmetric at s provided that $B(s) > B(s_1)$. Therefore, the density and the pressure are constant along the flux line if $B(s) > B(s_1)$. The stronger field region is in equilibrium with the central region and the transport of the particles between two regions is unlikely to have the selective effects on the distribution function if the number of particles is sufficiently large. Hence the density and the pressure are constant along the flux lines. Physically the interpretation is that the number of particles along a flux line decreases towards the stronger field region due to the mirror reflection but the volume of the flux tube decreases at the same rate to keep the density constant.

If the density and the pressure are constant along the flux lines, the hydromagnetic approximation ought to be good and the results obtained in Sect. 2 and 3 may be applied. In addition, the instabilities due to non-isotropic velocity distributions are avoided.

6. – Some practical considerations.

Of the many practical problems associated with the use of a multipole field for plasma storage the very objectional feature of having conductors close to and surrounded by plasma is probably the worst. Without going into the possibilities for terminating linear multipoles or for inducing currents in free but stably magnetically suspended rods in toroidal multipoles it is worth-while to point out that the very simple method of introducing supports for the current-carrying rods in a toroidal multipole results in a useful structure. The plasma flows to these supports with thermal velocity thus gradually draining the plasma away, but confinement times sufficiently long to be of interest are nevertheless possible.

To show this we calculate the time for N particles with ion velocity $v_{TH}/\sqrt{3}$ to be intercepted by a support of width W, with one support in a distance L, along the rod of a multipole of order $2m$. Then the volume drained by one support is $v = \pi R^2 L/(2m)$. The rate of loss to the support is

$$\mathrm{d}N/\mathrm{d}t = 2m v_{TH} W d/\sqrt{3}$$

and the loss time is

$$\tau_L \simeq \sqrt{3}\,\pi R^2 L \cdot 10^{-6}/(4m W \mathrm{d} T_i^{\frac{1}{2}}\ \mathrm{eV})\,.$$

R is the radius of the multipole structure.

If we note that the rod radius $r = R/(2m)$ and take $d/r \equiv \Gamma_1$, a geometrical proportion factor, and $L/W \equiv \Gamma_2$ as the ratio of support separation to support width,

$$\tau_L = 5.5 \cdot 10^{-6}(\Gamma_2/\Gamma_1)(mr/T_i^{\frac{1}{2}}\ \mathrm{eV}) = 3 \cdot 10^{-6}(\Gamma_2/\Gamma_1)(R/T^{\frac{1}{2}}) \tag{6.1}$$

with

$$\Gamma_1 = \tfrac{1}{5}\,, \qquad \Gamma_2 = 500\,, \qquad m = 10\,, \qquad r = 5\ \mathrm{cm}\,, \qquad T_{\mathrm{ions}} = 10^4\ \mathrm{eV}\,,$$

we find $\tau_L = 7.0 \cdot 10^{-3}$ s which is sufficiently long to be interesting in spite of the primitive nature of the supports which can be modified and guarded for the better in a variety of ways.

* * *

We are grateful to many members of the thermonuclear group, particularly to T. H. JENSEN, M. ROSENBLUTH, and F. R. SCOTT, for stimulating discussions during the development of this topic.

RIASSUNTO (*)

Un metodo per eliminare le perdite di plasma connettendo le cuspidi con un ponte formato dal campo magnetico è stato descritto da TUCK (4). Qui discutiamo una configurazione multipolare, facendo uso di quell'idea, ma senza campo periferico (B_z). Il plasma di β elevato è confinato senza superficie libera di plasma nel senso usuale del modello a cuspidi. Il diagramma di stabilità di tali configurazioni può essere ottenuto prendendo come parametro la pressione del plasma. In genere questa condizione per la struttura può essere formulata come $(B_2/B_1)^2 > r/d$, in cui r è il raggio delle sbarrette che portano la corrente che produce il campo multipolare, $2d$ è la distanza fra una sbarretta e la parete conduttrice (ampiezza del ponte), e B_2 e B_1 sono i campi massimo e minimo lungo la superficie della parete. Si tiene conto delle approssimazioni risultanti dalla trattazione magnetoidrodinamica. Si fa menzione di alcune questioni pratiche e si dimostra che in un caso campione ci si aspetta un tempo di confinamento di $\sim 10^{-2}$ s per una temperatura del plasma di 10^4 eV.

(*) *Traduzione a cura della Redazione.*

Primary Cosmic Radiation and Extensive Air Showers.

B. Peters

Institute for Theoretical Physics, University of Copenhagen - Copenhagen

(ricevuto il 19 Agosto 1961)

Summary. — The hypothesis, that separate sources of cosmic ray particles of widely differing strength predominate in different energy regions, has been examined. In particular the following questions are discussed: Can such separate sources dominate neighbouring energy intervals of the primary particle spectrum without introducing appreciable changes in slope or discontinuities in the size-frequency distribution of air showers? Can such separate contributions, if they exist, nevertheless be distinguished experimentally with existing techniques? Do available data on extensive air showers provide evidence for or against the hypothesis? It appears that, if such separate sources existed and even if they differed in strength by factors as large as thousand, no significant departure from smoothness in the size-frequency relation of air showers would occur, provided only that all chemical components in the primary radiation have identical spectra when expressed in terms of the magnetic rigidity of the particles or energy per nucleon, and provided further that the chemical composition of the accelerated particle beam does not deviate too radically from its composition at lower energies. While under these conditions even an infinitly sharp cut-off in rigidity of the particles supplied by the stronger of the contributing sources will not produce a significant disturbance in the size frequency spectrum of air showers, it will nevertheless produce discontinuities and irregularities in the dependence of certain other shower parameters on shower size.—Irregularities which so far have found no adequate plausible explanation have been reported by various investigators at a shower size corresponding to a primary energy of about 10^{15} eV. Each of these observations seems to support the hypothesis that a rather sharp rigidity cut-off occurs in the source which supplies most cosmic ray particles below this energy. Additional measurable irregularities can be predicted which have, however, not yet been discovered.—The considerations leading to this hypothesis emphasize the important role which the complexity of the chemical composition of primary cosmic radiation must play in the interpretation of air shower phenomena. In view of the resulting complexity in the origin of showers of a given size, it is suggested that a classification of

air showers according to the maximum energy of the nuclear-active particles in the axis may be more relevant to an understanding of the various underlying nuclear and electromagnetic processes than the customary classification on which is based the total number of shower particles.

1. – Introduction.

One of the most remarkable features of cosmic radiation is presented by the apparently smooth and uniform variation of particle number with energy over a very large energy range. This fact is usually expressed by the statement that a power law with an almost constant exponent represents the energy distribution adequately over nine or even ten orders of magnitude.

This is not easy to understand. If it were strictly true, it would seem to lead to either of the following conclusions about the sources which contribute cosmic ray particles observed in our neighbourhood:

a) One single source dominates all others and gives rise to particles whose energy follows a power spectrum over the entire energy range.

b) Several or many sources contribute comparable amounts over the major portion of this energy range. In that case the sources must have precisely the same energy spectra for their contributions to be comparable both at the high and at the low energy end.

c) The bulk of the particles in different and restricted energy intervals is contributed by different sets of sources. In that case the aggregate strength of the various sets must be very accurately adjusted in order to insure that the number of cosmic ray particles decreases smoothly with a power of the energy over many orders of magnitude.

A theory of the origin of cosmic radiation like that proposed by FERMI, in which particles are accelerated throughout galactic space, corresponds essentially to case *a*) and smoothness and uniformity in the energy spectrum could be expected. However, this particular feature of Fermi's theory, namely acceleration throughout the galactic volume, has generally been abandoned after the composition of the primary radiation and the physical conditions in the interstellar space had become better known.

If one accepts instead the hypothesis that a substantial fraction of cosmic rays originate in or near some specific stellar object, as f.i. Novae or Supernovae, then one approaches case *b*) or *c*). It would be surprising if these various sources contributed nuclei with the same energy spectra, the more so since historic supernovae which have been identified, like the *Crab* and *Cassiopeia*, A,

have different radio spectra and therefore are known to contain relativistic electrons whose energy distributions are quite different from each other.

In the third case, *c*), a nearly perfect correlation must exist over a very wide range between the number and strength of accelerators and the particle energy at which their main output occurs.

It is difficult to believe that either condition *b*) or *c*) could be satisfied with great accuracy over the entire range of observable cosmic ray energies. Thus, if careful examination of the intensity of the cosmic radiation as a function of energy should reveal no significant localized departures from a power law, it would seem difficult to avoid the conclusion that case *a*) prevails, namely that a single source of particles dominates the cosmic ray flux in our time and our region of space.

But before such a conclusion can be accepted, it is of great importance to establish whether or not there is any indication in the primary spectrum which points towards contributions from several different sources. It has generally been argued that the absence of marked discontinuities in the particle flux in the latitude-sensitive energy region and in the air shower region provides strong evidence against the presence of distinct, recognizable primary cosmic ray sources dominating different parts of the spectrum. This argument would be valid if cosmic radiation consisted of one kind of particles only, f.i. of protons only. If a complex radiation like that which arrives at the earth were subject to a cut-off, and another, much weaker source contributed the bulk of particles above this cut-off, the differential size-frequency spectrum of air showers f.i. would not show any gap; for the cut-off would occur at a critical *magnetic rigidity*; the *energy* at which the cut-off takes place will then be higher, the higher the atomic weight of the primary nuclei. Thus a cut-off in a complex spectrum can never be sharp as long as the quantities observed are functions of primary energy. The energy region in the primary spectrum which is affected by such a cut-off in rigidity will extend over at least a factor thirty, *i.e.* the energy ratio between iron nuclei and protons which have equal radii of curvature in interstellar magnetic fields. A factor thirty in energy corresponds to a factor of order 5000 in intensity. Another, much weaker source could therefore cut in, in such a way that the differential size-frequency spectrum for air showers does not exhibit a break, but only a discontinuity in slope, while the integral size-frequency spectrum remains almost smooth.

Nevertheless, one predicts very marked observable effects, when the primary radiation, coming from a source which dominates observations at lower energy, approaches such a critical magnetic rigidity. Such observable effects are discussed in this paper. There seems to be considerable, though not yet conclusive, experimental evidence in favour of at least one break in the primary spectrum, namely at a magnetic rigidity corresponding to that of protons with about 10^{15} eV.

2. – Observable effects produced by a primary rigidity cut-off.

In order to exhibit clearly the particular effects which a sharp cut-off in magnetic rigidity of primary particles will have on observable quantities in the air shower region, we approximate the charge composition of the primary radiation by a somewhat smoothed-out dependence of flux on a power of the atomic weight A in the range $A_{\mathrm{He}} < A < A_{\mathrm{Fe}}$. (A representation of the charge spectrum, which throughout varies inversely as the cube of the mass number A, gives a good approximation to the actual composition in the emulsion region (which extends up to about 10^{14} eV), as long as one is not interested in the finer details of the distribution of elements but only in the relative intensity of groups of elements.) (*)

The differential number spectrum of primary particles $n(\varepsilon, A)\,\mathrm{d}\varepsilon\,\mathrm{d}A$ can be written

$$(1)\qquad \begin{cases} n(\varepsilon, A) = \dfrac{F_0}{A^{\sigma+1}\varepsilon^{\gamma+1}}, & \text{for } A_{\mathrm{H}} \leqslant A \leqslant A_{\mathrm{Fe}} \text{ and } \varepsilon < \varepsilon_c, \\ = 0, & \text{for } \varepsilon > \varepsilon_c, \end{cases}$$

where F_0 is some constant.

A more accurate representation must take into account that presumably deuterium and ^{3}He, just as Li, Be, and B are rare in the primary radiation and also that the cut-off energy per nucleon is twice as high for protons as for the other elements. With these refinements,

$$(1')\qquad n(\varepsilon, A) = \frac{F_0}{\varepsilon^{\gamma+1}} \begin{cases} \dfrac{r_{\mathrm{H}}}{A_{\mathrm{H}}^{\sigma}}\,\delta_{A,1} + \dfrac{r_{\mathrm{He}}}{A_{\mathrm{He}}^{\sigma}}\,\delta_{A,4} + \dfrac{W}{A^{\sigma+1}}, & \text{for } \varepsilon < \varepsilon_c, \\ \dfrac{r_{\mathrm{H}}^{0}}{A_A^{\sigma}}\,\delta_{A,1}, & \text{for } \varepsilon_c < \varepsilon < 2\varepsilon_c, \\ 0 & \text{for } \varepsilon > 2\varepsilon_c. \end{cases}$$

Here δ is the Kronecker symbol, and

$$W = \begin{cases} 1, & \text{for } A_{\mathrm{C}} \leqslant A \leqslant A_{\mathrm{Fe}}, \\ 0, & \text{otherwise}. \end{cases}$$

r_{H} and r_{He} have the numerical values 0.47 and 0.45, respectively, and are related to the fraction of protons and α-particles in the primary beam at constant energy per nucleon, by

$$\sigma r_{\mathrm{H}}\, A_{\mathrm{H}}^{-\sigma} = A_{\mathrm{H}}^{-\sigma} - A_{\mathrm{He}}^{-\sigma} \approx \tfrac{15}{16}$$

$$\sigma r_{\mathrm{He}}\, A_{\mathrm{He}}^{-\sigma} = A_{\mathrm{He}}^{-\sigma} - A_{\mathrm{C}}^{-\sigma} \approx \tfrac{1}{18}.$$

(*) See Appendix.

In order to transform the primary spectrum into a size-frequency spectrum for air showers, one usually expresses the total number N of shower particles on the earth's surface in terms of the energy and mass of the primary by

$$N = \nu A \varepsilon^{\alpha}, \tag{2}$$

where ν, α are constants.

The size-frequency spectrum is obtained by inserting the value of ε from eq. (2) into eq. (1) or (1′) and integrating over the allowed range in mass numbers A. One obtains

$$n_{\sigma,\gamma}(N) = \frac{F_0}{A_{\mathrm{Fe}}^{\sigma} \varepsilon_c^{\gamma}} \frac{1}{\alpha N_M} \left(\frac{N_M}{N}\right)^{(\gamma/\alpha)+1} P_{\sigma,\gamma}, \tag{3}$$

where $N_M = A_{\mathrm{Fe}} N_1 = \nu A_{\mathrm{Fe}} \varepsilon_c$.

Depending on whether one uses the primary spectra of eq. (1) or (1′) one obtains (using the symbol $p = \sigma - (\gamma/\alpha)$)

$$P_{\sigma,\gamma} = \frac{1}{p} \begin{cases} [A_{\mathrm{Fe}}^{p} - 1], & \text{for } N \leqslant N_1, \\ \left| \left(\frac{N_M}{N}\right)^{p} - 1 \right|, & \text{for } N_1 \leqslant N \leqslant N_M, \end{cases} \tag{3a}$$

or

$$P_{\sigma,\gamma} = \begin{cases} A_{\mathrm{Fe}}^{\sigma} \left| \frac{r_{\mathrm{H}}}{A_{\mathrm{H}}^{\sigma}} \left(\frac{A_{\mathrm{H}}}{A_{\mathrm{Fe}}}\right)^{\gamma/\alpha} + \frac{r_{\mathrm{He}}}{A_{\mathrm{He}}^{\sigma}} \left(\frac{A_{\mathrm{Fe}}}{A_{\mathrm{He}}}\right)^{\gamma/\alpha} \right| + \frac{1}{p} \left| \left(\frac{A_{\mathrm{Fe}}}{A_{\mathrm{C}}}\right)^{p} - 1 \right|, & \text{for } N < N_c, \\ A_{\mathrm{Fe}}^{\sigma} \left| \frac{r_{\mathrm{H}}}{A_{\mathrm{He}}^{\sigma}} \left(\frac{A_{\mathrm{He}}}{A_{\mathrm{Fe}}}\right)^{\gamma/\alpha} \right| + \frac{1}{p} \left| \left(\frac{A_{\mathrm{Fe}}}{A_{\mathrm{C}}}\right)^{p} - 1 \right|, & \text{for } N_c < N < A_{\mathrm{He}} N_1, \\ \frac{1}{p} \left| \left(\frac{A_{\mathrm{Fe}}}{A_{\mathrm{C}}}\right)^{p} - 1 \right|, & \text{for } A_{\mathrm{He}} N_1 < N < A_{\mathrm{C}} N_1, \\ \frac{1}{p} \left| \left(\frac{N_M}{N}\right)^{p} - 1 \right|, & \text{for } A_{\mathrm{C}} N_1 < N < N_M. \end{cases} \tag{3b}$$

Here $N_c = \nu (2\varepsilon_c)^{\alpha}$ represents the cut-off shower size for protons.

The average value $\langle F(N) \rangle$ of an observable quantity, F, which depends on the energy per nucleon ε and the number A of nucleons composing the primary particle, as

$$F = A f(\varepsilon)$$

is given by

$$\langle F \rangle = \frac{\int A f(\varepsilon) (\mathrm{d}\varepsilon/\mathrm{d}N)_A \, n(\varepsilon, A) \, \mathrm{d}A}{\int (\mathrm{d}\varepsilon/\mathrm{d}N)_A \, n(\varepsilon, A) \, \mathrm{d}A}.$$

If one approximates F by

$$F = A\varepsilon^{\beta}, \tag{4}$$

one finds

$$\langle F \rangle = \frac{n_{\sigma-1,\gamma-\beta}}{n_{\sigma,\gamma}} = A_{\mathrm{Fe}}\varepsilon_c^{\beta}\left(\frac{N}{N_M}\right)^{\beta/\alpha}\frac{P_{\sigma-1;\gamma-\beta}}{P_{\sigma,\gamma}}. \tag{5}$$

Observables of the type F which, for a given energy per nucleon, depend *linearly* on the number of nucleons composing the primary particle, are for instance:

the number of secondary particles of a given type,
at a given altitude,
in a given energy interval,
at a given distance from the shower axis, or
making given angles with the shower axis.

The average value $\langle G(N) \rangle$ of an observable G, which is *independent* of the number of nucleons composing the primary particle and which can be approximated by

$$G = \varepsilon^{\beta} \tag{6}$$

is given by

$$G = \frac{n_{\sigma,\gamma-\beta}}{n_{\sigma,\gamma}} = \varepsilon_c^{\beta}\left(\frac{N}{N_M}\right)^{\beta/\alpha}\frac{P_{\sigma,\gamma-\beta}}{P_{\sigma,\gamma}}. \tag{7}$$

Observables of type G are f.i.:

shower age,
lateral distribution,
energy spectra of secondary particles,
intensity ratios between various types of secondary particles in different parts of the shower, etc.

The observables quantities represented by expressions of the type illustrated by eqs. (3), (5) or (7) exhibit a change in slope at the shower sizes corresponding to the cut-off value for protons ($N = N_c$) and for α-particles ($N = 4N_1$). The absence or rarity of deuterium and ^{3}He, and of Li, Be, and B, which is implicit in the assumed primary spectrum of eq. (1′), gives furthermore rise to small discontinuities at these values of shower size.

The differential shower-size spectrum based on a sharp cut-off in magnetic rigidity is shown in Fig. 1. The curve is drawn for an assumed exponent, γ, of the primary energy spectrum $\gamma = 1.65$. The exponent σ, which charac-

terizes the chemical distributions of elements in the primary cosmic radiation, has been taken as $\sigma = 2$, *i.e.* the value appropriate for energies up to

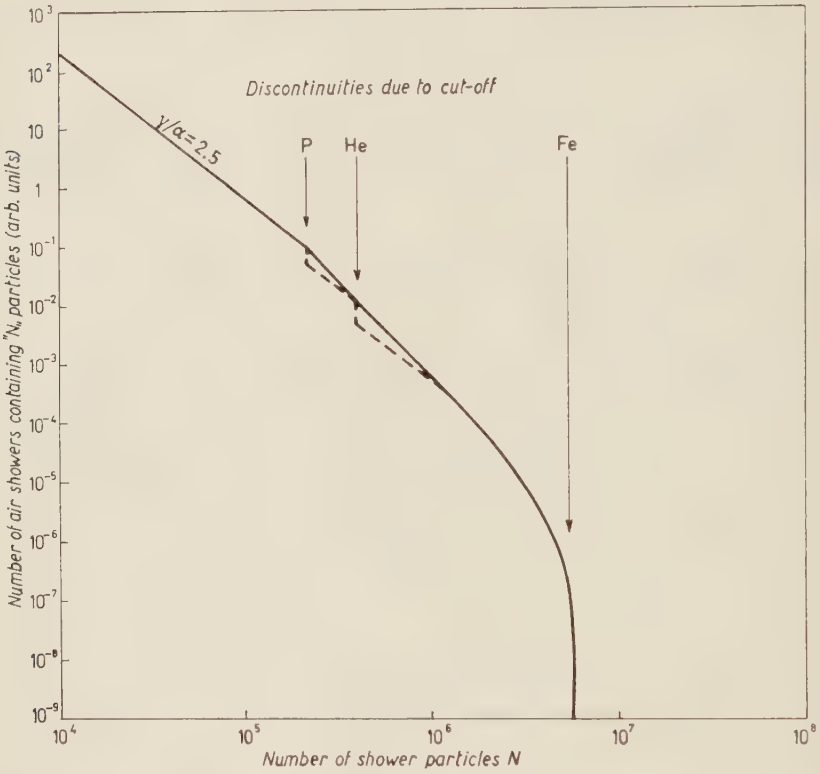

Fig. 1. – The curve represents the differential size distribution of air showers at mountain altitude in arbitrary units. This distribution results from a primary radiation which has: 1) the same chemical composition as that observed in nuclear emulsions; 2) an energy spectrum proportional to $E^{-\gamma}$ with $\gamma = 1.65$; 3) a sharp cut-off at a magnetic rigidity corresponding to protons with about 10^{15} eV. The discontinuities in the curve correspond to an assumed deficiency of ^{2}H, ^{3}He, Li, Be and B in the primary beam.

$\sim 10^{14}$ eV. The parameter α which characterizes the dependence of air-shower size on primary energy (eq. (2)) is usually assumed to lie between 1.0 and 1.2. In drawing Fig. 1, we have chosen $\alpha = 1.1$.

Fig. 2 shows the integral shower-size spectrum using the same parameters. It illustrates the fact that a *quite* smooth spectrum is obtained even in the extreme case when only two sources, differing by a factor 1000 in intensity, contribute to the particle flux and when the stronger of the two sources has an infinitely sharp cut-off at a particular magnetic rigidity.

Fig. 3 shows the behaviour of observables of type $\langle F \rangle$ and $\langle G \rangle$ as a function of shower size in the critical region. The curves are drawn for various values of the parameter β which characterizes the dependence of the observables on the energy of the incident nucleons and are based on the simpler of the two versions of the primary spectrum (eq. (1)).

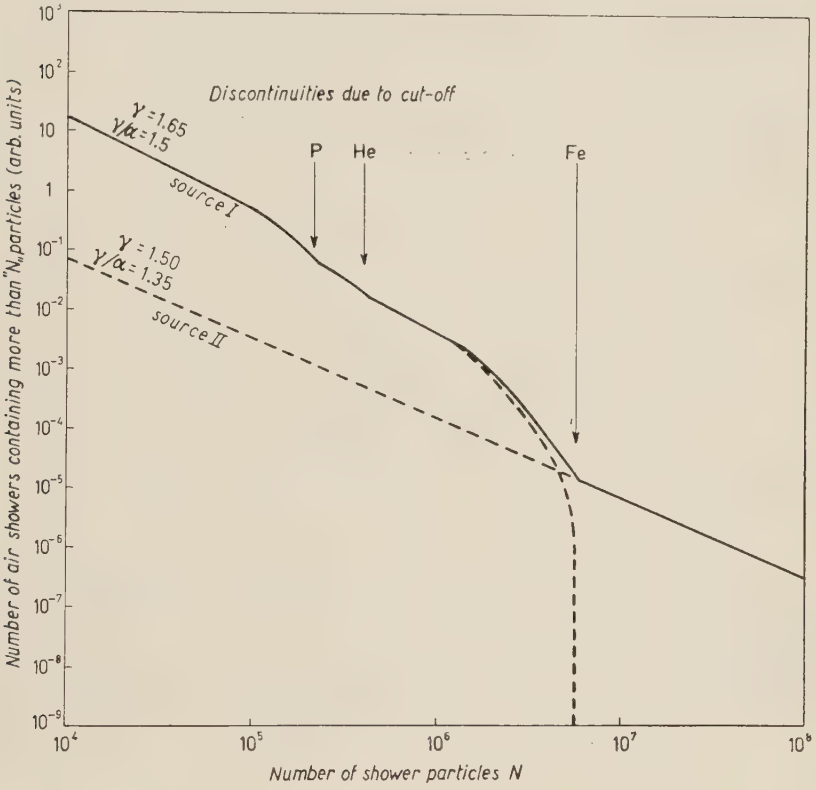

Fig. 2. – Curve I represents the integral size-frequency distribution of air showers, corresponding to the differential distribution of Fig. 1. Curve II represents the distribution contributed by a hypothetical and different source with the following properties: 1) an energy spectrum proportional to $E^{-\gamma}$ with $\gamma = 1.5$; 2) an energy output which is one thousand times smaller than that of source no. 1; 3) a cut-off which lies much higher than that of source no. 1. The solid line represents the combined effect of the two sources.

The most important conclusions which can be drawn from the curves and underlying considerations are the following:

a) Discontinuities in slope occur in the frequency of air showers and in the dependence on shower size of *all* observables of types F and G at the

same critical values of shower size. In the case of the logarithmic size-frequency shower curve the slope changes from $(\gamma/\alpha)+1 \approx 2.5$, which depends on the primary energy spectrum to $\sigma+1 \approx 3$ which is characteristic of the primary charge spectrum. The change in slope, therefore, is not very large.

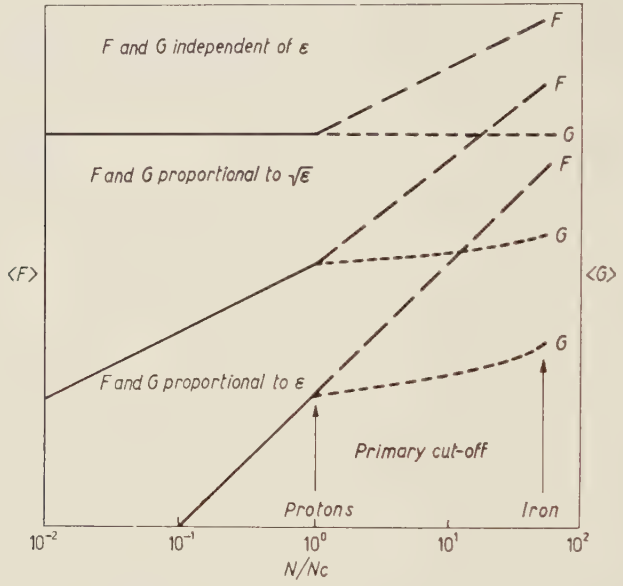

Fig. 3. – The variation of observable quantities of type F and G is shown as a function of the number of shower particles for various assumed dependences of these functions on the energy ε of primary nucleons. The curves show a break at the shower size at which a sharp magnetic rigidity cut-off in the primary spectrum begins to influence the nature of the showers. Dashed and dotted portions refer to variables of types F and G, respectively.

b) The behaviour of observables of types F and G above the critical region is well defined for a given dependence on shower size below the critical region.

c) Beyond the critical shower size, observables of types F and G behave quite differently from each other; differently from what one would predict if one assumed that both types of observables were simply functions of primary particle energy, without taking into account that they also depend in specific and distinct ways on the *mass* of the primary particle. Thus observables of type G *decrease* in their dependence on shower size and become essentially independent of shower size beyond the critical region, irrespective of whether they are slow or fast varying functions of the primary nucleon energy, while ob-

servables of type F *increase* in their dependence on shower size and tend to increase linearly or somewhat slowlier above the critical value (*).

d) Irregularities are introduced in the size dependence of shower properties by the gaps in the primary charge spectrum (*i.e.* the gap due to the presumably low abundance of deuterium and ^{3}He and the probably equally pronounced gap due to the low abundance of elements represented by the mass numbers $5 \leqslant A \leqslant 11$). For instance, the primaries responsible for showers with a particle number $N \geqslant N_c$ should, on the average, have a *lower* energy per nucleon than those responsible for showers of size $N \leqslant N_c$; the corresponding air showers should, therefore, show ar ather abrupt change in their absorption coefficient, zenith angle dependence, and barometric coefficient.

3. – Evidence for the existence of a rigidity cut-off in the primary spectrum.

The question arises now, whether experimental data support or contradict the existence of a critical air shower size beyond which

a) observables of type F become essentially proportional to shower size,
b) observables of type G become independent of shower size,
c) the absorption coefficient of the particles in the shower core shows a sudden increase,
d) the logarithmic differential size-frequency spectrum of showers suffers a (probably slight) change of slope.

If such discontinuities are observed and if they occur at the same shower size, they constitute a strong argument in favour of a sharp drop in the primary spectrum at the corresponding magnetic rigidity.

(*) The main features of this behaviour are easily derived if one simplifies eqs. (3), (5) and (7) with the help of the approximation $A_{\mathrm{Fe}} = 56 \gg 1$. One obtains

$$\left.\begin{aligned} n(N) &\sim N^{-((\gamma'/\alpha)+1)} \\ \langle F \rangle &\sim N^{\beta/\alpha} \\ \langle G \rangle &\sim N^{\beta/\alpha} \end{aligned}\right\} \quad \text{when } N \leqslant N_c$$

and

$$\left.\begin{aligned} n(N) &\sim N^{-(\sigma+1)} \\ \langle F \rangle &\sim N \\ \langle G \rangle &\sim \text{constant} \end{aligned}\right\} \quad \text{when } N > N_c \quad \text{and (if } \beta/\alpha > \tfrac{1}{2}\text{)}$$

Detailed measurements of the variation of quantities of types F and G with shower size have been carried out only during the last few years, mostly with the large air shower array in the Pamir mountains at a residual pressure of 650 g/cm².

3·1. *Observables of type F.* – The number of μ-mesons with energies above 1 GeV was found (1) to depend on shower size N as

$$n_\mu(>1\ \text{GeV}) \sim N^{0.62\pm0.12} \qquad \text{for } N < 4\cdot10^5 \text{ electrons}$$

and

$$n_\mu(>1\ \text{GeV}) \sim N^{0.95\pm0.05} \qquad \text{for } N > 4\cdot10^5 \text{ electrons.}$$

The number of nuclear-active particles with energies above 1 GeV was found (2) to depend on shower size N as

$$n_{N\cdot A.}(>1\ \text{GeV}) \sim N^{0.2}$$

$$n_{N\cdot A.}(>1\ \text{GeV}) \sim N\ .$$

Here also the discontinuity was placed at $N = 4\cdot10^5$ electrons. (See Fig. 4).

Both of these quantities are of course variables of type F, *i.e.*, for a given energy per nucleon of the primary, they must vary strictly proportional to the number of nucleons which constitute the pri-

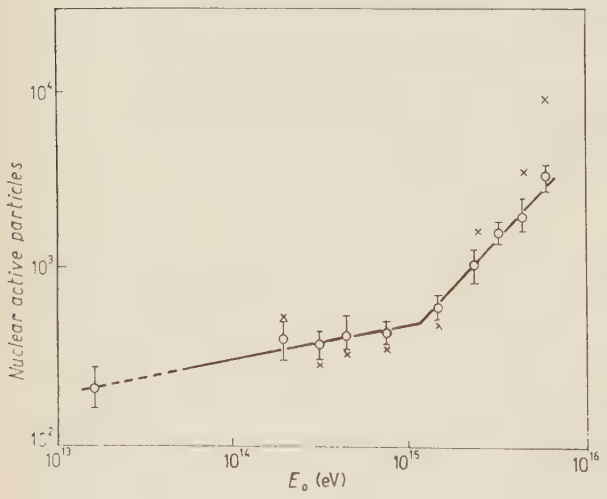

Fig. 4. – The number of nuclear-active particles, as given by Nikolskij *et al.* (4), as a function of shower size. The numbers on the abscissa represent primary energy in eV, obtained by multiplying the observed number of shower particles by $3\cdot10^9$.

(1) K. N. Vavilov, F. Estigneev and S. I. Nikolskij: *Žurn. Éksp. Teor. Fiz.*, **32**, 1319 (1957).

(2) S. I. Nikolskij, U. N. Vavilov and V. V. Batov: *Dokl. Akad. Nauk SSSR*, **111**, 71 (1956).

mary particle. They should, according to our model, become nearly proportional to N above the critical shower size N_c.

A special case of an observable of type F (when $\beta = 0$ in eq. (4)) is the atomic weight of primaries. The average atomic weight $\langle A \rangle$ of the primaries, responsible for air showers larger than N_c, should increase with N. If, as now seems likely, high energy nucleons lose only a minor fraction of their energy in meson producing collisions and always emerge as by far the most energetic product of the interaction, it follows that the number of very high energy nucleons in the shower core (at mountain altitude the energies should lie between 10^{12} and 10^{13} eV) constitute a measure of the atomic weight of the primary particle. From the transverse momenta which such nucleons transfer to π-mesons, one can estimate the scattering angles in inelastic collisions; one concludes that when the primary nucleons reach ground they should fall within a few square meters, if their energy ε_0 at the top of the atmosphere exceeded 10^{14} eV. In an apparatus of the type used by GRIGOROV *et al.* [3] and by NIKOLSKIJ and others [4], such primary nucleons shouldmani fest themselves as so-called « cores exhibiting structure ». Since, according to our hypothesis, the average atomic weight of primaries, $\langle A \rangle$, must increase proportional to N for $N > N_c$, we expect a strong increase in the probability of observing such « structure cores » when the shower size passes the critical value. Such a behaviour is for instance indicated by Table I, taken from a paper by NIKOLSKIJ *et al.* [4].

TABLE I.

Shower size N	Number of observations of at least one high energy nucleon in the shower axis	Number of cases where two or more nucleons are observed	
$1.5 \cdot 10^4$	7	2	
$2.9 \cdot 10^4$	10	3	
$5 \cdot 10^4$	8	2	$\approx 30\%$
$8 \cdot 10^4$	6	2	
$1.5 \cdot 10^5$	5	2	
$3.5 \cdot 10^5$	6	5	$\approx 85\%$
$5.8 \cdot 10^5$	1	1	

[3] N. L. GRIGOROV, V. IA. SHESTOPEROV, V. A. SOBINIAKOV and A. V. PODGURSKAIA: *Žurn. Èksp. Teor. Fiz.*, **33**, 1099 (1957).

[4] S. I. NIKOLSKIJ and A. A. POMANSKIJ: *Žurn. Èksp. Teor. Fiz.*, **35**, 618 (1958); and also O. DOVZKENKO, W. ZATSEPIN, E. MURZINA, S. NIKOLSKIJ, I. ROKOBOLSKAYA and E. TURKISH: *Dokl. Akad. Nauk SSSR*, **118**, 899 (1958).

The top curve for the observable of type F in Fig. 3 can be interpreted as representing $\langle A \rangle$, *i.e.* the average atomic weight of primaries responsible for an air shower, as a function of shower size. Below the critical region, for an air shower spectrum whose exponent $\gamma/\alpha = 1.5$, it has the value

$$\langle A \rangle \approx A_{\mathrm{Fe}} \frac{P_{\sigma-1,\gamma}}{P_{\sigma,\gamma}} = 7.5 \text{ or } 9.4$$

depending on whether one uses eq. (3*a*) or (3*b*). For larger showers, it increases towards the value $\langle A \rangle = A_{\mathrm{Fe}} = 56$.

The contribution of various groups of elements below the critical region can be easily calculated on the basis of the primary composition given in the Appendix, valid in the emulsion region which borders on, and even slightly overlaps, the air shower region. Assuming a value $\gamma/\alpha = 1.5$ the relative contributions are

$$\mathrm{H} = 49\,\%$$

$$\mathrm{He} = 24\,\%$$

$$\mathrm{C,\ N,\ O,\ F,} = 13\,\%$$

$$\mathrm{Ne,\ Mg,\ Si} = 7\,\%$$

$$\mathrm{Fe} = 7\,\%$$

3·2. *Observables of type G.* – We now turn to observables of type G, which according to this model should be independent of shower size in the interval $N_c \leqslant N < 56 N_1 \approx 30 N_c$, whatever their behaviour below $N = N_c$. There are many well-known experimental results which have a bearing on this question. Especially, the lateral distribution function and the shower age (variation of electron number with altitude) are known to be independent of shower size. Also the energy spectrum of μ-mesons is a quantity of type G and is independent of shower size ([5]).

However, more refined measurements are expected to show a somewhat more complicated behaviour of the average value of observables beyond N because of the large gaps in the chemical abundances between $A = 1$ and $A = 4$ and between $A = 4$ and $A = 12$. As we go to larger showers and pass the critical size N_c, where the proton contribution vanishes and the helium contribution becomes dominant, the energy per nucleon suddenly drops by a factor four from $2\varepsilon_c$ to $\frac{1}{2}\varepsilon_c$. By the time we reach $N = 4N_1$, it will have

([5]) O. I. Dovzhenko, B. A. Nelopo and S. I. Nikolskij: *Žurn. Èksp. Teor. Fiz.* **32**, 463 (1956).

partially recovered and have reached $\varepsilon = \varepsilon_c$. It will then drop again to $\varepsilon_c/3$. Once more it will recover and reach a value $\varepsilon = \varepsilon_c$ at $N = 12N_1$, etc.

On this picture, we expect that the high energy nucleons in the shower core should be harder, though less numerous, below N_c than they are above N_c and that therefore the absorption coefficient of particles in a shower core, when measured with thick absorbers, should show a sudden increase at the critical shower size N_c and then recover partially at $N = 12N_1 \approx 6N_c$.

Fig. 5 shows the result of measurements by NIKOLSKIJ and POMANSKIJ [4] on the absorption of air shower cores by 230 g cm^2 of aluminium and carbon absorber. The data have been interpreted by the authors as showing a significant increase in the absorption coefficient at $N \approx 2 \cdot 10^5$ followed by a partial recovery.

The discontinuity in absorption of shower cores as a function of air shower size should also reveal itself as a discontinuity in the barometric coefficient and the zenith angle distribution. Until those mutually related discontinuities have been detected, the observations of NIKOLSKIJ and POMANSKIJ, which constitute perhaps the strongest evidence to date for the existence of a magnetic rigidity cut-off, cannot yet be considered conclusive.

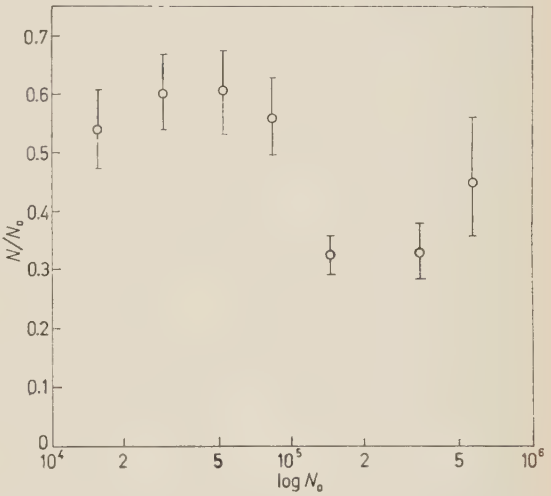

Fig. 5. – Results of NIKOLSKIJ *et al.* [4] showing the absorption of shower particles by 230 g/cm^2 of carbon plus aluminium as a function of shower size. The ordinate gives the ratio of particles below and above the absorber.

It seems, however, worth-while to point out that, if the interpretation given here is correct, such measurements, with only slightly better resolution, could lead to a determination of the relative abundance of elements among primaries in the energy range close to 10^{15} eV nucleon, *i.e.* an order of magnitude greater than obtainable with photographic emulsions.

One other effect which a hypothetical magnetic rigidity cut-off must produce on an observable of type G should be mentioned here.

A shower size between 2 and $4 \cdot 10^5$ at mountain altitude, where all these discontinuities seem to appear, corresponds approximately to a primary proton energy of $E_0 = 2\varepsilon_c \approx 10^{15}$ eV. Nucleons of such energy should arrive at 650 g/cm^2 with reduced energy E of order $E_0(1-\alpha)^{650/\lambda}$, where α is the fraction of energy transferred to mesons in each collision and λ the interaction

mean free path. If one uses $\lambda = 60$ g/cm^2 and $\alpha = 0.3$, one finds $E \approx 2 \cdot 10^{13}$ eV. One should then expect that, although the size of accompanying air showers keeps on increasing, the energy of nucleons in the shower core does not continue to increase when this value is reached. The flux of nuclei of energy larger than some value E, when plotted against the energy E, should show a decrease in the neighbourhood of $2 \cdot 10^{13}$ eV, whose sharpness will however be reduced by statistical fluctuations in the average number of inelastic atmospheric collisions.

Such a drop has been observed by MURZINA *et al.* [6] who measured the arrival rate of high energy nuclear-active particles (more than 80% of which occurred in air showers) as a function of energy. The drop seems to occur at $E = 1.5 \cdot 10^{13}$ eV.

3·3. *The size-frequency spectrum of air showers.* – Altogether, the experimental evidence regarding observables of types F and G seems to support the existence of a critical magnetic rigidity in the dominant part of the primary spectrum at a value which corresponds to a proton of energy 10^{15} eV and therefore to a value $\varepsilon_c = 5 \cdot 10^{14}$ eV. It is now necessary to discuss whether the observed size-frequency spectrum of air showers is in conflict with such a hypothesis.

At sea level the critical shower size corresponding to the assumed value of ε_c is about $N_c' = 7 \cdot 10^4$ electrons. The same peculiarities which have been observed at mountain altitude should have their counterpart at sea level at a somewhat smaller critical shower size. However, experimental data of sufficient accuracy are apparently not available.

If there was only one source of primary cosmic rays, then the sea level shower size spectrum should, for all practical purposes, terminate at a size

$$N_m = A_{\mathrm{Fe}} \frac{N_c'}{2^\alpha} \approx 1.8 \cdot 10^6 \text{ electrons} .$$

Evidently this is not the case. (See f.i. CLARK *et al.* [7]).

Let us, therefore, suppose that a second source exists which has the same or a slightly flatter energy spectrum than the first, characterized by an exponent γ', and which has a cut-off at a higher magnetic rigidity. Then, as illustrated in Fig. 2, no break in the differential shower size-frequency spectrum needs to occur, unless F_0', which is a measure of the intensity of this second source, is smaller than F_0 by a factor of the order of one thousand.

[6] E. MURZINA, S. I. NIKOLSKIJ and V. I. JAKOLEV: *Žurn. Èksp. Teor. Fiz.*, **35**, 1298 (1958).

[7] G. CLARK, J. EARL, W. KRAUSHAAR, J. LINSLEY, B. ROSSI and F. SCHERB: *Suppl. Nuovo Cimento*, **8**, 623 (1958).

Thus the differential shower size spectrum may well be continuous and only show a change of slope when there are different primary cosmic ray sources contributing to air showers in different size intervals. At the points corresponding to a cut-off, changes in the slope of the integral shower size spectrum could be quite small. The curves in Fig. 2 illustrate such a hypothetical situation.

KULIKOV and KHRISTIANSEN ([8]) have drawn attention to an apparent discontinuity in the slope of the integral size-frequency spectrum at sea level, which they place at $N = 8 \cdot 10^5$ electrons. It is, however, not clear as yet how this is connected with the various discontinuities observed at mountain altitude. Apart from the changes in slope of the size frequency distribution which should occur where the proton component of the dominant source cuts off and again in the region where the proton component of a new source becomes dominant, our hypothesis suggests that there should be a general tendency for the size frequency distribution of air showers to become flatter rather than steeper as the shower size increases. For, as long as we retain the existence of power laws as a characteristic feature of cosmic ray accelerators, the source which is unimportant at low energy but becomes dominant at high energy must have a flatter particle spectrum than the source which dominates at lower primary energy. Existing measurements on the air shower frequency spectrum do not contradict this conclusion; rather they seem to support it, although, within the as yet considerable statistical uncertainty, the observed flattening could well be spurious.

4. – Concluding remarks.

The hypothesis presented in this paper emphasizes the important role which the complexity of the primary cosmic radiation plays in the interpretation of air shower data.

Observations with nuclear emulsions show that at least those primaries which give rise to the smaller air showers ($N \lesssim 10^5$ particles) must be composed of comparable numbers of nuclei whose atomic weights (and therefore whose energy per nucleon) differ from each other by large factors. Since the average atomic weight of primaries contributing to the smaller showers ought to be close to $\langle A \rangle = 9.5$, it is clear that the traditional classification of air showers according to the total number of charged particles may not be the best suited one for comprehending the underlying basic nuclear and electromagnetic processes. The « normal » shower of size N is only in about half the cases produced by a nucleon of energy ε, and in about 7 % of the cases by 50 nucleons of energy $\varepsilon/50$. Thus one should expect, especially near the

([8]) G. V. KULIKOV and G. B. KHRISTIANSEN: *Žurn. Eksp. Teor. Fiz.*, **35**, 441 (1958).

core, large differences in the properties of showers of equal « size ». The interpretation of fluctuations of observables in showers of a given size in terms of fluctuations in fundamental processes seems hardly possible without taking this basic cause of fluctuations into account.

In order to arrive at a more natural classification of air showers one could start from the current picture that primary nucleons survive the meson producing collisions in the atmosphere and appear as the most energetic nuclear-active particles in the central area of the shower core. If this picture is correct, the nuclear-active particles within one meter from the shower axis could serve as a basis for classification. The events could then be classified according to the energy of the most energetic of these nuclear-active particles. This energy is presumably related to the *energy per nucleon* of the incident primary and determines all shower properties as well as the distribution of shower particles except for a scale factor. The *number* of nuclear-active particles of comparable energy close to the axis is presumably related to the atomic number of the incident primary and may furnish the scale factor.

Above energies of order 10^{14} to 10^{15} eV, nuclear emulsion data provide no guidance as to the nature of primaries. Certain measurements at mountain altitude show variations of shower properties with shower size which indicate an increasingly important role of heavy primaries in the energy region between 10^{15} and a few times 10^{16} eV. Such a preponderance of heavy nuclei could be interpreted as a magnetic rigidity cut-off in the source which contributes the bulk of primaries below 10^{15} eV. While experimental evidence in favour of this hypothesis is not yet conclusive, it appears to be fairly strong. There also seems to exist no difficulty in reconciling the hypothesis with all other observations on extensive air showers which have been reported so far.

* * *

An abbreviated version of this coork has been published in the *Proceedings of the Moscow Cosmic Ray Conference*, Vol. VIII, 157 (July 1960). [Considerations of a similar nature can also be found in the work of Ueda, *Progr. Theor. Phys.*, **24**, 1231 (1960)]. The complete article was not sent for publication, because many of the quoted experimental results were still controversial at that time. The author wants to express his gratitude to the members of the Air Shower Group of the Tata Institute of Fundamental Research, in particular to Dr. B. V. Sreekantan, Dr. S. Naranan and Mr. A. Subramanian who have pointed out to him that the salient features of the early experiments discussed in this paper are strongly supported by more recent and partially unpublished investigations. Publication of the manuscript seems, therefore, now appropriate. The author also would like to express his gratitude to Prof. H. J. Bhabha and Prof. M. G. K. Menon for the hospitality extended to him during his recent stay in Bombay.

Appendix

The composition and the energy distribution of the primary cosmic radiation in the mass interval

$$1 \leqslant A \leqslant 56 ,$$

and in the energy in interval from about $1.5A$ GeV to about 4500 GeV, is represented fairly accurately by

$$n(\varepsilon, A)\,\mathrm{d}\varepsilon\,\mathrm{d}A = \frac{F_0}{A^{\sigma+1}\varepsilon^{\gamma+1}}\,\mathrm{d}\varepsilon\,\mathrm{d}A ,$$

and the corresponding integral spectrum

$$\mathcal{N}_{A_1,A_2}(>\varepsilon) = \frac{F_0}{\gamma\sigma\varepsilon^{\gamma}}[A_1^{-\sigma} - A_2^{-\sigma}] , \tag{8}$$

Table II.

Energy per nucleon (GeV)	Group of elements	Particles/m² s sr		References
		calc.	obs.	
Texas $\varepsilon_H = 4.9$ $\lambda = 41°$, $\varepsilon_A = 2.6$	H	610	570 ± 50	McDonald [9]
	He	88.5	90 ± 9	
	C, N, O, F	7.1	7.5 ± 0.65	Appa Rao *et al.* [10]
	$Z \geqslant 10$	3.45	2.2 ± 0.35	
Guam $\varepsilon_H = 16.1$ $\lambda = 3°$, $\varepsilon_A = 8.3$	H	116	115 ± 12	McDonald [9]
	He	17.3	18 ± 2	
	C, N, O, F	1.38	0.93 ± .08	Jain *et al.* [11]
	$Z \geqslant 10$	0.68	0.36 ± .06	
$\varepsilon_H = 1600$ $\varepsilon_A = 1600$	H	0.19	0.29 ± 0.07	Lal [12]
	He	0.01	0.035 ± 0.025	
$\varepsilon_H = 4500$ $\varepsilon_A = 4500$	H	0.045	0.04 ± 0.015	Kaplon and Ritson [13]
	He	0.0026	~ 0.004	

[9] F. B. McDonald: *Phys. Rev.*, **109**, 1367 (1958).

[10] M. V. K. Appa Rao, S. Biswas, R. R. Daniel, K. A. Neelakantan and B. Peters: *Phys. Rev.*, **110**, 751 (1958).

[11] P. L. Jain, E. Lohrmann and M. W. Teucher: *Phys. Rev.* **115**, 654 (1959).

[12] D. Lal: *Proc. Ind. Acad. Sci.*, **38**, 93 (1953).

[13] M. F. Kaplon and D. M. Ritson: *Phys. Rev.*, **88**, 386 (1952).

where F_0 is a constant, and ε is the energy per nucleon including rest mass.

This formula does not actually reproduce the detailed chemical composition but gives a smoothed-out distribution of elements. However, it does represent the various mass groups correctly, provided one uses the following values for the constants:

$$F_0 = 1.7 \cdot 10^4 ,$$

$$\sigma = 2.0 ,$$

$$\gamma = 1.40 ,$$

and expresses ε in GeV and $\mathcal{N}$ in particles/m^2 s sr.

In Table II, flux values calculated with the help of eq. (8), are compared with measured values. (« H » in the Table stands for all elements with mass number $1 \leqslant A < 3$; « He » stands for all elements with mass numbers $4 < A < 11$ and includes therefore the elements Li, Be, and B. But hydrogen and helium are without doubt by far the dominant elements in their respective groups.)

The formula representing the spectrum must be slightly modified in the energy range which corresponds to air showers. The size frequency spectrum of air showers has an exponent which varies slowly with size. For showers of $N \approx 10^5$ electrons the exponent is $\gamma/\alpha \approx 1.5$, which probably corresponds to an exponent for the primary spectrum, $\gamma \approx 1.65$.

A very slowly increasing exponent of the form suggested by Cocconi [14] could probably represent the primary spectrum over the entire range of cosmic ray energies above $\sim 1.5A$ GeV adequately within the existing errors of measurement. This small dependence of exponent on energy has been neglected in this paper, since it does not affect the validity of the arguments.

The only data on chemical composition which are available in the energy range $10^3 < E < 10^{15}$ eV come from the observation of very large meson showers in nuclear emulsions. No accurate tabulation has been made; but roughly 50 % of the observed events are due to protons, and among the largest of the observed meson showers the very heavy primaries seem to be dominant.

([14]) G. Cocconi: *Suppl. Nuovo Cimento*, **8**, 560 (1958).

RIASSUNTO (*)

Si esamina l'ipotesi che sorgenti separate di particelle dei raggi cosmici di energie fortemente differenti predominino in differenti regioni di energia. In particolare si discutono le seguenti questioni: possono tali sorgenti separate essere predominanti in intervalli di energie dello spettro primario delle particelle adiacenti senza produrre variazioni apprezzabili della pendenza o discontinuità nella distribuzione grandezza-frequenza degli sciami atmosferici? Possono, tuttavia, tali contributi separati, se esistono, essere distinti sperimentalmente con le tecniche esistenti? I dati disponibili sugli sciami

(*) *Traduzione a cura della Redazione.*

estesi dell'aria forniscono prove a favore o contro tale ipotesi? Sembra che se tali sorgenti separate esistessero ed anche se differissero in energia per fattori fino a mille, non si dovrebbero avere scostamenti significativi dalla continuità della relazione grandezza-frequenza degli sciami dell'aria, purchè tutti gli elementi chimici componenti la radiazione primaria abbiano spettri identici se espressi in termini della rigidità magnetica delle particelle o di energia per nucleone, e purchè, inoltre, la composizione chimica del fascio di particelle accelerato non si scosti troppo radicalmente dalla sua composizione ad energie inferiori. Mentre in tali condizioni anche un taglio infinitamente netto della rigidità delle particelle derivanti dalla più forte delle sorgenti agenti non produrrà un'alterazione significativa nello spettro grandezza-frequenza degli sciami atmosferici, produrrà, tuttavia, discontinuità e irregolarità nella dipendenza di alcuni altri parametri dalla grandezza dello sciame. Da vari osservatori sono state riferite irregolarità per grandezze degli sciami corrispondenti a un'energia primaria di circa 10^{15} eV, che finora non hanno trovato una spiegazione adeguata. Ognuna di tali osservazioni sembra sostenere l'ipotesi che un taglio abbastanza netto avvenga nella sorgente che fornisce il massimo numero di particelle al disotto di tale energia. Si possono predire ulteriori irregolarità misurabili che, tuttavia, non sono ancora state osservate. Le considerazioni che conducono a questa ipotesi mettono in evidenza l'importanza che la complessità della composizione chimica della radiazione cosmica primaria deve avere nell'interpretazione dei fenomeni degli sciami atmosferici. In vista della complessità risultante dell'origine degli sciami di una data grandezza si pensa che una classificazione degli sciami dell'aria secondo la massima energia delle particelle nucleari-mente attive giacenti nell'asse sia più significativa per la comprensione dei vari processi nucleari ed elettromagnetici in atto, della consueta classificazione basata sul numero totale delle particelle dello sciame.

The Scattering of Positive 120 MeV Pions on Protons.

A. Loria, P. Mittner, R. Santangelo, I. Scotoni and G. Zago

Istituto di Fisica dell'Università - Padova
Istituto Nazionale di Fisica Nucleare - Sezione di Padova

B. Aubert, A. Brenner (*), Y. Goldschmidt-Clermont, F. Grard (**), G. R. MacLeod, A. Minguzzi Ranzi and L. Montanet

CERN - Genève

(ricevuto il 30 Agosto 1961)

Summary. — An investigation of the elastic scattering of 120 MeV positive pions by protons is described. The experiment was done by exposing a liquid propane chamber to the CERN 600 MeV synchro-cyclotron. The results refer to 5405 selected events in which the contamination from scattering on carbon nuclei is shown to be negligible. The values obtained for the phase-shifts are: $\alpha_{31} = -2.60° \pm 0.69°$, $\alpha_3 = -11.05° \pm 1.32°$, $\alpha_{33} = 31.67° \pm 1.01°$. The value of α_3 differs significantly from that expected if the linear dependence of α_3 on the momentum, which has been proposed by some authors, is assumed. The present result is discussed, particularly in connection with some recent theoretical developments.

Introduction.

Because of the current interest in the behaviour of the s-wave phase-shifts, the differential cross-section for the elastic scattering of positive 120 MeV kinetic energy pions by protons was measured by exposing the Padua propane chamber, without magnetic field, to the CERN 600 MeV synchro-cyclotron.

(*) Now at the Department of Physics, Harvard University, Cambridge, Mass.
(**) On leave of absence from the « Institut Interuniversitaire des Sciences Nucléaires ». Bruxelles.

A more detailed mimeographed report, giving special attention to the technical aspects of the work, has already appeared (1). The chamber and the auxiliary equipment used, including optics and timing circuits, have also been described (2).

Pions internally produced in the synchrocyclotron were used. The method of extraction is explained in detail by J. ASHKIN *et al.* (3). The general layout of the beam is shown in Fig. 1. The pions were first analysed and focussed by two bending magnets and then, after having been filtered by 2 cm of polythene in order to stop the protons, were collimated by means of a hole in a thick lead block. Monitoring was effected by two counters at either end of the hole. The bubble chamber was located at 80 cm distance from the second counter.

The energy was measured in the conventional manner, as shown in the insert of Fig. 2, by tracing differential range curves. One of these is reproduced in Fig. 2, and indicates a mean energy of 142 MeV, which was requested in order to have pions of 120 MeV in the middle of the chamber. The spread in beam energy was ± 2.5 MeV.

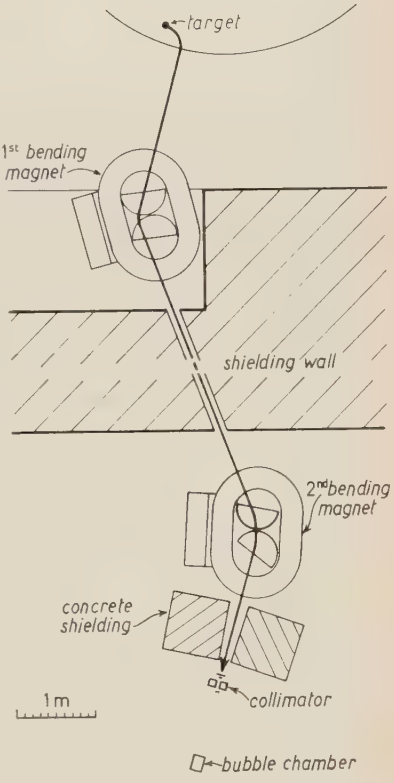

Fig. 1. – Layout of the pion beam.

Two exposures were effected. A suitable number of satisfactory tracks per picture, four on the average in the first and six in the second, was recorded by using the beam at the maximum available intensity. A photograph of some typical events, which consist of two-prong stars produced by beam tracks, is reproduced in Fig. 3.

During the first exposure, which took place in September 1958, 10 000 pictures were taken and the analysis was carried out at Padua. During the second, in April 1959, another 30 000 pictures were taken; 10 000 of these were also analysed by the Padua group, and 20 000 at Geneva by the CERN group. Preliminary results referring to the first exposure were quoted at the

(1) CERN 61-11 (1961).

(2) A. LORIA, P. MITTNER, I. SCOTONI and G. ZAGO: *Nuovo Cimento*, **11**, 718 (1959).

(3) J. ASHKIN, T. FAZZINI, G. FIDECARO, A. W. MERRISON, N. PAUL and A. V. TOLLESTRUP: *Nuovo Cimento*, **13**, 1240 (1959).

1959 Kiev Conference (4), and the Padua final results at the 1960 Rochester Conference (5).

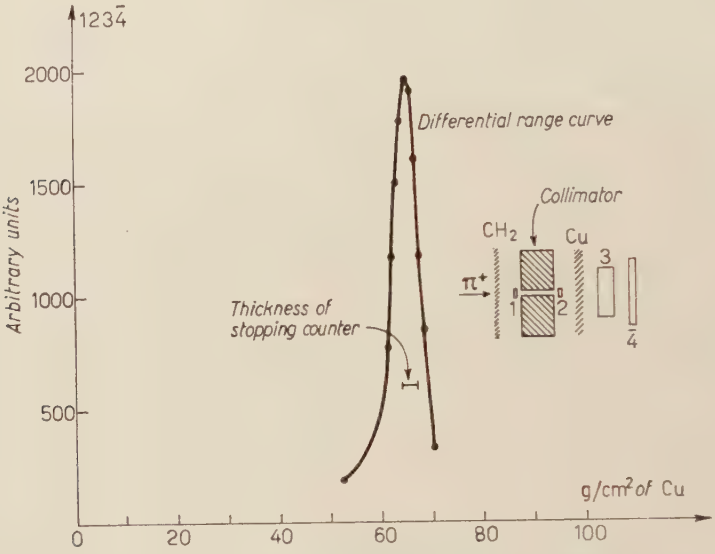

Fig. 2. – Differential range curve for a 142 MeV pion beam.

The events produced by the pions in the chamber are due to elastic collisions on hydrogen, and to collisions on carbon nuclei often leading to their disintegration. Most of the inelastic carbon events are recognizable immediately (many prongs) but some of them show two charged secondary particles with a configuration that cannot be directly distinguished by inspection from the pion-proton elastic scattering, but can be ascertained by measurements. The measurements performed on the events, and the subsequent analysis, must insure that the efficiency of detection of the events in the chamber and the separation of the carbon from the hydrogen collisions, leave systematic errors which are small with respect to the statistical ones. With a relatively large number of observed events, the analysis becomes therefore a crucial feature of the experiment. In the present paper, the experimental procedures are presented in Part I. Part II is a discussion of the results.

A list of abbreviations used throughout is given in Table I.

(4) B. PONTECORVO: *Proc. of the Ninth International Conference on High Energy Physics at Kiev* (1959), p. 100.

(5) A. LORIA, P. MITTNER, R. SANTANGELO, G. ZAGO, A. BRENNER, F. GRARD and L. MONTANET: *Proc. of the 1960 Annual International Conference on High Energy Physics at Rochester*, p. 188.

Fig. 3. – Photograph showing three typical scattering events.

TABLE I. – *List of abbreviations.*

x	coordinate perpendicular to y and z.
y	coordinate in the direction of the beam.
z	coordinate in the direction of the optical axes. The origin of the coordinates is the centre of the bubble chamber.
c.m.s.	the centre of mass system of reference; parameters referring to the c.m.s. are indicated by a star, *e.g.* θ^*.
π_i	the incident pion.
γ	the angle of π_i with the average direction of the beam.
π_s	the scattered pion.
p	the scattered proton.
p	momentum.
hydrogen event	the scattering of π_i by a free proton.
carbon event	the scattering of π_i by a proton of a carbon nucleus.
i, j, k	the unit vectors respectively of the π_i, π_s and p momenta.
θ_π	scattering angle of π_i: $\sin\theta_\pi = \lvert i\times j\rvert$.
θ_p	scattering angle of p: $\sin\theta_p = \lvert i\times k\rvert$.
c and d	deviation from coplanarity: $c = \cos\beta = (i\cdot j\times k)/(\lvert j\times k\rvert)$ CERN $d = \cos\alpha = (i\times j\cdot k)/(\lvert i\times j\rvert)$ Padua
φ	angle between the plane of π_i and π_s, and the glass windows.
θ'_p	angle between π_i and p, expected for the measured value of θ_π in the hypothesis of a 120 MeV hydrogen event.
Δ	$\theta'_p - \theta_p$.
σ_d	r.m.s. value of d.
σ_Δ	r.m.s. value of Δ.
σ	cross section.
Ω	solid angle.

PART I. – EXPERIMENTAL PROCEDURE

1. – Scanning criteria.

The pictures were examined using two projectors allowing the two stereoscopic views to be scanned side by side along the direction of the beam tracks. Pictures with more than 15 incident particles were disregarded, so as not to miss scattering close to 0 or 180°. Scanning was done by looking along all incident tracks for two-prong stars. Some of them could be excluded at the very first inspection from being hydrogen events because the transverse momentum was not conserved in at least one of the reprojections, or because the proton was scattered backwards in the laboratory system of reference. In addition, those interactions where the projection of γ was larger than 6° on one of the views were rejected, as well as any event where the incident particle underwent a scattering without visible recoil.

Further restrictions were placed on the initial selection of events by defining a fiducial volume in the central region of the chamber, and by choosing a lower limit for the accepted value of the pion scattering angle, as a too short proton range did not allow satisfactory measurements to be made. The choice of the volume and of the angle were made on the basis of exploratory work on samples of events in Padua, and by the systematic study of the distributions of the measured events at CERN. Table II indicates the limits chosen: they are practically almost identical for the two working groups as the interval of z includes, in both cases, all beam tracks.

TABLE II. – *Limits of acceptance of events.*

	Padua	CERN
x	$-5 \leqslant x \leqslant +5$ cm	$-5.1 \leqslant x \leqslant +5.1$ cm
y	$-6 \leqslant y \leqslant +6$ cm	$-6.1 \leqslant y \leqslant +7.0$ cm
z	$-2 \leqslant z \leqslant +2$ cm	$-3.3 \leqslant z \leqslant +3.0$ cm
c	see text	0.4
d	see text	—
Δ	see text	15°
θ_π	43°	40°
γ	see text	80°

Chamber dimensions: $14 \times 21 \times 7$ cm^3.

Some further events were rejected in the Padua analysis on the basis of quick estimates of kinematic relationships such as the coplanarity test mentioned by BASSI *et al.* (6).

In both cases, the films were scanned twice independently to estimate the scanning efficiency. For those events with $q < 60°$ and $\vartheta_\pi > 13°$ (proton range $\geqslant 5$ mm) it was found to be higher than 98%: it was higher than 95% for all events.

2. – Measurements and spatial reconstruction.

In Padua, a drawing was made from the two reprojected stereoscopic pictures, where, by shifting the paper, the images of the front fiducial marks of each view were brought into coincidence. Every track was approximated by eye with the « best » straight line, taking into account multiple scattering.

(6) P. BASSI, A. LORIA, J. A. MEYER, P. MITTNER and I. SCOTONI: *Nuovo Cimento*, 5, 1729 (1957).

It can be shown that, in the approximation in which straight lines in the chamber transform into straight lines in the pictures ([6]), the co-ordinates of points in space may be calculated, using simplified formulae, from measurements on the images ([7]). The geometric quantities useful in the description and in the analysis of the events were calculated by means of an electronic computer.

At CERN, measurements were made using two digitized instruments: the Digitized Protractor ([8]) and the IEP ([9]).

Reconstruction and kinematic analysis of the events were made using programs written for the CERN Mercury Computer ([10-12]). The reconstruction program calculated, for each co-ordinate of a measured point, an error determined by the method of least squares. Unfortunately this procedure could not be applied to the determination of track directions, as only two stereoscopic views were available for the reconstruction. Nevertheless, a set of repeated measurements on a series of selected tracks were used to estimate the precision of the digitized protractor. The standard deviations thus obtained were

x, y co-ordinates	0.3 mm
z co-ordinate	2.5 mm
Direction of tracks	1.2°
Coplanarity	0.03

The precision of IEP is superior to that of the digitized protractor, and we therefore used the IEP for the events which were intrinsically difficult to measure, and which therefore required the maximum available precision. These events were of two types: those where the recoil proton track was very short *i.e.* $\leqslant 5$ mm, and those where the pion was scattered at about 90° so that the image of its track lay nearly parallel to the x axis. For this second type we tried to measure on IEP the co-ordinates of corresponding points on the two views: some 90 cases were left at the end of the experiment as un-measurable since the quality of these photographs did not allow corres-

([7]) A. Loria: *Proc. of the Informal Meeting on Heavy Liquid Bubble Chambers*, CERN 59-24 (1959), p. 56.

([8]) G. R. Macleod: *Digitized protractors for the measurement of track chamber photographs*, CERN 60-14 (1960).

([9]) Y. Goldschmidt-Clermont: *Instruments for the analysis of track chamber photographs by digital computer*, CERN 58-4 (1958).

([10]) G. R. Macleod: *An input programme for measurements of track chamber photographs*, CERN 60-11 (1960).

([11]) G. R. Macleod: *Geometrical reconstruction of digitized protractor measurements*, CERN 60-12 (1960).

([12]) G. R. Macleod: *A kinematics programme for the analysis of pion-proton elastic scattering*, CERN 60-13 (1960).

ponding bubbles to be identified on the two views. The possible influence of these 90 events on the final result is discussed below. The quality of the measurements depends naturally on the apparatus used, and we have analysed the two groups of measurements independently. A further computer program was used to compile, from the measurements of individual events, the histograms needed to establish the fiducial limits of Table II and to reject the events erroneously accepted at the scanning, which could therefore be made with wide tolerances to avoid losses.

3. – Kinematic analysis and selection of hydrogen events.

The conservation of energy and momentum in the elastic collisions can be expressed in the form of the following criteria, which can be used to identify the pion-proton collisions:

a) π_i, π_s and p must be coplanar. The coplanarity was expressed by means of d in Padua, and c in CERN.

b) The correlation between the angles θ_π and θ_p must be consistent with the kinematics of the π-p collision at 120 MeV. This correlation is expressed by means of Δ.

c) The range of any particle stopping in the liquid must be consistent with the kinematics of the π-p collision at 120 MeV. In applying this criterion the fact that the proton range may be shorter than expected owing to interactions with carbon nuclei, *e.g.* the $^{12}C(p, n)^{12}N$ ([13]), was taken into account. This happened in about four percent of the hydrogen events.

As the dimensions of the chamber are comparable to the range of the stopping protons, a selection of events based on the measurement of the proton range would give rise to experimental bias. The selection was made instead by the criteria of coplanarity and angular correlation as follows.

For each event, a parameter ϱ was computed, defined by (the quantity d in the Padua analysis is replaced by c in the CERN work):

$$\varrho = \left| \left(\frac{d}{\sigma_d}\right)^2 + \left(\frac{\Delta}{\sigma_\Delta}\right)^2 \right|^{\frac{1}{2}}.$$

The values chosen for σ_d, σ_c and σ_Δ were obtained experimentally, as discussed below. Each event is characterized by two values of Δ, one for each of the

([13]) Yuin-Kwei Tai, G. P. Millburn, S. N. Kaplan and B. J. Moyer: *Phys. Rev.*, **109**, 2086 (1958).

two possible mass assignments for the secondary particles. Since the best angular correlation for a given measurement of a given event does not necessarily correspond to the best interpretation, we have always chosen the correct interpretation by a systematic comparison of the computed quantities with the original photographs. On the basis of the direction of the track, of the bubble density and of the δ-rays, π_i can generally be distinguished from π_s. In 70% of the cases the scattered proton was recognizable from the range; if this was not available the bubble density was almost always sufficient for a decision.

The precision of the measurement is affected by the geometry of the event. Histograms of the values of Δ and of d (Padua) and c (CERN) were therefore prepared for successive intervals of θ_π; of 45° (Padua) or 20° (CERN). From these histograms, the values of σ_d, σ_c and σ_Δ given in Table III were com-

TABLE III. – *Values of* σ_d, σ_c *and* σ_Δ.

Padua

θ_π	43°÷90°	90°÷135°	135°÷180°
σ_d	0.048	0.024	0.025
σ_Δ	1.8°	1.3°	1.4°

Cern

θ_π		40°÷60°	60°÷80°	80°÷100°	100°÷120°	120°÷140°	140°÷160°	160°÷180°
σ_c	*A*	0.102	0.134	0.136	0.120	0.109	0.098	0.086
	B	0.130	0.104	0.130	0.105	0.101	0.102	0.074
σ_Δ	*A*	3.15°	3.05°	3.25°	3.16°	3.07°	3.15°	2.70°
	B	3.33°	3.24°	3.49°	4.19°	3.44°	3.39°	2.26°

A: events measured on IEP. – *B*: events measured on Baby-IEP.

puted. The values of CERN and Padua are not directly comparable, as the Padua values are computed after a preliminary more effective exclusion of carbon events. For each event, the values of σ_d (or σ_c) and of σ_Δ corresponding to the proper θ_π interval were chosen to evaluate ϱ.

For the Padua analysis, the distribution of ϱ for all the events of both exposures is shown in Fig. 4, which was used to select the hydrogen events.

If $\varrho > 7$ the event was rejected. If $2 < \varrho < 7$ the event was remeasured and reanalysed with great care by taking into account all available information: on this basis a reasonable decision could always be reached. If $\varrho < 2$ the event was as a rule accepted: a few events in this category were also rejected because the proton range was appreciably greater than was consistent with the upper energy limit of the beam.

There were 1141 events from the first exposure and 1624 from the second exposure selected by the procedure described. All Padua results are based on these 2765 events.

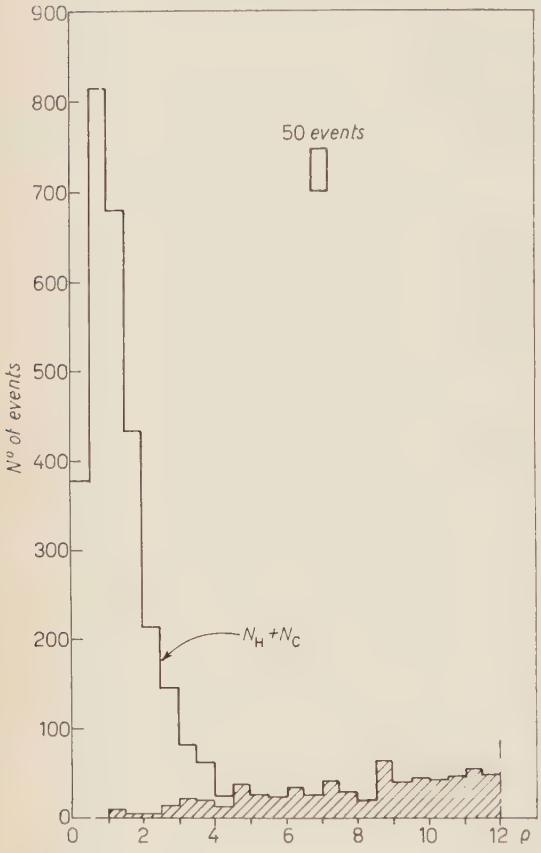

Fig. 4. – Padua analysis. Plot of the number of events accepted at the scanning of both exposures, *vs.* $\varrho = [(d/\sigma_d)^2 + (\Delta/\sigma_\Delta)^2]^{\frac{1}{2}}$.

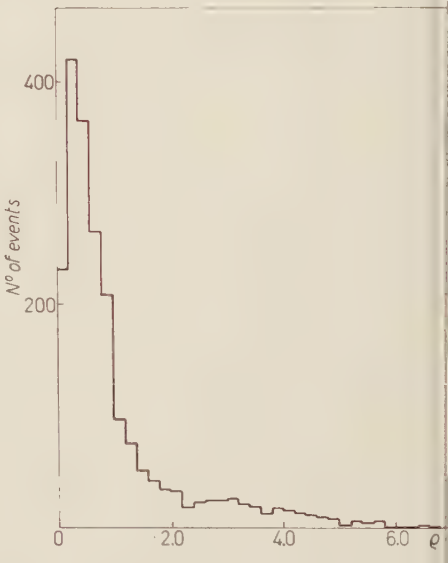

Fig. 5. – CERN analysis. Distribution of $\varrho = [(c/\sigma_c)^2 + (\Delta/\sigma_\Delta)^2]^{\frac{1}{2}}$.

In the CERN analysis, the histogram of ϱ is given by Fig. 5. The angular distribution of the events was prepared for $\varrho \leqslant 1.41$ and $\varrho \leqslant 2$ and, as no systematic difference could be seen, the limit $\varrho = 2$ was chosen, thus including 2640 events, 2100 of which were measured by the digitized protractor.

4. – Carbon contamination.

In the Padua analysis, the carbon contamination was evaluated by two methods. Using the method given by M. CHRÉTIEN *et al.* [14] we have first plotted in Fig. 6 the angular correlation of all the carbon events of both exposures for which $d < 2\sigma_d$. In the same figure five lines have been drawn:

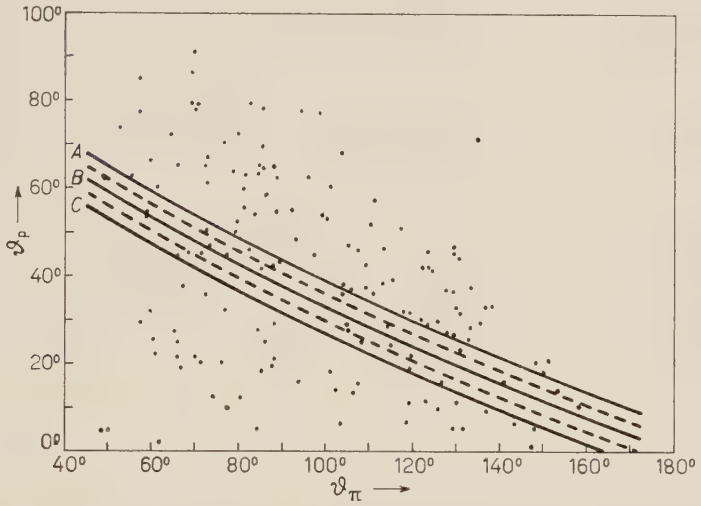

Fig. 6. – Padua analysis. Angular correlation of the coplanar carbon events ($d < 2\sigma_d$) of both exposures. Dashed lines include the acceptance region for hydrogen events (B). Region $A+C$ and region B have equal area.

the central one is the expected angular correlation for a π-p collision at 120 MeV and the others define two regions of equal area, a central one B, and a peripheral one consisting of two strips A and C. On the two regions we have, respectively, $\Delta < \sigma_\Delta$ and $\sigma_\Delta < \Delta < 2\sigma_\Delta$, were we adopted for σ_Δ a mean value of 1.5°.

It appears that the carbon events do not show any tendency to group themselves anywhere on the θ_p, θ_π-plane, so that the number of carbon events which have been included in the hydrogen events can be estimated by subtracting the carbon events in the region B from those in the region $A - C$. The result is, for the number c of the erroneously included events:

$$c = 1 \pm 5 .$$

[14] M. CHRETIEN, J. LEITNER, N. P. SAMIOS, M. SCHWARZ and J. STEINBERGER: *Phys. Rev.*, **108**, 383 (1957).

As a second method, we may assume that the carbon events are uniformly distributed both with respect to Δ/σ_Δ and d/σ_d. The distribution *vs.* ϱ is therefore given by the equation $dN_c = k\varrho\, d\varrho$, where k is a constant, and the histogram of the carbon events should be approximated, up to a certain value of ϱ, by a straight line passing through the origin of the co-ordinate system, and having a slope k.

For practically all the hydrogen events $\varrho < 4.5$.

From the carbon events distributed between $\varrho = 4.5$ and $\varrho = 12$ we have first calculated k by means of a weighted mean squares procedure, and then the number of carbon events expected to lie between $\varrho = 0$ and $\varrho = 4.5$. The number of events misinterpreted as hydrogen events is obviously given by the difference between expected and recognized carbon events in the same interval. Using this method we obtained for the contamination the value of $(0.8 \pm 0.3)\,\%$, where the error is purely statistical.

In the CERN analysis, the distribution of events as a function of ϱ (Fig. 5) allows an estimate to be made of the contamination of carbon scatters. Extrapolating the curve in the region $0 < \varrho < 2$ we find that an upper limit for the carbon contamination is of the order of $2.5\,\%$ for the events for which $\varrho < 2$.

5. – Experimental biases.

The detection efficiency was satisfactorily uniform throughout the fiducial volume. This was checked by comparing the spatial distribution of events to the distribution of 900 incident tracks in the fiducial volume.

It is clear however that even within the fiducial region some events get lost because the visibility is in some cases reduced. In fact when φ is near 90° or θ_π near 180°, the projected angles are small and the tracks difficult to distinguish from the beam, while when θ_π approaches its lower limit of 43° the recoil proton may be difficult to see.

As the methods used in Padua and in CERN to investigate the residual systematic errors due to these effects are somewhat different, they are presented separately.

Padua. – The number of selected events *vs.* the azimuthal angle φ for various intervals of θ^* is plotted on Fig. 7, which refers to the first, and on Fig. 8, which refers to the second exposure. Note that 53° in the c.m.s. are equivalent to 43° in the laboratory system of reference.

It may be seen that, within the limits of the statistical error, Fig. 7 *b*) and *c*) do not show any bias, while *a*) and *d*) indicate a possible small bias for big values of φ. A similar and bigger bias in noticeable in Fig. 8 *b*), *c*)

and *d*), but a new feature of Fig. 8 in comparison with Fig. 7 is the lack of events for small values of φ.

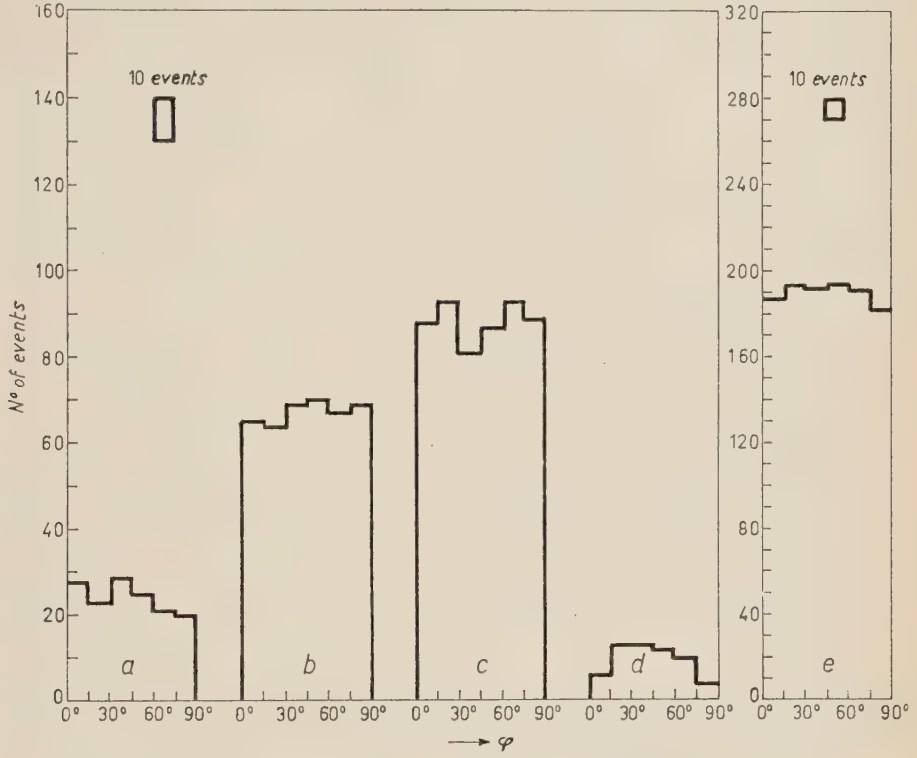

Fig. 7. – Padua analysis. First exposure. Plots of the number of selected events *vs.* the azimuthal angle φ, for various intervals of the pion scattering angle θ^*. *a*) $53° < \theta^* < 75°$; *b*) $75° < \theta^* < 120°$; *c*) $120° < \theta^* < 165°$; *d*) $165° < \theta^* < 180°$; *e*) $53° < \theta^* < 180°$.

A systematic study has convinced us, however, that this lack is not due to a loss of events, but either merely to a statistical fluctuation or to a shift of the events towards larger values of φ.

The study is first based on a check of the scanning efficiency for $q < 45°$, found to be better than $(98 \pm 1)\%$, and on the distribution of the carbon events, reported in Fig. 8 *e*), which shows that the missing events are not included in the carbon group. Secondly, the events lost in independent scannings were considered, from the distributions of which, reported in Fig. 9 *a*) and 10 *a*), no bias for small values of q appears. We may add that the direction of the beam in the second exposure had a dip of about 2°: this certainly caused a shift of events from small values of φ into greater ones.

In regard to observation biases for large and small values of θ_π, the curves of Fig. 9 *b*) and 10 *b*) indicate what the distribution of the events lost in

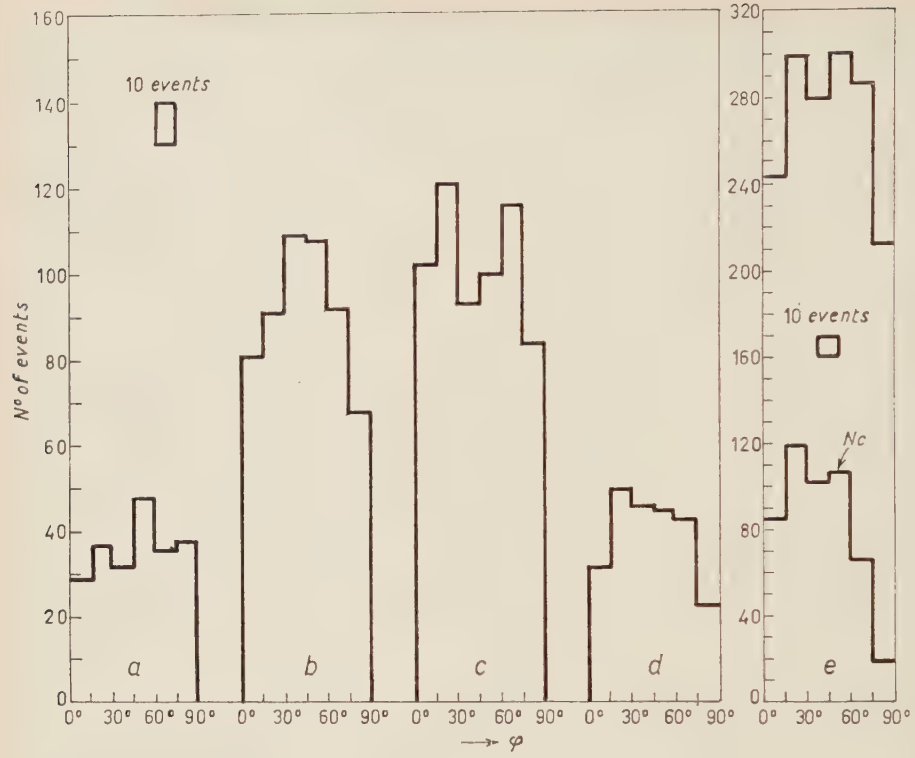

Fig. 8. – Padua analysis. Second exposure. Plots of the number of selected events and of the number of carbon events (N_C) *vs.* the azimuthal angle φ, for various intervals of the pion scattering angle θ^*. *a*) $53° < \theta^* < 75°$; *b*) $75° < \theta^* < 120°$; *c*) $120° < \theta^* < 150°$; *d*) $150° < \theta^* < 180°$; *e*) $53° < \theta^* < 180°$.

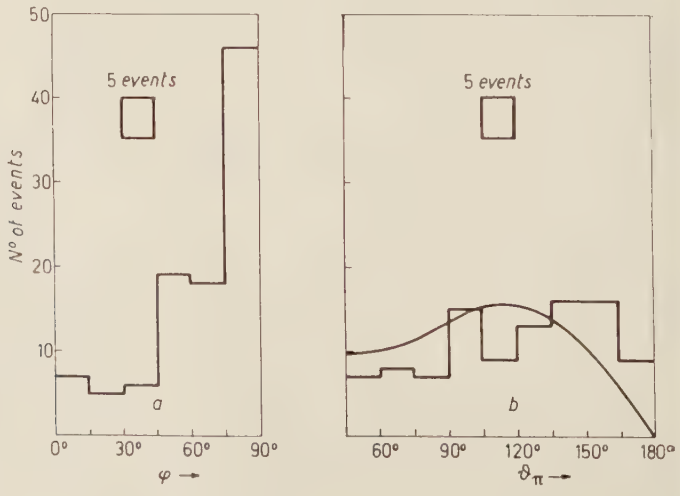

Fig. 9. – Padua analysis. First exposure. Plots of the number of events lost in three independent scannings, *vs.* φ and *vs.* θ_π.

independent scanning would have been in the absence of biases, on the basis of the final result of this work. As the curves fit the histograms rather well,

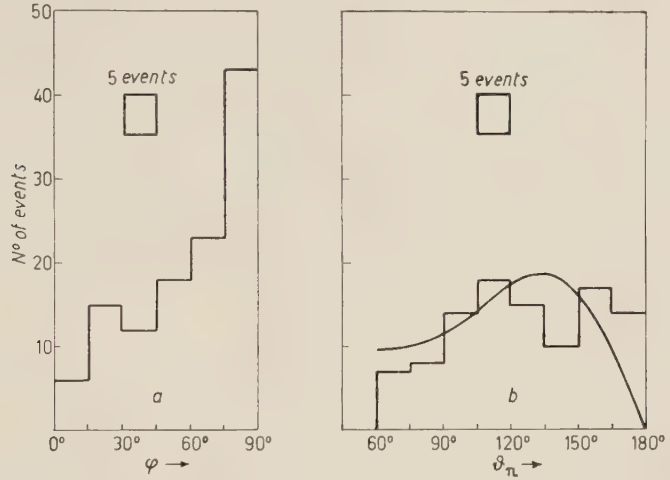

Fig. 10. – Padua analysis. Second exposure. Plots of the number of events lost in two independent scannings, *vs.* φ and *vs.* θ_π.

we can conclude that the biases against the detection of events with either great or small θ_π were not very important.

CERN. – The angular distribution was drawn by varying systematically the limits of acceptance of events as follows.

1) Useful volume

1.1	$-5.1 \leqslant x \leqslant 5.1$	$-6 \leqslant y \leqslant 6$	$-3.3 \leqslant z \leqslant 3.0$
1.2	$-4.5 \leqslant x \leqslant 4.5$	$-4.5 \leqslant y \leqslant 6$	$-2.8 \leqslant z \leqslant 2.5$
1.3	$-4 \leqslant x \leqslant 4.5$	$-4.5 \leqslant y \leqslant 5.5$	$-2.8 \leqslant z \leqslant 2.5$

2) Limits to φ

2.1 $\varphi \leqslant 80°$
2.2 $\varphi \leqslant 60°$

3) Limits to γ

3.1 $\cos\gamma \geqslant 0.994\,5$
3.2 $\cos\gamma \geqslant 0.998\,6$

4) Limits to ϱ, as already mentioned

4.1 $\varrho \leqslant 2$
4.2 $\varrho \leqslant 1.41$

Thus a total of 24 histograms were made.

The study of these histograms shows that the angular distribution is not affected by the following choice of criteria:

$$-5.1 \leqslant x \leqslant 5.1 \text{ cm} \qquad -6 \leqslant y \leqslant 6 \text{ cm} \qquad -33 \leqslant z \leqslant 3.0 \text{ cm}$$

$$\varphi \leqslant 60^\circ \qquad \cos\gamma \geqslant 0.9945 \qquad \varrho \leqslant 2 .$$

The distribution is not sensitive to the choice of γ and of the volume: on the other hand, the choice of φ and ϱ is indicated by inspection of the distributions.

In addition the histograms show a loss of events in the regions

$$\cos\theta^* > \quad 0.55 ,$$

$$\cos\theta^* < -0.95 .$$

It is to be noted that the angular distribution shows also an irregularity for

$$-0.15 > \cos\theta^* > -0.35 .$$

This region corresponds to angles θ_π between 85° and 95°: in the analysis of the angular distribution we have treated this anomaly in the two following ways:

1) by neglecting the zone defined by

$$-0.15 > \cos\theta^* > -0.35 ;$$

2) by correcting the distribution by a special analysis of the 90 unmeasurable events which correspond to this region (see Section 2). We estimate that one third of these events can be interpreted as elastic scatterings, and we have completed the angular distribution by taking account of the additional 30 unmeasurable events. By introducing larger errors on the points in this region, we find that the two methods give compatible results.

6. – Energy of the primary pions.

We have described how a suitable beam was used so as to have pions of 120 MeV energy in the middle of the chamber. It is of course desirable to check the beam energy by measurements of the events themselves. This was done separately, but with the same procedure, in Padua and at CERN.

We first plotted only the number of the events with stopping protons *vs.* the momentum of the primary pions at the point of interaction. The mo-

mentum was determined from the proton kinetic energy and the pion scattering angle, with a precision better than 3% on each event, as the angle θ_π is known to $\pm 1.2°$ and the proton range to ± 0.5 mm.

A cut-off was made to exclude temporarely also the events where the scattered proton had met a nuclear collision, and the remaining events were plotted *vs.* the momentum normalized to the central plane of the chamber. After a new cut-off due to the same reason as before, we calculated the mean normalized momentum and from it the energy which can be statistically attributed to the events

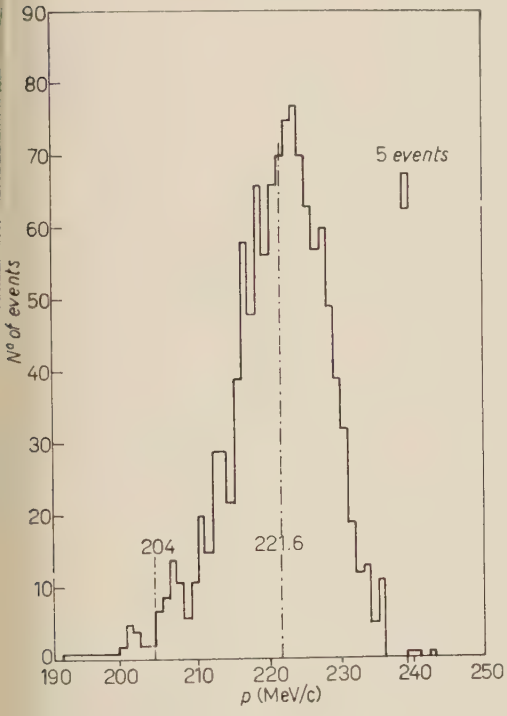

Fig. 11*a*. – Padua analysis. Second exposure. Plot of the number of 1211 selected events with stopping protons, *vs.* the momentum p of the primary pions at the point of interaction.

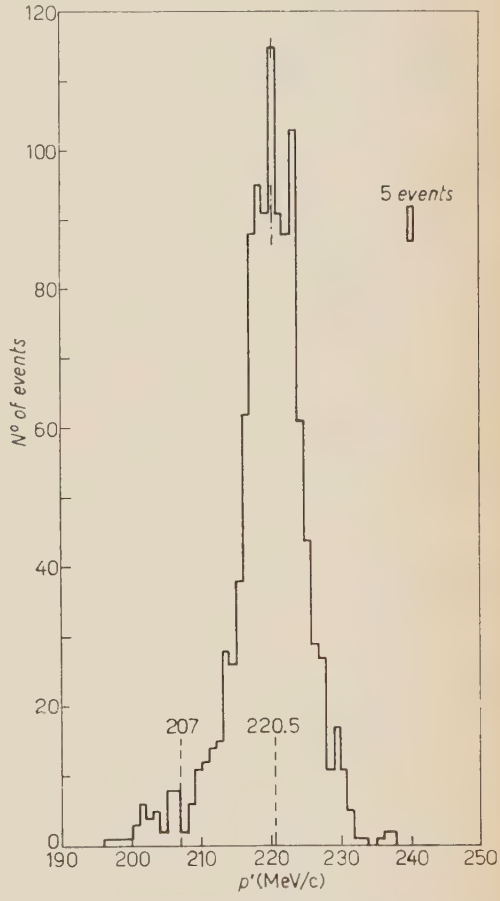

Fig. 11*b*. – Padua analysis. Second exposure. Plot of the number of selected events with stopping protons, *vs.* the momentum p' of the primary pions, normalized to the central plane of the chamber.

without stopping protons and to those previously excluded by the cut-offs. The histograms referring to the Padua events of the second exposure are reported in Fig. 11 *a*) and *b*) where the cut-offs are shown to have been made respectively at 204 and 207 MeV/c.

We obtained (119.9 ± 5.4) MeV for the events of the first exposure, (121.7 ; 5.6) MeV for the Padua events of the second exposure, and (121.5 ± 3) MeV for the CERN events.

As the difference of 1 MeV energy is irrelevant for the phase shift analysis, and in any case small in comparison with the energy spread of the primary pions, we have considered the events as if they were all due to positive pions of 120 MeV.

We may note that the energy spread deduced from Fig. 11 *b*), which is 3.6 MeV, is in good agreement with the value 2.5 MeV which can be deduced from Fig. 2.

7. – Angular distribution.

The angular distribution was approximated by means of the expression

$$A + 2B \cos\theta^* + 3C \cos^2\theta^* .$$

For Padua, Table IV gives the coefficients A, B and C for the distribution of the events of the first exposure, further referred to as first distribution,

TABLE IV. – *Values of the coefficients A, B and C for various distributions obtained in Padua, normalized to* $A=1$.

	First distribution	First distribution corrected for contamination	Second distribution	Second distribution cut at $\varphi=75°$	Second distribution cut at $\varphi=60°$
A	1.000 ± 0.059	1.000 ± 0.060	1.000 ± 0.049	1.000 ± 0.054	1.000 ± 0.060
B	-0.445 ± 0.060	-0.399 ± 0.062	0.376 ± 0.047	-0.389 ± 0.056	-0.389 ± 0.062
C	0.532 ± 0.082	0.582 ± 0.083	0.603 ± 0.064	0.617 ± 0.075	0.582 ± 0.083
χ^2	30.6	33.1	50	47.8	33.8
exp $[\chi^2]$	40	40	40	40	40

and the corresponding statistical errors, in comparison to which the geometrical biases and the contamination appear negligible. The Table also gives the coefficients of the distribution of the events of the second exposure, further referred to as second distribution, cut at $\varphi = 75°$ and $\varphi = 60°$, which show

that a possible loss of events for large values of φ has no significant influence.

The differential scattering cross-section as a function of θ^* was nevertheless finally deduced from a total distribution obtained by considering together the events of the corrected first distribution, and of the second distribution cut at $\varphi = 60^\circ$, as the decrease in statistical precision was small. This total distribution is given in Fig. 12.

For CERN, the limits of $\cos\theta^*$ were varied in intervals of 0.05 from 0.55 to 0.30, and from -0.95 to -0.75. Table V shows the results obtained; from these results we take the following values:

$$A = 0.340 \pm 0.010$$

$$B = -0.140 \pm 0.035$$

$$C = 0.247 \pm 0.053$$

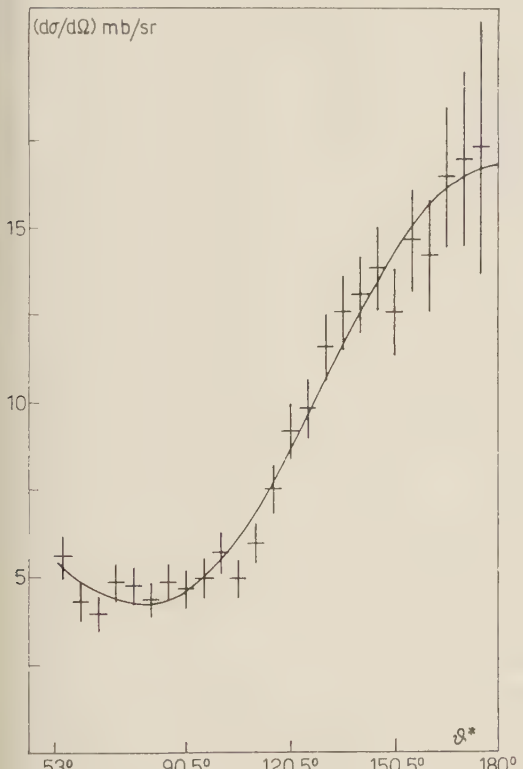

Fig. 12. – Padua analysis. Experimental normalized differential cross-section deduced from the total distribution. The curve shows the cross-section calculated with the phase shifts α_{31}, α_3 and α_{33} extracted from the total distribution.

Fig. 13. – CERN analysis. Accepted angular distribution: $\varphi \leqslant 60^\circ$, $\varrho \leqslant 2$.

after normalization to a total cross-section of (95 ± 6) mb, a value interpolated from other experimental evidence in the region of 120 MeV [15]. The distribution is shown by Fig. 13.

[15] J. ASHKIN: private communication.

TABLE V. – *Values of the coefficients A, B and C for various intervals of* cos θ^*, *obtained at CERN.*

cos θ^* <	cos θ^*>	— 0.95	— 0.90	— 0.85	— 0.80	— 0.75
0.55	A	48.79	49.37	49.60	48.60	49.45
	B	— 27.32	— 27.25	— 27.16	— 27.82	— 26.90
	C	27.14	25.47	24.72	28.42	24.69
0.50	A	48.83	49.47	49.74	48.61	49.62
	B	— 27.44	— 27.54	— 27.53	— 27.85	— 27.23
	C	27.00	25.10	24.24	28.38	24.13
0.45	A	48.37	49.03	49.29	47.91	49.04
	B	— 25.55	— 25.90	— 26.00	— 25.72	— 25.67
	C	29.05	27.10	26.15	31.32	26.52
0.40	A	47.65	48.24	48.39	46.61	47.83
	B	— 21.02	— 21.52	— 21.71	— 20.21	— 21.05
	C	33.72	32.90	31.12	38.21	33.05
0.35	A	47.84	48.54	48.79	46.95	48.35
	B	— 23.12	— 24.15	— 24.73	— 22.12	— 23.90
	C	31.50	28.90	28.00	35.95	25.43
0.30	A	47.76	48.29	48.34	46.02	47.36
	B	— 15.75	— 17.12	— 17.17	— 12.05	— 14.72
	C	38.72	36.02	35.95	47.81	40.07

8. – Phase shift analysis.

The calculation of the phase shifts from the Padua experimental data was made by the Department of Physics of Rochester University. The total distribution was grouped by intervals of 5 , and in each interval the error was taken as proportional to the square root of the number of events in the interval. The formulae used and the method by which the computation was performed have been explained in detail by BARNES *et al.* ([16]). The program was however modified to take into account the fact that the experimental results give only relative, and not absolute, values for the differential cross-sections. The proportionality factor was considered as a parameter in the fitting procedure. The total cross-section was fixed at (95 · 6) mb, as at CERN. The best values of

([16]) S. W. BARNES, B. ROSE, G. GIACOMELLI, J. KING, K. MIYAKE and K. KINSEY: *Phys. Rev.*, **117**, 226 (1960).

the phase shifts α_{31}, α_3 and α_{33} and of the proportionality factor k were found simultaneously.

The distributions of the two exposures were in addition analysed independently, and some auxiliary fits were performed to check the absence of sensitivity of the results to the cut-off of q and to small corrections for carbon contamination. The results were found to be all compatible, and the final data based on the total number of 2 765 events are:

$$\alpha_{31} = -3.15^\circ \pm 0.95^\circ , \quad \alpha_3 = -11.12^\circ \pm 2.10^\circ , \quad \alpha_{33} = 31.63^\circ \pm 1.15^\circ .$$

Similarly, in CERN, each solution in Table V has been analysed by a Mercury computer program to calculate the phase shifts α_3, α_{31} and α_{33} with their errors.

The inspection of these results leads to the choice

$$\alpha_3 = -11.0 \pm 1.7 , \quad \alpha_{31} = -2.0 \pm 1.0 , \quad \alpha_{33} = 31.8 \pm 2.1 ,$$

which corresponds to the limits

$$\cos\theta^* < 0.50 , \quad \cos\theta^* > -0.95 .$$

These results are based on 2 640 events.

PART II. – CONCLUSION

The results obtained at Padua and Geneva are consistent with each other. By combining them we have for the phase shifts:

$$\alpha_{31} = -2.60^\circ \pm 0.69^\circ , \quad \alpha_3 = -11.05^\circ \pm 1.32^\circ , \quad \alpha_{33} = 31.67^\circ \pm 1.01^\circ .$$

The values of α_{31} and α_{33} agree well with previous determinations and will not be discussed here. However, α_3 differs by more than two standard deviations from the value -8.2°, expected on the basis of the linear dependence on the momentum, which has been proposed by some authors, *e.g.* J. OREAR [17] and more recently S. W. BARNES *et al.* [16]. This dependence, previously thought to be valid at least up to a pion energy of about 200 MeV in the laboratory, can now be excluded.

Our result has in fact confirmed with markedly better precision the meas-

[17] J. OREAR: *Phys. Rev.*, **100**, 288 (1955).

urements with nuclear plates in the region around 100 MeV [18] which gave for α_3 values significantly smaller than indicated by that linear dependence. More evidence from other sources has accumulated in the meantime both at higher and at lower energies. We have plotted some representative points in Fig. 14, where three lines are drawn.

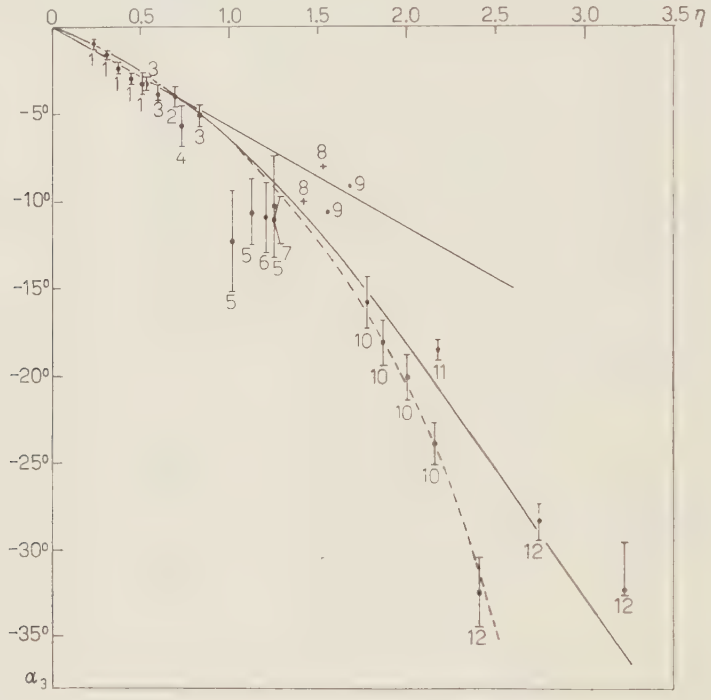

Fig. 14. – α_3 *vs.* momentum.

1. G. E. Fisher and E. W. Jenkins: *Phys. Rev.*, **116**, 749 (1959).
2. S. W. Barnes *et al.*: *Phys. Rev.*, **117**, 226 (1960).
3. *CERN Conference* (1958), p. 43, Fig. 7.
4. J. Orear *et al.*: *Phys. Rev.*, **93**, 575 (1954).
5. Bologna Group: *Nuovo Cimento*, **5**, 1651, 1658, 1660 (1957).
6. J. Orear: *Phys. Rev.*, **96**, 1417 (1954).
7. This experiment.
8. J. Ashkin *et al.*: *Phys. Rev.*, **101**, 1149 (1956).
9. A. I. Mukhin *et al.*: *CERN Symposium* (1956), p. 217.
10. *Kiev Conference* (1959), Pontecorvo's Report, p. 30.
11. J. H. Foote *et al.*: *Rochester Conference* (1960), p. 52 (*).
12. W. D. Walker *et al.*: *Phys. Rev.*, **118**, 1612 (1960) (*).

(*) *D* waves are also considered.

(18) G. Ferrari, E. Manaresi and G. Quareni: *Nuovo Cimento*, **5**, 1651 (1957); R. Gessaroli, G. Quareni, G. Dascola, S. Mora and G. Todesco: *Nuovo Cimento*, **5**, 1658 (1957); L. Ferretti, G. Quareni, M. Della Corte and T. Fazzini: *Nuovo Cimento*, **5**, 1660 (1957).

The straight line represents the linear dependence.

By neglecting the re-scattering one can easily obtain from the dispersion relations by G. F. CHEW *et al.* [19] the following equations

$$(1)\qquad \begin{cases} \sin\alpha_3\cos\alpha_3 = \eta\,\dfrac{M}{\omega+M}\left(-2\lambda^+ - \dfrac{\omega}{M}\lambda^-\right), \\ \sin\alpha_1\cos\alpha_1 = \eta\,\dfrac{M}{\omega+M}\left(-2\lambda^+ + \dfrac{2\omega}{M}\lambda^-\right), \end{cases}$$

where η is the momentum in the c.m.s. in units of $m_\pi c$, M is the mass of the proton and ω is the total energy in the c.m.s., minus the mass of the proton.

The dashed curve corresponds to the above relations with:

$$\lambda^+ = +\,0.007 \qquad \text{and} \qquad \lambda^- = +\,0.562\,.$$

The values of λ^+ and λ^- have been obtained by normalizing the eq. (1) to the phase shifts

$$\alpha_3 = -\,4.01^\circ \qquad \alpha_1 = +\,6.65^\circ$$

measured by S. W. BARNES *et al.* [16] in an experiment of π^+-p and π^--p elastic scattering at 41.5 MeV.

Neglecting the re-scattering though could hardly be justified, as the phase shifts are already too big in the energy region which we consider; in fact the curve appears to be too low, especially towards the higher energies.

It is certainly more correct to neglect the re-scattering for the expression

$$(2)\qquad \tfrac{1}{2}(\sin 2\alpha_1 - \sin 2\alpha_3)$$

as the value of $\sin^2\alpha_1 - \sin^2\alpha_3$, which appears in the integral representing the re-scattering, is experimentally known to be very small.

In fact J. BOWCOCK *et al.* [20] have recently calculated the expression (2), neglecting the re-scattering and taking instead into account a possible π-π interaction in the $J=1$, $T=1$ state.

Taking now for α_3 our experimental value and for α_1 the value calculated

[19] C. R. CHEW, M. L. GOLDBERGER, F. E. LOW and Y. NAMBU: *Phys. Rev.*, **106**, 1337 (1957).

[20] J. BOWCOCK, N. COTTINGHAM and D. LURIÉ: *Nuovo Cimento*, **19**, 142 (1961).

at 120 MeV, and assuming that

$$\alpha_1 = \eta \times (0.166\,8 \pm 0.023\,0) \quad (16)$$

we obtain for the above expression the value 0.390 ± 0.034.

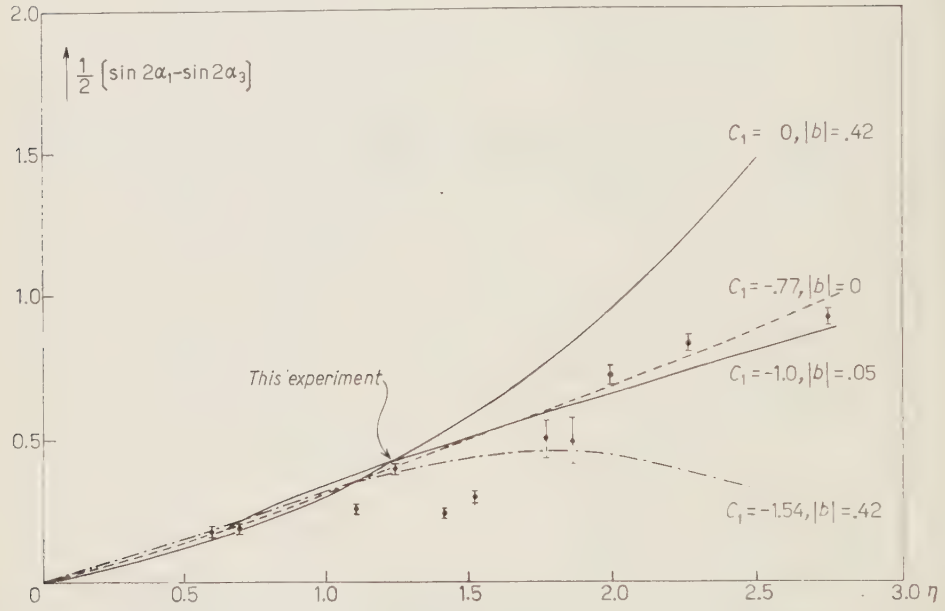

Fig. 15. – Theoretical curves for S-waves, from J. Bowcock *et al.* See text for reference.

We have inserted the resulting point in Fig. 15 which is a copy from J. Bowcock *et al.*: the agreement with the theoretical predictions is very good. Unfortunately the energy at which our experiment was planned, when the problem had not yet arisen, is too low in order to choose among the various curves, and therefore no indication on the π-π interaction can be given.

It might perhaps be of some interest to note that, if we replace empirically $\sin\alpha\cos\alpha$ by $\mathrm{tg}\,\alpha$ in the eq. (1), we obtain from

$$\mathrm{tg}\,\alpha_3 = \eta \cdot \frac{M}{\omega + M}\left(-2\lambda^+ - \frac{\omega}{M}\lambda^-\right),$$

the solid curve of Fig. 14, which fits rather well the experimentally data up to 600 MeV.

* * *

We are very grateful to Prof. A. ROSTAGNI for his warm support and to Prof. P. BASSI for his active interest in the construction and use of the apparatus. We would also like to thank Prof. G. PUPPI and Prof. S. FUBINI for helpful suggestions.

We express our deep gratitude to Prof. G. BERNARDINI for his encouragement and advice, and we take this opportunity to express our indebtedness to Prof. G. FIDECARO, Dr. A. LUNDBY, Prof. A. W. MERRISON and Dr. D. E. G. MICHAELIS for assistance in preparing the beam: further we are indebted to Prof. S. W. BARNES and his colleagues for having kindly calculated with their program the phase shifts from the Padua data. We have also great pleasure in thanking Dr. A. GRIGOLETTO for helping us in measurements and in calculations, and Dr. M. TONIN for interesting discussions.

Further thanks are due to Mr. O. FREDRIKKSON and the cyclotron crew, to Mr. B. TIVERON for the running of the bubble chamber and to Mr. M. MERLIN, Mr. G. PASQUALI and Mr. R. RAMPAZZO for their efficient scanning work.

RIASSUNTO

Si descrive una ricerca sull'urto elastico di pioni positivi di 120 MeV su protoni. L'esperimento è stato fatto esponendo una camera a bolle a propano al sincrociclotrone da 600 MeV del CERN. I risultati si riferiscono a 5405 eventi opportunamente scelti, per i quali si dimostra che la contaminazione da urti su nuclei di carbonio è trascurabile. I valori ottenuti per le fasi sono

$$\alpha_{31} = -2.60^\circ \pm 0.69^\circ , \qquad \alpha_3 = -11.05^\circ \pm 1.32^\circ , \qquad \alpha_{33} = 31.67^\circ \pm 1.01^\circ .$$

Il valore della fase α_3 differisce notevolmente da quello che ci si attenderebbe assumendo che essa dipenda linearmente dal momento, come è stato proposto da alcuni autori; questo risultato viene discusso, particolarmente in relazione ad alcuni recenti sviluppi teorici.

LETTERE ALLA REDAZIONE

(La responsabilità scientifica degli scritti inseriti in questa rubrica è completamente lasciata dalla Direzione del periodico ai singoli autori)

Remarks on Complex Singularities of the Vertex Function and Nakanishi's Conjecture.

S. DEMBINSKI (*)

Institute of Theoretical Physics, University of Wrocław - Wrocław

(ricevuto il 17 Giugno 1961)

Recently NAKANISHI (1) discussed the possibility of double dispersion representation for various matrix elements. He has pointed out, that the non existence of dynamic singularities, is not a sufficient condition for the validity of the above mentioned representation. As an example he considered the non trivial lowest order vertex function with one internal mass equal to 0. In the following, let us look if really this vertex function is free from many-variable singularities. Due to KARPLUS *et al.* (2) and FOWLER *et al.* (3), for vertex as in Fig. 1, the geometry of the Landau curves, in the real s, t plane, is given in Fig. 2 *a*, *b*. The solid straight lines are normal thresholds and the shaded portion of the s, t plane is the region R where V is real.

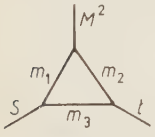

Fig. 1.

Using Tarski's (4) method of investigating the complex surfaces attached to Landau curves and analytical continuation under Feynman's integrals, in

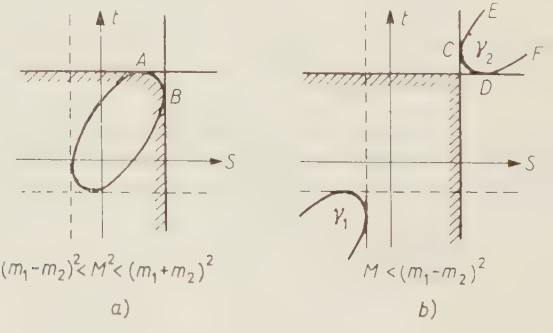

Fig. 2.

(*) Present address: Theoretical Physics Department, N. Copernicus University, Toruń.

(1) N. NAKANISHI: *Progr. Theor. Phys.*, **24**, 1275 (1960); **25**, 155 (1961).

(2) R. KARPLUS, C. M. SOMMERFIELD and E. H. WICHMAN: *Phys. Rev.*, **111**, 376 (1958).

(3) M. FOWLER, P. V. LANDSHOFF and R. W. LARDNER: *Nuovo Cimento*, **17**, 956 (1960).

(4) J. TARSKI: *Journ. Math. Phys.*, **1**, 149 (1960).

the terminology of EDEN *et al.* [5], one has: the arc AB is singular on the physical sheet in appropriate and inappropriate limits as well, the remaining part of an ellipse is always regular on the physical sheet. The singular hypersurface has the form

$$(1) \qquad t' = -\frac{M^2 - m_1^2}{2m_1^2} m_2^2 s' + \frac{1}{2m_1^2}\sqrt{(M^2 - m_1^2 - m_2^2)^2 s'^2 - 4[m_2^2 s'^2 - 4m_1^2 m_2^2 m_3^2 + m_3^2(M^2 - m_1^2 - m_2^2)^2]m_1^2}\,.$$

where

$$t' = t - m_2^2 - m_3^2; \qquad s' = s - m_1^2 - m_3^2\,.$$

In the limit $\operatorname{Im} s \to 0+$ and $\operatorname{Im} s \to 0-$, from the first and second Riemann surfaces respectively, on the portion

$$m_1^2 + m_3^2 - \frac{m_3}{m_2}(M^2 - m_1^2 - m_2^2) < \operatorname{Re} s < (m_1 + m_3)^2\,,$$

of the cut, of the function (1), one obtains the singular arc AB. In both cases we are on the physical sheet.

The curve γ_1 is regular and so is the hypersurface Σ, which joins γ_1 and γ_2. γ_2 consists of virtual singularities *i.e.* is singular in inappropriate limits (CD is singular in limits from the corresponding half planes, CE and DF are singular in limits from the opposite half planes).

When $m_3 = 0$, the ellipse reduces to a point $s = m_1^2$, $t = m_2^2$, which is now the point of intersection of two normal threshold lines. The hypersurface

$$(2) \qquad t - m_2^2 = (s - m_1^2) R \exp[i\vartheta]\,,$$

which follows from (1), remains singular on the physical sheet and is responsible for the relative shift of s and t cut planes. This fact was given by NAKANISHI, through explicit calculations. Now it is clear, that nothing else but dynamic singularities makes the double representation impossible, in the same fashion as before the limit $m_3 = 0$ was taken.

When $M^2 < (m_1 - m_2)^2$, the degenerate case gives two straight lines and in the region $s > m_1^2$, $t > m_2^2$ they bound that portion of the real s, t plane, where the spectral function is different from zero.

In general, following conditions are sufficient for the invalidity of the double dispersion representation:

1) The region R (*i.e.* the region where the function is real) is bounded with some piece of the Landau curve.

2) When R is bounded with one variable singularity only, there exists a hypersurface Σ, that is entirely attached to parts of the Landau curve from the region, O, where cuts overlap (region of virtual singularities).

[5] R. J. EDEN, P. V. LANDSHOFF, J. C. POLKINGHORNE and J. C. TAYLOR: *Phys. Rev.*, **122**, 307 (1961).

The first case is obvious and it contains among others an example of Nakanishi's «curious singularities» discussed above. The second one needs some comments: The Σ quoted above is singular always. This is not in general true for Σ constructed between curves laying in the remaining part of the s, t plane outside R and O. All limits onto the real boundary of the physical sheet give there the same curves and some parts of these, though not directly connected to R, could be regular.

Nakanishi's conjecture for the invalidity of double representation states that when $F(s, t) = 0$, for s, $(t) > s_0$, (t_0), t, (s) is complex. Here $F(s, t) = 0$ is the equation for the Landau curve and s_0, t_0 are static cuts (normal or anormal).

When such a situation occurs, it gives necessarily rise to the singular hypersurface invariant 1) or 2). This may be easily verified by considering the possible branches of the Landau curve and its relations to one-variable singularities.

Summing up, in our opinion, Eden's [6] proof of Mandelstam representation does not suffer from neglect of the curious singularities.

Note added in proof.

After this letter has been mailed, the author was informed of the paper by R. J. Eden, P. V. Landshoff, J. C. Polkinghorne and J. C. Taylor: *Acnodes and Cusps on Landau curve* (Cambridge University, Department of Applied Mathematics and Theoretical Physics, preprint, March 1961) (*). In Nakanishi's example, considered above, there is one acnode, beside two static cuts, on the real boundary of the physical sheet. The proof of double dispersion relations is not complete till now, as it is not well established, that there are no acnodes and cusps on the physical sheet. They may appear not only due to the special choice of masses, as we believed.

[6] R. J. Eden: *Phys. Rev.*, **121**, 1567 (1961).

(*) I wish to express my thanks to Prof. R. J. Eden for sending me his *Lectures on the Use of Perturbation Methods in Dispersion Theory* (University of Maryland, March-April 1961).

Investigation of Styrene Polymerization by Means of Nuclear Magnetic Relaxation Measurements.

G. Bonera, P. De Stefano and A. Rigamonti
Istituto di Fisica dell'Università - Pavia

(ricevuto il 1° Agosto 1961)

The purpose of this letter is that of showing how it is possible to obtain information about the polymerization processes by studying nuclear magnetic relaxation.

A systematic investigation of the polymerization of vinyl compounds of which the polymer is soluble in the respective monomer is being pursued at present. We were able to see that generally during the polymerization process the substances we have studied exhibit two very differnt spin-lattice relaxation times T_1. The existence of these two spin-lattice relaxation times can be demonstrated with the technique of fast adiabatic passages. It is well known [1] that if we perform two successive fast adiabatic passages through the resonance with an interval of time τ between them, the height of the signal due to the second passage depends on τ. It is possible to choose such an interval of time between the two passages that the second signal is null: this happens when $\tau = T_1 \ln 2$. But if in a sample there are two groups of protons having different enough spin-lattice relaxation times T_{1L} and T_{1S}, we can choose the experimental conditions for which the passages through the resonance are fast for the protons that have the long spin-lattice relaxation time T_{1L} but are slow for the protons that have the shorter spin-lattice relaxation time T_{1S}: in these conditions the second signal can never be null. For $\tau = T_{1L} \ln 2$ the second signal has the appearance of a dispersion signal and is due to the protons with spin-lattice relaxation time T_{1S}. This is clearly seen in Fig. 1 in which three recordings relative to a sample of styrene are reproduced.

It has been possible to confirm the existence of the relaxation time T_{1S} by choosing such experimental conditions that the passages were fast also for the protons with spin-lattice relaxation time T_{1S} and performing a sequence of passages so frequent that the signals due to the protons with spin lattice relaxation time T_{1L} are practically cancelled because of a saturation effect. In these

[1] G. Bonera, P. L. Chiodi, G. Lanzi and A. Rigamonti: *Nuovo Cimento*, **17**, 198 (1960).

conditions it is possible to perform an accurate enough meaurement of T_{1S} [2].

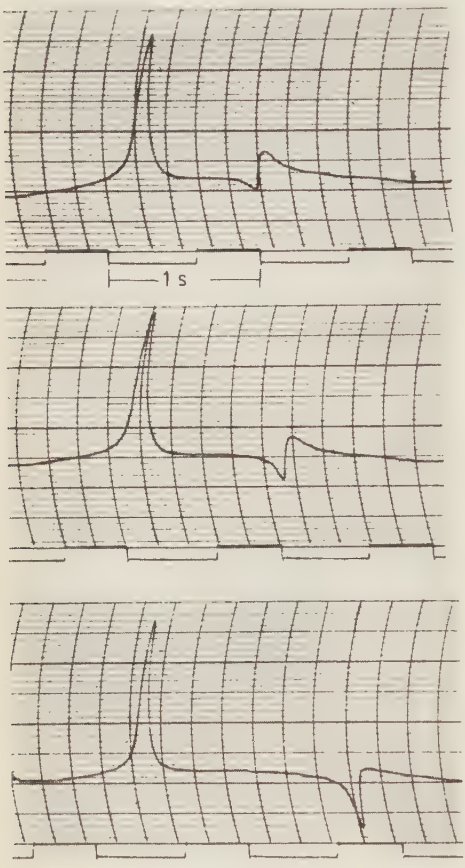

Fig. 1. – Recordings obtained for a sample of styrene at 25 °C during thermal polymerization when the percent of polystyrene was 30 %. The interval of time τ between the two adiabatic passages through the resonance is different in each recording. In recording (*a*) $\tau < T_{1L} \ln 2$; in recording (*b*) $\tau = T_{1L} \ln 2$; in recording (*c*) $\tau > T_{1L} \ln 2$.

Considerations of a general character and the fact that the height of the dispersion signal increases with increasing concentration of polymer in the syrup let us think that the relaxation time T_{1L} is to be ascribed to the monomer protons and that the relaxation time T_{1S} is to be ascribed to the polymer protons.

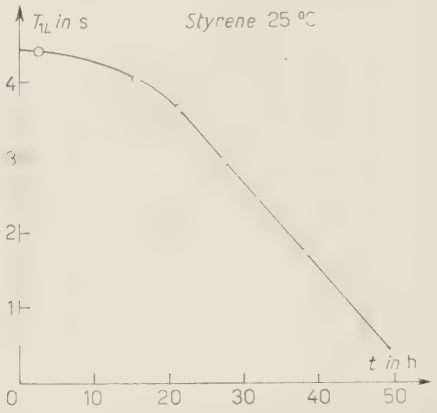

Fig. 2. – Spin-lattice relaxation time T_{1L} of styrene *vs.* time t of duration of thermal treatment. The sample was kept at 90 °C continuously except the short interruptions necessary for the measurements; the measurements were performed at 25 °C.

The results we have obtained for styrene are shown in Figg. 2 and 3 and in Table I.

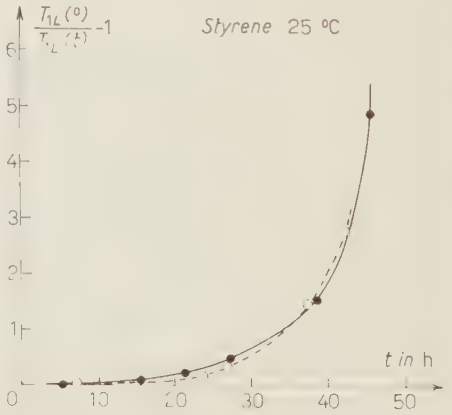

Fig. 3. $T_{1L}(0)/T_{1L}(t) - 1$ for styrene *vs* time t of duration of exposition to ultraviolet light (dashed line) and of thermal treatment (full line).

From the results shown in Table I it is possible to see that the polymer

[2] G. CHIAROTTI, G. CRISTIANI, L. GIULOTTO and G. LANZI: *Nuovo Cimento*, **12**, 519 (1954).

TABLE I. – *Per cent of polymer (estimated from refractive index measurements) and viscosity of the syrup during thermal polymerization of styrene.*

time t (h)	%	viscosity (poise)
0	0	$0.73 \cdot 10^{-2}$
3	0	$0.73 \cdot 10^{-2}$
4.5	—	$22 \cdot 10^{-2}$
14.5	13	32
17.6	—	60
20	23	~ 200
24	32	—
39	60	—
63	~ 90	

concentration increases with time following the exponential law

$$P(t) = A(1 - \exp[-kt]) ,$$

in agreement with the general assumptions one is allowed to make about the polymerization kinetics ([3,4]) and taking into account a short inhibition period. These results are consistent with those obtained by several researchers ([5]).

We see that during the first 20 h of the polymerization process the viscosity increases by several orders of magnitude while the spin-lattice relaxation time T_{1L} decreases only slightly. It is therefore not possible to assume that during the polymerization process the spin-lattice relaxation time T_{1L} decreases with increasing viscosity as required by the theory of Bloembergen, Purcell and Pound ([6]). We may say that the monomer molecules although trapped among the polymer chains retain most of their degrees of freedom.

Measurements of spin-spin relaxation time T_2 ([7]) for the protons of the monomer were occasionally performed only at low polymer concentrations: the results show that in general T_2 is almost equal to T_1.

We were able to measure T_{1S} only for high polymer concentrations. Because of the experimental error, which is still very large, the values we have obtained are only indicative. For a sample with 60% of polystyrene we found $T_{1S} = 3 \cdot 10^{-2}$ s. From measurements performed at higher concentrations of polymer it seems that also this relaxation time decreases with proceeding polymerization.

The values of T_{1S} we found seem to be larger than those one would expect from consideration of the dimensions of the polymer chains and the very large values of viscosity; it is therefore very probable that also at high polymer concentrations some hindered motions of the chains are possible.

Our results seem to point out that measurements of nuclear magnetic relaxation can give new information for a microscopic interpretation of the polymerization process.

* * *

The AA. thank Prof. L. GIULOTTO for the interest he has shown in this work and for some useful suggestions. They thank the C.N.R. which with its financial support has made possible to initiate this research.

([5]) G. F. D'ALELIO: *Fundamental Principles of Polymerization* (New York, 1952).

([4]) A. CHARLESBY: *Atomic Radiation and Polymers* (London, 1960).

([5]) C. E. SCHILDKNECHT: *Vinyl and Related Polymers* (New York, 1952).

([6]) N. BLOEMBERGEN, E. M. PURCELL and R. V. POUND: *Phys. Rev.*, **73**, 679 (1948).

([7]) G. BONERA, P. L. CHIODI, L. GIULOTTO and G. LANZI: *Nuovo Cimento*, **14**, 119 (1959).

Two Modes of Measuring Spurious Scattering in Nuclear Emulsions (*).

E. Dahl-Jensen
Institute for Theoretical Physics - Copenhagen

M. Gailloud (**)
Ecole Polytechnique - Lausanne

W. O. Lock and G. Vanderhaeghe
CERN - Geneva

(ricevuto il 29 Agosto 1961)

On May 12 th and 13th an informal discussion meeting took place in Lausanne on Problems of Distortion and Spurious Scattering in Nuclear Emulsions. During the course of the discussions it became clear that groups had differing concepts and definitions of spurious scattering, and in particular differing methods of measuring the mean second difference, $\bar{D}_{ss}$, corresponding to the signal from spurious scattering effects. It was therefore extremely difficult to compare the results of different groups obtained from scattering measurements in emulsions treated and/or processed in different ways. We discuss here the two common methods of measuring spurious scattering (or rather, $\bar{D}_{ss}$, the mean absolute second difference corresponding to spurious scattering effects) which we hope will be adopted as standard methods in the work with spurious scattering, simply in order to facilitate the comparisons of results. For the same reason we also give some recommendations on the actual measurements and on the scattering constant, eventually to be used.

Let us consider first the case in which scattering measurements are carried out on isolated tracks of *known* energy in an emulsion. For a given cell size the measured absolute mean difference, $\bar{D}_{\text{meas}}$, may be written as

$$(1) \quad \bar{D}_{\text{meas}} = \sqrt{\bar{D}_c^2 + \bar{D}_\varepsilon^2 + \bar{D}_\gamma^2 + \bar{D}_{ss}^2} \,,$$

where the absolute mean second difference due to Coulomb scattering is written as $\bar{D}_c$, that due to reading, grain and irreproducible microscope noise as $\bar{D}_\varepsilon$, that due to the stage profile noise as $\bar{D}_\gamma$ and that due to spurious

(*) The contents of this paper arose out of discussions held at the Lausanne Meeting at which representatives of the following laboratories were present: Bern, Bristol, Brussels, Caen, CERN, Copenhagen, Dublin, Durham, Hamburg, Karachi, Lausanne, Milan, Munich, Rome, Strasbourg, UC London.

(**) Secretary of the Lausanne Meeting, May 12-13, 1961.

scattering as $\bar{D}_{ss}$. (It will be noted that $\bar{D}_\gamma$ is added quadratically to the terms under the square root. This can be done only if the distribution of D_γ has been found to be gaussian. If this is not the case one must correct every reading for the known displacement of the microscope stage with respect to an arbitrary straight line, as should be done for the contribution of general distortion, which we assume here to be negligible.)

In this way we define spurious scattering as the signal which remains after all known effects have been allowed for. Thus $\bar{D}_{ss}$ can be calculated from eq. (1):

$$(2) \quad \bar{D}_{ss} = \sqrt{\bar{D}^2_{\text{meas}} - \bar{D}^2_c - \bar{D}^2_\varepsilon - \bar{D}^2_\gamma} .$$

This method of evaluating $\bar{D}_{ss}$ implies the knowledge of momentum of the beam particles, the scattering constant for the cell length used (which is not known very well in the 25 GeV region) and accurate measurements of $\bar{D}_\varepsilon$ and $\bar{D}_\gamma$. (We discuss later the ways in which $\bar{D}_\varepsilon$ and $\bar{D}_\gamma$ should be measured.)

When the flux density of incident beam particles in the emulsion under study is rather high it becomes possible to make relative scattering measurements on pairs of tracks which are close together. Let $\bar{D}_r$ be the absolute mean second difference obtained from the relative scattering measurements. Then, since no reference is made to the stage movement of the microscope, we may write

$$(3) \qquad \bar{D}_r = \sqrt{\bar{D}^2_{c1} + \bar{D}^2_{c2} + 2\,\bar{D}^2_\varepsilon} ,$$

where $\bar{D}_{c1}$, and $\bar{D}_{c2}$ are the absolute mean second differences due to Coulomb scattering of the two particles.

In order to explain the reliability of excluding $\bar{D}_{ss}$ from (3) consider Fig. 1 which shows two tracks on which measurements are being made at points A and A', B and B', C and C' etc., where the distance $AB = BC$ etc. is the basic cell length employed. Now the phenomenon of spurious scattering defined in (1) and (2) arises from some change in the emulsions between point A and point B, point B and point C

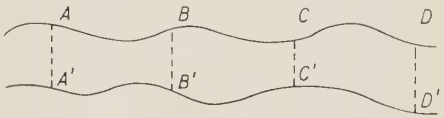

Fig. 1.

and so on. If A and A', B and B' C and C', etc. are sufficiently close together then the same change affects A', B' and C' ... so that $\bar{D}_{ss}$ is eliminated by taking relative scattering measurements. From the measurements of Biswas *et al.* (1), the validity of this assumption seems to be proved.

By making relative scattering measurements one can automatically be provided with the measurements of $\bar{D}_{\text{meas}}$ for the two tracks used in the relative scattering measurements. When (1) and (3) are combined one obtains

$$(4) \quad \bar{D}_{ss} = \sqrt{\bar{D}^2_{\text{meas}\,1} + \bar{D}^2_{\text{meas}\,2} - \bar{D}^2_r - 2\,\bar{D}^2_\gamma} ,$$

where $\bar{D}_{\text{meas}1}$ and $\bar{D}_{\text{meas}2}$ are the absolute mean second differences obtained from the individual measurements of the two tracks.

It is worth noting that $\bar{D}_{ss}$ derived from eq. (4) is independent of the calculated values of $\bar{D}_{c1}$, and $\bar{D}_{c2}$, and hence of the momenta of the two particles (which could be somewhat different) and of the scattering constant. It is also independent of $\bar{D}_\varepsilon$. Therefore, assuming that statistical errors can be rendered small enough, relative scattering measurements provide us with a better measure of $\bar{D}_{ss}$ than individual scattering measurements which involve the knowledge of more parameters.

For technical studies of spurious scattering we suggest that whenever possible relative scattering measurements should be used to evaluate $\bar{D}_{ss}$. On

(1) S. Biswas, N. D. Prasad and S. Mitra: *Proc. Ind. Acad. Sci.*, **46** A, 167 (1957).

the other hand we recognise that this may not be possible for many emulsion stacks exposed to a rather low flux of incident particles, from an accelerator, for nuclear physics purposes. In such cases eq. (2) should be used to evaluate $\bar{D}_{ss}$, but it should be borne in mind that it is not reliable to compare quantitatively values of $\bar{D}_{ss}$ obtained using eq. (2) with those obtained from eq. (4). Similarly a comparison of the level of spurious scattering in different emulsion stacks based only on eq. (2) could be misleading.

For the actual measurements in the GeV region we recommend that:

1) an oil objective of approximately $50\times$ magnification be used together with an $\times 10 \div \times 15$ eyepiece;

2) the basic cell size for measurements should be 2 mm with $\bar{D}_{\text{meas}}$ calculated for cell size of 2 mm and multiples of 2 mm;

3) a filar micrometer be used in the eyepiece and that only one reading be taken of each position;

4) $\bar{D}_{\varepsilon}$ is usually measured by taking readings at $(50 \div 100)$ μm intervals. However, $\bar{D}_{\varepsilon}$ measured in this way includes some contributions (such as micrometer screw noise and stage profile noise) not appearing in the $\bar{D}_{\varepsilon}$ for the proper cell size. In addition that part of $\bar{D}_{\varepsilon}$ arising from irreproducible microscope noise may not be determined correctly if the actual cell length is not used in measuring $\bar{D}_{\varepsilon}$. It is, therefore, preferable to use the method outlined in the paper of BISWAS *et al.* [2] which gives the $\bar{D}_{\varepsilon}$ for the actual of readings;

5) the stage profile D_y should be determined either by using an interferometer or by using the so-called « Swedish line » of BØGGILD and SCHARFF [3]. Note that the profile should be measured in such a way that no kind of additional noise (*e.g.* reading noise) is included in the numbers;

6) the cut-off should be applied at $4\bar{D}_c$ with replacement;

7) the scattering constant used should be that of PICKUP and VOYVODIC [4] with cut-off and using the experimental relation determined by the Bristol group [5] between the scattering constant $4\bar{D}_c$ cut-off with replacement ($K_{4\bar{D}_c}$-replacement) and the constant with $4\bar{D}$ cut-off only viz. ($K_{4\bar{D}_c}$-replacement) $= 1.043$ ($K_{4\bar{D}_c\,\text{cut-off}}$). When making scattering measurements in the 25 GeV region it has been observed that the distributions of measured second differences do not appear to fit with the theory (extremely few $4\bar{D}_c$ values have been found) [6]. In addition there is some indication from the work of HOSSAIN *et al.* [7] that at cell sizes above 8 mm a lower value of $\bar{D}_{\text{meas}}$ is obtained than that expected from the usual theory. It seems to us very desirable to know better the scattering constant in this energy region for the cell sizes normally used;

8) for relative scattering measurements the procedure suggested by BISWAS *et al.* [2] should be followed for microscopes of the Cosyns type stage. The separation between the two tracks should be < 50 μm in the plane of the emulsion and < 20 μm in depth. In the case of other constructions (*e.g.* Koristka *R*4) relative scattering measurements should be made by measuring successively the distances AA', BB', CC' etc. (see Fig. 1).

[2] S. BISWAS, B. PETERS and RAMA: *Proc. Ind. Acad. Sci.*, **41**, 154 (1955).

[3] J. K. BØGGILD and M. SCHARFF: *Suppl. Nuovo Cimento*, **12**, 374 (1954).

[4] E. PICKUP and L. VOYVODIC: *Phys. Rev.*, **85**, 91 (1952).

[5] Bristol group (private communication from A. BONETTI).

[6] E. DAHL-JENSEN: Report on Lausanne Meeting on Spurious Scattering and Distortion in Nuclear Emulsions (1961), p. 6.

[7] A. HOSSAIN, M. F. VOTRUBA and A. WATAGHIN: *Nuovo Cimento*, in the press (1961).

IL NUOVO CIMENTO Vol. XXII, N. 4 16 Novembre 1961

Protons from ^{32}S Bombarded by 14.4 MeV Neutrons.

B. Antolković

Institute Rudjer Bošković - Zagreb

(ricevuto il 18 Settembre 1961)

The experiemental data on the $^{32}S(n, p)^{32}P$ and $^{32}S(n, np)^{31}P$ reactions published so far ([1-5]) show notable fluctuations in the value of the total cross section for the reactions resulting in the proton emission. There are also differences in assigning the relative contributions of these reactions to the total cross section. No data are known on the « *nuclear temperature* » (*) of the residual nucleus from the ^{32}S (n, np) ^{31}P reaction. The purpose of this paper is to present some of our recent results on the $^{32}S(n, p)^{32}P$ and $^{32}S(n, np)^{31}P$ reactions. So far the « *nuclear temperature* » of the residual nucleus from the $^{32}S(n, np)^{31}P$ reaction has been obtained, the angular distribution of the backward angles being in the course of study.

The energy spectrum and the angular distribution of protons emitted from

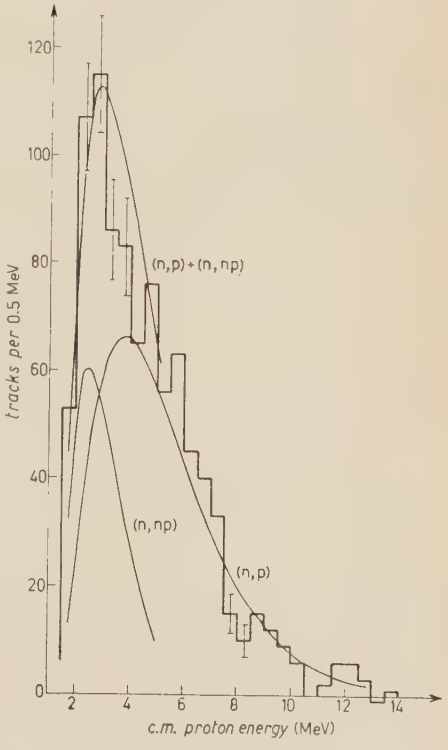

Fig. 1. – Energy distribution of protons from ^{32}S. The smooth curves represent the normalized theoretical proton distributions calculated for (n, p), (n, np) and (n, p) + (n, np) processes.

(*) In the case of n,np reactions the slope of the spectrum of proton gives an « apparent temperature »

([1]) E. B. Paul and R. L. Clarke: *Can. Journ. Phys.*, **31**, 267 (1953).

([2]) L. Allen, Jr., W. A. Biggers, R. S. Prestwood and K. R. Smith: *Phys. Rev.*, **107**, 1363 (1957).

([3]) H. P. Eubank, R. A. Peck, Jr. and F. L. Hassler: *Nucl. Phys.*, **9**, 273 (1958).

([4]) L. Colli, I. Iori, G. Marcazzan, F. Merzari, A. M. Sona and P. G. Sona: *Nuovo Cimento*, **17**, 634 (1960).

([5]) D. L. Allan: *Nucl. Phys.*, **24**, 274 (1961).

^{32}S bombarded by 14.4 MeV neutrons have been determined using a photographic plate method. Nuclear plates allow measurements of low energy protons, and so it is possible to estimate the nuclear temperature of the (n, np) reaction.

The energy spectrum of protons emitted in the angular interval from 0° to 65° was examined. The spectrum is represented in Fig. 1. Although it is expected that protons from direct interaction should be present, nevertheless the hystogram has a Maxwellian distribution shape indicating that the main contribution to the proton spectrum comes from the decay of the compound nucleus. By plotting the data from Fig. 1 in a $\ln N(E_p)/\sigma_c(E_p)E_p$ versus E_p diagram (Fig. 2), where $N(E_p)$ is the number of protons observed in an energy interval $E_p \pm 0.25$ MeV and σ_c is the cross section for the formation of the compound nucleus by bombarding the residual nucleus with protons of energy E_p, one obtains two straight lines. From the slope of these lines it is possible to estimate the nuclear temperature of the residual nucleus for the compound nucleus part of the (n, p) and (n, np) reactions. The change of the slope at 5.15 MeV illustrates the outset of the (n, np) reaction.

For the diagram represented on Fig. 2 all the measured tracks were used, while the diagram on Fig. 3 contains only the tracks making an angle greater than 45° with the incident neutrons. The first diagram could therefore contain direct interaction protons from the $^{32}S(n, p)^{32}P$, as well as deuterons from the $^{32}S(n, d)^{31}P$ reactions. The deuteron tracks were measured simultaneously with the proton tracks because the poor resolution between proton and deuteron tracks in nuclear emulsions

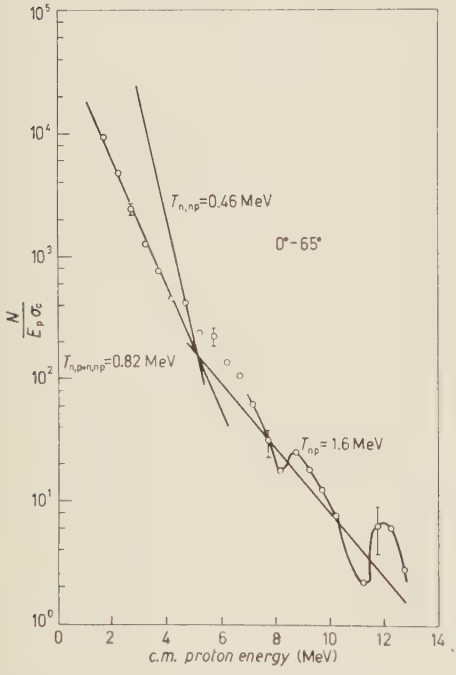

Fig. 2. – Statistical theory plot for protons emitted in the angle interval of 0°÷65°.

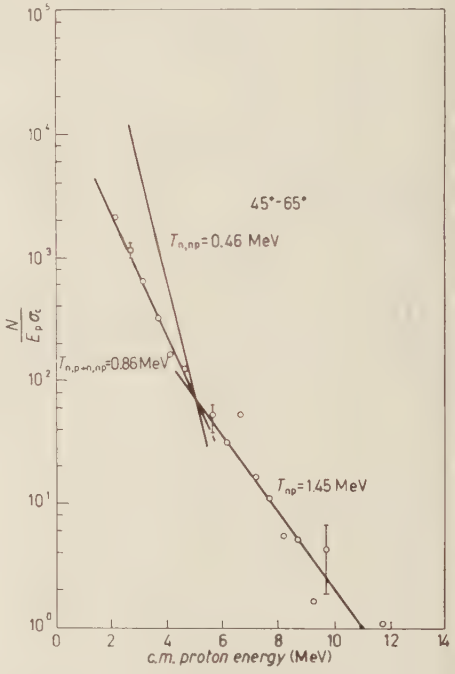

Fig. 3. – Statistical theory plot for protons emitted in the angle interval of 45°÷65°.

does not allow an accurate identification of the kind of particles in consideration (6). As the ground state transition of the $^{32}S(n, d)^{31}P$ reaction gives deuterons of energy 7.07 MeV in the C.M. system and the tracks of these deuterons have the same length as the 5.5 MeV protons, they are expected at the position of (5.5 ± 0.7) MeV on the proton energy scale. The fact that the experimental points in this energy interval all lie above the lines corresponding to (n, p) and (n, np) reactions shows the presence of the deuterons. Therefore the points in the energy interval of (5.5 ± 1.0) MeV were omitted in the calculation of the nuclear temperature. The least squares fit restricted to the energy intervals from 1.7 to 4.5 MeV and from 6.5 to 13.5 MeV gives the values: $T_{(n,p)+(n,np)} = 0.82$ MeV and $T_{n,p} = 1.6$ MeV. The latter value is based on few experimental points and it is difficult to say whether the peaks of the curve drawn through the experimental points represent a gross structure of the proton distribution, or they are only statistical fluctuations. The energy spectrum based on the data of protons making an angle greater than 45° gives the nuclear temperatures: $T_{n,p} = 1.45$ MeV and $T_{(n,p)+(n,np)} = 0.86$ MeV.

The value of $T_{(n,p)+(n,np)}$ was corrected for the contribution of the (n, p) process, and the nuclear temperature of $T_{n,np} = 0.46 \pm 0.06$ MeV, was obtained for the $^{32}S(n, np)^{31}P$ process.

With the above values for nuclear temperatures $T_{n,p} = 1.5$ MeV, $T_{n,np} = 0.46$ MeV, the theoretical proton distribution for the (n, p) and (n, np) reactions based on the statistical theory (7) were calculated. They are shown on Fig. 1 Supposing an isotropic angular distribution, the ratio of the areas under the (n, np) and (n, p) proton distribution curves gives the ratio of the cross sections of the (n, np) and (n, p) processes, both going via the formation of the compound nucleus. The value obtained is $\sigma_{n,np}/\sigma_{n,p} = 0.33$. This considerable value for the (n, np) process can be understood taking into account the Q values for the (n, 2n) and (n, np) reactions which are -14.71 MeV and -8.85 MeV respectively. One can see that the (n, 2n) reaction on ^{32}S induced by neutrons of 14.4 MeV is completely inhibited by its big negative Q value.

(6) D. L. ALLAN: *Proc. Phys. Soc.*, A **70**, 195 (1957).

(7) J. M. BLATT and V. F. WEISSKOPF: *Theoretical Nuclear Physics* (New York, 1952).

Scattering of Low Energy K^--Mesons by Nuclei (*).

J. H. Hetherington and D. G. Ravenhall

Physics Department, University of Illinois - Urbana, Ill.

(ricevuto il 18 Settembre 1961)

We present the results of a calculation which links the low-energy K^--proton scattering amplitudes with the optical potential for K^--mesons in nuclei. A comparison of the predicted K^--nucleus scattering with the appropriate low-energy emulsion data (1) is made, from which it appears that the $(a-)$ zero-range solution of Dalitz and Tuan (2) is a significantly poorer fit than the $(a+)$ and $(b+)$ solutions. Our results do not favor the $(b-)$ solution either, but they are less reliable in this case.

The importance of making this comparison at energies low enough that effective-range contributions to the scattering amplitudes do not change their character has been discussed by Hill *et al.* (1), following the remarks of Karplus *et al.* (3). The data of Hill *et al.* are fortunate in this respect, covering an energy range from 35 to 85 MeV, centered at 50 MeV. Our calculation assumes the validity at these energies of the zero-range approximation to the K^--nucleon center of mass scattering matrix:

$$(1) \quad t_i = -(4\pi/2\mu) f_i = (4\pi/2\mu) A_i/(1 - ikA_i) .$$

A_i is the complex scattering length in the isospin state $i(=0, 1)$, k is the relative momentum and μ the reduced mass. For all four sets of solutions (2), expression (1) represents an attractive interaction since for the $(+)$ solutions $\mathrm{Re}\, t_i$ is negative and for the $(-)$ solutions the t_i have poles in the second quadrant

(*) This work has been supported by the joint program of the U.S. Office of Naval Research and the U.S. Atomic Energy Commission.

(1) R. D. Hill, J. H. Hetherington and D. G. Ravenhall: *Phys. Rev.*, **122**, 267 (1961).

(2) R. H. Dalitz and S. F. Tuan: *Ann. Phys.*, **8**, 100 (1959). We have in fact used the following more recent set of scattering lengths [R. H. Dalitz: *Rev. Mod. Phys.*, **33**, 471 (1961)]:

$(a-)$, $A_0 = 0.05 + i\,1.10$, $A_1 = 1.45 + i\,0.35$;

$(b-)$, $1.15 + i\,2.00$, $0.70 + i\,0.15$;

$(a-)$, $-0.75 + i\,2.00$, $-0.85 + i\,0.21$;

$(b-)$, $-1.85 + i\,1.10$, $-0.10 + i\,0.65$.

All lengths are in fermi. We thank Dr. Dalitz for this information.

(3) R. Karplus, L. Kerth and T. Kycia: *Phys. Rev. Lett.*, **2**, 510 (1959).

of k (4). While the (+) solutions must necessarily produce an attractive optical potential, it is not at all obvious what is to be expected from the (—) solutions. Because of the energy restrictions mentioned earlier, the Watson high-energy limit (5), in which $\mathrm{Re}\, U \propto -\mathrm{Re}\, t$, is not a reliable guide. The effects of nucleon Fermi-motion and binding energy, and of the self-consistent inclusion of U, the meson optical potential, are to make accessible the pole in t_i. In effect, the meson is able to appreciate the fact that the interaction is attractive, although $\mathrm{Re}\, t_i$ had led it to understand a repulsion. Thus for the (—) solutions $\mathrm{Re}\, U$ is expected to depend on meson energy and nuclear density in a sensitive way, which must be examined by many-body techniques. A calculation with the same object as ours has been made by MARTIN (6). So far as we can ascertain, however, he does not include the effect of the pole in t by calculating the bound matrix τ (see below). This, because it can even change the sign of $\mathrm{Re}\, U$, is crucial.

The basic calculation is of the optical potential U (single-particle potential) of a meson in nuclear matter. The nuclear matter is described by a degenerate Fermi gas, with the nucleon single-particle potential $W(p)$ determined by BRUECKNER and GAMMEL (7). Keeping only collisions of the K meson with one nucleon at a time, but in the presence of all the other nucleons, we express U as the sum of all meson-*bound nucleon* collision amplitudes τ (8):

$$U = \sum_{\text{nucleons}} \tau \,, \tag{2}$$

where

$$\tau = t\{1 + [(E_0 - a + i\varepsilon)^{-1} - (E_1 - h + i\varepsilon)^{-1}]\tau\} \,. \tag{3}$$

Both t and τ are matrices involving absorption into the pion-hyperon channels, as well as elastic scattering. We ignore the *nuclear interaction* of these reaction products, so that the presence of nuclear matter does not affect the reaction channels. It then turns out that (3) involves only the elastic scattering channel. Thus $h = T_{\mathrm{K}} + T_{\mathrm{p}}$ is the Hamiltonian of the meson and a single free nucleon, and

$$a = T_{\mathrm{K}} + U + \sum_i (T_{\mathrm{p}_i} + W_{\mathrm{p}_i}) \,,$$

is the Hamiltonian of the whole system, including U. The boundary condition is for outgoing scattered waves. The operator τ, for any given incident energy T_{K}, depends on both the meson virtual momentum and the momentum of the struck nucleon. U is obtained, as in (2), by integrating over the nucleon momenta. It still depends on the meson virtual

(4) To represent a truly repulsive interaction, in which $\mathrm{Re}\, t_i$ is positive but with no accessible pole in the second quadrant of k, one can use for the (—) solutions the zero range approximation $\delta = kR$. With R a complex length, $\mathrm{Re}\, R < 0$, this is a trivial generalization of the corresponding potential-scattering result. The K⁻-proton scattering data can be fitted just as well as with the usual zero-range assumption $k \operatorname{ctg} \delta = 1/A$. The quantities $|R|$ are somewhat smaller than the corresponding $|A|$, but some are still considerably larger than the expected range $(2m_\pi)^{-1}$, an undesirable feature for a repulsive interaction (3). In any case, the predicted optical potentials would be repulsive for all densities, and so could be ruled out by the emulsion experiments.

(5) See, for example, K. M. WATSON: *Rev. Mod. Phys.*, **30**, 565 (1958).

(6) A. D. MARTIN: *Nuovo Cimento*, **21**, 88, (1961). We thank Dr. MARTIN for a preprint of his paper.

(7) K. A. BRUECKNER and J. L. GAMMEL: *Phys. Rev.*, **109**, 1023 (1958); K. A. BRUECKNER, J. L. GAMMEL and J. T. KUBIS: *Phys. Rev.*, **118**, 1438 (1960). We have used as an approximation to the single-nucleon energy $E_1(p, \Sigma)$, for $\Sigma = 0.95$, including the rearrangement energy.

(8) See, for example, K. M. WATSON: *Phys. Rev.*, **105**, 1388 (1957); A. KERMAN, H. MCMANUS and R. M. THALER: *Ann. Phys.*, **8**, 551 (1959).

momentum, and parametrically on the nucleon density and T_K. Because of the extremely simple form (1) of t_i, the formal eq. (3) has the solution

$$\tau = -(4\pi/2\mu)\, A/[1 - i(k_1 - B)A]\,, \tag{4}$$

where B is a two-dimensional definite integral involving U, and k_1 characterizes a particular collision. The form of eq. (4) justifies our earlier remarks about the influence of the pole in t_i: B is complex and for some accessible situations $\mathrm{Re}\,\tau$ for the (—) solutions is negative. The integrals involved in B, (4), and in evaluating U, (2), are performed numerically, and the whole process iterated until a self-consistent function U of the virtual meson momentum is obtained [9]. Because of this momentum dependence, the Fourier transform of U would not be local in configuration space. We ignore this nonlocality, and choose as the appropriate local value $U(k_0)$, where k_0 is the solution of

$$T_K = k_0^2/2m_K + U(k_0)\,. \tag{5}$$

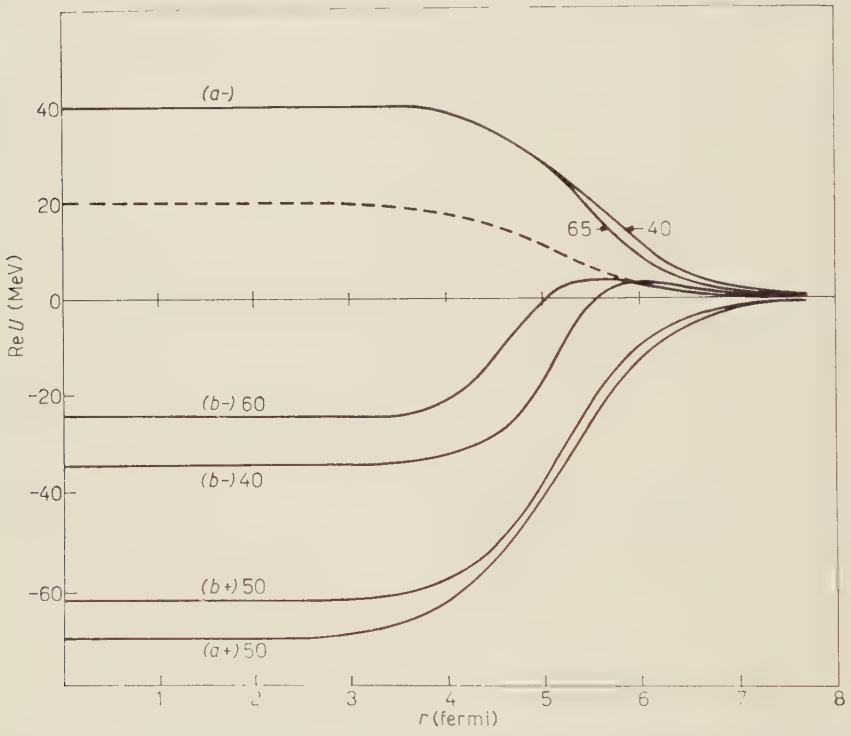

Fig. 1. – Re U, the real part of the meson optical potentials, in MeV, *vs.* radius in fermi, for silver. The Fermi shape assumed for the nucleon density is the dashed line. The labels on the curves indicate the corresponding Dalitz-Tuan solution, and the meson kinetic energy.

k_0 is complex in general. We obtain $U(k_0)$ by making an analytic continuation of a suitable approximate expression fitted to our $U(k)$ on the real axis. All of this procedure thus obtains a local

[9] The computations were performed on ILLIAC. We thank Dr. J. N. SNYDER and members of the Illinois Digital Computer Laboratory for their support of this work.

optical potential, for any particular T_K, at some particular density.

The radial dependence of $U(r)$ near the nuclear surface is obtained by repeating the above calculation (for infinite nuclear matter) at the density appropriate to each value of r, with values of $W(p)$ extrapolated from those of BRUECKNER and GAMMEL [7]. With this assumption, the bound scattering matrix τ approaches the free scattering matrix t at the nuclear edge. The (—) solutions, in which the influence of the pole depends sensitively on nuclear density, lead to radial dependences for U which can be surprising, and which certainly cannot be approximated by the nuclear density itself. With $(b-)$, where the pole is close to threshold and easily accessible, U is negative in the center of the nucleus, but becomes positive at the edge, as $\tau \to t$. The effect is not so marked for $(a-)$ because the pole is further from threshold. For the (+) solutions, as we have implied earlier, no changes of sign occur, and everything is straightforward.

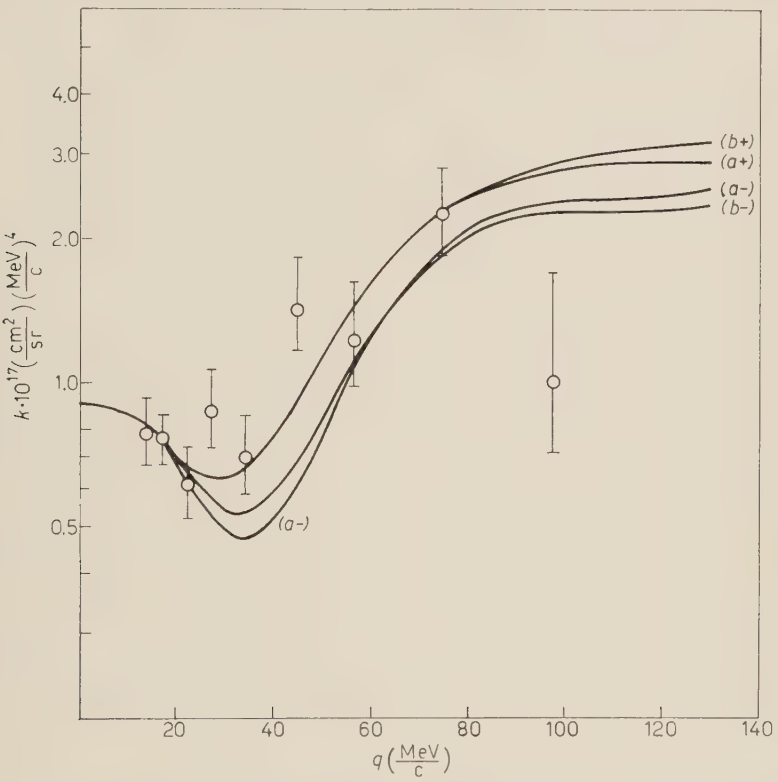

Fig. 2. - The quantity $k \cdot q^4(d\sigma/d\Omega)$, averaged over incident energy and emulsion elements, *vs.* recoil momentum q. The experimental points are taken from HILL *et al.* [1].

The optical potentials $U(r)$ shown in Fig. 1 are obtained by assuming a Fermi radial density distribution, with parameters determined from electron scattering [10]. Cross sections calculated by means of a partial wave analysis [1], at $T_K = 65$ MeV and 40 MeV for the (—)

[10] B. HAHN, D. G. RAVENHALL and R. HOFSTADTER: *Phys. Rev.*, **101**, 1131 (1956).

solutions, and 50 MeV for the (+) solutions, and for three typical nuclei, $Z=8$, 35, and 47, are compared with the experimental data of Hill *et al.* [1], Fig. 2. From a least-squares analysis, the χ^2 for the four solutions $a+$, $b+$, $a-$, $b-$ are respectively 12, 12, 55, and 37. The discrimination among the solutions seems to be greater than in the corresponding K^--p experimental comparisons [11]. Additional emulsion data in this energy range are very desirable.

Of the many approximations necessary in this calculation, we think that the most fundamental is the treatment of the surface as infinite nuclear matter at reduced density [12]. For the $(b-)$ solution it is the fact that Re $U(r)$ is repulsive at the edge of the nucleus which determines the cross section in the interference region, because of the strong absorption of the meson wave in the nucleus. For the other solutions, however, including $(a-)$, Re $U(r)$ does not change sign, and the results should not depend crucially on this approximation. Also, in the case of $(b-)$, the extrapolation to $U(k_0)$, eq. (5), is rather sensitive to small variations. It is worth remarking that in all cases it is the relative values of Re $U(r)$ and Im $U(r)$ which are important, not the actual radial dependence of the density. This we checked by repeating some of the cross-section calculations using instead of the Fermi density distribution the equally preferable modified Gaussian distribution [9].

In the many-body part of the calculations, eq. (2) keeps only the first term of a multiple-scattering series. We expect higher terms of the series to be small if the range of the K^--p interaction is short. MARTIN [6] estimates such effects (nucleon correlation) to be small, and certainly not big enough to affect our conclusion qualitatively. Other approximations, of a more computational nature, may need further study, although we are not aware of any substantial defects. Our results do depend on the zero-range scattering lengths, of course, and will have to be recalculated as these parameters are modified by further K^--p experiments.

A more detailed discussion of the many-body aspects of the calculation, and of possible extensions, will be given elsewhere.

[11] R. C. KING, R. E. LANOU jr. and S. F. TUAN: *Phys. Rev. Lett.*, **6**, 500 (1961).

[12] For a discussion of the corresponding treatment for nuclear matter see K. A. BRUECKNER, J. L. GAMMEL and H. WEITZNER: *Phys. Rev.*, **110**, 431 (1958).

On the Behaviour of the Multiple Scattering Constant, K, for Nuclear Emulsions, at Large Cell Sizes.

A. Hossain (*), M. F. Votruba (**), A. Wataghin (***) and D. Evans

CERN, European Organization for Nuclear Research - Geneva

(ricevuto il 7 Ottobre 1961)

In a previous paper Hossain *et al.* (1) have reported results on multiple scattering measurements on the tracks of high energy particles in nuclear emulsions. Indications were found of a possible discrepancy between the theoretically expected values of the mean scattering angle and that found experimentally at cell sizes, t, greater than 1 cm.

In this letter we *a*) present the results of measurements on a further sample of tracks produced by negative pions of 16.2 GeV/c momentum, which confirm the measurements, made in the same stack, reported in (1); *b*) present the results of measurements on the tracks of 8.2 GeV/c muons, which also show the same effect as was obtained from the measurements on the pion tracks; and *c*) calculate the value of the scattering constant, K, needed to fit our data for values of t greater than 1 cm.

The experimental procedure has already been described (1). The microscope used was a Koritska type R-4. The total noise (stage, reading and grain noise) was ~ 0.2 μm, which for $t > 1$ cm is negligible compared with the signal ($\geqslant 8$ μm) from the multiple Coulomb scattering. A 30× objective was employed giving a field of view of 150 μm width. A basic cell size of 1 cm was used for the measurements and values of the mean second difference $\bar{D}$ for 2 cm and 3 cm cell sizes were obtained using non-overlapping cells.

We have considered carefully the question of bias in our experimental data. Due to the low-power objective used no tracks had to be abandoned due to a large angle scattering along its path. All the tracks that were measured have been included in the results. The « flat chamber effect » (caused by the finite thickness of the emulsion) is negligible at the scattering angles with which we are concerned (see Menon *et al.* (2)). The low resolution

(*) On leave from Pakistan Atomic Energy Commission. Ford Foundation Fellow, CERN.

(**) On leave from Physical Institute of Czechoslovak Academy of Sciences, Prague, IAEA Fellow, Vienna.

(***) On leave from Centro Brasileiro de Pesquisas Físicas, Rio de Janeiro, Ford Foundation Fellow, CERN, Geneva.

(1) A. Hossain, M. F. Votruba and A. Wataghin: *Nuovo Cimento* (1961), in press.

(2) M. G. K. Menon, C. O'Ceallaigh and O. Rochat, *Phil. Mag.*, **42**, 932 (1951).

of the optical system we have used could only have the effect of adding noise to the measured $\bar{D}$ and hence increasing the experimental value of K. This effect is seen to be small since within statistical errors the present results from the pion stack agree with those reported in (1), which were obtained using a 55× objective.

($(8.12 \pm 0.35)\,\mu$m) is in agreement with that obtained from the previous measurements and reported in (1), viz. $(7.9 \pm 0.6)\,\mu$m. In Fig. 1 are also plotted the expected variations of K with cell-size following the Williams' (3) theory for a point charge nucleus (curve 1), and his correction for the finite size of the nucleus (curve 2). We have taken Williams'

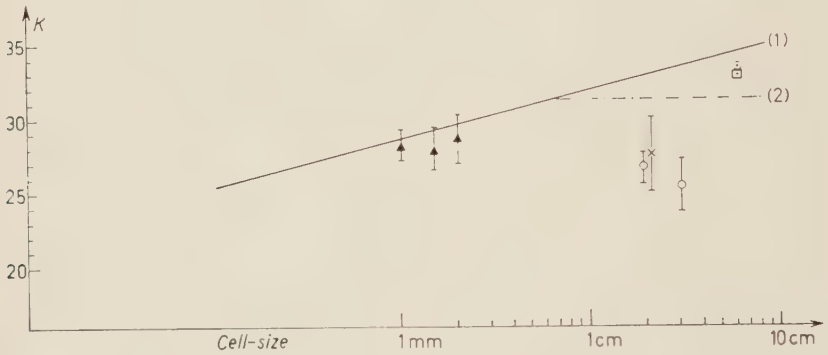

Fig. 1. – The variation of scattering constant, K, with cell size t. For curves (1) and (2) see text. ▲ points of BRISBOUT *et al.* (5); ○ present work, pion data; × present work, muon data; ⊙ from COOPER and RAINWATER (6); ⊡ from OLBERT (7).

The scattering constant K was calculated from the experimental values of the mean second difference $\bar{D}$, using the known momenta of the beam particles, and assuming spurious scattering to be zero. Any correction for a finite amount of spurious scattering will only make the calculated values of K smaller.

The values of $\bar{D}$ and of K are given in Table I and Fig. 1. The value of $\bar{D}$ for 2 cm cells in the pion stack curves from the paper of VOYVODIC and PICKUP (4).

For our energy range, the measurements in the region of cell-sizes up to ~ 1 cm are likely to overestimate the value of $\bar{D}$ by $\leqslant 10\%$ because of

TABLE I.

Cell-size (mm)	π^--mesons (16.2 GeV/c)		μ^--mesons (8.2 GeV/c)	
	$\bar{D}$ (in μm)	K	$\bar{D}$ (in μm)	K
20	8.12 ± 0.35	26.6 ± 1.15	16.58 ± 1.5	27.5 ± 2.5
30	14.20 ± 1.00	25.4 ± 1.8	—	—

(3) E. J. WILLIAMS: *Proc. Roy. Soc.* (*London*), A **169**, 531 (1939).

(4) L. VOYVODIC and E. PICKUP: *Phys. Rev.*, **85**, 91 (1952).

the influence of spurious scattering, and so we have not used them for the purpose of studying the behaviour of the scattering constant.

The experimental points obtained at 1 mm, 1.5 mm and 2 mm cell sizes by BRISBOUT *et al.* [5], which are free from spurious scattering since they were obtained by relative scattering measurements, are also given in Fig. 1.

Our data for 2 cm and 3 cm cell-sizes and the Brisbout points suggest that the simplest assumption for practical purposes is to take a constant value of scattering constant $K=27.6\pm0.6$ (the weighted average of the experimental points in Fig. 1) in the cell size range 1 mm to 3 cm. This value of $K=27.6$ is, at the 2 cm cell-size, about 15% lower than curve 1 and about 11% lower than curve 2.

COOPER and RAINWATER have calculated the angular distribution for multiple scattering of 1 GeV μ-mesons in 1 cm of lead [6]. The average angle is about 3% lower than the Molière calculation (which is equivalent to the Williams' point-charge calculation).

Olbert's calculation [7] gives an average angle 4% lower than Molière's prediction. The points of Cooper and Rainwater and of Olbert are plotted in Fig. 1, at a cell size of 6 cm of emulsion, which is approximately equivalent to 1 cm of lead.

The agreement between our muon and pion data suggests that, within the errors of the measurements, the contribution of nuclear forces is not important in the phenomena discussed in this paper. The introduction of an extended charge for the nucleus brings the theoretical curve for K nearer to the experimental points. Possibly, some changes in the statistical treatment of the theory of multiple Coulomb scattering may further contribute to a better fit of our data to theoretical predictions.

* * *

Our grateful thanks are due to Dr. W. O. LOCK and Dr. G. VANDERHAEGHE for many fruitful discussions during the course of the work. The emulsions used were exposed in muon and pion beams set up at the CERN PS by the Group of Dr. B. D. HYAMS and by Dr's H. BINGHAM, B. DE RAAD and R. G. P. VOSS respectively. We are indebted to them and to the PS machine Division for their kind cooperation. The emulsions exposed in the pion beam were processed by Mr. M. A. ROBERTS, Mr. R. STERCHI and Dr. G. VANDERHAEGHE. We are indebted to Dr. M. GAILLOUD and his colleagues at the Ecole Polytechnique, Lausanne, for the loan of their emulsions which they exposed in the muon beam.

[5] F. A. BRISBOUT, C. DAHANAYAKE, A. ENGLER, P. H. FOWLER and P. B. JONES: *Nuovo Cimento*, **3**, 1400 (1956).

[6] L. N. COOPER and J. RAINWATER: *Phys. Rev.*, **97**, 492 (1955).

[7] S. OLBERT: *Phys. Rev.*, **96**, 1400 (1954).

$V-A$ or $V+A$ Interaction in μ-Meson Capture?

R. Silbar and H. Überall

Harrison M. Randall Laboratory of Physics, University of Michigan - Ann Arbor, Mich.

(ricevuto il 7 Ottobre 1961)

We wish to investigate to what extent the μ-meson capture interaction is determined by present evidence, and in particular whether a negative relative sign of vector and axial vector coupling is established. The analysis is based on the effective muon capture interaction as given by Primakoff ([1,2]), and considers the observable quantities: capture rates, neutron asymmetries, and hyperfine effect.

Total capture rates have been measured on many nuclei ([3-5]), but Primakoff's formula ([2]) describes only their gross features, and is handicapped by our ignorance of the average neutrino momentum, as are the few existing shell model calculations ([6]). The best way for a determination of the coupling seems to be the partial rate of

$$(1) \qquad \mu^- + {}^{12}\mathrm{C} \to {}^{12}\mathrm{B} + \nu \,,$$

leading to the ^{12}B ground state, recently re-measured ([7]) to be

$$\lambda_B = (6.31 \pm 0.24) \cdot 10^3 \ \mathrm{s}^{-1} \,,$$

in agreement with three other results (and disagreeing with two) ([8-12]). The theoretical rate is given in ref. ([1]) (in close agreement with the results of other workers ([13])), in terms of the effective

([1]) A. Fujii and H. Primakoff: *Nuovo Cimento*, **12**, 327 (1959).

([2]) H. Primakoff: *Rev. Mod. Phys.*, **31**, 802 (1959).

([3]) J. C. Sens: *Phys. Rev.*, **113**, 679 (1959).

([4]) A. Astbury, M. A. R. Kemp, N. H. Lipman, H. Muirhead, R. G. P. Voss, G. Zangger and A. Kirk: *Proc. Phys. Soc.*, **72**, 494 (1958).

([5]) A. Astbury, I. M. Blair, M. Hossain, M. A. R. Kemp and H. Muirhead: to be published (1961).

([6]) G. H. Burkhardt and C. A. Caine: *Phys. Rev.*, **117**, 1375 (1960).

([7]) E. J. Maier, B. L. Bloch, R. M. Edelstein and R. T. Siegel: *Phys. Rev. Lett.*, **6**, 417 (1961).

([8]) T. N. K. Godfrey: *Thesis*, Princeton Univ. (1954): 5.9 ± 1.5.

([9]) J. G. Fetkovich, T. H. Fields and R. L. McIlwain: *Phys. Rev.*, **118**, 319 (1960): 6.8 ± 1.1.

([10]) B. L. Bloch: *Thesis*, Carnegie Institute of Technology (1960): 5.8 ± 1.3.

([11]) F. B. Harrison, H. V. Argo, H. W. Kruse and A. D. McGuire: *Phys. Rev.*, **114**, 626 (1959): 9.05 ± 0.95.

([12]) J. O. Burgman, J. Fischer, B. Leontic, A. Lundby, R. Meunier, J. P. Stroot and J. D. Teja: *Phys. Rev. Lett.*, **1**, 469 (1958): 9.18 ± 0.5.

([13]) G. Flamand and K. W. Ford: *Phys. Rev.*, **116**, 1521 (1959); L. Wolfenstein: *Nuovo Cimento*, **13**, 319 (1959).

coupling constants

$$(2)\qquad \begin{cases} G_V = g_V\left(1 - \dfrac{\nu}{2m_p}\right), \\ G_A = g_A - g_V\,(1+\mu_p-\mu_n)\dfrac{\nu}{2m_p}, \\ G_P = [g_P - g_A - g_V(1+\mu_p-\mu_n)]\dfrac{\nu}{2m_p}, \end{cases}$$

with ν the neutrino momentum, m_p the proton mass, μ_p and μ_n the nucleon anomalous magnetic moments, and the dressed coupling constants

$$(3)\qquad g_V = 0.97 g_V^\beta,$$

assuming a conserved vector current [14];

$$(4)\qquad g_P = 8 g_A,$$

determined phenomenologically [15] and from dispersion relations [16] (including the sign); we further take from β-decay

$$(5)\qquad g_A^\beta = -1.21 g_V^\beta,$$

and finally set

$$(6)\qquad g_A = x g_V,$$

with x (and its sign) to be determined. WOLFENSTEIN [17] estimates a 20% uncertainty in the shell model calculations. Assuming that and taking the value of λ_B of ref. [7], we find from [1]

$$(7)\qquad \Gamma_A^2 = (0.87\pm 0.17)(g_A^\beta)^2,$$

with

$$\Gamma_A^2 = G_A^2 + \tfrac{1}{3}G_P^2 - \tfrac{2}{3}G_A G_P.$$

the two possible values

$$(8)\qquad \begin{cases} x^{(+)} = 1.46\pm 0.13, \\ x^{(-)} = -1.10\pm 0.13. \end{cases}$$

One check is provided by the asymmetry of the emitted neutrons, measured [18] relative to the muon decay electron asymmetry in S and Mg as $a = -0.32$, -0.39, respectively (if one assumes a smearing factor [19] $\varphi = 0.773$ due to the nuclear proton motion). The difference of the a's reflects the large uncertainty in φ and suggests we take

$$a = -0.35\pm 0.10.$$

From [2]

$$(9)\qquad a = \frac{G_V^2 - G_A^2 + \tfrac{1}{3}G_P^2 - \tfrac{2}{3}G_A G_P}{G_V^2 + 3G_A^2 + G_P^2 - 2G_A G_P},$$

and (8), we find two sets

$$(10)\qquad \begin{cases} a^{(+)} = -0.19\mp 0.06, \\ a^{(-)} = -0.37^{+0.06}_{-0.04}, \end{cases}$$

favoring $x^{(-)}$, but not in a very convincing fashion, due to the uncertainties in measuring a.

The hyperfine effect, recently suggested [20] to be measured via the neutral products of the capture reaction, depends on $\delta = \Delta\lambda/\lambda$, where

$$\lambda = n_+\lambda_+ + n_-\lambda_-, \qquad \Delta\lambda = \lambda_+ - \lambda_-,$$

($\lambda_\pm$ = capture rates in $F = J \pm \frac{1}{2}$ hyperfine states, $n_\pm$ = hyperfine populations). In $^{19}_{9}$F, the nucleus most suitable for the experiment, both λ and $\Delta\lambda$ were calculated on the shell model [6,21]. Both

[14] R. P. FEYNMAN and M. GELL-MANN: *Phys. Rev.*, **109**, 193 (1958).

[15] L. WOLFENSTEIN: *Nuovo Cimento*, **8**, 882 (1958).

[16] M. L. GOLDBERGER and S. B. TREIMAN: *Phys. Rev.*, **111**, 355 (1958).

[17] L. WOLFENSTEIN: *Proc. of the 1960 Annual International Conference on High-Energy Physics at Rochester* (New York, 1960), p. 529.

[18] V. L. TELEGDI: *Proc. of the 1960 Annual International Conference on High-Energy Physics at Rochester* (New York, 1960), p. 713.

[19] H. ÜBERALL: *Nuovo Cimento*, **6**, 533 (1957).

[20] R. WINSTON and V. L. TELEGDI: *Phys. Rev. Lett.*, **7**, 104 (1961).

[21] H. ÜBERALL: *Phys. Rev.*, **121**, 1219 (1961).

are proportional to $\bar{\nu}^2$, the (largely unknown) average squared neutrino momentum, so $\delta = \Delta\lambda/\lambda$ is practically free of it:

$$\delta = 1.59 \cdot \frac{0.879b - 1.003b' + 0.436b''}{G_V^2 + 3G_A^2 + G_P^2 - 2G_A G_P} \,, \tag{11}$$

where

$$\begin{cases} b = 2G_A(G_V - G_A) - \frac{2}{3}G_V G_P + \frac{4}{3}G_A G_P, \\ b' \quad G_V(G_A - \frac{1}{3}G_P) \,, \\ b'' \quad G_A(G_A - \frac{2}{3}G_P) \,, \end{cases} \tag{11a}$$

and with (8), comes out as (for $^{19}_{9}\mathrm{F}$)

$$\begin{cases} \delta^{(+)} = -0.26 \mp 0.03 \,, \\ \delta^{(-)} = -0.78 \pm 0.01 \,. \end{cases} \tag{12}$$

Due to the large difference between these values, their considerable insensitivity to the uncertainties in $x^{(\pm)}$ and their resulting accuracy, this will be a decisive method for determining the sign of x, or the sign in the muon capture interaction $V \pm A$.

Corresponding values of $\bar{\nu}$ can be obtained assuming that the capture rate measured ([3]) really represents

$$\lambda_- = \lambda - \tfrac{3}{4}\Delta\lambda \,,$$

due to the fast hyperfine conversion ([20]), and we find

$$\begin{cases} \bar{\nu}^{(+)} = (0.88 \mp 0.08)\, m_\mu \,, \\ \bar{\nu}^{(-)} \quad (0.75 \pm 0.06)\, m_\mu \,, \end{cases} \tag{13}$$

whereas an *a priori* estimate is ([2])

$$\bar{\nu} = (0.75 \div 0.80)\, m_\mu .$$

Another determination of the sign of x has been attempted ([22]). It is however based on a μ-decay asymmetry parameter in ^{31}P, for which two contradicting values of $\frac{1}{2}$ ([23]) and zero ([24]) have been reported. Therefore, this question awaits another decisive experiment before it can be accepted as evidence.

Finally, one could take, again for ^{19}F, λ from Primakoff's formula ([2,3]), again assuming that Sens' value $2.54 \cdot 10^5\ \mathrm{s}^{-1}$ is really λ_-, and so explain its deviation from the Primakoff line. This would give $\lambda = 1.54 \cdot 10^5\ \mathrm{s}^{-1}$, and taking into account uncertainties in the measured capture rate as exemplified by another measurement ([4]) $(\lambda_- = (2.72 \pm 0.20) \cdot 10^5\,\mathrm{s}^{-1})$, we get further $\Delta\lambda = (-1.33 \mp 0.48) \cdot 10^5\ \mathrm{s}^{-1}$. Then obtaining $\bar{\nu}$ from the condition that λ is on the Primakoff line, we get from the shell model ([21])

$$(\Delta\lambda)^{(+)} = (-0.62 \mp 0.09) \cdot 10^5\ \mathrm{s}^{-1} \,,$$

$$(\Delta\lambda)^{(-)} \quad (-1.90 \pm 0.01) \cdot 10^5\ \mathrm{s}^{-1} \,.$$

Both values contradict the above $\Delta\lambda$.

Alternatively, (as pointed out to us by Professor PRIMAKOFF), if we use $(\Delta\lambda)^{(\pm)} = \delta^{(\pm)} \cdot \lambda$ with $\lambda = 1.54 \cdot 10^5\ \mathrm{s}^{-1}$ and with $\delta^{(\pm)}$ from (12), we obtain

$$(\Delta\lambda)^{(+)} = (-0.40 \pm 0.13) \cdot 10^5\ \mathrm{s}^{-1} \,,$$

$$(\Delta\lambda)^{(-)} = (-1.20 \pm 0.40) \cdot 10^5\ \mathrm{s}^{-1} \,,$$

and thus the $V-A$ result for $\Delta\lambda$ compares favorably with the above «experimental» $\Delta\lambda$.

* * *

We wish to thank Mr. R. WINSTON for a discussion of his proposed experiment, and Prof. H. PRIMAKOFF for his comments.

([22]) L. B. EGOROV, G. V. ZHURAVLEV, A. E. IGNATENKO, A. V. KUPTSOV, LI SUAN-MIN and M. G. PETRASCU: Laboratory of Nuclear Problems (Dubna) Report D-701 (1961), unpublished.

([23]) L. B. EGOROV, A. E. IGNATENKO and D. CHULTÉM: *Žurn. Eksp. Teor. Fiz.* (*USSR*), **37**, 1517 (1959) [translation: *Sov. Phys. JETP*, **10** (37), 1077 (1960)].

([24]) J. L. LATHROP, R. A. LUNDY, V. L. TELEGDI and R. WINSTON: *Žurn. Eksp. Teor. Fiz.* (*USSR*), to be published.

IL NUOVO CIMENTO Vol. XXII, N. 4 16 Novembre 1961

Integral Equations for the Process $3\pi \to 3\pi$ (*).

P. Carruthers

Laboratory of Atomic and Solid State Physics, Cornell University - Ithaca, N. Y.

(ricevuto il 9 Ottobre 1961)

The report of a resonance in the three-pion state [1] no longer permits the luxury of regarding this system as theoretically intractable. Perhaps the most suggestive remark made to date is that of Chew [2], who pointed out that the antisymmetry of the isospin zero three-pion wave function under interchange of any pair permits each pion to interact with the others through the strong p-wave, isospin 1 π-π force. In order to implement this idea we have considered a model in which the pions interact two at a time in the p-wave, isospin 1 (resonant) state. The essential point we wish to make is that all graphs of this type are summed by a simple integral equation for the scattering amplitude $3\pi \to 3\pi$.

In order to carry out the calculation sketched below it is necessary to use some notions of perturbation theory and also to have some way of representing the π-π resonance. The structure of the resulting equations suggests that the answer could also be obtained from what are usually considered to be more fundamental theories. One of the main advantages of our approach is clarity, in a region where dispersion-theoretic approaches are apt to be especially opaque. To be definite we represent the π-π resonance by an unstable vector, isovector Boson as suggested by Sakurai [3], and Lee and Vaughn [4]. In this picture the approximation of the first paragraph is equivalent to keeping only processes in which the pions coalesce into the Boson (π-π resonance), and neglecting the non-resonant π-π scattering via Boson exchange.

In (Fig. 1*a*) we show the simplest process by which three pions can scatter in the model under consideration [5]. The solid line represents the complete renormalized propagator of the unstable Boson, or more generally whatever mechanism is assumed responsible for the π-π resonance. The next simplest

(*) This research received partial support from the A. E. C.

(1) B. C. Maglic, L. W. Alvarez, A. H. Rosenfeld and M. L. Stevenson: *Phys. Rev. Lett.*, **7**, 178 (1961).

(2) G. F. Chew: *Phys. Rev. Lett.*, **4**, 142 (1960).

(3) J. J. Sakurai: *Ann. Phys.*, **11**, 1 (1960).

(4) B. W. Lee and M. T. Vaughn: *Phys. Rev. Lett.*, **4**, 578 (1960).

(5) The pion propagator in Fig. 1*a*) can have a pole for physical external momenta, as was pointed out to the author by Dr. D. Harrington.

process (Fig. 1*b*) is that in which the recoil pion in the final state of (Fig. 1*a*) interacts with one of the « decay » pions.

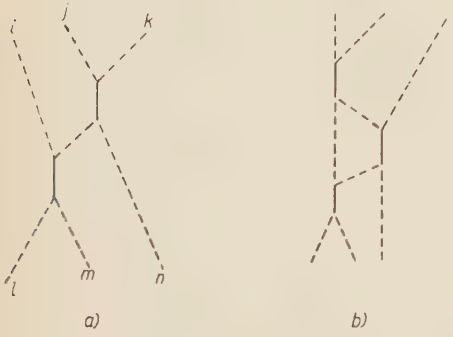

Fig. 1. – The simplest processes leading to 3π scattering are shown. The dashed lines represent pions; the solid line represents the unstable Boson (or π-π resonance) propagator.

This illustrates the essential point: to form the graph with $n+1$ unstable Bosons one scatters the recoil pion off a decay pion in the graph with n Bosons. The structure of the general term is

Fig. 2. - The structure of the general term in our approximation is shown.

indicated in Fig. 2. (According to CUTKOSKY [6], graphs such as (Fig. 1*b*) have logarithmic singularities in the physical region.)

The entire set of such graphs is generated by iteration of an integral equation written down easily by inspection. The correct interweaving of mesons is accomplished by choosing the notation carefully. Denote the initial isospin labels by (l, m, n); the final isospin labels by (i, j, k). (The momenta are to be treated in identical fashion.) Denote the Green's function [7] for which the initial pions l, m and final pions j, k interact via the p-wave resonance by $S_{ijk,lmn}$. The corresponding quantities for Figs. (1*a* and (1*b*) are $T^{(2)}_{ijk,lmn}$ and $T^{(3)}_{ijk,lmn}$, respectively. Then the entire set of graphs is summed by the equation

$$(1) \qquad S_{ijk,lmn} = T^{(2)}_{ijk,lmn} + T^{(3)}_{ijk,lmn} + \int \mathrm{d}\varrho\, S_{ijk,\lambda\mu\nu} T^{(2)}_{\lambda\mu\nu,lmn} .$$

In this equation $\int \mathrm{d}\varrho$ signifies summation over repeated isospin labels and integration over the four-momenta (only one is independent) with relevant δ-functions and numerical factors. It should be noted that eq. (1) is very similar to the usual Bethe-Salpeter equation.

Eq. (1) must be symmetrized to allow each initial (and final) pion to be the « recoil » pion. Introducing isospin projection operators, eq. (1) is reduced to a set of coupled equations for the isospin amplitudes. However the isospin zero channel is especially simple in that it is not coupled to any other channels. An angular momentum decomposition is probably necessary as well. These details will be reported elsewhere. $T^{(2)}$ and $T^{(3)}$ are to be calculated explicitly, for example, using the unstable Boson model [3,4]. Once this is done it is clear that the intregral eq. (1), so easy to derive, has a very complicated structure. Therefore one of the purposes of this note is to stimulate interest in the analytic properties of this equation.

Although we are at this time unable to solve eq. (1) the physical picture implied by our graphs is entirely compatible with the observed three-pion « mass » of 790 MeV [1]. In the model here proposed the π-π resonance energy, localized at

[6] R. E. CUTKOSKY: *Rev. Mod. Phys.*, 33, 448 (1961).

[7] The propagators of the three incoming pions are to be omitted as is clear from eq. (1).

a given time between one pair, is passed from pair to pair. Taking the « recoil » pion to be nearly at rest, we have for the « mass » of the three-pion state $M^* \cong M + \mu - B$, where M is the mass of the π-π resonance ($M \approx 750$ MeV), μ is the pion rest energy and B the binding energy. This picture leads to a plausible binding energy of $B \approx 100$ MeV. The above argument should be contrasted with the purely kinematical requirement that all three pairs of initial pions have the di-pion « mass » M in their c.m. frames, which leads to too high a « mass » in the total c.m. system. Denoting the initial pion four-momenta by p_1, p_2 and p_3, the restriction

$$(p_1 + p_2)^2 = (p_1 + p_3)^2 = (p_2 + p_3)^2 = M^2$$

determines the total c.m. energy W by the relation

$$W^2 = (p_1 + p_2 + p_3)^2 = 3(M^2 - \mu^2) .$$

The result $W \approx 1.7\, M$ disagrees with the result of ref. (1).

Finally we note that similar techniques can be applied to the scattering of four pions. In this case it is useful to introduce the 3π amplitude as deduced from (1) as well as the 2π scattering amplitude. If only the 3π amplitude is kept, the graphs contributing to the process $4\pi \to 4\pi$ have a structure very similar to that of Fig. 2. In this way the influence of the 3π resonance on 2π scattering through the 4π intermediate state can be studied (8). Thus one is led to a self-consistent procedure in which the position, width, and existence of either resonance may depend on its coupling to the other resonance. The practical problems of such a program seem exceedingly difficult at present.

* * *

The author would like to thank Dr. David Harrington for many helpful discussions.

(8) Cf. R. Blankenbecler: *Phys. Rev.*, (to be published).

Three-Pion Form Factor from Electron-Positron Experiments.

G. Da Prato and G. Putzolu

Laboratori Nazionali del C.N.E.N. - Frascati

(ricevuto il 10 Ottobre 1961)

A recent work (1) has shown the possibility of a direct measurement of the photon-(n-pion) vertices through processes of the kind $e^+ + e^- \to n\pi$. Such processes will be studied with the storage rings presently under development in Frascati (2).

Particularly the reaction

$$e^+ + e^- \to \pi^+ + \pi^- + \pi^0 , \tag{1}$$

can be used to obtain information on the vertex $\gamma - 3\pi$, which is important in the theory of the isoscalar nucleon structure. Following reference (1) the differential cross-section in the C.M.S. for the process (1) is given by

$$\frac{\mathrm{d}^2\sigma}{\mathrm{d}\omega^{(+)}\,\mathrm{d}\omega^{(-)}} = \frac{\alpha}{(2\pi)^2}\,\frac{|H|^2}{64\,E^2}\,|(\boldsymbol{p}^{(+)} \times \boldsymbol{p}^{(-)})^{\,2}\,\mathrm{sen}^2\,\theta\,\mathrm{d}(\cos\theta) , \tag{2}$$

where $\boldsymbol{p}^{(+)}$, $\omega^{(+)}$, $\boldsymbol{p}^{(-)}$ and $\omega^{(-)}$ are the momenta and the energies of the π^+ and π^-, E is the energy of the electrons, θ is the angle between the normal to the plane in which the three pions are produced and the line of collision, and H is the form factor of the vertex $\gamma \to \pi^+ + \pi^- + \pi^0$. Recently Blankenbecler an Tarski (3) have calculated this vertex essentially in terms of the $T=1$, $J=1$ 2-pion resonance.

From their work we obtain

$$|H|^2 = (2\pi)^9\,|F_0|^2\,|\exp\,[\Delta_{12} + \Delta_{23} + \Delta_{31}|^2\,D^{-2}(t)\,|_{t=4E^2} , \tag{3}$$

where F_0 is a constant that must be determined experimentally; $|\exp\,[\Delta_{ij}]|^2$ are

(1) N. Cabibbo and R. Gatto: *Phys. Rev. Lett.*, **4**, 313 (1960).

(2) See the reports by B. Touschek and by R. Gatto in the *Procedings of the International Conference on the Theoretical Aspects of very high energy phenomena* CERN, June 1961 (CERN Report 61-22, pag. 75), and R. Gatto, *Proceedings of the Conference on the elementary particles* Aix-en-Provence, 1961 (to be published).

(3) R. Blankenbecler and J. Tarski: *Phys. Rev.* (to be published).

the pion-pion phase functions; t is the square of the four momentum transfer; and $D(t)$ is the function that sums the connected three pions diagrams (see [3]).

For the total cross-section we have obtained the expression

$$\sigma(E) = \frac{\alpha}{3}\frac{(2\pi)^7}{(4E)^4}\,|F_0|^2 D(4E^2)^{-2}\int_{4\mu^2}^{(2E-\mu)^2} dx \int_{y_1}^{y_2} dy \cdot$$

$$\cdot\,|\exp[\Delta(x)+\Delta(y)+\Delta(4E^2-x-y+3\mu^2)]|^2\,|\boldsymbol{p}^{(+)}\times\boldsymbol{p}^{(-)}|^2 . \tag{4}$$

Where μ is the pion mass, and

$$\omega^{(+)} = \frac{1}{4E}(4E^2+\mu^2-y)\,, \tag{5}$$

$$\omega^{(-)} = \frac{1}{4E}(4E^2+\mu^2-x)\,. \tag{6}$$

$$\cos(\widehat{\boldsymbol{p}^{(+)}\boldsymbol{p}^{(-)}}) = \frac{1}{2|\boldsymbol{p}^{(+)}||\boldsymbol{p}^{(-)}|}\cdot$$

$$\cdot[x-2\omega^{(+)}(2E-\omega^{(-)})]\,, \tag{7}$$

$$y_{1,2} = 2E\omega\boldsymbol{p}^{(-)} \mp |^{(-)}|\sqrt{\frac{x-4}{x}}\,. \tag{8}$$

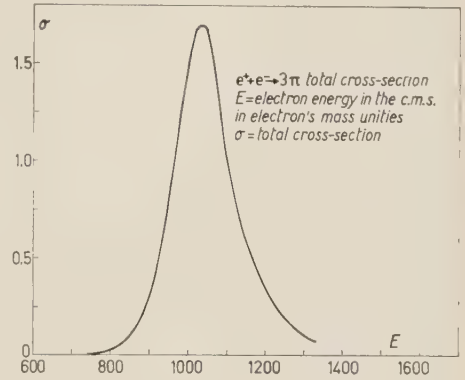

Fig. 1.

We have integrated (4) for the value $t_R = 20\mu^2$ of the π-π resonance, in the approximation $D(t)=1$.

The results are reported in Fig. 1, that gives $\sigma(E)$ in arbitrary units.

However recently experimental evidence [4] has been found for a narrow three pion resonance around $\sqrt{t}=787$ MeV, with a half-width less than 15 MeV. The rescattering function $D^{-1}(t)$ should therefore show a strong resonance in this zone, and the cross-section $\sigma(E)$ should have a peak around $E=395$ MeV.

Our results give another peak at $E=525$ MeV. It seems difficult at present to evaluate the relative importance of the two resonances.

* * *

We thank Doctor N. Cabibbo for helpful adwice, and the Frascati computing staff for help in calculations.

[4] B. C. Maglic, L. W. Alvarez, A. H. Rosenfeld and M. L. Stevenson: *Phys. Rev. Lett.*, **7**, 178 (1961).

Possible Interpretation of the 1815 MeV K^-p Resonance as a $\bar{K}^*\mathcal{N}$ Bound State.

W. Królikowski (*)

Department of Physics, University of Washington - Seattle, Wash.

(ricevuto l'11 Ottobre 1961)

It was recently reported that the total cross-section for K^-p scattering displays a bump corresponding to a $\bar{K}\mathcal{N}$ resonance in a $T=0$ state of the mass about 1815 MeV and full width about 120 MeV (1).

As it was pointed out by Kerth and Pais (2) not only the $\frac{3}{2}\,\frac{3}{2}$ $\pi\mathcal{N}$ resonance but also the higher $\pi\mathcal{N}$ resonances should have their counterparts in pion-hyperon scattering, if baryon-pion interactions had the global symmetry and baryon-kaon interactions did not disturb too badly this symmetry. These higher πY resonances could be also observed as resonances in $\bar{K}\mathcal{N}$ scattering. In particular, one of two πY counterparts of the third $\pi\mathcal{N}$ resonance ($T=\frac{1}{2}$) would have isospin $T=0$ and the mass and full width about 1855 MeV and 66 MeV, respectively (2). Since the predicted value 1855 MeV is not too far from the value 1815 MeV, this resonance may be tentatively identified with the experimental broad $\bar{K}\mathcal{N}$ resonance (2). In this case the experimental $\bar{K}\mathcal{N}$ resonance ought to be dominated by the $F_{\frac{5}{2}}$ wave like the third $\pi\mathcal{N}$ resonance.

The aim of the present letter is to propose another possible interpretation for the 1815 MeV K^-p resonance. To this end let us observe that the sum of masses of the nucleon ($M_{\mathcal{N}}=939$ MeV) and the $\bar{K}^*$ meson (3) ($M_{\bar{K}^*}=885$ MeV) is 1824 MeV. Since this value is very close to 1815 MeV, it is appealing to interpret the 1815 MeV $\bar{K}\mathcal{N}$ resonance as a $\bar{K}^*\mathcal{N}$ bound state with isospin $T=0$ and binding energy about 9 MeV. This $K^*\mathcal{N}$ bound state would be an analogy of the $\bar{K}\mathcal{N}$ bound state suggested (4) by the Dalitz-Tuan approach as an explanation for the 1405 MeV Y_0^*-hyperon (5). In both the cases the bound states would have isospin $T=0$ and could not be explained by a globally symmetric mechanism. A difference between both

(*) On leave from Institute for Nuclear Research, Polish Academy of Sciences, Warsaw, and Institute of Theoretical Physics, University of Warsaw. Present address: Institute for Advanced Study, Princeton, N. J.

(1) L. T. Kerth: *Rev. Mod. Phys.*, **33**, 389 (1961).

(2) L. T. Kerth and A. Pais: *On the gentle art of hunting bumps in pion-hyperon system* (preprint).

(3) M. Alston, L. Alvarez, Ph. Eberhard, M. L. Good, W. Graziano, H. K. Ticho and S. G. Wojcicki: *Phys. Rev. Lett.*, **6**, 300 (1961).

(4) J. Franklin, R. C. King and S. F. Tuan: *Possible theoretical interpretation of the excited hyperons* (preprint).

(5) M. Alston, L. Alvarez, Ph. Eberhard, M. L. Good, W. Graziano, H. K. Ticho and S. G. Wojcicki: *Phys. Rev. Lett.*, **6**, 698 (1961).

bound states might be caused by spins of $\bar{K}$ and $\bar{K}^*$-mesons (0 for $\bar{K}$ and presumably 1 for $\bar{K}^*$). If the analogy between these states extended to their space structure, the $\bar{K}^*\mathcal{N}$ bound state would be a S-state. Then its total spin could be $J=\frac{1}{2}$ or $J=\frac{3}{2}$. Thus our $T=0$ $\bar{K}^*\mathcal{N}$ bound state would have assignment $S_{\frac{1}{2}}$ or $S_{\frac{3}{2}}$ (parity as for the kaon). It would cause, therefore, the $T=0$ $\bar{K}\mathcal{N}$ resonance in wave $S_{\frac{1}{2}}$ or $D_{\frac{3}{2}}$ or in a state being a superposition of both waves.

To compare qualitatively the binding energies of $(\bar{K}^*\mathcal{N})_S$ and $(\bar{K}\mathcal{N})_S$, notice that for S-bound-states we can put:

(1) wave function $=$

$$= \frac{1}{(4\pi\mu r_0)^{\frac{1}{2}}} \frac{\exp[-r/r_0]}{r},$$

and

(2) $$\text{binding energy} = -\frac{1}{2\mu r_0^2},$$

where μ is the reduced mass, r_0 the « radius » of the state. Thus, the smaller binding energy of $(\bar{K}^*\mathcal{N})_S$ (~ 9 MeV) compared to $(\bar{K}\mathcal{N})_S$ (~ 28 MeV) might be ascribed partly to the reduced mass, larger for $\bar{K}^*+\mathcal{N}$ (~ 456 MeV) than for $\bar{K}+\mathcal{N}$ (~ 324 MeV), and partly to a larger « radius » of $(\bar{K}^*\mathcal{N})_S$ in comparison with $(\bar{K}\mathcal{N})_S$ (because $(\bar{K}^*\mathcal{N})_S$ could be considered as an excited state $(\bar{K}\mathcal{N})_S$).

The second fundamental feature of $(\bar{K}^*\mathcal{N})_S$ to be explained, if our model were true, would be its width that should be much greater than the width of $(\bar{K}\mathcal{N})_S$ (~ 120 MeV and ~ 20 MeV, respectively). This difference might be due to the following reasons:

(i) phase space factor in the case of decay channel $\pi\Sigma$ would be about 3.5 times larger for $(\bar{K}^*\mathcal{N})_S$ than for $(\bar{K}\mathcal{N})_S$, if the difference caused by non-zero orbital angular momentum of the first decay would be neglected in the transition matrix;

(ii) decay channels $\bar{K}\mathcal{N}$ and $\pi\bar{K}\mathcal{N}$ would be open for $(\bar{K}^*\mathcal{N})_S$.

When speaking about the width of the 1815 MeV K⁻p resonance there is still another possibility pointed out by KERTH [1] that the observed broad bump is caused by two different resonances close to each other. In our case these resonances might be the $T=0$ $\bar{K}^*\mathcal{N}$ bound state and the $T=0$ πY counterpart of the third $\pi\mathcal{N}$ resonance considered by KERTH and PAIS. In this case the observed bump would display no simple partial wave structure.

The question about the binding mechanism would be similar in the cases of $(\bar{K}^*\mathcal{N})_S$ and $(\bar{K}\mathcal{N})_S$. This mechanism might be provided by forces trasmitted by pairs of resonating pions (*e.g.* in the $J=1$, $T=1$ state, denoted by π^*) or in accordance with Sakurai and Gell-Mann point of view by elementary vector mesons (*e.g.* $J=1$, $T=1$ mesons, denoted by ρ). It is known that this mechanism leads in the lowest order (exchange of one ρ-meson) to the following static potential

(3) $$V(r) = \frac{\gamma_{\mathcal{N}\rho}\gamma}{4\pi} \boldsymbol{\tau}_{\mathcal{N}}\cdot\boldsymbol{\tau} \frac{\exp[-M_\rho r]}{r},$$

where M_ρ is the mass of ρ-meson, $\gamma_{\mathcal{N}\rho}$ and γ are $\mathcal{N}\mathcal{N}\rho$ and $\bar{K}^*K^*\rho$ (or $\bar{K}K\rho$) coupling constants (>0), and finally $\boldsymbol{\tau}_{\mathcal{N}}$ and $\boldsymbol{\tau}$ the nucleon and $\bar{K}^*$ (or $\bar{K}$) meson isospin matrices. This potential gives attraction for $T=0$ and repulsion for $T=1$, as it is desired in our discussion. Let us notice that this lowest order static potential does not depend on ordinary spins of the particles involved. It can be seen that the dependence on the spin of $\bar{K}^*$-meson does not appear also in higher orders and non-static terms, if $\bar{K}^*K^*\rho$ interaction is provided by the coupling of ρ-mesons to the isospin current of $\bar{K}^*$-mesons. In this case, therefore, there is no spin-spin coupling in the $\bar{K}^*\mathcal{N}$ system and hence the possible bound state, $(\bar{K}^*\mathcal{N})_S$,

is a superposition of states with $J=\frac{1}{2}$ and $J=\frac{3}{2}$.

The above binding mechanism would not exclude the globally symmetric mechanism leading to the nucleon and hyperon excited states (isobars) discussed by KERTH and PAIS. Let us remark that in the case of global symmetry the Kerth-Pais general discussion covers in principle all special models using baryon-pion and pion-pion interactions only, as *e.g.* the Peierls' model (6).

Concluding, we can say that till now four interpretations of 1815 MeV K^-p resonance were proposed:

(i) globally symmetric isobar (KERTH and PAIS (2));

(ii) scattering effect of intermediate π and Y_1^* (PEIERLS (6));

(iii) $\bar{K}^*\mathcal{N}$ threshold effect of inelastic scattering (BALL and FRAZER (7));

(iv) bound state of $\bar{K}^*$ and $\mathcal{N}$.

In the case (i) the resonance is dominated by $F_{\frac{5}{2}}$ wave, whereas in the cases (iii) and (iv) the wave $D_{\frac{3}{2}}$ appears provided the $\bar{K}^*$ has spin 1. It is possible that some of the proposed mechanisms contribute to this resonance simultaneously. The author hopes to be able to discuss this problem in detail later.

* * *

The author would like to thank Dr. S. F. TUAN and Dr. J. J. SAKURAI for many valuable conversations and Professor B. A. JACOBSOHN for the hospitality extended to him at the Physics Department of the University of Washington in Seattle during the Summer of 1961.

Note added in proof.

Quite recently a new K^-p resonance corresponding to a $T=0$ state of mass 1520 MeV and full width 20 MeV has been reported (R. D. TRIPP, M. FERRO-LUZZI and M. B. WATSON: abstract UCRL-9948). The spin assignment for this resonance is probably $D_{\frac{3}{2}}$. This resonance also does not fit the global symmetry like Y_0^*. On the other hand, it is amusing that the mass 1520 MeV is very close to the sum of masses of the Y_1^*-hyperon and π-meson (1385 MeV + 140 MeV = 1525 MeV). In this situation a question arises, whether this resonance can be interpreted as a πY_1^* quasi-bound state or alternatively as a πY_1^* threshold effect. It may be interesting to remark that the lowest order static potential for πY_1^* interaction via ϱ mesons gives the strongest attraction for $T=0$ states. A $T=0$ S-bound state of π and Y_1^* would give the $T=0$ $\bar{K}\mathcal{N}$ resonance in a $D_{\frac{3}{2}}$ state, provided the Y_1^*-hyperon is a $P_{\frac{3}{2}}$ state in accordance with the global symmetry. The very narrow width of the new resonance ($\sim$ 20 MeV) is, however, a serious obstacle for this bound-state interpretation, because the width of Y_1^* is much broader ($\sim$ 50 MeV). It does not seem to be any obstacle for the threshold-effect interpretation.

(6) R. F. PEIERLS: *Phys. Rev. Lett.*, **6**, 641 (1961).

(7) J. S. BALL and W. R. FRAZER: *Phys. Rev. Lett.*, **7**, 204 (1961).

Multiple-Wire Spark Counters for Counting α-Particles and Neutrons.

S. Kawata and T. Aragaki

Institute of Physics, Konan University - Kobe

(ricevuto il 13 Ottobre 1961)

The Chang-Rosenblum type spark counters have several attracting features for detection of α-particles including their insensitiveness to low specific ionization radiations. To get higher efficiency for detection several investigators have devised multiple-wire counters ([1-9]), some of them having intended to detect neutrons. One of the present writers (S.K.) has constructed a counter with 14 wires, studied its working characteristics and found that the operation has been greatly improved by insertion of a high resistance to each wire ([10]).

In the former investigation, a counter was made with 14 wires at an interval of 2.5 mm between adjacent wires. Thus in this time narrower spacings were aimed at, but after some trial it was found that counters of spacing of less than 2 mm were too unstable to use, accompanied frequently by false pulses. So, the writers have constructed and

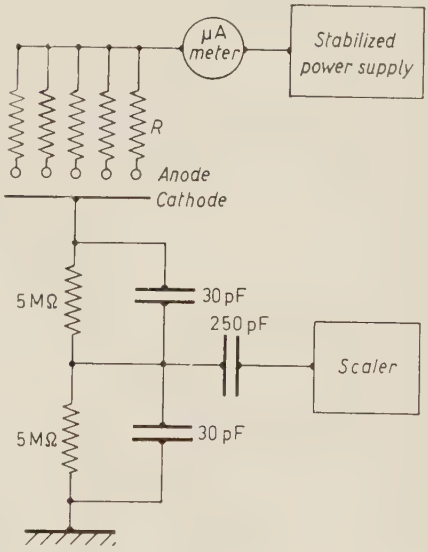

Fig. 1.

studied a counter with a spacing of 2.5 mm consisting of 15 wires (named counter I) and one with a spacing of

([1]) W. Y. Chang and S. Rosenblum: *Phys. Rev.*, **67**, 222 (1945).

([2]) G. G. Eichholtz: *Nucleonics*, **10**, No. 10, 46 (1952).

([3]) R. D. Connor: *Journ. Sci. Instr.*, **29**, 12 (1952).

([4]) M. J. Swetnick and N. G. Anton: *Nucleonics*, **15**, No. 6, 93 (1957).

([5]) N. K. Saha and Narendra Nath: *Nucleonics*, **15**, No. 6, 94 (1957).

([6]) E. Leisk: *Nucleonics*, **16**, No. 7, 95 (1958).

([7]) L. Reiffel: *Rev. Sci. Instr.*, **29**, 1151 (1958).

([8]) C. W. Peters and F. E. Jablonski: *Rev. Sci. Instr.*, **30**, 728 (1959).

([9]) A. El-Nadi and F. M. Ally: *Journ. Sci. Instr.*, **36**, 434 (1959).

([10]) S. Kawata: *Journ. Phys. Soc. Japan*, **16**, 1 (1961).

2 mm consisting of 5 wires (counter II). Tungsten wires 0.1 mm thick and 40 mm long were stretched on a frame of acrylresin of $(60\times70\times20)$ mm at a distance of 1.1 mm above a plate of stainless steel separated by two spacers of glass. The counters were operated by a circuit shown in Fig. 1.

circular hole of 0.8 mm in diameter and 5.3 mm in length placed immediately below the source. Fig. 2 shows variation of count with the counter I when the source was moved parallel to the cathode plate and perpendicularly to the wires by applying 5.0 kV with $R=0$ in the circuit. In Fig. 3 curves a and b show

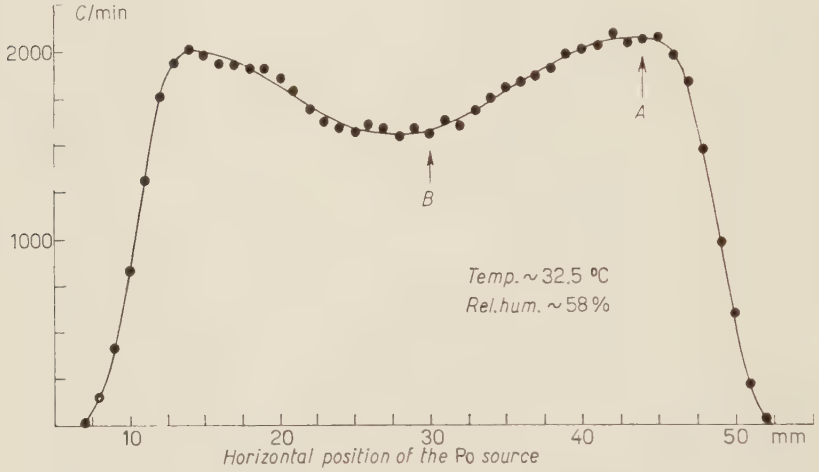

Fig. 2. – Horizontal position of the Po source.

To study working characteristics a ^{210}Po source was placed 28 mm above

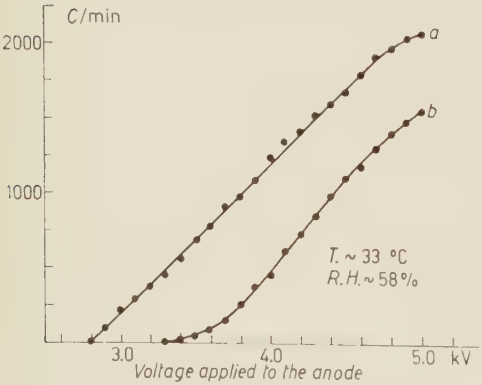

Fig. 3. – Voltage applied to the anode.

the plane of wires and irradiation was made in end-on direction through a

relations between count and voltage applied to the wires respectively at points A and B in the curve in Fig. 2. Curve m in Fig. 4 is similar to that in Fig. 2 but with $R=10\,\mathrm{M}\Omega$. Curves a' and b' in Fig. 5 show relations of count *vs.* applied voltage taken respectively at points A' and B' in Fig. 4. It will be seen that voltage to initiate spark for b' is higher than a', the rising form of b' is different from that of a' and the voltage giving saturation count is distinctly higher in b'. Again by comparing curves in Fig. 5 and curve m in Fig. 4 respectively with curves in Fig. 3 and curve in Fig. 2 it may be found that insertion of a high resistance R in the circuit will reduce saturation voltage and make counting rate become uniform through the main part of the acting region of the counter. (However, when the source is brought

near the anode wires curve m begins to show periodic variation giving maximum counts at points directly above each wire). For comparison of efficiencies of counters of single-wire and multiple-wire types for counting α-particles especially from a wide source, curve s is drawn for a single-wire counter in Fig. 4. Figs. 6 and 7 represent curves obtained with counter II similar to those of Figs. 4 and 5(b') with counter I.

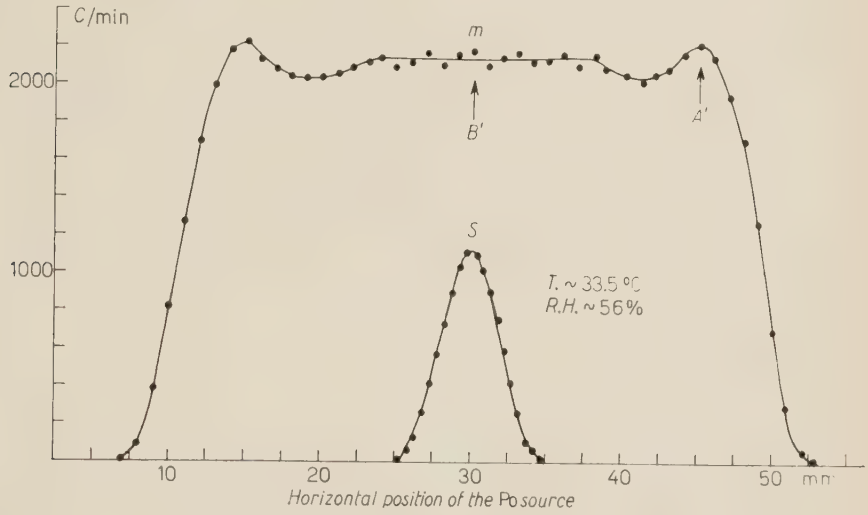

Fig. 4. – Horizontal position of the Po source.

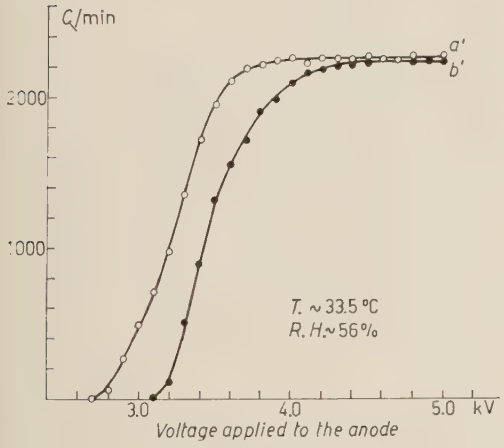

Fig. 5. – Voltage applied to the anode.

Lastly, detection of neutrons was undertaken with counter I. A boron-coated glass plate of (40 × 40) mm in area and 1.4 mm thick was put at various distances d from the wires, and the assembly was placed in paraffin piles as

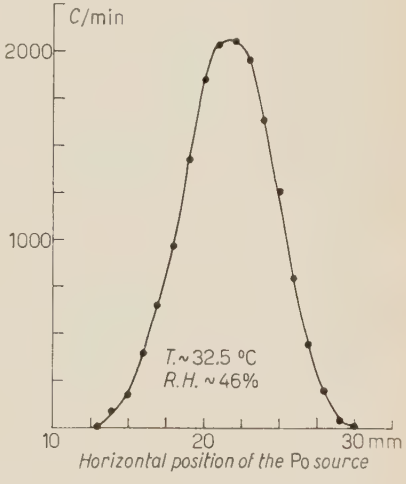

Fig. 6. – Horizontal position of the Po source.

shown in Fig. 8. To prepare the boron-coated plate, fine boron (natural) powders

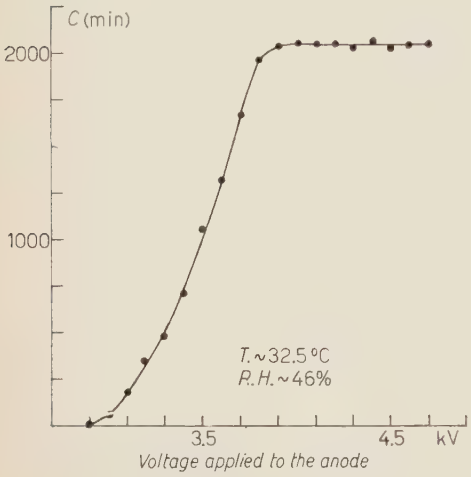

Fig. 7. Voltage applied to the anode.

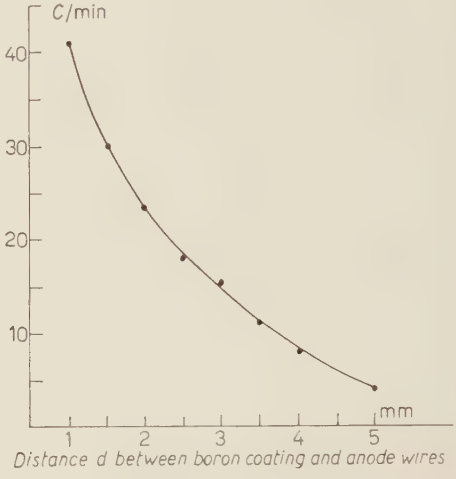

Fig. 9. – Distance d between boron coating and anode wires.

were separated out from commercial samples by electrostatic separation meth-

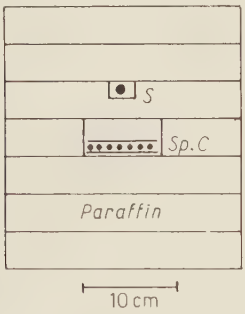

Fig. 8.

od and sprayed with benzene upon glass plates. The method seems fairly satisfactory, but making ideally thin (~ 0.5 mg/cm^2) uniform coating was far beyond the writers' technical skill. Thickness of coating actually employed was ~ 2.5 mg/cm^2. A (10 mC RaD+Be) neutron source emitting $\sim 2.5 \cdot 10^4$ n/s was enclosed in paraffin as marked by S. Fig. 9 shows variation of count of sparks *vs.* d. Count was practically zero without either the neutron source or the boron-coated plate. As a method of increasing efficiency of detection two similar counters were combined with their cathode plates in contact *i.e.* one of the counters being held upside down and placed in paraffin. Then counting rate increased about 80%. The efficiency may be made more than 10 times greater by using powders of ^{10}B and making coating of optimum thickness.

IL NUOVO CIMENTO Vol. XXII, N. 4 16 Novembre 1961

Some Remarks on the Wick Product of Interacting Fields (*).

A. Campolattaro and M. Marinaro

Istituto di Fisica Teorica dell'Università - Napoli
Istituto Nazionale di Fisica Nucleare - Sottosezione di Napoli

(ricevuto il 21 Ottobre 1961)

1. – It is customary to write the Lagrangian or Hamiltonian of a quantized field theory by replacing the ordinary products of wave functions of the non-quantized theory with the Wick products (1) of the corresponding field operators. As is well known, however, when there is interaction the definition of the Wick product is somewhat artificial and not wholly unambiguous (if at least, as it is usually stated, it is attained by imposing only that it reduce to the one for free fields when the interaction vanishes).

The question arises, what difference does it actually make if one changes the definition, or gives up the use of the Wick product. This comes naturally to the routine problem of field theory, giving unambiguous rules for disposing of ambiguous terms. The answer one would intuitively expect, in this case, is that the difference show up simply as a phase factor. We shall find that this does indeed happen, but only if all calculations involving formally divergent integrals are made so as to satisfy some specific consistency requirements; neglect of these might lead to erroneous numerical results. With different physical considerations, the same conclusions hold also for many-body problems (in which case the corresponding integrals are finite, but our proofs still apply).

Our discussion uses the formalism developed by Caianiello (2), to whose works the reader is referred for further details. His branching equations that connect the propagation kernels, or Green's functions, of field theory permit to exploit the formal advantages offered in our case by the use of perturbative expansions — where only products of free fields occur — while giving in fact a treatment which is independent of any hypothesis on the convergence of these expansions.

2. – Let

$$K_{N_0P_0}\begin{pmatrix} x_1 \dots x_{N_0} \\ y_1 \dots y_{N_0} \end{pmatrix} | t_1 \dots t_{P_0}\Big),$$

(*) The research reported in this document has been sponsored in part by the Air Force Research Division of the Air Research and Development Command, United States Air Force, through its European Office.

(1) G. C. Wick: *Phys. Rev.*, **80**, 268 (1950).

(2) E. R. Caianiello: *Nuovo Cimento*, **13**, 637 (1959) and references quoted therein.

denote the propagation kernel which describes, in a two-field theory, all processes involving N_0 initial, N_0 final fermions and P_0 bosons; (x, y), $[x, y]$ will denote the free fermion and boson propagators (or Feynman, or causal functions $S^F(x-y)$ and $D^F(x-y)$).

If one views the perturbative expansions it is apparent [3] that adopting the standard definition of Wick product amounts simply to defining $(xx)=0$.

This was also explicitly assumed by CAIANIELLO, and is clearly legitimate, because at equal time and space points the free propagators, which originate in the theory as time-ordered products, are wholly indeterminate and can therefore be given any arbitrary value (to avoid unnecessary discussions, we assume, whenever convenient, that auxiliary regularizing parameters — to be removed after algebraic manipulations are made — are introduced in the theory; for instance, that the free propagators are sums over a finite number N of modes, which later will increase to infinity). We assume here, more generally, that

$$(x, x) = f(x, m), \tag{1}$$

$$[x, x] = g(x, \mu) , \tag{2}$$

where f and g are arbitrarily given, infinitely differentiable functions of the fermionic mass m and of the square μ of the bosonic mass, and of position if there are external fields.

It is then straightforward to re-derive Caianiello's equations [4] for the derivatives of the kernels with respect to the parameters λ (coupling constant), m and μ. We find, by using the same combinatorial techniques:

$$\frac{\partial}{\partial\lambda} K\begin{pmatrix} x_1 \dots x_{N_0} \\ y_1 \dots y_{N_0} \end{pmatrix} t_1 \dots t_{P_0}\Big) = \int \mathrm{d}\xi \sum \gamma^{\xi} K\begin{pmatrix} x_1 \dots x_{N_0}\xi \\ y_1 \dots y_{N_0}\xi \end{pmatrix} t_1 \dots t_{P_0}\xi\Big) , \tag{3}$$

$$\frac{\partial}{\partial m} K\begin{pmatrix} x_1 \dots x_{N_0} \\ y_1 \dots y_{N_0} \end{pmatrix} t_1 \dots t_{P_0}\Big) = -i\int \mathrm{d}\xi\, K\begin{pmatrix} x_1 \dots x_{N_0}\xi \\ y_1 \dots y_{N_0}\xi \end{pmatrix} t_1 \dots t_{P_0}\Big) + \tag{4}$$

$$+ i\int \mathrm{d}\xi(\xi\xi)\, K\begin{pmatrix} x_1 \dots x_{N_0} \\ y_1 \dots y_{N_0} \end{pmatrix} t_1 \dots t_{P_0}\Big) ,$$

$$\frac{\partial}{\partial\mu} K\begin{pmatrix} x_1 \dots x_{N_0} \\ y_1 \dots y_{N_0} \end{pmatrix} t_1 \dots t_{P_0}\Big) = -\frac{i}{2}\int \mathrm{d}\xi\, K\begin{pmatrix} x_1 \dots x_{N_0} \\ y_1 \dots y_{N_0} \end{pmatrix} t_1 \dots t_{P_0}\xi\xi\Big) + \tag{5}$$

$$+ \frac{i}{2}\int \mathrm{d}\xi[\xi\xi]\, K\begin{pmatrix} x_1 \dots x_{N_0} \\ y_1 \dots y_{N_0} \end{pmatrix} t_1 \dots t_{P_0}\Big) .$$

No change occurs in the other equations [5] which do not contain derivatives of the kernels.

[3] E. R. CAIANIELLO: *Nuovo Cimento*, **10**, 1634 (1953), Section 4.5.
[4] E. R. CAIANIELLO: *Nuovo Cimento*, **13**, 637 (1959), eq. (23), (24), (25).
[5] E. R. CAIANIELLO: *Nuovo Cimento*, **13**, 637 (1959), eq. (20), (21), (22).

It is then apparent that the change of functions:

$$(6)\qquad K\begin{pmatrix} x_1 \dots x_{N_0} \\ y_1 \dots y_{N_0} \end{pmatrix} t_1 \dots t_{P_0}\Big) = \exp\left[i\int \mathrm{d}\xi \left[\int^{m} \mathrm{d}m' f(\xi, m') + \frac{1}{2}\int^{\mu} \mathrm{d}\mu' g(\xi, \mu') \right] \right] \cdot \widetilde{K}\begin{pmatrix} x_1 \dots x_{N_0} \\ y_1 \dots y_{N_0} \end{pmatrix} t_1 \dots t_{P_0}\Big),$$

reduces (3), (4), (5) to the form

$$(7)\qquad \frac{\partial}{\partial\lambda}\widetilde{K}\begin{pmatrix} x_1 \dots x_{N_0} \\ y_1 \dots y_{N_0} \end{pmatrix} t_1 \dots t_{P_0}\Big) = \int \mathrm{d}\xi \sum \gamma^{\xi}\, \widetilde{K}\begin{pmatrix} x_1 \dots x_{N_0}\, \xi \\ y_1 \dots y_{N_0}\, \xi \end{pmatrix} t_1 \dots t_{P_0}\, \xi\Big),$$

$$(8)\qquad \frac{\partial}{\partial m}\widetilde{K}\begin{pmatrix} x_1 \dots x_{N_0} \\ y_1 \dots y_{N_0} \end{pmatrix} t_1 \dots t_{P_0}\Big) = -\,i\int \mathrm{d}\xi\, \widetilde{K}\begin{pmatrix} x_1 \dots x_{N_0}\, \xi \\ y_1 \dots y_{N_0}\, \xi \end{pmatrix} t_1 \dots t_{P_0}\Big),$$

$$(9)\qquad \frac{\partial}{\partial\mu}\widetilde{K}\begin{pmatrix} x_1 \dots x_{N_0} \\ y_1 \dots y_{N_0} \end{pmatrix} t_1 \dots t_{P_0}\Big) = -\,\frac{i}{2}\int \mathrm{d}\xi\, \widetilde{K}\begin{pmatrix} x_1 \dots x_{N_0} \\ y_1 \dots y_{N_0} \end{pmatrix} t_1 \dots t_{P_0}\, \xi\xi\Big),$$

which is that which obtains if one sets in (4) and (5)

$$(10)\qquad f(x, m) = g(x, \mu) = 0\,.$$

This demonstrates that a change in the definition of the free propagators for coincident space-time points has no consequence except that shown by the transformation (6), which does not affect, in particular, the ratios $K_{N_0P_0}/K_{00}$. The same formal result might be obtained, as easily, by any of the several methods available for the derivation of these equations, once attention is fixed on the definitions (1) and (2).

One might define thus — as it is relevant to do when handling many-body systems — (xx) as $\lim_{y^0 \to x_0^-} (\boldsymbol{x}, x^0; \boldsymbol{x}, y^0)$; or adopt any other convention, provided all computations are made afterwards *consistently* with the chosen rule. From the connection between Caianiello's perturbative expansions and his branching equations it is apparent that, in his formalism, the question is as trivial as it should be. Furthermore, as was proved several times by him and others, the branching equations among propagation kernels are in turn fully equivalent to the Hamiltonian or Lagrangian formalisms; since, then, once kernels are known, Hamiltonians and Lagrangians can be expressed in terms of these, this procedure can give a precise definition of the products thus found of field operators at coincident space-time points, i.e. of Hamiltonians and Lagrangians. Any possible ambiguity of the sort we were considering in the first section can be analyzed and removed in this fashion: kernels differing by a phase factor such as we have derived may serve to define equivalent types of « Wick products » for interacting fields.

3. – We come now to a point which, in our opinion, deserves explicit mention: the requirement that computations be made « consistently » in order to assure that the indeterminates (1) and (2) be correctly factored out of the kernels as in (6) is by no means automatically met, so that, if special care is not taken, numerical errors,

or at least incorrect attributions of renormalizative counterterms, might be the consequence.

We observe first that all the equations reported before are valid also for non-relativistic theories, including models with cut-offs which make everything convergent and well defined (6); there is therefore no way of bypassing the inconsistencies one may meet, as is shown below, by attributing them to the divergent or ill-defined nature of some quantities. Suppose that one starts, without thought of possible inconsistencies, with the assumptions $(xx)=[xx]=0$ and no other requirement. Straightforward combinatorics shows then, through steps entirely similar to those which let to Caianiello's equations for electrodynamics, that (4) must be replaced with

$$(11)\qquad \frac{\partial}{\partial m} K\begin{pmatrix} x_1 \dots x_{N_0} \\ y_1 \dots y_{N_0} \end{pmatrix} t_1 \dots t_{P_0}\Big) = -i\int \mathrm{d}\xi\, K\begin{pmatrix} x_1 \dots x_{N_0}\,\xi \\ y_1 \dots y_{N_0}\,\xi \end{pmatrix} t_1 \dots t_{P_0}\Big) + \\ + i\lambda \iint \mathrm{d}\xi_1\, \mathrm{d}\xi_2\, \gamma^{\xi_2}\begin{pmatrix} \xi_1 \xi_2 \\ \xi_1 \xi_2 \end{pmatrix} K\begin{pmatrix} x_1 \dots x_{N_0} \\ y_1 \dots y_{N_0} \end{pmatrix} t_1 \dots t_{P_0}\,\xi_1\Big)\,.$$

(3) is always correct, (5) reduces identically to the correct expression. We may note here that, in the case of a P.S. neutral meson theory with additional $\lambda'\varphi^4$ coupling, eq. (5) must be written, if $[xx]=0$, in the form:

$$(12)\qquad \frac{\partial}{\partial \mu} K\begin{pmatrix} x_1 \dots x_{N_0} \\ y_1 \dots y_{N_0} \end{pmatrix} t_1 \dots t_{P_0}\Big) = -\frac{i}{2}\int \mathrm{d}\xi\, K\begin{pmatrix} x_1 \dots x_{N_0} \\ y_1 \dots y_{N_0} \end{pmatrix} t_1 \dots t_{P_0}\,\xi\,\xi\Big) + \\ + 3i\lambda' \iint \mathrm{d}\xi_1\, \mathrm{d}\xi_2 [\xi_1\,\xi_1\,\xi_2\,\xi_2]\, K\begin{pmatrix} x_1 \dots x_{N_0} \\ y_1 \dots y_{N_0} \end{pmatrix} t_1 \dots t_{P_0}\,\xi_1\,\xi_1\Big)\,.$$

In any case, clearly, such equations, which are also fully correct as they stand, permit to compute all *mixed* derivatives of the kernels with respect to λ, m and μ in terms only of the integral expressions which can be read at their r.h.s.'s. It is now quite easy to see, by a similar combinatorial exercise, that in general *all mixed derivatives* involving the coupling constant do not commute: this is the manifest sign of an inconsistent situation which cannot be accepted.

The reason is that propagators and their derivatives are connected by the well-known relations:

$$(13)\qquad \frac{\partial (x, y)}{\partial m} = i\int \mathrm{d}\xi\,(x\,\xi)(\xi\,y)\,,$$

$$(14)\qquad \frac{\partial [x\,y]}{\partial \mu} = -i\int \mathrm{d}\xi\,[x\,\xi][\xi\,y]\,.$$

Commutability, and consistency, are restored throughout only if we impose explicitly, together with $(xx)=0$ and $[xx]=0$, also the condition that all their derivatives with respect to the masses, as given by (13) and (14), are vanishing (or proceed in a like manner from assumptions (1) and (2): one finds then immediately that

(6) E. R. CAIANIELLO: *Nuovo Cimento*, **3**, 223 (1956); A. BUCCAFURRI and E. R. CAIANIELLO: *Nuovo Cimento*, **8**, 170 (1958); D. R. YENNIE and S. GARTENHAUS: *Nuovo Cimento*, **9**, 59 (1958).

all mixed derivatives of the kernels do commute as they should, so that eq. (3), (4) and (5) retain their consistency in all cases. We prefer however, in view of the finding of the next section, to keep eq. (3), (4) and (5) as they stand, without assuming a priori any special value for (xx) and $[xx]$.

The crux of the question is that, while it is readily assumed that $(xx)=0$, $[xx]=0$ (or f, g) the r.h.s.'s of eq. (13) and (14) are divergent integrals when $x \equiv y$. This paradoxical, but typical, situation was explicitly commented by CAIANIELLO (7), who also showed that it suffices to replace ordinary with finite-part integrals in order to change *ipso facto* the unrenormalized into the renormalized theory. His proof shows that all the divergent terms which are eliminated by this change are identical with Dyson's classical counterterms.

We may infer, therefore, that if caution against possible mistakes stems from Caianiello's renormalizative procedure, attention should be given to the same points also with other techniques. If we renormalize by means of finite-part integrals, we have to put, from (1), (2) and (13), (14):

$$f'_m(x, m) = i \int \mathrm{d}\xi\, (x\,\xi)(\xi\, x)\,, \tag{15}$$

$$g'_\mu(x, \mu) = -i \int \mathrm{d}\xi\, [x\,\xi][\xi\, x]\,. \tag{16}$$

But finite-part integrals, although they may be defined in a variety of ways, need be given always *the same* definition, once one is adopted: we may not, for instance, for arbitrary m and μ, impose consistently a priori that both (15) and (16) be vanishing. Factorization out of a kernel (or matrix element) of the ambiguous terms is guaranteed, however, if these matters are handled with due care. Conversely, neglect of this circumstance might lead to numerical errors.

We remark, finally, that the present considerations become quite intuitive if applied to a simple mathematical model of field theory which was recently discussed (8), which consists in replacing, in neutral scalar meson theory, the meson propagator with a constant: then all mass derivatives of the free fermion propagator coincide with the various possible vacuum graphs, and the overall contributions of these are explicitly summed, as may be easily verified, into the phase factor

$$K_0 = \exp\left[i \int \mathrm{d}\xi \int^m (\xi\xi)_{m'}\, \mathrm{d}m'\right] \exp\left[-\frac{\lambda^2}{2}\frac{\partial^2}{\partial m^2}\right] \exp\left[-i \int \mathrm{d}\xi \int^m (\xi\xi)_{m'}\, \mathrm{d}m'\right] \quad \text{(cfr. eq. (6))}.$$

The bearing of these results on the practical computational aspects of renormalization through finite-part integrals is now being investigated and will be discussed in a future occasion.

* * *

We express our sincerest thanks to Prof. E. R. CAIANIELLO for his helpful criticism and constant encouragement during the preparation of this work.

(7) E. R. CAIANIELLO: *Nuovo Cimento*, **14**, 185 (1959), Section 5.2.

(8) E. R. CAIANIELLO and A. CAMPOLATTARO: *Nuovo Cimento*, **20**, 422 (1961). We are indebted to Drs. S. OKUBO and I. BIALINICKI-BIRULA, whose correspondence on this point with Prof. E. R. CAIANIELLO stimulated the present research. Thanks are also due to them for pointing out that work similar in contents, although not in method, to that of the note quoted here was made by V. G. SOLOV'EV: *Sov. Phys. JETP*. **5**, 459 (1957).

LIBRI RICEVUTI E RECENSIONI

J. C. SLATER – *Quantum Theory of Atomic Structure.* McGraw-Hill, New York, N.Y.; Vol I, pp. XII-502, prezzo 85 s. 6 d.; Vol. II, pp. IX-439 senza indicazione di prezzo.

La prolifica famiglia dei libri Slater è alla terza generazione, come si apprende dalla prefazione-predigree del primo di questi volumi.

« And I hope that there are a number of volumes still to come ». Allora il lettore si ferma, perplesso (a pag. v), e pensa: forse conviene leggere il prossimo, più generale, più vasto, più aggiornato. Ma la fatica è così ragionevolmente diluita, nelle mille pagine dell'opera, da favorire la lettura immediata.

Dopo una prima impressione di superfluo nell'impostazione del 1° volume, ci si accorge che in fondo esso rimpiazza in biblioteca un buon numero di testi onorati. Il 2° volume è decisamente più attraente, almeno per un fisico.

Com'è facile immaginare, i pezzi forti di questi due libri sono il metodo auto-consistente e la struttura dei multipletti: è qui che qualunque lettore impara qualcosa di nuovo con il piacere di non cercarlo tra le pubblicazioni speciali. Anche se la trattazione dell'atomo di idrogeno finisce a pag. 187, dopo qualche sbadiglio.

La bibliografia è assolutamente straordinaria, particolarmente nel 2° volume (da pag. 383 a pag. 436, in ordine alfabetico, oltre alla bibliografia speciale alla fine dei vari capitoli).

Vorrei soltanto lamentare l'assenza dell'effetto Stark e l'insufficienza dell'indice analitico del 2° volume.

C. BERNARDINI

Direttore responsabile: G. POLVANI

Tipografia Compositori - Bologna

Questo fascicolo è stato licenziato dai torchi il 7-XI-1961